Tectonophysics

Hanging-wall deformation at the active Sierra Palomera extensional fault (Jiloca basin, Spain) from structural, morphotectonic, geophysical and trench study

--Manuscript Draft--

Manuscript Number:	TECTO15283R1
Article Type:	Research Paper
Keywords:	Active fault antithetic fault rollover magnetometry Pleistocene Iberian Chain
Corresponding Author:	Alba Peiro Universidad de Zaragoza Zaragoza, Aragón SPAIN
First Author:	Alba Peiro
Order of Authors:	Alba Peiro
	José Luis Simón
	Luis Eduardo Arlegui
	Lope Ezquerro
	Ana I. García-Lacosta
	M. Teresa Lamelas
	Carlos Luis Liesa
	Arantxa Luzón
	Leticia Martín-Bello
	Óscar Pueyo-Anchuela
	Nausica Russo
Abstract:	The NNW-SSE trending Sierra Palomera fault is characterized as an active, nearly pure extensional fault with mean transport direction towards N230ºE, consistent with the ENE-WSW extension trajectories of the recent to present-day regional stress field. Its macrostructure is described from surface geology and magnetometric and electromagnetic surveys, which have allowed identifying two subsidiary, nearly parallel normal faults (antithetic and synthetic, respectively). The structural contour map of an extensive planation surface, dated to 3.8 Ma, provides a maximum fault throw s.s. of 330 m for the main fault (480 m including bending), and a net slip rate of 0.09 mm/a (0.13 mm/a including bending). Trench study focussed on the subsidiary antithetic fault shows evidence of its activity during Middle-Late Pleistocene times, offsetting ca. 2.5 m the slope of a well-preserved alluvial fan. Detailed analysis and retrodeformation of the antithetic fault and other minor ruptures in the trench has allowed defining seven deformation events. The lack of a consistent age model for the involved sedimentary sequence makes them almost meaningless in terms of paleoseismic history. However, geometry and sequential development of meso-scale faults (intermediate between seismic-scale and analogue models) allows unravelling the extensional deformation history within the hanging-wall block of the Sierra Palomera fault. Progressive rupture patterns reveal shifting from dominantly synthetic to dominantly antithetic faulting, suggesting both kinematical control linked to rollover growth, and dynamical control by the regional stress field.

Abstract

The NNW-SSE trending Sierra Palomera fault is characterized as an active, nearly pure extensional fault with mean transport direction towards N230ºE, consistent with the ENE-WSW extension trajectories of the recent to present-day regional stress field. Its macrostructure is described from surface geology and magnetometric and electromagnetic surveys, which have allowed identifying two subsidiary, nearly parallel normal faults (antithetic and synthetic, respectively). The structural contour map of an extensive planation surface, dated to 3.8 Ma, provides a maximum fault throw *s.s.* of 330 m for the main fault (480 m including bending), and a net slip rate of 0.09 mm/a (0.13 mm/a including bending). Trench study focussed on the subsidiary antithetic fault shows evidence of its activity during Middle-Late Pleistocene times, offsetting 2.6 m the slope of a well-preserved alluvial fan. Detailed analysis and retrodeformation of the antithetic fault and other minor ruptures in the trench has allowed defining seven deformation events. The lack of a consistent age model for the involved sedimentary sequence makes them almost meaningless in terms of paleoseismic history. However, geometry and sequential development of meso-scale faults allows unravelling the extensional deformation mechanisms within the hanging-wall block of the Sierra Palomera fault, suggesting both kinematic control linked to rollover growth, and dynamic control by the regional stress field.

Keywords: Active fault, antithetic fault, rollover, magnetometry, Pleistocene, Iberian Chain.

HIGHLIGHTS

- The Sierra Palomera fault bounds the central sector of the active Jiloca Graben
- This fault offsets ca. 480 m a mid-Pliocene (3.5 Ma) planation surface
- A large antithetic fault in the hanging-wall block accommodates simple shear associated to roll-over
- The antithetic fault was active during Late Pleistocene time, at the rate of XXX
- Hanging-wall subsidiary faulting is controlled by both roll-over kinematics and the regional extensional stress field

Hanging-wall deformation at the active Sierra Palomera extensional fault (Jiloca basin, Spain) from structural, morphotectonic, geophysical and trench study

J.L. Simón[1], A. Peiro[1], L.E. Arlegui[1], L. Ezquerro[2], A.I. García-Lacosta[1], M.T. Lamelas[3], C.L. Liesa[1], A. Luzón[1], L. Martín-Bello[1], Ó. Pueyo-Anchuela[1], N. Russo[1]

[1]Departamento de Ciencias de la Tierra, Universidad de Zaragoza, Pedro Cerbuna, 12, 50009 Zaragoza, Spain. GEOTRANSFER Research Group-IUCA. jsimon@unizar.es, apeiro@unizar.es, arlegui@unizar.es, anagarcialacosta@hotmail.com, carluis@unizar.es, luzon@unizar.es, leticia.martin.bello@gmail.com, opueyo@unizar.es, nausicarusso@gmail.com

[2]GEOBIOTEC, Department of Earth Sciences, NOVA School of Science and Technology, Campus de Caparica, P-2829 516 Caparica, Portugal. lopezquerrro@gmail.com

[3]Centro Universitario de la Defensa, Academia General Militar, Ctra. de Huesca s/n, 50090 Zaragoza, Spain. GEOFOREST Research Group-IUCA. tlamelas@unizar.es

Corresponding author: A. Peiro, apeiro@unizar.es

Abstract

The NNW-SSE trending Sierra Palomera fault is characterized as an active, nearly pure extensional fault with mean transport direction towards N230ºE, consistent with the ENE-WSW extension trajectories of the recent to present-day regional stress field. Its macrostructure is described from surface geology and magnetometric and electromagnetic surveys, which have allowed identifying two subsidiary, nearly parallel normal faults (antithetic and synthetic, respectively). The structural contour map of an extensive planation surface, dated to 3.8 Ma, provides a maximum fault throw *s.s.* of 330 m for the main fault (480 m including bending), and a net slip rate of 0.09 mm/a (0.13 mm/a including bending). Trench study focussed on the subsidiary antithetic fault shows evidence of its activity during Middle-Late Pleistocene times, offsetting 2.6 m the slope of a well-preserved alluvial fan. Detailed analysis and retrodeformation of the antithetic fault and other minor ruptures in the trench has allowed defining seven deformation events. The lack of a consistent age model for

the involved sedimentary sequence makes them almost meaningless in terms of paleoseismic history. However, geometry and sequential development of meso-scale faults allows unravelling the extensional deformation mechanisms within the hanging-wall block of the Sierra Palomera fault, suggesting both kinematic control linked to rollover growth, and dynamic control by the regional stress field.

Keywords: Active fault, antithetic fault, rollover, magnetometry, Pleistocene, Iberian Chain.

1. Introduction

Our understanding of geometry and kinematics of extensional fault systems has been significantly improved thanks to analytical and scaled analogue models, particularly concerning deformation of the hanging-wall block of listric faults. Such models provide interesting inferences about controls that the shape of the main fault surface exerts on the development of hanging-wall folds and fractures. Fault surfaces with irregular geometry induce antithetic simple shear along a deformation band that nucleates at shallowing fault bends, while synthetic shear is induced at steepening fault bends (McClay and Scott, 1991; Xiao and Suppe, 1992; Withjack *et al.*, 1995; Delogkos *et al.*, 2020). Depending on the mechanical properties of materials, such overall simple shear results in either fault-related folding (rollover and drag folds, respectively) or faulting (antithetic and synthetic, respectively). Analogue models provide insights into both differential behaviours, *e.g.*, by comparing experimental materials as clay and sand (*e.g.*, Withjack *et al.*, 1995). Nevertheless, as discussed by Xiao and Suppe (1992), models give limited information about the actual small-scale mechanisms that accommodate deformation. Therefore, contribution of data directly supplied by field examples is necessary for full understanding of kinematics of extensional systems.

Methodology of trench analysis, extensively used and standardized for paleoseismological studies (*e.g.*, McCalpin, 1996), offers new insights for detailed analysis of progressive extensional deformation. Each identified paleoseismic event can be considered as an incremental or 'infinitesimal' deformation episode, and hence the reconstructed paleoseismic sequence provides a realistic view of extension kinematics (although ineludibly constrained to a given space and time window).

The Sierra Palomera fault is one of the most conspicuous recent, hypothetically active extensional faults in the central Iberian Chain (Spain). Nevertheless, in contrast with other neighbouring faults (Concud, Teruel, Valdecebro, Calamocha, Munébrega faults), in which numerous trench studies have been carried out in the last two decades (Gutiérrez *et al.*, 2009;

Lafuente, 2011; Lafuente *et al.*, 2011a, 2014; Martín-Bello *et al.*, 2014; Simón *et al.*, 2016, 2017, 2019), no paleoseismological analysis has been developed in the Sierra Palomera fault owing to lack of appropriate sites for digging a trench at the main fault zone.

The Sierra Palomera fault belongs to the Jiloca graben, the youngest Neogene-Quaternary basin of the central-eastern Iberian Chain (eastern Spain; Fig. 1) linked to rifting of the Valencia Trough (Vegas *et al.*, 1979). In overall, it is a half-graben that exhibits a NNW-SSE trend resulting from en-échelon, right-lateral arrangement of NW-SE striking normal faults at its eastern, active border. This basin has developed since Late Pliocene time, under a nearly biaxial or multidirectional extension regime ($\sigma_2 \approx \sigma_3$) with maximum extension trajectories (σ_3) oriented ENE-WSW (Simón, 1983, 1989; Arlegui *et al.*, 2005; Liesa *et al.*, 2019).

[PREFERENTIALLY, FIG.1 SHOULD BE INSERTED HERE, AS A 2-COLUMN FIGURE]

The northern and southern sectors of the Jiloca basin are bounded by the Calamocha and Concud faults, respectively (Fig. 1c). Both faults cut and offset the uppermost, early Pliocene lacustrine deposits of the neighbouring Calatayud and Teruel basins, respectively. Based on clearly recognized stratigraphic markers, the corresponding maximum throws are calculated at about 210 m for the Calamocha fault (Martín-Bello *et al.*, 2014), and 260 m for the Concud fault (Ezquerro *et al.*, 2020).

In the central segment of the basin (Fig. 2), the displacement at the Sierra Palomera fault cannot be calculated in the same way since no recent stratigraphic marker is available. The tectonic nature of the boundary itself, and particularly the discrimination between the role of erosive lowering and vertical tectonics in the creation of the mountain scarp has been the object of controversy indeed. After Cortés and Casas (2000), its topography is essentially a result of erosive incision in response to orogenic uplift. Gracia *et al.* (2003) reinterpret the Jiloca depression as a polje, developed during Late Pliocene-Quaternary times on an incipient half graben. Rubio and Simón (2007) and Rubio *et al.* (2007) analyse these arguments and provide new sedimentary, geomorphological and hydrogeological evidence on the tectonic origin of the Jiloca depression, from both surface and subsoil data. These authors conclude that: (i) the basin is a tectonic graben limited by Plio-Quaternary faults; (ii) the Sierra Palomera fault has a maximum throw approaching 350-400 m; and (iii) although the basin is noticeably underfilled, its sedimentary infill shows thickness and facies distribution consistent with such basin model.

[PREFERENTIALLY, FIG.2 SHOULD BE INSERTED HERE, AS A 1.5-COLUMN FIGURE]

Concerning the signs of Quaternary activity, these are again conspicuous in the northern and southern sectors of the graben. The Concud fault has been object of intense paleoseismological research at both natural outcrops and trenches, which have allowed reconstructing a wide paleoseismic succession of eleven events since ca. 74 ka BP to the present day, with average recurrence period of 7.1-8.0 ka, total net accumulated slip of about 20 m, and average slip rate of 0.29 mm/a (Lafuente, 2011; Lafuente *et al.*, 2011a,b, 2014; Simón *et al.*, 2016). Quaternary activity of the Calamocha fault is revealed by the mechanical contact between Neogene units of the Calatayud basin and Late Pleistocene alluvial deposits that infill the northernmost Jiloca basin. Three distinct fault branches are well exposed at the slopes of the A-23 highway and an industrial area in the neighbourhoods of Calamocha town (Martín-Bello *et al.*, 2014).

On the contrary, no exposure of the Sierra Palomera fault cutting Quaternary deposits has been described. It is mainly due to the fact that the Quaternary fluvial incision is virtually absent. Endorheic conditions in this sector have remained until historical times, with development of a palustrine area at the basin centre (ancient Cañizar lake; Rubio and Simón, 2007). Observation of Quaternary surficial ruptures has not been possible, thus their evidence is only indirect.

The purpose of the present work is contributing to fill this gap, with three specific objectives: (i) improving our overall knowledge on the structure and evolution of the Jiloca basin; (ii) reporting evidence on the activity of the Sierra Palomera fault during the Quaternary, and (iii) characterizing the style of extensional deformation within its hanging-wall block. Especial attention will be paid to structural features that indicate recent activity of the Sierra Palomera fault and other structures associated to it, showing how geophysical exploration provides complementary subsoil information with that respect. We will go deeper into the morphotectonics of the area, analysing the effects of fault activity on the relief. In the absence of stratigraphic markers, extensive Late Neogene planation surfaces existing in the region will be especially useful as geomorphological markers of deformation. Finally, we will address a detailed analysis of ruptures within a portion of the hanging-wall block of the Sierra Palomera fault by using trenching techniques.

2. Geological setting

The Iberian Chain is a NW-SE trending, 450 km long intraplate mountain range located in the eastern Iberian Peninsula (Fig. 1a). This chain developed in Paleogene to Early Miocene times due to the convergence between the Africa and Eurasia plates, under which an heterogeneous ensemble of fold-and-thrust belts, depicting a roughly double-vergence structure, was built by positive inversion of the extensional Mesozoic Iberian basin (Álvaro *et al.*, 1979; Guimerà and Álvaro, 1990; Capote *et al.*, 2002; Liesa *et al.*, 2018). After a transition period during the Early Miocene, in which the longitudinal Calatayud basin developed under a transpressional regime (Colomer and Santanach, 1988; Simón *et al.*, 2021), a new extensional stage associated to rifting of the Valencia Trough took place. Extensional deformation propagated onshore towards the central part of the Iberian Chain (Álvaro *et al.* 1979, Vegas *et al.*, 1979), inducing both reactivation of the main inherited Mesozoic faults and formation of new normal faults, and generating a number of diversely oriented intracontinental grabens and half-grabens (Simón, 1982, 1989; Gutiérrez *et al.*, 2008, 2012; Ezquerro, 2017; Liesa *et al.*, 2019).

Relationships of extensional macrostructures with geomorphic features and stress evolution in the Iberian Chain allow defining two main extensional phases. During the first phase (Late Miocene to Early Pliocene in age), the 90-km-long, NNE-SSW trending Teruel half-graben basin developed, filled with terrestrial sediments up to 500 m thick (Simón, 1982, 1983; Moissenet, 1983; Anadón and Moissenet, 1996; Ezquerro, 2017; Ezquerro *et al.*, 2020). Throughout this period, the Teruel basin propagated northwards, acquiring a N-S trend at its northern sector (El Pobo fault zone; Fig. 1b; Ezquerro *et al.*, 2019, 2020), while other N-S trending half-grabens were settled in its footwall block (western and eastern El Pobo basins; Simón-Porcar *et al.*, 2019). The second extensional phase started in the Late Pliocene and shows a more widespread deformation. In the central Iberian Chain, a large number of compressional and extensional structures were reactivated, producing new NNW-SSE trending grabens and half-grabens that are inset or cross-cut the pre-existent Teruel and Calatayud basins (Simón, 1983, 1989; Gutiérrez *et al.*, 2008, 2020; Liesa *et al.*, 2019). They include (Fig. 1): (i) the 80-km-long Jiloca graben, which results from en-échelon, right releasing arrangement of the NW-SE striking Concud, Sierra Palomera and Calamocha faults (Simón, 1983; Rubio and Simón, 2007; Simón *et al.*, 2012, 2017; Peiro *et al.*, 2019, 2020); (ii) the 30-km-long Daroca half-graben (Colomer, 1987; Gracia, 1992; Gutiérrez *et al.*, 2008, 2020; Casas *et al.*, 2018); (iii) the 88-km-long Río Grío-Pancrudo Fault Zone, made of two main faults, Río Grío-Lanzuela and Cucalón-Pancrudo (Peiro and Simón, 2021). In the first extensional phase, the direction of maximum extension (σ_3) was E-W to ESE-WNW (under a triaxial extensional regime), whereas 'multidirectional' extension with ENE-WSW σ_3 trajectories characterizes the second phase (Simón, 1982, 1983, 1989; Cortés, 1999; Capote *et al.*, 2002; Arlegui *et al.*, 2005, 2006; Liesa, 2011; Ezquerro, 2017; Liesa *et al.*, 2019). Regional uplift during the Late Pliocene-Quaternary resulted in: (i) constraining sedimentation to underfilled residual basins, with a modest sedimentary infill (normally less than 100 m thick), and (ii) driving most of the area to exorheic conditions.

Geometric construction of normal fault profiles of the Teruel fault system locates the sole detachment at a depth of 14-17 km b.s.l. (Ezquerro *et al.*, 2020), *i.e.*, in an intermediate location within the ~30-km-thick crust of the central Iberian Chain, although it diminishes up to ~14 km in the central part of the Valencia Trough (*e.g.* Roca and Guimerà, 1992). Ezquerro *et al.* (2020) estimate an average E-W stretching factor ß=1.1 since the formation of the Teruel basin (11.2 Ma ago), accommodated by major faults that have vertical slip between a few hundred metres and 1 km. The total vertical slip rate (considering fault throw and associated bending) shows a similar value (0.09 mm/a) for distinct transects across the Teruel half graben, but a clear increase between both extensional phases (from 0.05-0.07 mm/a to 0.12-0.16 mm/a) has been reported (Ezquerro *et al.*, 2020). Slip rate increase has been attributed to: (i) onshore, westwards propagation of extensional deformation from the inner parts of the Valencia Trough, enhanced by crustal doming that would have affected the eastern Iberian Chain; (ii) change of the regional stress field, which evolved to multidirectional extension driven by a crustal doming mechanism; (iii) progressive fault linkage since the beginning of the Late Miocene, which is documented from tectono-stratigraphic information.

Mountains surrounding the Teruel and Jiloca basins show extensive erosion surfaces modelling Mesozoic-Palaeogene rocks and bevelling compressional structures. Two large planation surfaces, whose remnants appear at different heights either on the upthrown blocks or in the basin floors, have been traditionally defined (Gutiérrez and Peña, 1976; Peña *et al.*, 1984; Sánchez-Fabre *et al.*, 2019): (i) *Intra-Miocene Erosion Surface* (*IES*, middle Miocene), generally recognized in the upper part of the main reliefs, and (ii) *Fundamental Erosion Surface* (*FES*, middle Pliocene), easily recognizable as a vast planation level at lower heights. They approximately correspond to the *Iberian Chain Surface* and the *Lower Pliocene Surface* by Pailhé (1984), and the S1 and S2 by Gutiérrez and Gracia (1997), respectively. Recent detailed studies (Simón-Porcar *et al*., 2019; Ezquerro *et al.*, 2020) have demonstrated that the *FES* splits into three different surfaces: an Upper Sublevel, the *FES s.s.* (the most widely developed), and a Lower Sublevel. In this work, these surfaces will be called as *FES1*, *FES2* and *FES3*, respectively. Based on mammal sites as well as on magnetostratigraphic constraints, the *Intra-Miocene Erosion Surface* has been dated close to the Aragonian-Vallesian limit (~11.2 Ma; Alcalá *et al.*, 2000; Ezquerro, 2017), *FES1* and *FES2* to the Late Ruscinian (both merging around ~3.8 Ma), and *FES3* to the Early Villafranchian (~3,5 Ma) (Ezquerro *et al.*, 2020).

Qualitative and quantitative geomorphological features of the mountain fronts and the associated piedmonts of the eastern margin of the Jiloca graben are those typical of active normal faults. At the Concud fault, Lafuente *et al.* (2011b) described conspicuous triangular facets and short, non-incised alluvial fans, and provided a significantly low value of the mountain-front sinuosity index defined by Bull and McFadden (1977) (S_{mf} = 1.24). At the Sierra Palomera fault, García-Lacosta (2013) described trapezoidal facets and V-shaped gullies, and provided a similar value for the sinuosity index (S_{mf} = 1.27).

Historic and instrumental seismicity of the central-eastern Iberian Chain is low to moderate. In the Teruel region, the epicentres are concentrated at the Jiloca graben margins, the central-southern sector of the Teruel basin, and the Albarracín and Javalambre massifs. Apart from the Albarracín massif, epicentres can be reasonably associated to Neogene-Quaternary known faults. Measured magnitudes (Mb) usually range from 1.5 to 3.5, with maximum Mb = 4.4 in the Teruel Graben and Mb = 3.8 in the Albarracín massif (data from seismic database of Instituto Geográfico Nacional, IGN: https://www.ign.es/web/ign/portal/sis-catalogo-terremotos).

3. Methodology

The structural study is based on recognizing and mapping the main structures on aerial photographs at 1: 18,000 and 1: 33,000 scale, and satellite imagery, complemented with field surveys involving outcrop-scale observations. Data of orientation of rupture surfaces and slickenlines have been collected in a number of sites within the Sierra Palomera fault damage zone, as well as within the trench described below. Stereoplots (equal-area, lower hemisphere) of those data sets have been elaborated using Stereonet 8 software (Allmendinger *et al.*, 2012; Cardozo and Allmendinger, 2013).

To characterize the geometry of recent vertical deformation, the three erosional planation surfaces (*FES1*, *FES2* and *FES3*) described above were used as markers. This required mapping of erosion surfaces and morphotectonic analysis based on aerial photographs (scales 1: 18,000 and 1: 33,000) and orthorectified photographs (1: 5000), as well as on digital elevation models (DEM, pixel = 5 m) and the resulting hillshade images. A structural contour map of *FES2* was elaborated by interpolating the altitude of their remnants, which permits measuring vertical displacement across the main fault and hence calculating slip rate. Changes of vertical displacement along the fault zone were inferred from 1-km-spaced transects orthogonal to the fault trace and analysed on a throw *vs.* distance (T-D) graph.

Once constrained the age of a planation surface (see Section 2), the main challenge to be addressed when using it as a marker is ensuring its degree of flatness, being aware of the degree of error involved in height treatment. Continental planation surfaces can show gentle (short- to middle-wavelength) unevenness, or locally connect with residual, non-flattened reliefs through pediment slopes. Amplitude of their unevenness advises to use adequate spacing for contours in order to represent its present-day geometry with the suitable precision. Both the local difference in height between *FES2* and *FES3* and the local unevenness within each one usually lies within the range of 10-40 m. Therefore, we assume that: (i) vertical fault throws calculated from them implicitly include a maximum error bar of ±40 m, and (ii) a 50-m-spaced contour map can be considered as reasonable for assessing recent movements (as previously proposed by Ezquerro *et al.*, 2020). Such level of uncertainty in the calculated fault throws results in errors for slip rates around 0.01 mm/a.

Subsurface information was acquired by means of geophysical exploration. Two different techniques were utilised, which had rendered interesting results in other neighbouring sectors (*e.g.*, Pueyo *et al.*, 2016): magnetometry and electromagnetic (EM) multifrequency survey. A twofold approach was taken: first, a regional analysis by means of ten transects approximately orthogonal to the Sierra Palomera mountain front; second, a detailed analysis of a sector where the highest geophysical anomalies were identified and also where geomorphological evidences hinted at the presence of a previously unknown antithetic fault. For the magnetometry survey, a GSM-19 equipment with built-in GPS was used to measure both Earth magnetic field intensity and vertical magnetic gradient (sensors separation of 0.5 m). Diurnal correction was performed from a second, stationary, magnetometer (PMG-01) that permitted to exclude natural earth magnetic field changes during the survey and to compare the results performed during different days. Then, the regional general trend was identified and subtracted to highlight anomalies in the form of residual values. The EM multifrequency survey was performed by a GEM-02 device for a range of frequencies between 65 and 0.5 kHz.

Subsoil information has been complemented with borehole data extensively compiled by Rubio (2004), whose synthetic results were presented by Rubio and Simón (2007). Such subsoil information, together with surface geology, was used for constructing geological cross sections that have allowed characterizing the general geometry of macrostructure.

A trench study has been carried out following the classical methodology (see, *e.g.*, McCalpin, 1996): excavating and shoring; cleansing and gridding the most suitable wall; identifying and marking sedimentary boundaries and deformation structures; drawing a detailed log and taking photographs of each grid cell; analysing the relationship between units and faults to identify individual events; and sampling materials for dating. Sedimentary units were defined on the basis of lithology, bed geometry, texture, colour and sedimentary structures. Dating of trench samples was achieved by the Luminiscence Dating Laboratory of University of Georgia, USA using the Optically Stimulated Luminiscence (OSL) technique. Unfortunately, five of them were saturated samples that only provided minimum ages, which drastically decreased the consistency of the age model. Additional, preliminary OSL dating of shallow alluvial fan sediments had been achieved by Laboratorio de Datación y Radioquímica de la Universidad Autónoma de Madrid.

Please add some text about how displacement along faults are measured/calculated, at which interval are measured for which fault activity event and how/if measured values are backstripped.

4. Structure and morphotectonics of the Sierra Palomera area

The NNW-SSE trending Sierra Palomera extensional fault makes the eastern boundary of the Jiloca graben at its central sector (Figs. 1b, 2). In the footwall block, Jurassic marine carbonates are unconformably covered by Paleogene continental clastic materials (Figs. 2, 3). In the western, hanging-wall block, *i.e.*, the central sector of the Jiloca basin, the sedimentary infill is made of: (i) Late Pliocene (Villafranchian) to Pleistocene alluvial and episodic palustrine deposits, all of them exposed at the ~~land~~ surface; (ii) an underlying carbonate unit, only observed in boreholes, that could represent an early lacustrine stage of Late Miocene-Early Pliocene age (Rubio and Simón, 2007). Isopach maps elaborated from borehole information show how the maximum thickness of the total infill approaches ~~one hundred metres~~, and its geometry is partially controlled by NW-SE to NNW-SSE striking normal faults (Rubio and Simón, 2007).

[PREFERENTIALLY, FIG.3 SHOULD BE INSERTED HERE, AS A 2-COLUMN FIGURE]

The Jiloca basin runs slightly oblique to previous Paleogene, NW-SE trending folds (Fig. 1b). Their hinges can be tentatively interpolated beneath the Neogene-Quaternary infilling from geology of the basin margins, borehole data and hydrogeological criteria (Rubio and Simón, 2007; Rubio *et al.*, 2007). In particular, the Sierra Palomera extensional fault follows the eastern limb, nearly vertical, of an eastwards verging anticline (Fig. 3), suggesting that it could result from negative inversion of a previous reverse fault linked to that fold. Its core is represented by the Lower and Middle Triassic rocks that crop out in the neighbourhoods of Singra village, making two gentle reliefs not completely buried by the basin filling. Its periclinal closure is partially preserved close to the southern tip of Sierra Palomera fault (Fig. 2).

The Sierra Palomera fault trace is ca. 26 km long and trends N152ºE in average. The main fault surface only crops out in a few, very small exposures (1 to 4 m^2 in area). A number of rupture surfaces observed within the damage zone show orientations consistent with the map trend: they strike between NW-SE and N-S, and dip between 54º and 87º W (mean orientation: N155ºE, 70º W; Fig. 4). Slickenlines show pitch ranging from 75ºN to 70ºS, therefore indicating almost pure normal movement, with mean transport direction towards N230ºE.

[PREFERENTIALLY, FIG.4 SHOULD BE INSERTED HERE, AS A 1-COLUMN FIGURE]

The Sierra Palomera fault is expressed in the landscape by a conspicuous, 20-km-long fault mountain front (Fig. 5a,b), which attains heights of 200 to 300 m above its toe, 450 to 550 with respect to the bottom of the Jiloca basin. It is quite rectilinear, with a significantly low value of the sinuosity index (S_{mf} = 1.27; García-Lacosta, 2013). A number of gullies (most of them exhibiting V-shaped transverse profiles) run across the fault scarp and delimit some well-preserved trapezoidal facets (Fig. 5c). Gullies feed short, high-slope alluvial fans (Fig. 5d) that are barely incised, only partially connected to the axial fluvial system, and exhibit signs of present-day functionality (*e.g.*, gravel aggradation affecting bush vegetation).

[PREFERENTIALLY, FIG.5 SHOULD BE INSERTED HERE, AS A 2-COLUMN FIGURE]

The envelope of relief at the footwall block is largely represented by the *FES2* planation surface, which cuts Triassic, Jurassic and Paleogene units, and attains a maximum height of 1430 m close to the edge (Fig. 6). The summit of Sierra Palomera (1533 m a.s.l.) and its surrounding area constitutes a residual relief that stands out from the *FES2* erosion level, while remains of an upper erosion sublevel (*FES1*) extend at the eastern foothills. A lower sublevel (*FES3*, usually lying 10-40 m below *FES2*) is also present: (i) eastwards of Sierra Palomera, over large areas of the northern Teruel basin; (ii) northwards and southwards, at the relay zones with the Calamocha and Concud faults, respectively; and (iii) along a narrow band westwards of the Sierra Palomera divide.

[PREFERENTIALLY, FIG.6 SHOULD BE INSERTED HERE, AS A 2-COLUMN FIGURE]

Within the sedimentary infill of the Teruel basin, these planation surfaces can be physically correlated with different coeval sedimentary horizons (lacustrine-palustrine carbonates) that were precisely characterized and dated by Ezquerro (2017) based on both paleontological and magnetostratigraphic data. As stated above, the age of *FES1* and *FES2* is constrained at about 3.8 Ma (Late Ruscinian, mammal zone MN15), while *FES3* is dated to 3.5 Ma (Early Villafranchian, MN16) (Ezquerro *et al.*, 2020).

The height of *FES2* and *FES3* surfaces within the Jiloca depression can only be inferred indirectly. Both have been mapped at the eastern margin of the Jiloca depression, W of Santa Eulalia town, where they descend to ca. 1100 and 1050 m, respectively (Fig. 6). Then they are supposed to be covered by the Plio-Pleistocene infill, while gentle residual reliefs at the Singra-Villafranca del Campo area (made of Triassic and Jurassic rocks belonging to the core of the Sierra Palomera anticline) stand out above the depression bottom. Having in mind the morpho-sedimentary setting at the nearby Teruel basin, the subsoil data provided by Rubio and Simón (2007) for the central Jiloca basin can be used for constraining heights of those planation surfaces. In this way, the boundary between Plio-Pleistocene alluvial deposits and the underlying carbonate unit, lying at about 950 m a.s.l. in the Santa Eulalia area, could be correlated with either *FES2* or *FES3*. This piece of data will allow reasonably approaching the total tectonic offset at the Sierra Palomera fault zone since 3.8-3.5 Ma.

Within the Sierra Palomera block, *FES2* and its correlative Late Ruscinian carbonates of the Teruel basin systematically lose height towards east. Both are in continuity with each other and show a quite homogeneous slope of about 1.5-2% along a distance of 20 km, in which the altitude of this morpho-sedimentary marker diminishes from 1400-1430 m (central sector of Sierra Palomera) to 1090-1120 m (Alfambra area) (Fig. 6). This morphotectonic setting defines a conspicuously tilted block whose edge has undergone a tectonic uplift of about 300 m relative to the bottom of the Teruel depression, as can be visualized from structural contours in Figure 6.

The latter value closely approaches the topographic amplitude of the Sierra Palomera scarp itself, and also the maximum fault throw inferred from offset of the *FES2* marker. Such fault throw, and its variation along the Sierra Palomera fault, have been analysed on a series of 1-km-spaced transects across the fault trace on the contour map of Figure 6, assuming that *FES2* within the Jiloca basin coincides with the base of the Plio-Pleistocene infill. The result is shown in the throw *vs.* distance (T-D) graph of Figure 7, where two distinct curves depict values of (i) fault throw *s.s.*, and (ii) total tectonic offset of *FES2* between the Sierra Palomera summits and the Jiloca depression bottom (including the bending component). The T-D curves show an overall bell-shape, while exhibiting slight bimodality in detail. The maximum values, 330 m and 480 m, respectively, are found at the central sector. Considering the age of the *FES2* morpho-sedimentary marker (3.8 Ma), and assuming an average dip of 70º for the fault plane and a pure normal movement, a maximum net slip rate of 0.09 mm/a can be inferred (0.13 mm/a for the total rate between Sierra Palomera and the Jiloca bottom).

[PREFERENTIALLY, FIG.7 SHOULD BE INSERTED HERE, AS A 1-COLUMN FIGURE]

Although the initial appearance of the Sierra Palomera fault is that of a single major rupture that accommodates the entire ~~vertical~~ throw, there are indications of a parallel, synthetic fault (Las Vallejadas fault) located west of the main escarpment at its southern sector (Fig. 2). Both delimit an intermediate step within the mountain front, in which *FES2* lies at an altitude of 1140-1220 m, furthermore offset (ca. 10 m) by a minor antithetic rupture (La Peñuela fault). Recent activation of both subsidiary faults is revealed by local deformation of Villafranchian alluvial deposits: (i) back tilting (up to 25ºE), due to rollover kinematics, observed at the foot of the morphological escarpment of Las Vallejadas fault; (ii) accommodation monocline (dip up to 22ºE) in the case of La Peñuela fault (Fig. 8; see location in Fig. 2).

[PREFERENTIALLY, FIG.8 SHOULD BE INSERTED HERE, AS A 1-COLUMN FIGURE]

5. Geophysical exploration of the overall Sierra Palomera piedmont

Data of magnetic intensity field and vertical magnetic gradient were extensively collected along ten transects, roughly orthogonal to the Sierra Palomera fault trace and ranging from 2.0 to 5.2 km in length (Fig. 9a). Spacing between successive measurement points was about 0.8

m. The two northernmost transects (profiles 01 and 02) and the southernmost one (profile 10) show a narrow distribution of residuals due to their lesser contrast with respect to the general, regional trend (Fig. 9b). The central transects (03 to 09) have spikes and lows that depart considerably from the general trend, and therefore, when data of the ten transects are considered as a whole, they define the range of the distribution (more specifically, profile 03 has the lowest and the highest values of residual magnetic intensity). Nonetheless, transects 01, 02 and 10 show a similar (albeit reduced in magnitude) outline to the rest.

[PREFERENTIALLY, FIG.9 SHOULD BE INSERTED HERE, AS A 2-COLUMN FIGURE]

The magnetic and EM profiles follow a common pattern of variation of residuals, portraying three domains that broadly parallel the Sierra Palomera fault (Fig. 9b):

a) Closest to the fault, domain A is an area where residual values of magnetic intensity are close to zero and barely change, except for a subtle decrease to the west.

b) Westwards, a sharp change of attitude marks the onset of domain B, a zone of anomalies expressed as variations of residuals up to 20-30 nT over decametric distances. Such anomalies reflect the presence of small magnetic dipoles, a slightly higher mean value of Earth magnetic field, while still homogeneous values for apparent conductivity.

c) Finally, domain C is separated from domain B by a sharp decrease in magnetic intensity (it goes down about 100 nT) with lower relative values of Earth magnetic field, presence of a lower density of magnetic dipoles (including those of higher wavelength), and higher apparent conductivity and magnetic susceptibility.

In map view, Figure 9a shows the location of transects, on which the residual values of field intensity (nT) are plotted as a colour palette. The spatial correlation of the described domains on successive transects is depicted. While the boundary between A and B domains is largely evident, the northern profiles show a more direct correlation than the southern ones, where the contact progresses through a magnetic dipole.

The reported geophysical results (Earth magnetic field, apparent conductivity, and susceptibility) suggest the presence of a body of relatively higher susceptibility underlying domain A, which gets shallower under domain B, and gets again deeper under domain C. Boundaries between those domains are sharp and clear. This setting can be interpreted as an uplifted block (made of Paleozoic and Triassic materials belonging to the core of the Sierra Palomera anticline) bounded by faults nearly parallel to the Sierra Palomera fault trace.

6. Detailed study at La Sima alluvial fan: linear topographic anomaly and its geomagnetic expression

In the absence of any visible surficial rupture across Quaternary sediments of the Sierra Palomera piedmont, the need to excavate and survey a trench arose. After careful field survey in search of a suitable location for such trench, no locality could be selected on the Sierra Palomera fault trace itself, owing to non-favourable topographic, lithologic and access conditions. Our search was then focused on the surface of two of the recent alluvial fans sourced at the mountain front, at La Cecilia and La Sima areas (see location in Figs. 2 and 5d). Both exhibit well-preserved alluvial fan morphology at its proximal sectors, with evidence of present-day aggradation at the apex. Shallow sand and silty sedimentary horizons in those alluvial fans have provided ages of 28.9 ± 2.0 ka BP (La Cecilia) and 19.2 ± 1.1 ka BP (La Sima) (see Table 1; location in Fig. 2).

In the middle sector of La Sima alluvial fan, a sharp NNW-SSE trending lineament is clearly visible on aerial photographs and DEM images, beyond which the fan surface is more deeply incised by the local drainage network (Fig. 10a). That lineament involves a morphological anomaly, a break in the fan slope, which becomes null or even negative up to take locally the appearance of a gentle, degraded uphill-facing scarplet (Fig. 10c). In view of these features, it came to mind the hypothesis of an antithetic fault that would have raised the middle sector of the fan with respect to the proximal one by about 2.6 m. The described lineament coincides with the boundary between domains A and B defined from geophysical results (Fig. 9b). Moreover, it is virtually prolonged towards SSE ~~up to~~ connect with the antithetic La Peñuela fault (Fig. 2).

[PREFERENTIALLY, FIG.10 SHOULD BE INSERTED HERE AS A 1.5-COLUMN FIGURE]

In order to test the hypothesis of an antithetic fault cutting the La Sima alluvial fan, the subsoil in the neighbourhoods of the morphological lineament was intensively explored by means of a magnetic and electromagnetic survey. Seeing at the geophysical domains described in Section 5, the lineament coincides with the A/B boundary, which is clearly expressed in the detailed map of residual magnetic anomalies shown in Figure 10b. The area east of the sharp linear, NNW-SSE trending limit clearly visible on this map shows low residual values with wide (hectometre-scale) wavelength variations. To the west, an increase of more than 30 nT is observed, as well as a decrease of more than 50 mS/m in the total conductivity; moreover, the texture of the residual map changes noticeably, showing sharper magnetic dipoles of decametric wavelength.

The amplitude and morphology of the linear anomaly is not consistent with the susceptibility values of surficial sediments, and suggest the contrast, at shallow levels, between a high-susceptibility rock body to the west (domain B, as defined in section 5) and the domain A to the east. In addition, Figure 10b shows other NW-SE trending linear anomalies in domain B, which involve a lower contrast of magnetic field values. Both the main anomaly and the secondary ones show high gradient and sharpness of the observed dipoles, suggesting near-surface, high dipping discontinuities or rock boundaries compatible with recent faults.

7. Trench study at La Sima alluvial fan

Once verified that geophysical and topographic analysis of La Sima lineament reinforced our preliminary hypothesis about the northwards prolongation of the antithetic La Peñuela fault, we selected an easily accessible site for trench study. A 40 m long, 1.4 m wide trench was dug along a N067ºE direction, roughly orthogonal to the linear anomaly. A segment of 19 m on its southern wall, with depth ranging from 3.0 to 3.5 m, was logged and analysed in detail (Fig. 11a).

[PREFERENTIALLY, FIG.11 SHOULD BE INSERTED HERE IN VERTICAL IF POSSIBLE]

7.1. Sedimentary units

The materials exposed at La Sima trench essentially correspond to relatively well-bedded Pleistocene alluvial sediments (Fig. 11a). Sedimentary features indicate alternating energetic flows, sometimes flash floods, recorded by gravel channel and bar deposits, and waning discharges that settled fines over the gravel deposits. All the succession includes clear signs of calcrete development and periods of time with negligible sedimentation. Bioturbation signs and carbonate precipitation are related to pedogenesis, and suggest wetting and drying episodes of the sedimentary surface. The sedimentary succession has been subdivided into twelve lithological units (Fig. 11a):

- Unit 1 (up to 50 cm in thickness): Massive reddish mudstone with isolated, mm- to cm-sized angular limestone clasts (more abundant at the base), with bioturbation traces and smooth carbonate nodules.

- Unit 2 (25 to 55 cm): Orange massive sandy mudstone with floating angular-subangular grey limestone granules and pebbles, and some irregular cm-thick gravel bed. Grey mudstones laminae towards the top.

- Unit 3 (55 to 75 cm): Tabular laminated, indurated and brecciated, carbonate crust with some cm-thick interbedded silts with carbonate clasts. Carbonate fragments are smaller in the upper part; laminated fragments are less abundant towards W.

- Unit 4 (20 to 35 cm): Reddish massive silty sand and mudstone in a tabular level with vertical root traces filled by fine sands. Some carbonate nodules, plant remains and scattered grey, angular limestone and caliche clasts up to 10 cm in size can be recognized.

- Unit 5 (15 to >50 cm): Clast-supported gravel with silty to sandy matrix in a tabular, locally channelized sedimentary body with crude horizontal stratification. Gravel is made of angular-subrounded limestone clasts (up to 8 cm) and smaller caliche clasts.

- Unit 6 (25-55 cm): Orange to brownish massive silt and mudstone with greyish limestone angular clasts and floating whitish caliche rounded nodules (up to 2 cm). Clast content increases locally. Root traces, plant remains and organic matter patches can be recognized in the western sector.

- Unit 7 (30 to >150 cm): Heterogeneous unit mainly made of grain-supported gravel, locally cemented, with angular-subrounded limestone clasts (up to 15 cm in size) and caliche nodules. It includes red mudstone discontinuous intercalations, up to 20 cm in thickness, with floating cm-sized angular clasts (labelled as 7a in Fig. 11a). The overall geometry of the unit is tabular in the footwall block and channelized in the hanging-wall block. A level of calcrete gravel, >50 cm in thickness, appears at the top of this unit within the footwall block.

- Unit 8 (10-60 cm): Reddish silt with floating limestone angular granules and pebbles (up to 8 cm) with evidence of bioturbation.

- Unit 9 (45-120 cm): Grey gravel in a channeled body with limestone angular clasts (up to 12-14 cm in size) and caliche rounded clasts. Crude finning upwards cycles can be recognized. Pedogenic features increase towards the top, where brecciated limestones locally appear.

It wold be helpful if original, uninterpreted trench is also shown.

- Unit 10 (55 to 70 cm): Reddish massive silts with floating subangular limestone clasts (up to 7 cm), whitish carbonate nodules and an interbedded discontinuous clast-supported gravel level (10b) with subangular clasts up to 10 cm in size.

- Unit 11: Wedge-shaped body of orange and whitish massive, highly cemented silt, with carbonate floating subangular limestone clasts (up to 10 cm) and caliche clasts arranged with the A-axis subvertical.

- Unit 12 (20 to 50 cm): Surface regolith made of silt with angular to subangular clasts, reworked by agricultural labours.

7.2. OSL dating

Dating of a total of seven samples of alluvial sediments within the trench (see Fig. 11a for location) has allowed approaching their age distribution, although, unfortunately, the results show a high level of uncertainty (see Table 1). Other three collected samples did not contain enough sand grains for providing a representative dose distribution and therefore OSL dates were not reliable in this case. These samples are not located in Fig. 11a.

Samples S2, S3, S4, S6 and S7 have presented signal saturation, *i.e.*, their natural luminescence signal lies beyond the saturation of the OSL response with dose, making it impossible to provide adequate results. According to laboratory results, their ages should be older than 193 to 378 ka, although such figures should not be taken *sensu stricto*. Only one of the alluvial sedimentary units is directly dated: S1 provides an age 97.4±10.2 ka for the top of unit 9. Unit 11 (sample S5), which will be next interpreted as a fissure infill, is dated to 49.2±5.4 ka. As a result, the chronology of unit 10, overlapping unit 9 and being cut by the fissure, can be broadly constrained between both numerical ages.

Without the support of further anchors, building an age model for the overall alluvial succession exposed in the trench is not feasible. In any case, the ensemble of OSL dating results and geomorphological observations in the study area suggest that: (i) most of that alluvial succession belongs to the Middle Pleistocene; (ii) a rapid decrease of sedimentation rate occurs by the Middle-Late Pleistocene transition; and (iii) sedimentation persisting in proximal and middle sectors of the alluvial fans during Late Pleistocene to present-day times only represents a small contribution to the surficial aggradation and landscape modelling.

7.3. Deformation structures

In a first approach, the trench log shows a main extensional fault zone at the central sector, dipping eastward and hence antithetic with respect to the Sierra Palomera fault (Fig.

11a), and full consistent with the uphill-facing scarplet described in section 6. The footwall block of that fault zone shows a gentle monocline, while other normal (both synthetic and antithetic) faults, cutting most of the sedimentary succession, are distributed along the entire section. The orientations of all these structures are overall consistent, as depicted in stereoplots of Fig. 11b,c,d,e.

The central fault zone is made of three significant structural elements: (i) Main rupture, expressed by θ_1 and θ_2 fault surfaces. (ii) Splay faults κ1, κ2, κ3 and κ4, associated to the tip of the main rupture and propagated through unit 7. Both the main, westwards dipping rupture surfaces and the nearly vertical splay faults consistently strike NNW-SSE (Fig. 11b). Such structural arrangement suggests that, at certain stage of its development, the main rupture θ_1-θ_2 was covered by unit 7, and then reactivated in the form of splay faults related to refraction at the extensional tip (horse-tail structure, in the sense of Granier, 1985). (iii) Open fissure bounded by surfaces θ_3 and η, and filled with unit 11. The interpretation is based on its wedge shape, the massive internal structure of the infill, and the occurrence of clasts with nearly vertical A-axes. According to this interpretation, surfaces θ_3 (smooth) and η (more irregular) would have represented both walls of a single, also NNW-SSE striking fault, then disengaged from each other when the fissure opened up and, in the case of η, partially crumbled before infilling took place.

The footwall block is deformed by the monocline and cut by a number of NNW-SSE striking normal faults (Fig. 11c), all of them synthetic with the Sierra Palomera fault and exhibiting dip separations in the range of 10 to 20 cm (Fig. 11a). Faults ρ, π_1 and π_2 cut the horizontal limb of the monocline, and have apparently kept their original, high dip. The rest of faults (τ, σ, μ, χ, λ_1 and λ_2) appear at the hinge and the abrupt limb of the monocline. They show a progressive decrease in dip towards the east as the bedding dip increases, and some individual faults (μ, λ_1, λ_2) exhibit conspicuously arched traces, so that the angle between faults and bedding remains broadly constant (mostly within the range of 55-65º). Such geometrical setting strongly suggests that they were folded by the monocline. Concerning the relationships between faults and sedimentary units, ρ and π_1 uniformly offset (15-20 cm) the base of units 2 to 6, while they suddenly vanish and does not affect the base of unit 7. Also fault σ shows similar relationships, although in this case it does not propagated through the lower units, probably detached within low-viscosity materials of unit 4. As a consequence, ρ, π_1 and σ produce a noticeable thickening of unit 6 in their respective hanging-wall blocks. Faults π_2, τ, μ, χ, λ_1 and λ_2) also offset rather uniformly the sedimentary boundaries, and at least two of them (π_2 and μ) propagated across unit 7.

The hanging-wall block shows two ensembles of intersecting faults that cut younger units (Fig. 11a). Individual faults show distinct offsets for different sedimentary markers, which indicates diachronic development. The ε_0-ε_1 couple offsets more than 1.4 m the base of unit 7, while it produces a rather uniform dip separation of 8-10 cm in the bases of units 8, 9 and 10. We should therefore interpret that ε_0-ε_1 underwent most of its present-date displacement (>1.3 m) before sedimentation of unit 8, and was then reactivated after the lower part (at least) of unit 10 was deposited. Splaying from ε_1, fault ε_2 cuts units 7 and 8, and is covered by unit 9, while ε_3 cuts the base of unit 9, thus making the three faults a footwall rupture sequence. The antithetic ε_4 propagated up to the lower unit 10. At the easternmost trench sector we find a similar pattern in the NNW-SSE striking faults α and β. Fault β offsets more than 0.7 m the base of unit 7, while (together with its splay faults γ_1, γ_2 and γ_3) produces a smaller separation (0.4 m) in the bases of units 8 and 9. We interpret that β underwent displacement $\approx$ 0.3 m before sedimentation of unit 8, and was then reactivated after deposition of unit 9. Fault α propagated through unit 7, previous to sedimentation of unit 8, and did not undergo further reactivation.

We should emphasize the strict consistence of orientations of the described structures. All faults systematically strike NNW-SSE (Fig. 11e), and so does the limb of the monocline (Fig. 11c). There is no doubt that the latter is (i) genetically linked to faults, and (ii) responsible for the decrease in dip of faults σ, μ, χ, λ_1 and λ_2. Bedding and fault surfaces are rotated around a common, well-defined horizontal axis ca. N160ºE (Fig. 11c). Strikes of minor fractures measured along the trench are also clustered around NNW-SSE, although a small number among them are oriented NNE-SSW (in blue in Fig. 11d). A brief discussion about the dynamic framework (stress fields) in which such fault and fracture pattern developed will be made in Section 7.6.

7.4. Evolutionary model: deformation events

According to the former structural description, in particular to the relationships between structures ~~themselves and with~~ the sedimentary units, we propose the evolutionary model explained below, tested by means of careful retrodeformation analysis (Fig. 12). The evolution has been conventionally divided into a succession of "deformation events", following the common practice in paleoseismological reconstruction. Several post-event sedimentary stages have been also included for better understanding.

[PREFERENTIALLY, FIG.12 SHOULD BE INSERTED HERE, AS A 1-COLUMN FIGURE]

A number of identifiable faults were either formed, propagated of reactivated during each deformation event (Fig. 12 and Table 2). Dip separation directly measured on the trench log is taken as the first approach to the net slip on each fault, since: (i) bedding is roughly horizontal, (ii) the trench, oriented N067ºE, is nearly orthogonal to the prevailing strike of faults, and (iii) the only kinematical indicator observed during trench survey (slickenlines with pitch 82ºS on fault μ), as well as those collected at the Sierra Palomera fault zone itself (see Fig. 4b), suggest nearly pure normal movement for the overall extensional fault system. A precision of 5 cm has been adopted for net slip measurements; those that are synthetic to the Sierra Palomera fault (downthrown block to the west) are compiled as positive in Table 2, while those antithetic are compiled as negative.

Below we summarize the main features of each of the seven deformation events (T to Z) distinguished in the La Sima trench (Fig. 12):

- **Event T**: Slip on faults ρ, π_1, τ and σ after deposition of unit 6 and previous to unit 7. Accumulated net slip: +45 cm.

- **Event U**: Slip on faults π_2, τ, μ, χ, λ_1, λ_2 and ε_1, subsequent or coeval with deposition of the lower part of unit 7. Accumulated net slip: +110 cm.

- **Event V**: Slip on fault θ_2, subsequent to deposition of lower unit 7, then covered by upper unit 7. Development of the monocline begins; according to our progressive deformation model depicted in Fig. 12, in which the main rupture had always propagated through units 1 to 6, this monocline should be interpreted as a drag fold. Net slip: −5 cm.

- **Event W**: Reactivation of the main, central fault through the rupture surfaces θ_1-θ_2, which propagates across upper unit 7 splitting into κ1, κ2, κ3 and κ4. Progress of the monocline produces rotation of faults τ, σ, μ, χ, λ_1 and λ_2. Slip on faults ε_0-ε_1, α and β, all of them subsequent to top of unit 7 and previous to unit 8. Accumulated net slip: +100 −105 = −5 cm.

- **Event X**: Propagation of the main fault zones, θ and ε, through new rupture surfaces: θ_2-θ_3 and ε_2, respectively. Both are younger than unit 8 and older than unit 9. Accumulated net slip: +05 −95 = −90 cm.

- **Event Y**: Activation of fault ε_3, and propagation of β splitting into γ_1, γ_2 and γ_3. Both processes are subsequent to deposition of unit 9 and probably previous to unit 10, therefore close to (or slightly younger than) the numerical age provided by sample S1 (97.4 ± 10.2 ka). Accumulated net slip: −40 cm.

- **Event Z**: Formation of fault ε_4 and propagation of ε_1 cutting the lower part of unit 10. Slip on θ_2 that passively activates the θ_3 surface with extensional component, giving rise to an open fissure (from fault η) that tears apart units 7 to 10 and is subsequently filled with unit 11. This event should be dated just prior to the numerical age provided by sample S5 (49.2 ± 5.4 ka). Accumulated net slip: +10 −135 = −125 cm.

8. Overall interpretation and discussion

8.1. Geometry and kinematics of macrostructures

We have seen how geophysical results reported in Section 5, defining three adjacent, NNW-SSE trending elongated domains (A, B, C) suggest the existence of an uplifted block bounded by faults nearly parallel to the Sierra Palomera fault trace. At the southern sector of the study area, local coincidence of the A/B and B/C domain boundaries with La Peñuela and Las Vallejadas faults, respectively, strongly supports such interpretation. The antithetic rupture exposed in La Sima trench unequivocally represents that map-scale antithetic La Peñuela fault and corroborates the extensional character of such structure. In this way, the results of subsoil exploration by geophysical methods and trench survey allow refining the structural model of the central Jiloca graben, *i.e.*, deformation style of the hanging-wall block of the Sierra Palomera fault. These new inferred faults separating domains A, B and C have been incorporated to the geological map of Fig. 2.

The Sierra Palomera fault probably resulted from negative inversion, during the Late Pliocene-Quaternary extensional phase, of a previous contractive structure developed under the Paleogene-Early Miocene compression. Such origin is suggested by its spatial coincidence with the eastern, nearly vertical limb of an eastwards verging anticline. Evidence of the same inversion setting has been described for the other master faults bounding the Jiloca graben, namely the Concud fault (Lafuente *et al.*, 2011a) and the Calamocha fault (Liesa *et al.*, 2021).

The attitude of the main fault surface is N155ºE, 70º W in average, while most ruptures visible along and close to it are systematically parallel to it. The fault shows pure normal movement, with mean transport direction towards N230ºE. These features are similar to those of the Concud and Calamocha faults, the other structures that make the eastern boundary of the Jiloca graben. In particular, the average transport direction of those faults is N220ºE (Lafuente *et al.*, 2014) and W to SW (Martín-Bello *et al.*, 2014), respectively, thus jointly making a geometrically and kinematically consistent major extensional fault system.

Two wide right relay zones separate the Sierra Palomera fault from the Calamocha and Concud faults. The dominant trend of recent, extensional faults and fractures distributed within both relay zones is similar to that of the main fault or slightly deviates to approach the N-S direction. Close to the southern tip, such fractures mainly affect Upper Miocene and Villafranchian sediments, while close to the northern tip they cut Jurassic carbonates giving rise to narrow N-S trending grabens filled with Pleistocene alluvial sediments (Capote *et al.*, 1981). These relay zones dominated by along-strike fractures were described in detail and interpreted by Peiro *et al.* (2019, 2020) with the help of analogue modelling. Fracturing in this new type of fault relay is controlled by both the structural inherited grain and the remote stress field, and efficiently contribute to slip transfer and dynamical interaction between adjacent faults. It strongly contrasts with the classical models reported in the literature (*e.g.*, Peacock and Sanderson, 1994; Young *et al.*, 2001; Fossen and Rotevatn, 2016), in which transverse connecting faults controlled by the own relay kinematics prevail. According to Peiro *et al.* (2020), the overall fault system at the eastern boundary of the Jiloca basin is at an intermediate stage between complete independence and coalescence, and will probably evolve to an along-strike propagation of the master faults through the distributed longitudinal fracture ensembles. The slightly bimodal throw *vs.* distance (T-D) curve depicted in Fig. 7 suggests that the Sierra Palomera fault itself resulted from coalescence of two distinct fault segments, although their overall bell-shape indicates full linkage between them. Moreover, the persistence of an important bending component beyond both tips of the fault trace reveals that the total length of the Sierra Palomera fault is larger than that exposed at the surface, thus being propagated towards NNW and SSE as a blind fault.

Geophysical and morphotectonic data have allowed characterizing the overall structure of the hanging-wall block beyond the apparently flat appearance of the Sierra Palomera pediment. We have explained (sections 5 and 6) how magnetic field linear anomalies parallel to the Sierra Palomera fault trace suggest a distribution of subsoil lithological domains consistent with a gentle horst-and-graben setting.

The most conspicuous linear anomaly coincides with a morphological lineament (a gentle uphill-facing scarplet) across the middle sector of La Sima alluvial fan (section 6), and with the uphill-facing fault scarp east of Las Vallejadas fault. The hypothesis that all of these elements represent an antithetic fault has been corroborated by the exposure of that antithetic rupture in La Sima trench. In summary, the available information reveals a more complex structure in the Sierra Palomera hanging-wall block than the one assumed so far, including: (i) a synthetic fault, located at about 1.5 km basinwards, which at its southern sector emerges at surface (Las Vallejadas fault); (ii) a recent antithetic fault, at a distance of 0.7-1.0 km, which would have displaced the surface of the La Sima alluvial fan and would extend southwards up to La Peñuela fault.

In order to depict the refined structural model of the Sierra Palomera hanging-wall block, both faults have been incorporated to the geological map of Figure 2, as well as to a new version of the cross section (Fig. 13a). Furthermore, the latter depicts a reinterpretation of the geometry of the master fault. It is known that the shape of the main fault surface strongly controls the style of accommodation folding and subsidiary faulting in the hanging-wall block of extensional faults. Rollover folds and antithetic faults develop above concave-upward fault bends, whereas drag folds and synthetic faults form above convex-upward fault bends, their propagation being facilitated by high curvature of such fault bends (McClay and Scott, 1991; Xiao and Suppe, 1992; Withjack *et al.*, 1995; Delogkos *et al.*, 2020). In our case, the occurrence of the antithetic and the synthetic inferred subsidiary faults strongly suggests the presence, at a depth of less than 1 km, of a relative flat in the main fault surface (*i.e.*, a double, convex-concave bend), probably located at the Middle-Upper Triassic lutite and evaporite units (Middle Muschelkalk and Keuper facies).

[PREFERENTIALLY, FIG.13 SHOULD BE INSERTED HERE, AS A 2-COLUMN FIGURE]

8.2. Planation surfaces as structural markers: inferred offsets and slip rates

In contrast to the other master faults bounding the Jiloca graben, namely the Calamocha and Concud faults, no dated stratigraphic marker is available at the Sierra Palomera fault in order to precisely calculate its total offset and slip rate. In such context, the use of planation surfaces (in our case, the mid-Pliocene *FES2* and *FES3* surfaces; Fig 13b) is necessary for characterizing the macrostructure and measuring fault throws. As explained in Section 4, fault throw *s.s.* and total tectonic offset of *FES2* at the Sierra Palomera graben margin attain maximum values of 330 m and 480 m, respectively, resulting in slip rates of 0.09 and 0.13 mm/a.

We should draw attention to the fact that our main geomorphological marker, *FES2*, is poorly represented within the Jiloca bottom, *i.e*., the hanging-all block of the Sierra Palomera fault, which makes difficult to calculate the actual throw. We interpret that the boundary between Plio-Pleistocene alluvial deposits and the underlying carbonate unit probably represents the first approach to the position of *FES2* (Fig. 13b), although it also could be correlated with *FES3*. According to the results provided by Ezquerro *et al.* (2020), such uncertainty introduces a potential error of either 10-40 m in the height of the marker (equivalent to the thickness of Villafranchian palustrine carbonates ≈ M8 megasequence of Ezquerro, 2017), or 0.3 Ma in its age. If the top of the buried carbonate unit would be Early Villafranchian in age (3.5 Ma, therefore correlative of *FES3*): (i) the fault throw *s.s.* and the total tectonic offset calculated in section 4 (330 m and 480 m, respectively) should be applied to a 3.5 Ma time span, therefore resulting in slightly higher slip rates (0.10 *vs*. 0.09 mm/a, 0.15 *vs*. 0.13 mm/a, respectively); (ii) *FES2* would lie 10-40 m lower within the downthrown block, and hence the fault throw *s.s.* and the maximum total tectonic offset could increase up to 370 m and 520 m, respectively, giving rise to slip rates of 0.10 and 0.15 mm/a for the last 3.8 Ma. In any case, such height uncertainty is of the same order as the unevenness of the planation surfaces themselves, and results in a very small error in slip rate (0.01-0.02 mm/a).

The consistency of this interpretation is further reinforced if a broader morphotectonic perspective is adopted, considering the whole setting of footwall and hanging-wall blocks of the Sierra Palomera fault and neighbouring structures. We have explained how the morpho-sedimentary *FES2* marker defines a tilted Sierra Palomera-Alfambra block whose edge is tectonically uplifted ca. 300 m relative to the bottom of the Teruel basin. A similar morphostructural outline can be drawn for the Sierra de Albarracín-Jiloca block, in which *FES2* shows a progressive eastwards decrease in altitude, from 1400-1500 m to <1100 m. Therefore, the inference that the fault separating such tilted blocks has a throw in the range of 300-400 m seems well-founded. On the other hand, the notion of recent vertical displacement on the Sierra Palomera fault being larger than those on Calamocha and Concud faults (210 and 260 m, respectively; Martín-Bello *et al.*, 2014; Ezquerro *et al.*, 2020) fits a common structural feature of segmented extensional fault zones, in which maximum throws are found in central segments (self-similar pattern as that of individual faults; Cowie and Roberts, 2001). Gracia *et al.* (2003) aimed to minimize the role of tectonic subsidence in benefit of erosional lowering in the development of the central Jiloca depression, and hence to underestimate the throw of the Sierra Palomera fault (see further discussion by Rubio and Simón, 2007; Rubio *et al.*, 2007; Gracia *et al.*, 2008). Nevertheless, such controversy is currently out of place.

It is also pertinent to compare the displacement and slip rates on the Sierra Palomera fault with those in the neighbouring Teruel graben. During the last 3.8 Ma (Late Pliocene-Quaternary extensional phase), fault zones making the eastern margin of the Teruel basin underwent total vertical displacement (including bending component) in the range of 440 to 620 m, and hence long-term vertical slip rates of 0.12 to 0.16 mm/a (Ezquerro *et al.*, 2020). Assuming an average dip of 70º for the fault plane and a pure normal movement, the resulting total net slip rates for this period are 0.13 to 0.17 mm/a, similar to that calculated for the Sierra Palomera fault (0.15 mm/a) and higher than those for the Concud (0.07-0.08 mm/a; Lafuente *et al.*, 2011a), Calamocha (0.06-0.09 mm/a; Martín-Bello *et al.*, 2014), and Teruel (0.075 mm/a; Simón *et al.*, 2017) faults.

8.3. Geomorphic indices of the mountain front: assessing fault activity

Geomorphic indices constitute an auxiliary tool for assessing fault activity, as enhanced by, *e.g.*, Bull and McFadden (1977), McCalpin (1996), Silva *et al.* (2003), or Burbank and Anderson (2012). With this respect, it is interesting to compare the values proposed for the Sierra Palomera mountain front with those of other faults in the same geodynamic framework.

At Sierra Palomera, García-Lacosta (2013) calculated values of two significant geomorphic indices defined by Bull and McFadden (1977), *i.e.*, mountain-front sinuosity (S_{mf}), and valley width/height ratio (V_f). The value of S_{mf} is 1.27. The average width/height ratio calculated for 10 gullies crossing the fault is V_f = 0.22 (measured 250 m upstream from the fault trace). These values, together with other mentioned qualitative attributes of the mountain front (trapezoidal facets, V-shaped gullies, small alluvial fans not connected to the regional fluvial system), indicate 'rapid' fault slip according to the classification by McCalpin (1996), and 'active' (according to Silva *et al.*, 2003) (Fig. 14). The range of slip rates that those authors estimate for such categories in their respective classifications (0.08 to 0.5 mm/a) encloses the value calculated for our fault from offset of the *FES2* marker (0.09-0.13 mm/a).

[PREFERENTIALLY, FIG.14 SHOULD BE INSERTED HERE, AS A 1-COLUMN FIGURE]

The sinuosity index S_{mf} at the Sierra Palomera mountain front is very similar to that at the Concud fault (S_{mf} =1.24; Lafuente *et al.*, 2011b), and to those calculated by Perea (2006) for twenty fault-generated mountain fronts at the Maestrat grabens, eastern Iberian Chain (S_{mf} = 1.04-1.60; mean = 1.27). They also resemble those obtained at well-known active faults of the

Betic Chains (SE Spain), such as the Carboneras, Lorca-Alhama or Baza faults, in which S_{mf} usually ranges from 1.05 to 1.4 (Silva *et al.*, 2003; García-Tortosa *et al.*, 2008).

The average value of the V_f index computed at a distance of 250 m upstream from the Sierra Palomera fault trace (V_f = 0.22) does not differ very much from that of the Concud fault (V_f = 0.30; Lafuente *et al.*, 2011b), while higher and more variable values have been reported in the Maestrat grabens (V_f = 0.12-1.5; Perea, 2006), and Betic Chains: Baza fault (V_f = 0.28-0.86; García-Tortosa *et al.*, 2008); Carboneras and Lorca-Alhama faults (0.38 to 0.59; Silva *et al.*, 2003).

Plotting S_{mf} *vs.* V_f values on the diagram proposed by Silva *et al.* (2003) allows us assessing the relative position of the Sierra Palomera fault among extensional fault-generated mountain fronts of eastern Spain (Fig. 14). The relatively low values of both S_{mf} and V_f indices found at the Sierra Palomera mountain front (1.27 and 0.22, respectively) represent a morphotectonic signal similar to that of the Concud fault, and also consistent with extensional faults studied by Silva *et al.* (2003) in the Valencia area and Betic Chains, which draw the tendency curve plotted in Fig. 14. The position of our geomorphic indices on that diagram: (i) demonstrates that the Sierra Palomera fault fits the same tendency, and (ii) corroborates that it lies within Class 1 (active).

8.4. Pleistocene fault activity and paleoseismological relevance

Although morphotectonic data indicate that the Sierra Palomera fault has a significant degree of activity, no outcrop observation on the main trace has unequivocally evidenced its Quaternary activity. Therefore, it is very relevant the finding, in La Sima trench, of Pleistocene faults that accommodate extensional deformation associated to the hanging-wall rollover, since they indirectly confirm, for the first time, Pleistocene activity of the main fault.

As explained in section 6.4, seven deformation events (T to Z) have been recognized after detailed trench analysis, which could be conventionally considered as paleoseismic events according to usual criteria in Paleoseismology. Individual faults activated in each event have been recognized; their displacements have been quantified (individual net slip in the range of 5 to 125 cm; mean = 28 cm; Table 2), and the overall faulting history has been carefully reconstructed by means of retrodeformational analysis (Fig. 12). Nevertheless, we should critically admit that the meaning of these results in relation to paleoseismicity of the Sierra Palomera fault is very imprecise, since:

(i) Instead of crossing the main fault, the trench only represents a short transect within the hanging-wall block, at a distance of 1.0 km from the Sierra Palomera fault trace.

(ii) During each event, faults widely distributed along the surveyed transect underwent both synthetic slip with Sierra Palomera fault (downthrown block to the west; positive values in Table 2) and antithetic slip (negative). The algebraic sum of those values has no meaning in relation to the real slip on the main fault.

(iii) The poor quality of OSL results precludes us from having an age model of the exposed sedimentary succession; therefore, the age constraints of the individual events are very limited. Only the last two events, Y and Z, could be dated to ca. 97±10 ka and 49±5 ka, respectively.

Concerning net slip accumulated by faults (see Table 2): (i) the first two events (T and U) involve significant synthetic slip (+45 and +110 cm, respectively); (ii) for V and W, synthetic and antithetic movements almost counterbalanced each other; (iii) the last three events (X, Y, Z) involve significant antithetic slip (−90, −40 and −125 cm, respectively). The cumulative global fault slip, −110 cm, considering an average fault dip of 65º, represents an antithetic throw of ca. 100 cm. We should add the vertical offset accommodated as continuous deformation in the bending monocline (amplitude: ca. 120 cm), not included when computing fault slip *s.s.* The total tectonic, antithetic throw at the transect should be therefore estimated at 220 cm (net slip ≈ 230 cm). This value reasonably approaches the total throw (190 cm) that can be directly measured from offset of the top of unit 6 (youngest sedimentary marker previous to the recorded faulting episodes). It is also consistent with the apparent height of the gentle uphill-facing scarplet that breaks the natural slope of La Sima alluvial fan (260 cm; Fig. 10c). In summary, the morphological expression of the fault zone exposed in the trench fits well the antithetic sign of the displacements during the most recent faulting episodes.

The youngest, antithetic faulting events have associated net slip values (40 to 125 cm) that should be accommodated on faults several km long (11 to 23 km, according to the empirical relationships proposed by Wells and Coppersmith, 1994). This inference plays in favour of: (i) the interpretation of the antithetic fault exposed at La Sima trench as a large structure, comparable in length to the Sierra Palomera fault itself, as the macrostructural and geophysical data suggested (see section 7.1); (ii) the notion that faulting events recorded at the trench, in particular those dated to ca. 97±10 ka and 49±5 ka, very probably respond to coseismic slip events on the main fault.

Could the timing of those younger events be taken as a reference for approaching seismic recurrence periods and slip rates of the Sierra Palomera fault during Pleistocene times? This is a very difficult question to answer from the available information. The tempting hypothesis that the two aforementioned ages correspond to the last two major paleoearthquakes would suggest a single interseismic period of around 48 ka. According to the empirical relationship by Villamor and Berryman (1999), such a recurrence period is reliable for faults moving at an average slip rate around 0.1 mm/a; therefore, it fits well the long-term slip rate estimated for the Sierra Palomera fault (in the range of 0.09 to 0.15 mm/a).

Nevertheless, we do not consider this as the most reliable scenario. The space and time window examined in our trench is too narrow for providing a representative paleoseismological record. Subsidiary faults similar to those exposed at La Sima could have form at other sites within the hanging-wall block in response to other slip events on the Sierra Palomera fault. Furthermore, each slip event on this main fault did not necessarily reactivate the antithetical fault exposed at La Sima trench. Accordingly, the actual slip rate on the main fault during Late Pleistocene times could be significantly higher than the long-term one, as evinced in other active faults of the region. Slip rate increased during Late Pleistocene times with respect to its average value since Late Pliocene times in the most documented structures south of Sierra Palomera: the Concud fault (0.29 *vs*. 0.07-0.08 mm/a) and Teruel fault (0.19 *vs*. 0.07 mm/a) (Lafuente *et al*., 2014; Simón *et al*., 2016, 2017). The same tendency has been revealed for other large faults of the neighbouring Teruel basin (Ezquerro *et al*., 2020; see Section 2) and Calatayud basin (Peiro and Simón, 2021). We therefore consider that the Sierra Palomera fault, larger than the Concud and Teruel faults, very probably underwent a slip rate higher than 0.09-0.15 mm/a, and an average recurrence period shorter than 48 ka, since Late Pleistocene time.

With this respect, the estimation of short-term slip rate that can be made for the antithetic La Peñuela fault from offset of Unit 9 in the studied trench is irrelevant. The top of that unit is dated to 97.4 ± 10.2 ka, and has been displaced by the last two deformation events defined (Y and Z), totalizing a cumulative antithetic net slip of 165 cm. This results in a slip rate of 0.015-0.019 mm/a, which only reflects the local deformation rate on a subsidiary fault for a very narrow, non-representative time window.

8.5. Internal deformation of the hanging-wall fault block: a close look from trench analysis

Although the succession of deformation events identified at La Sima trench have a very limited paleoseismic meaning, it allows understanding progressive stretching within the hanging-wall block of the Sierra Palomera fault. In particular, sequential activation of synthetic and antithetic individual faults has been carefully reconstructed by means of retrodeformation analysis (Fig. 12) and can be precisely compared with faulting patterns observed in published analogue models and field examples of rollover deformation.

Usually, the hanging-wall rollover geometry is not entirely achieved through continuous deformation. Examples from analogue models (*e.g.*, Withjack and Schlische, 2006), outcrops and high-resolution seismic profiles (*e.g.*, Song and Cawood, 2001; Delogkos *et al.*, 2020) indicate that a portion of the hanging-wall deformation is accommodated by smaller-scale faults. Antithetic faults directly materialize the antithetic simple shear band that nucleates at the transition zone from the main ramp to the basal detachment (Withjack *et al.*, 1995). Therefore, they occur above, and frequently abutting, the connection line between the steep and flat segments of the main fault surface (Bruce, 1973; Song and Cawood, 2001; Withjack and Schlische, 2006). In addition, together with subsidiary synthetic faults, they can accommodate layer-parallel extension along the rollover. Such extension mainly operates at the hinge zone of the rollover, giving rise to crestal collapse grabens that are well documented from both analogue models (*e.g.*, McClay, 1990; McClay and Scott, 1991; Buchanan and McClay, 1991; Soto *et al.*, 2007) and field examples (*e.g.*, Imber *et al.*, 2003; Fazlikhani *et al.*, 2017).

The locus of active hanging-wall antithetic faulting, as well as that of crestal graben formation, have the appearance of having migrated landwards during development of extensional systems. Each individual antithetic fault (or fault fan) forms near the fault bend, moves passively within the hanging-wall block beyond the fault bend, and becomes inactive, while a new fault zone propagating from the same fault bend replaces it. Thus, secondary faults tend to be progressively older basinwards (Christiansen, 1983; McClay, 1990; Withjack *et al.*, 1995; Withjack and Schlische, 2006). That tendency can be enhanced by repeated footwall collapse (footwall faulting sequence) at the main structure (Imber *et al.*, 2003).

In any case, such overall time polarity of hanging-wall growth faults does not exclude significant overlap in their periods of activity (Imber *et al.*, 2003), as well as variations in the relative occurrence of synthetic and antithetic faults. The great majority of analogue models of rollovers show a faulting sequence that begins with an antithetic fault, then alternating synthetic and antithetic ones eventually joining and reciprocally offsetting at depth (McClay, 1990; McClay *et al.*, 1991; T. Román-Berdiel, personal communication). Nevertheless, sandbox experiments have been reported in which alternating activation of synthetic and antithetic faults is initiated with a synthetic one (*e.g.*, Buchanan and McClay, 1991).

The fault sequence interpreted at La Sima trench share some of the former evolutionary patterns typical of rollover deformation: (i) relevance and persistence of a subsidiary antithetic fault; (ii) activation of additional, younger antithetic ruptures closer to the main fault; (iii) overall alternating onset of synthetic and antithetic ruptures. On the other hand, we have found a non-typical feature: the oldest recorded meso-scale faults are synthetic with the Sierra Palomera fault, despite having formed in the same area where the persistent antithetic fault will later appear. The first two deformational events (T and U) involve accumulation of significant synthetic slip (+155 cm), while in the following two (V and W) synthetic and antithetic movements almost counterbalanced each other, and the last three ones (X, Y, Z) involve substantial antithetic slip (−255 cm). Such "irregularity" suggests the existence of other controls on the hanging-wall deformation in addition to the rollover kinematics itself.

On the other hand, the accumulated net slip has an associated component of horizontal extension that enables another quantitative kinematical approach (see Table 2). The total extension recorded at La Sima trench is ≈385 cm, which represents about 20% of the total logged transect (local β factor = 1.2). The antithetic faults accommodate much more extension (200 cm) than the synthetic ones (115 cm). Considering that the bending monocline represents additional antithetic offset, it also involves additional horizontal extension, which can be estimated at 70 cm assuming a fault dip of 65º. Two main events (W, equally represented by synthetic and antithetic faults, and Z, mostly antithetic) accumulate about one half of the total extension (85 cm, ca. 4.5%, each one).

8.6. Stress regime and tectonic framework

Geometry and kinematics of faults exposed in the trench, as well as of those inferred at a macrostructural scale from surface mapping and geophysical exploration, overall fits the expected deformation within the hanging-wall block of the Sierra Palomera fault. ~~But, at the same time,~~ it is also consistent with the regional extensional stress field, whose σ_3 trajectories trend ENE-WSW (Simón, 1982, 1989; Arlegui *et al.*, 2005, 2006; Liesa *et al.*, 2019), orthogonal to the overall trend of the Jiloca graben, and only slightly oblique to the Sierra Palomera fault trace itself. Stress inversion from the most representative, non-rotated conjugate faults measured within the trench, according to Anderson's model, provides local stress axes matching those regional trajectories (Fig. 15).

[PREFERENTIALLY, FIG.15 SHOULD BE INSERTED HERE, AS A 1-COLUMN FIGURE]

It is not easy to discriminate whether the faults propagated through the hanging-wall block are kinematically or dynamically controlled, *i.e.*, they essentially accommodate extensional deformation associated to the rollover monocline, or they are directly linked to regional stress conditions. The extension direction expectable for the first scenario could be constrained between N065ºE (orthogonal to the average strike of the Sierra Palomera fault; an inherited feature indeed) and N050ºE (transport direction). The extension trend expectable for the second scenario would approach N075ºE (seeing at the average trend of the Jiloca graben), or would range from N055ºE to N080ºE (seeing at paleostress results reported by Arlegui *et al.*, 2005, and Liesa *et al.*, 2019). The similarity between both inferences prevents us from discriminating among those hypothetical controls based solely on the orientation of structures (stereoplots of Fig. 11 show how the strongly clustered directions of normal faults in La Sima trench fit equally well the two scenarios). Nevertheless, some details of the faulting succession suggest that both controls probably coexist. The kinematical control has been attested and discussed in sections 8.1 and 8.5. The dynamical one could explain the early occurrence of synthetic meso-scale fault at La Sima site.

Additionally, the imprint of the regional stress field is revealed by certain fracture features directly linked to characteristic heterogeneities of the extensional Plio-Quaternary stress field in the eastern Iberian Chain. First, under the biaxial or multidirectional extension regime characterizing such stress field, a strong tendency for the σ_2 and σ_3 axes to switch typically results in secondary faults striking at right angles to the master faults (Simón *et al.*, 1988; Simón, 1989; Arlegui *et al*. 2005, 2006). Second, both E-W to ESE-WNW, and ENE-WSW extension directions (characterizing the Late Miocene-Early Pliocene and the Plio-Quaternary rift episodes, respectively) are recorded during the entire extensional period indeed (Liesa *et al.*, 2019), suggesting stress partitioning (in the sense of Simón *et al.*, 2008) of the composite extensional field that results from combination of intraplate NNW-SSE compression (Africa-Iberia convergence) and WNW-ESE extension (rifting of the Valencia trough) (Simón, 1989; Herraiz *et al.*, 2000; Capote *et al.*, 2002). Fractures observed at La Sima trench only reveal the second type of stress heterogeneity. There is no orthogonal fault or fracture, and hence no evidence of permutation of σ_2 and σ_3 axes. Nevertheless, a minority NNE-SSW trending set can be distinguished among fractures that do not show any sign of displacement (Fig. 11e), which records the WNW-ESE extensional component of the regional, locally and episodically partitioned stress field.

9. Conclusions

1) The NNW-SSE trending, 26 km long Sierra Palomera extensional fault probably resulted from negative inversion of a previous contractive structure developed under the

Paleogene-Early Miocene compression of the Iberian Chain.

2) The Sierra Palomera extensional fault has been active during Late Pliocene-Quaternary times. In has undergone nearly pure normal movement with mean transport direction towards N230ºE, consistent with the ENE-WSW extension trajectories of the recent to present-day regional stress field.

3) Magnetic and electromagnetic profiles, together with local geological and geomorphological evidence, suggest that the hanging-wall block of the Sierra Palomera fault is cut by two subsidiary parallel ruptures: (i) the synthetic Las Vallejadas fault, located at about 1.5 km basinwards, and (ii) the antithetic La Peñuela fault, at a distance of 0.7-1.0 km, which apparently offsets the surface of the La Sima alluvial fan giving rise to a gentle uphill-facing scarplet.

4) In the absence of recent stratigraphic markers visible in the both fault blocks, the *FES2* planation surface (3.8 Ma) has constituted a useful marker for estimating the extensional net slip on the main fault. The corresponding contour map has allowed calculating a maximum value of 330 m for the fault throw *s.s.*, and 480 m for the total tectonic offset at the graben margin (including the bending component). Assuming an average dip of 70º for the fault plane and a pure normal movement, a net slip rate of 0.09 mm/a is inferred (0.13 mm/a including bending). Based on the natural unevenness of the *FES2* marker, the error bar for the calculated throws and net slip values is ±40 m, which results in errors for slip rates around 0.01 mm/a.

5) The Sierra Palomera fault is expressed in the landscape by a conspicuous fault mountain front. Qualitative geomorphological features (trapezoidal facets; V-shaped gullies; small, steep alluvial fans not fully connected to the axial drainage), as well as values of geomorphic indices, are consistent with a significant degree of recent fault activity.

6) Trench study has demonstrated the existence of the above-mentioned antithetic subsidiary fault, accompanied by a number of minor synthetic and antithetic ones. Their detailed kinematical analysis has allowed building an evolutionary model made of seven deformation events recorded in Middle-Late Pleistocene alluvial deposits. Net slip on individual faults ranges from 5 to 125 cm (mean = 28 cm). The cumulative global throw at the antithetic fault zone, including fault slip *s.s.* and bending, is estimated at 220 cm, which reasonably approaches the apparent offset of the natural slope of La Sima alluvial fan at the uphill-facing scarplet (260 cm).

7) Unfortunately, it was not feasible to achieve a consistent age model for the entire

sedimentary sequence, since the majority of samples dated by Optically Stimulated Luminiscence (OSL) presented signal saturation. Only the last two deformation events have been dated to ca. 97±10 ka and 49±5 ka, respectively. In addition, the surveyed trench only represents a short transect within the hanging-wall block, not across the main fault itself, so that its paleoseismic significance is limited. Nevertheless, it is worth highlighting the fact that, for the first time, Pleistocene activity of the Sierra Palomera fault has been unequivocally (although indirectly) proved from outcrop observation.

8) Despite its poor paleoseismic meaning, the succession of faulting events identified at La Sima allows unravelling the extensional deformation mechanisms within the hanging-wall block of the Sierra Palomera fault. The total horizontal extension recorded at La Sima trench is ≈385 cm (local β factor = 1.2). The evolutionary model built from retrodeformation analysis indicates that synthetic slip prevailing in early deformation events was gradually substituted by antithetic slip, the latter being clearly predominant during the younger ones. Geometry and sequential development of meso-scale faults suggest the concurrence of: (1) a kinematic control, *i.e.*, antithetic simple shear linked to rollover kinematics (mostly resulting in the main antithetic fault zone), eventually accompanied by layer-parallel extension orthogonal to the rollover axis, and (2) a dynamic control, *i.e.*, response to the regional stress field.

Acknowledgments

The research has been financed by projects LMP127_18 (Gobierno de Aragón-Programa Operativo del Fondo Europeo de Desarrollo Regional Aragón 2014-2020), and PID2019-108705-GB-I00 of the Spanish Government (Ministerio de Ciencia e Innovación). This work is a contribution of the Geotransfer Research Group (E32_20R) funded by Gobierno de Aragón. A. Peiro benefits from an FPU contract (FPU17/02470) of the Spanish Government. We thank G. Brook, Luminiscence Dating Laboratory of University of Georgia (US), and P. Beneítez, Laboratorio de Datación y Radioquímica of the Universidad Autónoma de Madrid (Spain), for OSL dating. A. Medialdea advised us on issues related to OSL dating, and T. Román-Berdiel helped us comparing the results with analogue models.

References

Alcalá, L., Alonso-Zarza, A.M., Álvarez, M.A., Azanza, B., Calvo, J.P., Cañaveras, J. C., van Dam, J.A., Garcés, M., Krijgsman, W., van der Meulen, A.J., Morales, J., Peláez, P., Pérez-González, A., Sánchez, S., Sancho, R., Sanz, E., 2000. El registro sedimentario y faunístico de las cuencas de Calatayud-Daroca y Teruel. Evolución paleoambiental y paleoclimática durante el Neógeno. Revista Sociedad Geológica España. 13, 323-343.

Allmendinger, R.W., Cardozo, N., Fisher, D., 2012. Structural geology algorithms: Vectors and tensors in structural geology. Cambridge University Press.

Álvaro, M., Capote, R., Vegas, R., 1979. Un modelo de evolución geotectónica para la Cadena Celtibérica. Acta Geológica Hispánica. 14, 172-177.

Anadón, P., Moissenet, E., 1996. Neogene basins in the Eastern Iberian Range, in: Friend, P.F., Dabrio, C.F. (Eds.), Tertiary basins of Spain. The stratigraphic Record of Crustal kinematics. World and Regional Geology series 6, Cambridge University press, Cambridge, pp. 68-76.

Anderson, E.M., 1951. The dynamics of faulting and dyke formation with application to Britain. Oliver & Boyd, Edinburgh.

Arlegui, L.E., Simón, J.L., Lisle, R.J., Orife, T., 2005. Late Pliocene-Pleistocene stress field in the Teruel and Jiloca grabens (eastern Spain): contribution of a new method of stress inversion. Journal of Structural Geology. 27, 693-705. https://doi.org/10.1016/j.jsg.2004.10.013.

Arlegui, L.E., Simón, J.L., Lisle, R.J., Orife, T., 2006. Analysis of non-striated faults in a recent extensional setting: the Plio-Pleistocene Concud fault (Jiloca graben, eastern Spain). Journal of Structural Geology. 28, 1019-1027. https://doi.org/10.1016/j.jsg.2006.03.009.

Bruce, C.H., 1973, Pressured shale and related sediment deformation: mechanism for development of regional contemporaneous faults. AAPG Bulletin. 57, 878-886. https://doi.org/10.1306/819A4352-16C5-11D7-8645000102C1865D.

Buchanan, P.G., McClay, K.R., 1991. Sandbox experiments of inverted listric and planar fault systems. Tectonophysics. 188, 97-115. https://doi.org/10.1016/0040-1951(91)90317-L.

Bull, W.B., McFadden, L.D., 1977. Tectonic Geomorphology north and south of the Garlock fault California, in: Doehring, D.O. (Ed.), Geomorphology in arid regions. Allen & Unwin, London, pp. 115-138.

Burbank, D.W., Anderson, R.S., 2012. Tectonic Geomorphology. Wiley-Blackwell, Oxford.

Capote, R., Gutiérrez, M., Hernández, A., Olivé A., 1981. Movimientos recientes de la fosa del Jiloca (Cordillera Ibérica). Proceedings V Reunión del Grupo Español de Trabajo del Cuaternario, Sevilla, pp. 245-257.

Capote, R., Muñoz, J.A., Simón, J.L., Liesa, C.L., Arlegui, L.E., 2002. Alpine tectonics I: The Alpine system north of the Betic Cordillera, in: Gibbons, W., Moreno, T., (Eds.), Geology of Spain. The Geological Society, London, pp. 367-400.

Cardozo, N., Allmendinger, R.W., 2013. Spherical projections with OSXStereonet: Computers & Geosciences. 51, 193-205, https://doi.org/10.1016/j.cageo.2012.07.021.

Casas-Sainz, A.M., Gil-Imaz, A., Simón, J.L., Izquierdo-Llavall, E., Aldega, L., Román-Berdiel, T., Osácar, M.C., Pueyo-Anchuela, Ó., Ansón, M., García-Lasanta, C., Corrado, S., Invernicci, C., Caricchi, C., 2018. Strain indicators and magnetic fabric in intraplate fault zones: Case study of Daroca thrust, Iberian Chain, Spain. Tectonophysics. 730, 29-47. https://doi.org/10.1016/j.tecto.2018.02.013.

Christiansen, A.F., 1983. An example of a major syndepositional listric fault, in: Bally, A.W. (Ed.), Seismic expression of structural styles. AAPG Studies in Geology. 15 (2.3.1), 36-40.

Colomer, M., 1987. Estudi geològic de la vora sud-oest de la Fossa de Calataiud-Daroca, entre Villafeliche i Calamocha. BSc thesis, Univ. Barcelona.

Colomer, M., Santanach, P., 1988. Estructura y evolución del borde sur-occidental de la Fosa de Calatayud-Daroca. Geogaceta. 4, 29-31.

Cortés, A.L., Casas, A.M., 2000. ¿Tiene el sistema de fosas de Teruel origen extensional? Revista de la Sociedad Geológica de España. 13(3-4), 445-470.

Cortés, A.L., 1999. Evolución tectónica reciente de la Cordillera Ibérica, Cuenca del Ebro y Pirineo centro-occidental. Unpublished PhD thesis. Univ. Zaragoza.

Cowie, P., Roberts, G.P., 2001. Constraining slip rates and spacings for active normal faults. Journal of Structural Geology. 23, 1901-1915. https://doi.org/10.1016/S0191-8141(01)00036-0.

Delogkos, E., Saqab, M.M., Walsh, J.J., Roche, V., Childs, C., 2020. Throw variations and strain partitioning associated with fault-bend folding along normal faults. Solid Earth. 11, 935-945. https://doi.org/10.5194/se-11-935-2020.

Ezquerro, L., 2017. El sector norte de la cuenca neógena de Teruel: tectónica, clima y sedimentación. PhD thesis, Univ. Zaragoza, http://zaguan.unizar.es/record/77098#

Ezquerro, L., Simón, J.L., Luzón, A., Liesa, C.L., 2019. Alluvial sedimentation and tectono-stratigraphic evolution in a narrow extensional zigzag basin margin (northern Teruel Basin, Spain). Journal of Palaeogeography, *8*, 1-25. https://doi.org/10.1186/s42501-019-0044-4

Ezquerro, L., Simón, J.L., Luzón, A., Liesa, C.L., 2020. Segmentation and increasing activity in the Neogene-Quaternary Teruel Basin rift (Spain) revealed by morphotectonic approach. Journal of Structural Geology. 135, 104043. https://doi.org/10.1016/j.jsg-2020.104403.

Fazlikhani, H., Back, S., Kukla, P. A., Fossen, H., 2017. Interaction between gravity-driven listric normal fault linkage and their hanging-wall rollover development: a case study from the western Niger Delta, Nigeria. Geological Society. London, Special Publications. 439(1), 169-186. https://doi.org/10.1144/SP439.20.

Fossen, H., Rotevatn, A., 2016. Fault linkage and relay structures in extensional settings-A review. Earth-Science Reviews. 154, 14-28. https://doi.org/10.1016/j.earscirev.2015.11.014.

García-Lacosta, A.I., 2013. La falla de Sierra Palomera: evolución estructural y actividad reciente. Unpublished MSc thesis, Univ. Zaragoza.

García-Tortosa, F.J., Sanz de Galdeano, C., Sánchez-Gómez, M., Alfaro, P., 2008. Geomorphologic evidence of the active Baza Fault (Betic Cordillera, South Spain), Geomorphology. 97, 374-391. https://doi.org/10.1016/j.geomorph.2007.08.007.

Gracia, J., 1992. Tectónica pliocena de la Fosa de Daroca (prov. de Zaragoza). Geogaceta, 11, 127-129.

Gracia, F.J., Gutiérrez, F., Gutiérrez, M., 2003. The Jiloca karst polje-tectonic graben (Iberian Range, NE Spain). Geomorphology. 52, 215-231. https://doi.org/10.1016/S0169-555X(02)00257-X.

Gracia, F.J., Gutiérrez, F., Gutiérrez, M., Rubio, J.C., Simón, J.L., 2008. Discussion of ‘Tectonic subsidence vs erosional lowering in a controversial intramontane depression: the Jiloca basin (Iberian Chain, Spain)’. Geological Magazine. 145, 591-597.

Granier, T., 1985. Origin, damping, and pattern of development of faults in granite. Tectonics. 4, 721-737. https://doi.org/10.1029/TC004i007p00721.

Guimerà, J., Alvaro, M., 1990. Structure et evolution de la compression alpine dans la Chaine Cotiere Catalane (Espagne). Bulletin Société Géologique France. 8, 339-348. https://doi.org/10.2113/gssgfbull.VI.2.339.

Gutiérrez, M., Gracia, F.J., 1997. Environmental interpretation and evolution of the Tertiary erosion surfaces in the lberian Range (Spain), in: Widdowson, M. (Ed.), Palaeosurfaces: Recognition, Reconstruction and Palaeoenvironmental Interpretation. Geological Society. London, Special Publications. 120, 147-158.

Gutiérrez, M., Peña, J.L., 1976. Glacis y terrazas en el curso medio del río Alfambra (provincia de Teruel). Boletín Geológico y Minero. 87, 561-570.

Gutiérrez, F., Gutiérrez, M., Gracia, F.J., McCalpin, J.P., Lucha, P., Guerrero, J., 2008. Plio-Quaternary extensional seismotectonics and drainage network development in the central sector of the Iberian Range (NE Spain). Geomorphology. 102, 21-42. https://doi.org/10.1016/j.geomorph.2007.07.020.

Gutiérrez, F., Masana, E., González, Á., Lucha, P., Guerrero, J., McCalpin, J.P., 2009. Late Quaternary paleoseismic evidence on the Munébrega half-graben fault (Iberian Range, Spain). International Journal of Earth Sciences. 98, 1691-1703. https://doi.org/10.1007/s00531-008-0319-y.

Gutiérrez, F., Gracia, F.J., Gutiérrez, M., Lucha, P., Guerrero, J., Carbonel, D., Galve, J.P., 2012. A review on Quaternary tectonic and nontectonic faults in the central sector of the Iberian Chain, NE Spain. Journal of Iberian Geology. 38, 145-160. https://doi.org/10.5209/rev_JIGE.2012.v38.n1.39210.

Gutiérrez, F., Carbonel, D., Sevil, J., Moreno, D., Linares, R., Comas, X., Zarroca, M., Roqué, C., McCalpin, J.P., 2020. Neotectonics and late Holocene paleoseismic evidence in the Plio-Quaternary Daroca Half-graben, Iberian Chain, NE Spain. Implications for fault source characterization. Journal of Structural Geology. 131, 103933. https://doi.org/10.1016/j.jsg.2019.103933.

Herraiz, M., De Vicente, G., Lindo, R., Giner, J., Simón, J.L., González, J.M., Vadillo, O., Rodríguez, M.A., Cicuéndez, J.I., Casas, A., Rincón, P., Cortés, A.L., Lucini, M., 2000. The recent (Upper Miocene to Quaternary) and present tectonics stress distributions in the Iberian Peninsula. Tectonics. 19, 762-786. https://doi.org/10.1029/2000TC900006.

Imber, J., Childs, C., Nell, P.A.R., Walsh, J.J., Hodgetts, D., Flint, S., 2003. Hanging wall fault kinematics and footwall collapse in listric growth fault systems. Journal of Structural Geology. 25(2), 197-208. https://doi.org/10.1016/S0191-8141(02)00034-2.

Lafuente, P., 2011. Tectónica activa y paleosismicidad de la falla de Concud (Cordillera Ibérica central). Unpublished PhD thesis, Univ. Zaragoza.

Lafuente, P., Arlegui, L.E., Liesa, C.L., Simón, J.L., 2011a. Paleoseismological analysis of an intraplate extensional structure: the Concud fault (Iberian Chain, Eastern Spain). International Journal of Earth Sciences. 100, 1713-1732. https://doi.org/10.1007/s00531-010-0542-1.

Lafuente, P., Lamelas, T., Simón, J.L., Soriano, M.A., 2011b. Comparing geomorphic and geologic indices of activity in an intraplate extensional structure: the Concud fault (central Iberian Chain, Spain). Geodinamica Acta. 24, 107-122. https://doi.org/10.1007/S00531-010-0542-1.

Lafuente, P., Arlegui, L.E., Liesa, C.L., Pueyo, O., Simón, J.L., 2014. Spatial and temporal variation of paleoseismic activity at an intraplate, historically quiescent structure: the Concud fault (Iberian Chain, Spain). Tectonophysics. 632, 167-187. https://doi.org/10.1016/j.tecto.2014.06.012.

Liesa, C.L. 2011. Evolución de campos de esfuerzos en la Sierra del Pobo (Cordillera Ibérica, España). Revista Sociedad Geológica España. 24, 49-68.

Liesa, C.L., Simón, J.L., Casas, A.M., 2018. La tectónica de inversión en una región intraplaca: La Cordillera Ibérica. Revista Sociedad Geológica España. 31, 23-50.

Liesa, C.L., Simon, J.L., Ezquerro, L., Arlegui, L.E., Luzón, A., 2019. Stress evolution and structural inheritance controlling an intracontinental extensional basin: The central-northern sector of the Neogene Teruel Basin. Journal of Structural Geology. 118, 362-376. https://doi.org/10.1016/j.jsg.2018.11.011.

Liesa, C.L., Corral, M.B., Arlegui, L.A., Peiro, A., Simón, J.L., 2021. Inversión tectónica negativa y estructuración de la zona de relevo entre las fallas normales plio-cuaternarias de Calamocha y Daroca. *X Congreso de Geología de España*, Sociedad Geológica de España, Vitoria, Spain.

Martín-Bello, L., Arlegui, L.E., Ezquerro, L., Liesa, C.L., Simón, J.L., 2014. La falla de Calamocha (fosa del Jiloca, Cordillera Ibérica): estructura y actividad pleistocena, in: Álvarez-Gomez, J.A., Martín González, F. (Eds.), Una aproximación multidisciplinar al estudio de las fallas activas, los terremotos y el riesgo sísmico. Segunda reunión ibérica sobre fallas activas y paleosismología, Lorca, (Murcia, España), pp. 55-85.

McCalpin, J.P., 1996. Paleoseismology. Academic Press, New York.

McClay, K.R., 1990. Extensional fault systems in sedimentary basins: a review of analogue model studies. Marine and Petroleum Geology. 7, 206-233. https://doi.org/10.1016/0264-8172(90)90001-W.

McClay, K.R., Scott, A.D., 1991. Experimental models of hangingwall deformation in ramp-flat listric extensional fault systems. Tectonophysics. 188, 85-96. https://doi.org/10.1016/0040-1951(91)90316-K.

McClay, K.R., Waltham, D.A., Scott, A.D., Abousetta, A., 1991. Physical and seismic modelling of listric normal fault geometries. Geological Society. London, Special Publications. 56, 231-239. https://doi.org/10.1144/GSL.SP.1991.056.01.16.

Moissenet, E., 1983. Aspectos de la Neotectónica en la fosa de Teruel, in: Comba, J.A. (Ed.), Geología de España. Libro Jubilar J.M. Ríos. 2, IGME, Madrid, pp. 427-446.

Pailhé, P., 1984. La Chaîne Ibérique Orientale. Étude géomorphologique, PhD thesis. Univ. Bordeaux.

Peacock, D.C.P., Sanderson, D.J., 1994. Geometry and development of relay ramps in normal fault systems. Bull. Am. Ass. Petrol. Geol. 78, 147-165. https://doi.org/10.1306/BDFF9046-1718-11D7-8645000102C1865D.

Peiro, A., Simón, J.L., 2021. The Río Grío-Pancrudo Fault Zone (central Iberian Chain, Spain): recent extensional activity revealed by drainage reversal. Geological Magazine. (in press).

Peiro, A., Simón, J.L., Román-Berdiel, T., 2019. Zonas de relevo de falla en el margen oriental de la fosa del Jiloca (Cordillera Ibérica): geometría, cinemática y modelización analógica. Boletín Geológico y Minero. 130 (3): 393-416. https://doi.org/10.21701/bolgeomin.130.3.002.

Peiro, A., Simón, J.L., Román-Berdiel, T., 2020. Fault relay zones evolving through distributed longitudinal fractures: the case of the Teruel graben system (Iberian Chain, Spain). Journal of Structural Geology. 131, 103942. https://doi.org/10.1016/j.jsg.2019.103942.

Peña, J.L., Gutiérrez, M., Ibáñez, M., Lozano, M.V., Rodríguez, J., Sánchez, M., Simón, J.L., Soriano, M.A., Yetano, L.M., 1984. Geomorfología de la provincia de Teruel. Instituto de Estudios Turolenses. Teruel.

Perea, H., 2006. Falles actives i perillositat sísmica al marge nord-occidental del solc de Valencia. Unpublished PhD thesis Univ. Barcelona.

Pueyo, Ó., Lafuente, P., Arlegui, L.E., Liesa, C.L., Simón, J.L., 2016. Geophysical characterization of buried active faults: the Concud Fault (Iberian Chain, NE Spain). International Journal of Earth Sciences. 105, 2221-2239. https:// doi.org/10.1007/s00531-015-1283-y.

Roca, E.; Guimerà, J., 1992. The Neogene structure of the eastern Iberian margin: structural constraints on the crustal evolution of the Valencia trough (western Mediterranean). Tectonophysics. 203, 203-218. https:// doi.org/10.1016/0040-1951(92)90224-T.

Rubio, J.C., 2004. Los humedales del Alto Jiloca: estudio hidrogeológico e histórico-arqueológico. Unpublished PhD thesis, Univ. Zaragoza.

Rubio, J.C., Simón, J.L., 2007. Tectonic subsidence vs. erosional lowering in a controversial intramontane depression: the Jiloca basin (Iberian Chain, Spain). Geological Magazine. 144, 1-15. https://doi.org/10.1017/S0016756806002949.

Rubio, J.C., Simón, J.L., Soriano, A., 2007. Interacting tectonics, hydrogeology and karst processes in an intramontane basin: the Jiloca graben (NE Spain). Hydrological Journal. 15, 1565-1576. https://doi.org/10.1007/s10040-007-0190-0.

Sánchez-Fabre, M., Peña-Monné, J.L., Sampietro-Vattuone, M.M., 2019. Geomorphology of the northern sector of the Alfambra-Teruel depression (Iberian ranges, NE Spain). Journal of Maps. 15, 112-121. https://doi.org/10.1080/17445647.2018.1551157.

Silva, P.G.; Goy, J.L.; Zazo, C., Bardají, T., 2003. Fault-generated mountain fronts in southeast Spain: geomorphologic assessment of tectonic and seismic activity. Geomorphology. 50, 203-225. https://doi.org/10.1016/S0169-555X(02)00215-5.

Simón, J.L., 1982. Compresión y distensión alpinas en la Cadena Ibérica oriental. PhD thesis. Universidad de Zaragoza, Instituto de Estudios Turolenses, Teruel.

Simón, J.L., 1983. Tectónica y neotectónica del sistema de fosas de Teruel. Teruel. 69, 21-97.

Simón, J.L., 1989. Late Cenozoic stress field and fracturing in the Iberian Chain and Ebro Basin (Spain). Journal of Structural Geology. 11, 285-294. https://doi.org/10.1016/0191-8141(89)90068-0.

Simón, J.L., Serón, F.J., Casas, A.M., 1988. Stress deflection and fracture development in a multidirectional extension regime. Mathematical and experimental approach with field examples. Annales Tectonicae. 2, 21-32.

Simón, J.L., Arlegui, L.E., Lafuente, P., Liesa, C.L., 2012. Active extensional faults in the central-eastern Iberian Chain, Spain. Journal of Iberian Geology. 38, 127-144. https://doi.org/10.5209/rev_JIGE.2012.v38.n1.39209.

Simón, J. L., Arlegui, L. E., Ezquerro, L., Lafuente, P., Liesa, C. L., Luzón, A., 2016. Enhanced palaeoseismic succession at the Concud Fault (Iberian Chain, Spain): new insights for seismic hazard assessment. Natural Hazards. 80, 1967-1993. https://doi.org/10.1007/s11069-015-2054-6.

Simón, J.L., Arlegui, L.E., Ezquerro, L., Lafuente, P., Liesa, C.L. Luzón, A. 2017. Assessing interaction of active extensional faults from structural and paleoseismological analysis: The Teruel and Concud faults (eastern Spain). Journal of Structural Geology. 103, 100-119. https://doi.org/10.1016/j.jsg.2017.08.003.

Simón, J.L., Ezquerro, L., Arlegui, L.E., Liesa, C.L., Luzón, A., Medialdea, A., García, A., Zarazaga, D., 2019. Role of transverse structures in paleoseismicity and drainage rearrangement in rift systems: the case of the Valdecebro fault zone (Teruel graben, eastern Spain). International Journal of Earth Sciences. 108, 1429-1449. https://doi.org/10.1007/s00531-019-01707-9.

Simón, J. L., Casas-Sainz, A. M., Gil-Imaz, A., 2021. Controversial epiglyptic thrust sheets: The case of the Daroca Thrust (Iberian Chain, Spain). Journal of Structural Geology. 145, 104298. https://doi.org/10.1016/j.jsg.2021.104298.

Simón-Porcar, G., Simón, J.L., Liesa, C.L., 2019. La cuenca neógena extensional de El Pobo (Teruel, Cordillera Ibérica): sedimentología, estructura y relación con la evolución del relieve. Revista Sociedad Geológica España. 32, 17-42.

Song, T., Cawood, P.A., 2001. Effects of subsidiary faults on the geometric construction of listric normal fault systems. AAPG Bulletin. 85(2), 221-232. https://doi.org/10.1306/8626C7A3-173B-11D7-8645000102C1865D.

Soto, R., Casas-Sainz, A. M., Del Río, P., 2007. Geometry of half-grabens containing a mid-level viscous décollement. Basin Research. 19(3), 437-450. https://doi.org/10.1111/j.1365-2117.2007.00328.x.

Vegas, R., Fontboté, J.M., Banda, E., 1979. Widespread neogene rifting superimposed on alpine regions of the Iberian Peninsula. Proceedings Symposium Evolution and Tectonics of the Western Mediterranean and Surrounding Areas, EGS, Viena. Instituto Geográfico Nacional, Madrid, Special Publication. 201, 109-128.

Villamor, P., Berryman, K.R., 1999. La tasa de desplazamiento de una falla como aproximación de primer orden en las estimaciones de peligrosidad sísmica. I Congreso Nacional de Ingeniería Sísmica, Asociación Española de Ingeniería Sísmica, Abstracts, 1.

Wells, D.L., Coppersmith, K.J., 1994. New Empirical Relationships among Magnitude, Rupture Length, Rupture Width, Rupture Area, and Surface Displacement. Bull. Seismol. Soc. Am. 84, 974-1002.

Withjack, M.O., Schlische, R.W., 2006. Geometric and experimental models of extensional fault-bend folds. Geological Society, London, Special Publications. 253(1), 285-305.

Withjack, M.O., Islam, Q.T., La Pointe, P.R., 1995. Normal faults and their hanging-wall deformation: An experimental study. AAPG Bulletin. 79, 1-18. https://doi.org/10.1144/GSL.SP.2006.253.01.15.

Young, M.J., Gawthorpe, R.L., Hardy, S., 2001. Growth and linkage of a segmented normal fault zone; the Late Jurassic Murchison-Statfjord North Fault, northern North Sea. Journal of Structural Geology. 23, 1933-1952. https://doi.org/10.1016/S0191-8141(01)00038-4.

The authors declare that they have no known competing financial interests or personal relationships that could have appeared to influence the work reported in this paper.

FIGURES AND FIGURE CAPTIONS:

Figure 1:

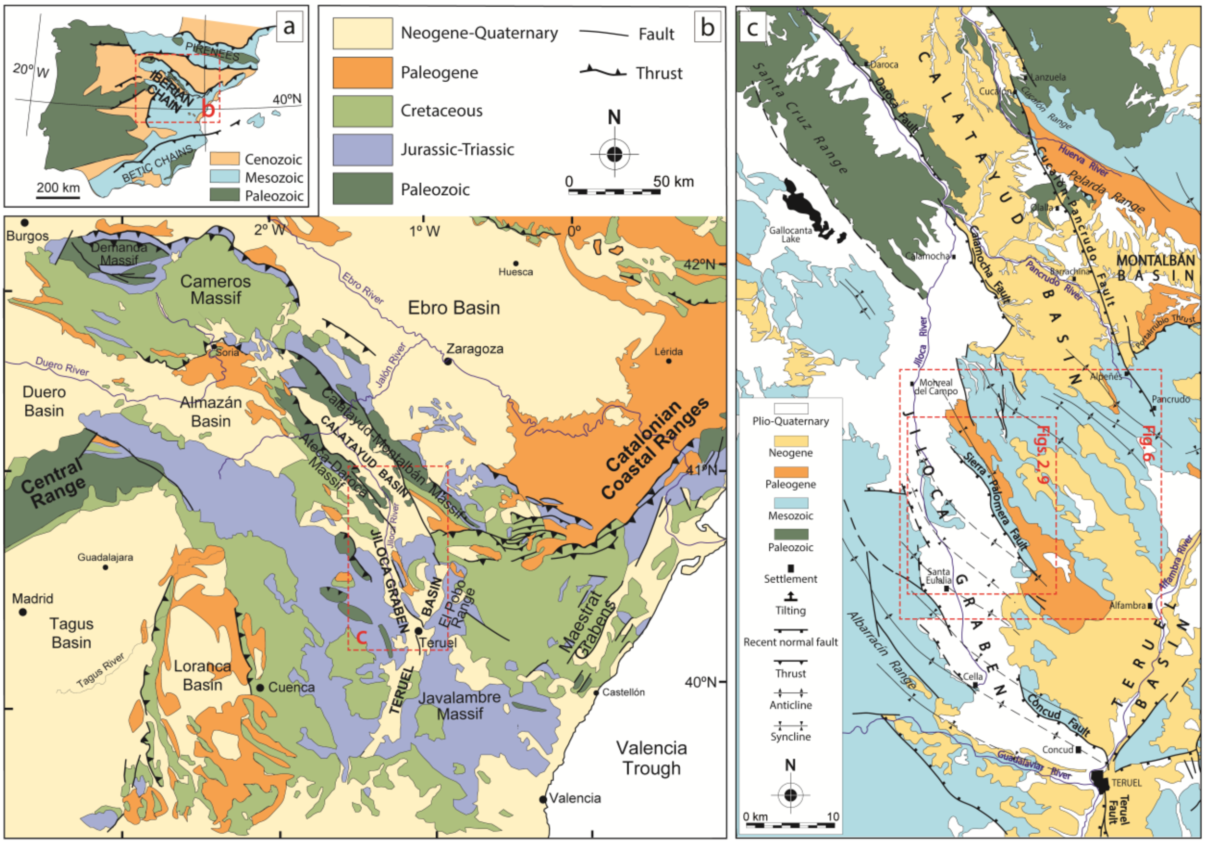

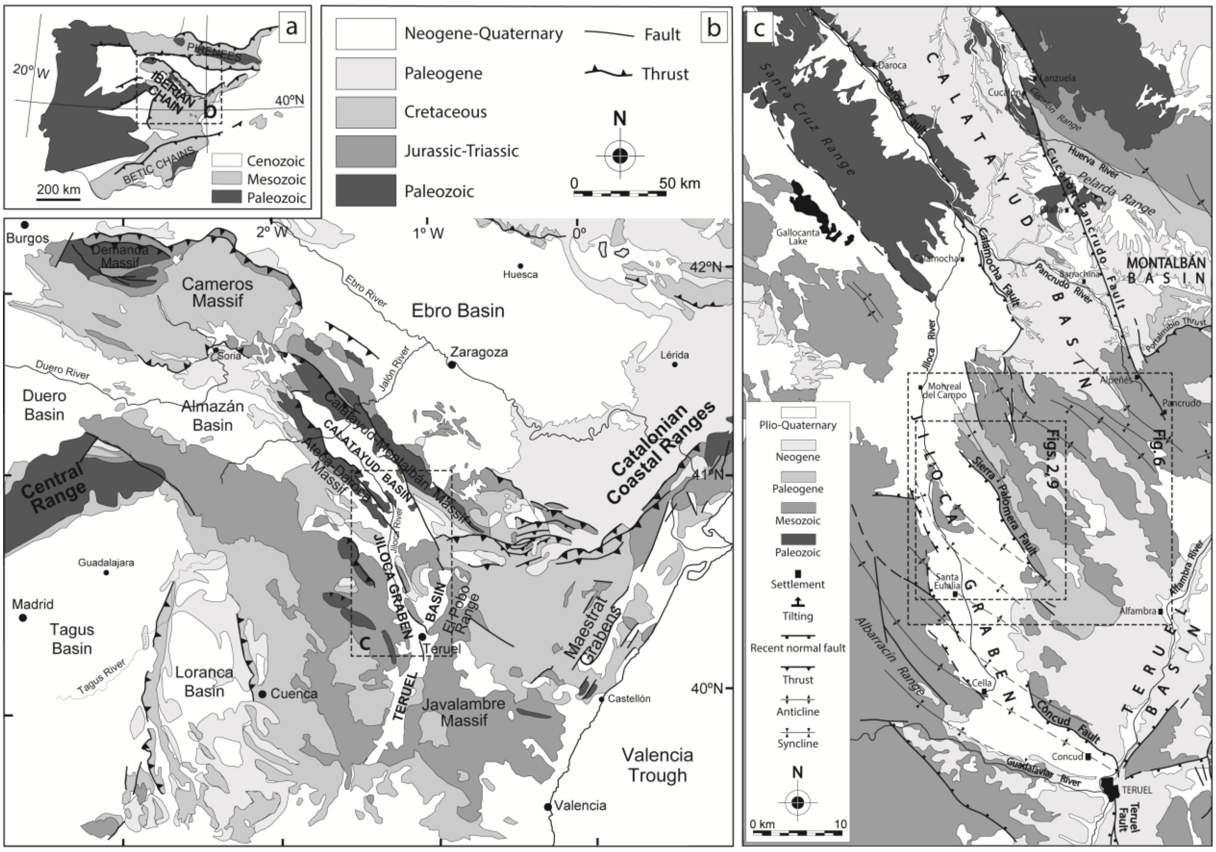
a
PIRENEES
IBERIAN CHAIN
BETIC CHAINS
20° W
40°N
200 km
Cenozoic
Mesozoic
Paleozoic
b
Neogene-Quaternary
Paleogene
Cretaceous
Jurassic-Triassic
Paleozoic
Fault
Thrust
N
0
50 km
2° W
1° W
0°
42°N
41°N
40°N
Burgos
Demanda Massif
Cameros Massif
Ebro River
Ebro Basin
Huesca
Zaragoza
Lérida
Soria
Duero River
Duero Basin
Almazán Basin
Jalón River
Calatayud-Montalbán Massif
CALATAYUD BASIN
Ateca-Daroca Massif
Jiloca River
JILOCA GRABEN
TERUEL BASIN
El Pobo Range
Catalonian Coastal Ranges
Central Range
Guadalajara
Madrid
Tagus Basin
Tagus River
Loranca Basin
Cuenca
Teruel
Javalambre Massif
Maestrat Grabens
Castellón
Valencia Trough
Valencia
c
Daroca
Santa Cruz Range
Gallocanta Lake
Calamocha
Calamocha Fault
CALATAYUD BASIN
Lanzuela
Huerva River
Pelarda Range
Pancrudo Fault
Pancrudo River
MONTALBÁN BASIN
Alpeñés
Pancrudo
Jiloca River
Monreal del Campo
Figs 2, 9
Fig. 6
Sierra Palomera Fault
JILOCA GRABEN
Santa Eulalia
Albarracín Range
Alfambra
Alfambra River
Cella
Concud Fault
Concud
Guadalaviar River
TERUEL
Teruel Fault
TERUEL BASIN
Plio-Quaternary
Neogene
Paleogene
Mesozoic
Paleozoic
Settlement
Tilting
Recent normal fault
Thrust
Anticline
Syncline
N
0 km
10

Figure 1:

(a) Location of the Iberian Chain within the Iberian Peninsula. (b) Geological sketch of the Iberian Chain, with location of the main Neogene-Quaternary extensional basins. (c) Simplified geological map of the Jiloca graben, with location of Figures 2, 6 and 9.

Figure 2:

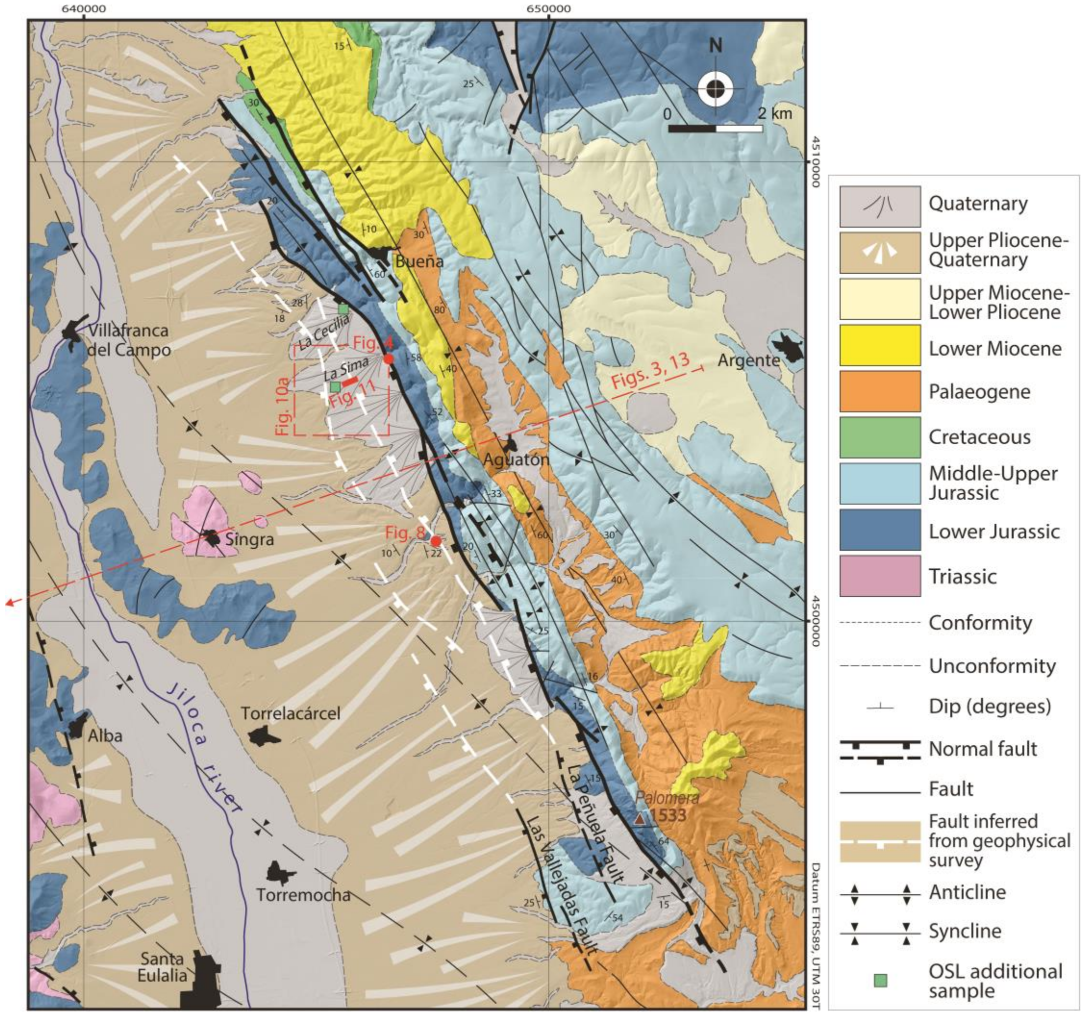

640000
650000
4510000
4500000
N
0
2 km
Datum ETRS89, UTM 30T
Bueña
Villafranca del Campo
La Cecilia
La Sima
Fig. 4
Fig. 10a
Fig. 11
Figs. 3, 13
Argente
Aguatón
Singra
Fig. 8
Torrelacárcel
Alba
Jiloca river
Torremocha
Santa Eulalia
La Peñuela Fault
Las Vallejadas Fault
Palomera
1533
Quaternary
Upper Pliocene-Quaternary
Upper Miocene-Lower Pliocene
Lower Miocene
Palaeogene
Cretaceous
Middle-Upper Jurassic
Lower Jurassic
Triassic
Conformity
Unconformity
Dip (degrees)
Normal fault
Fault
Fault inferred from geophysical survey
Anticline
Syncline
OSL additional sample


640000
650000
N
0
2 km
4510000
4500000
Datum ETRS89, UTM 30T
Bueña
Villafranca
del Campo
La Cecilia
Fig. 4
La Sima
Fig. 11
Fig. 10a
Figs. 3, 13
Argente
Aguatón
Singra
Fig. 8
Jiloca river
Torrelacárcel
Alba
Torremocha
Santa
Eulalia
La Peñuela Fault
Las Vallejadas Fault
Palomera
1533
Quaternary
Upper Pliocene-Quaternary
Upper Miocene-Lower Pliocene
Lower Miocene
Palaeogene
Cretaceous
Middle-Upper Jurassic
Lower Jurassic
Triassic
Conformity
Unconformity
Dip (degrees)
Normal fault
Fault
Fault inferred from geophysical survey
Anticline
Syncline
OSL additional sample

Figure 2:

Geological map of the Sierra Palomera area (on DEM image from Instituto Geográfico Nacional) showing the main structures associated to the Sierra Palomera fault. Location of Figures 3, 4, 8, 10a, 11 is indicated, as well as that of OSL samples in La Cecilia and La Sima alluvial fans (see Table 1).

Figure 3:

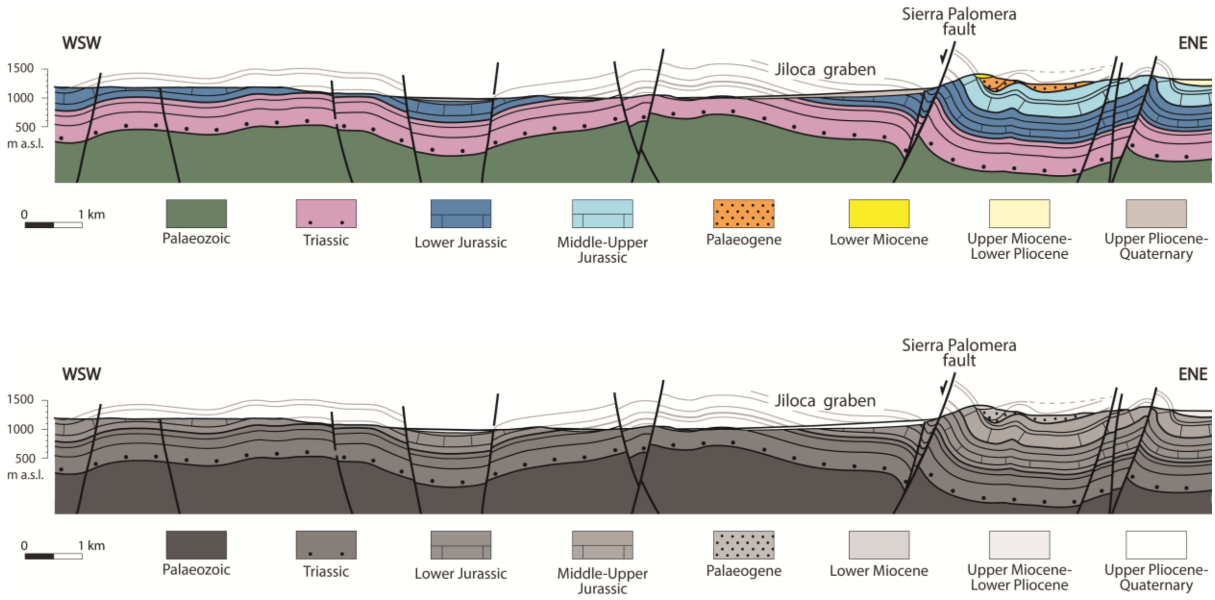
WSW
ENE
Sierra Palomera fault
Jiloca graben
1500
1000
500
m a.s.l.
0
1 km
Palaeozoic
Triassic
Lower Jurassic
Middle-Upper Jurassic
Palaeogene
Lower Miocene
Upper Miocene-Lower Pliocene
Upper Pliocene-Quaternary
WSW
ENE
Sierra Palomera fault
Jiloca graben
1500
1000
500
m a.s.l.
0
1 km
Palaeozoic
Triassic
Lower Jurassic
Middle-Upper Jurassic
Palaeogene
Lower Miocene
Upper Miocene-Lower Pliocene
Upper Pliocene-Quaternary

Figure 3:

Cross section of the Jiloca Graben at its central sector, initially reconstructed from surface geology and shallow borehole data (modified from Rubio and Simón, 2007). See location in Figure 2.

Figure 4:

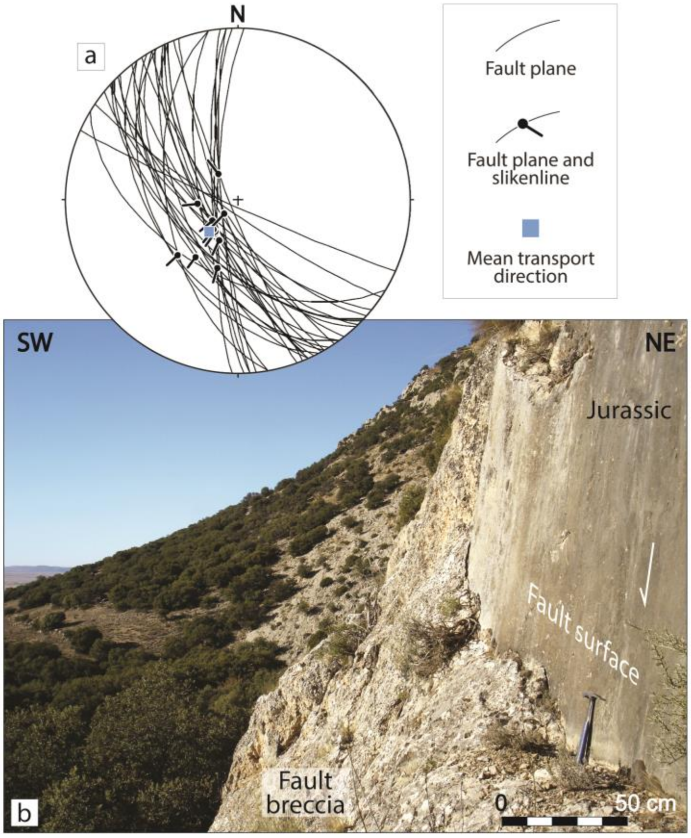
N
a
Fault plane
Fault plane and slikenline
Mean transport direction
SW
NE
Jurassic
Fault surface
Fault breccia
b
0
50 cm

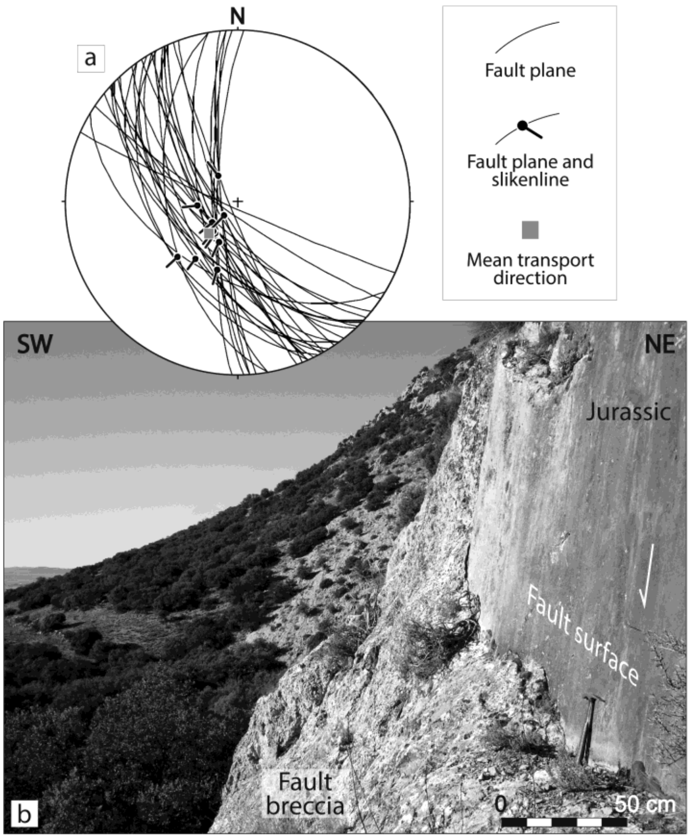
N
a
Fault plane
Fault plane and slikenline
Mean transport direction
SW
NE
Jurassic
Fault surface
Fault breccia
b
0
50 cm

Figure 4:

(a) Field view of one of the rupture surfaces within the damage zone of the Sierra Palomera fault; it cuts Lower Jurassic limestones and shows associated fault breccia. (b) Stereoplot (equal area, lower hemisphere) showing orientations of fault planes and slickenlines collected in that zone.

Figure 5:

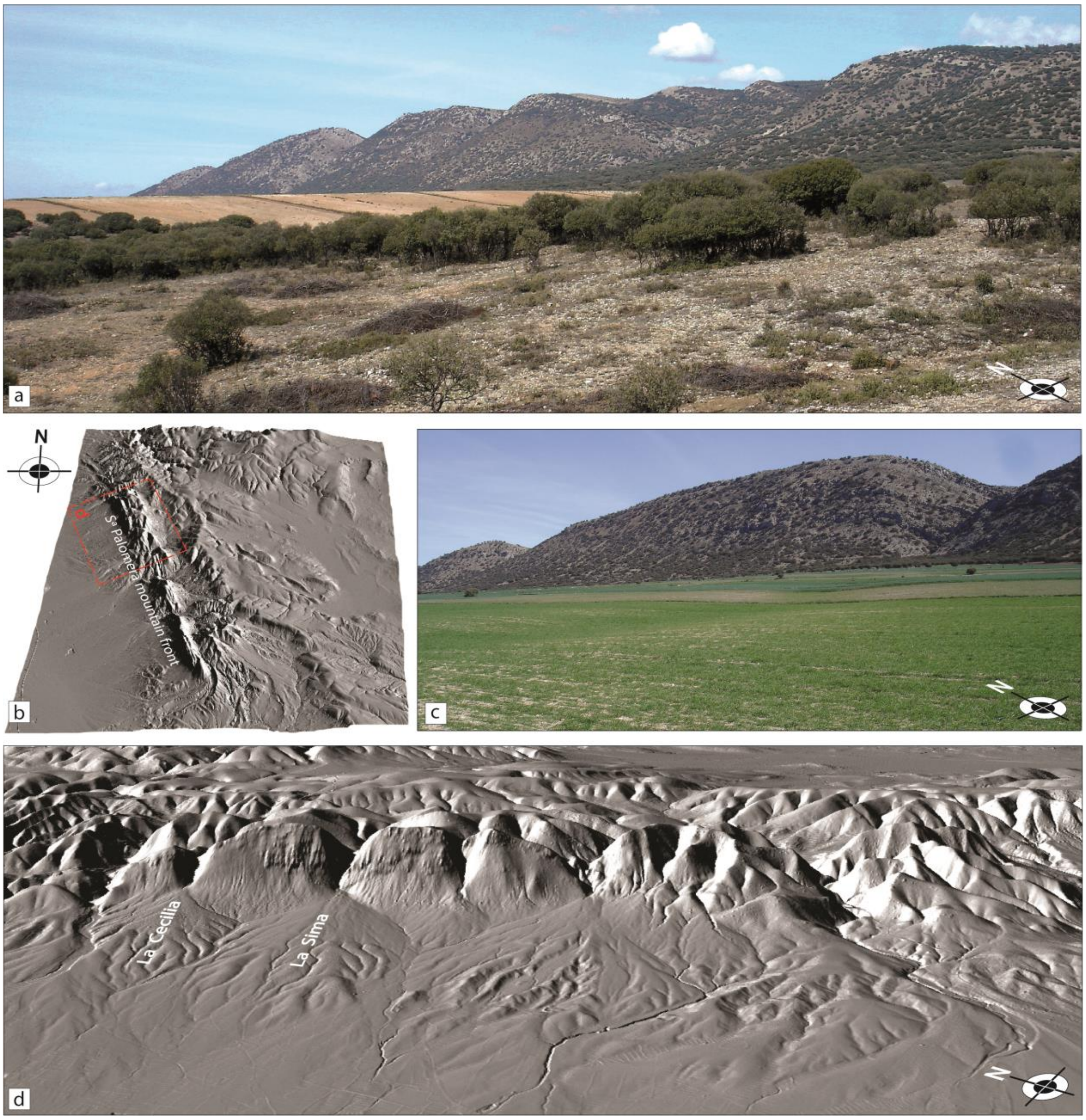

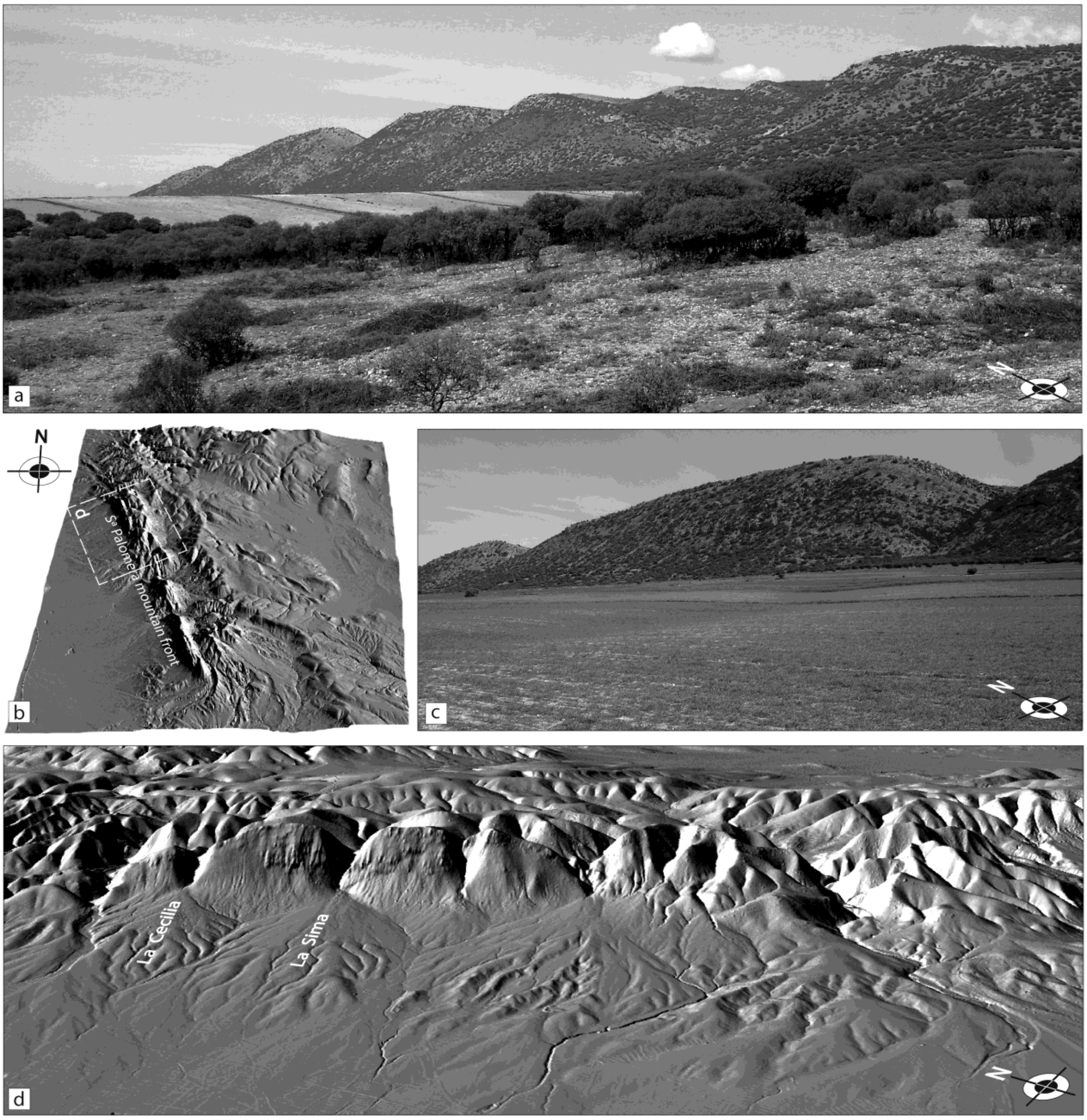
a
N
d
Sª Palomera mountain front
b
c
La Cecilia
La Sima
d

Figure 5:

The Sierra Palomera mountain front. (a) Field panoramic view. (b) Hillshade oblique image rendered from Digital Elevation Model (5 m grid) of Instituto Geográfico Nacional (IGN). (c) Detail of a trapezoidal facet within the fault scarp. (d) Hillshade oblique image (5-m-grid DEM, IGN) showing a close view to the alluvial fans sourced at the mountain front; La Cecilia and La Sima alluvial fans are identified.

Figure 6:

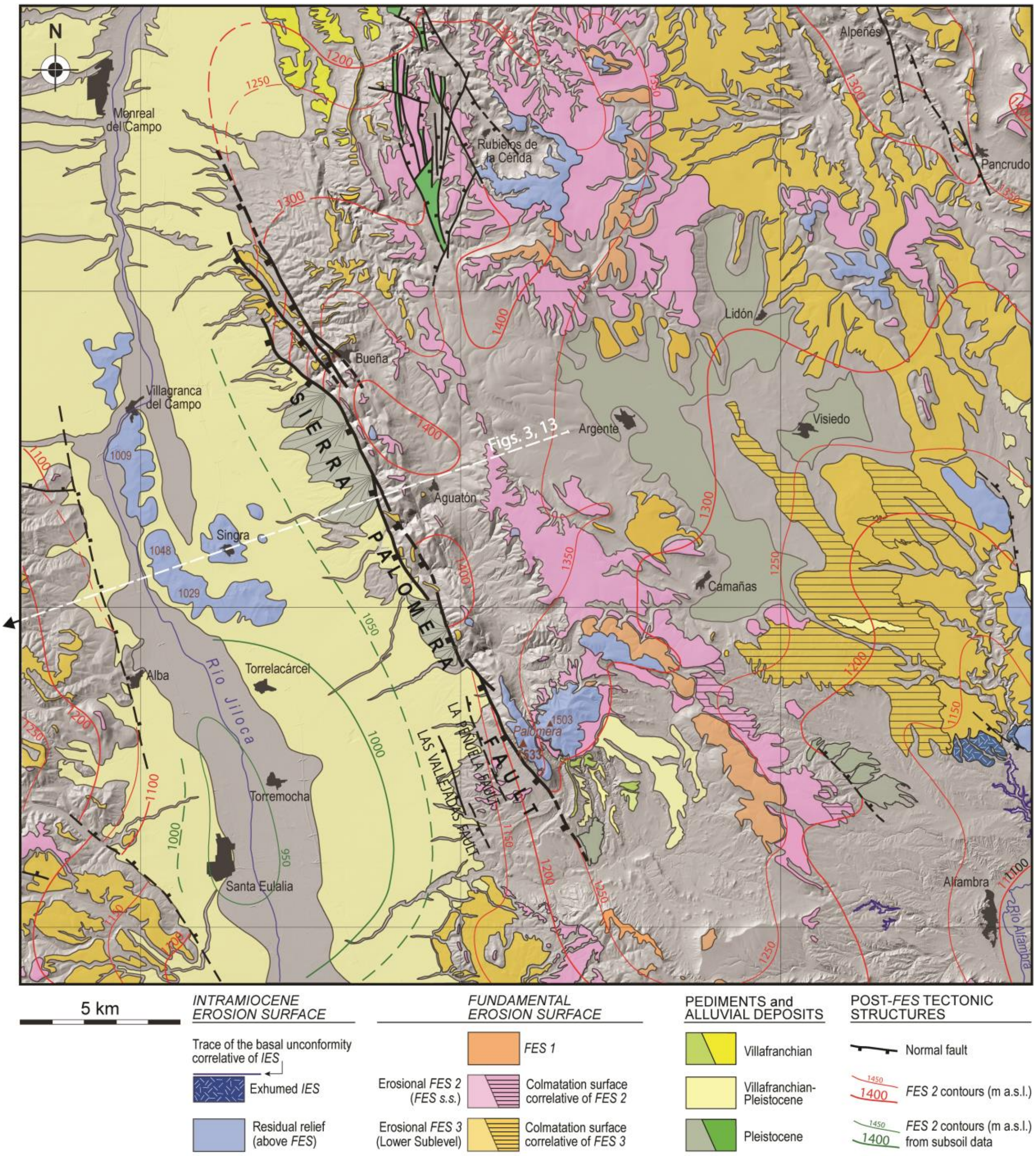
N
Monreal del Campo
Rubielos de la Cerda
Alpeñes
Pancrudo
Lidón
Bueña
Villagranca del Campo
Argente
Visiedo
Figs. 3, 13
Aguatón
Singra
Camañas
SIERRA PALOMERA
FAULT
Alba
Río Jiloca
Torrelacárcel
Torremocha
Santa Eulalia
LA PEÑUELA FAULT
LAS VALLEJADAS FAULT
Palomera
1503
Alfambra
Río Alfambra
5 km
INTRAMIOCENE EROSION SURFACE
Trace of the basal unconformity correlative of IES
Exhumed IES
Residual relief (above FES)
FUNDAMENTAL EROSION SURFACE
FES 1
Erosional FES 2 (FES s.s.)
Colmatation surface correlative of FES 2
Erosional FES 3 (Lower Sublevel)
Colmatation surface correlative of FES 3
PEDIMENTS and ALLUVIAL DEPOSITS
Villafranchian
Villafranchian-Pleistocene
Pleistocene
POST-FES TECTONIC STRUCTURES
Normal fault
FES 2 contours (m a.s.l.)
FES 2 contours (m a.s.l.) from subsoil data

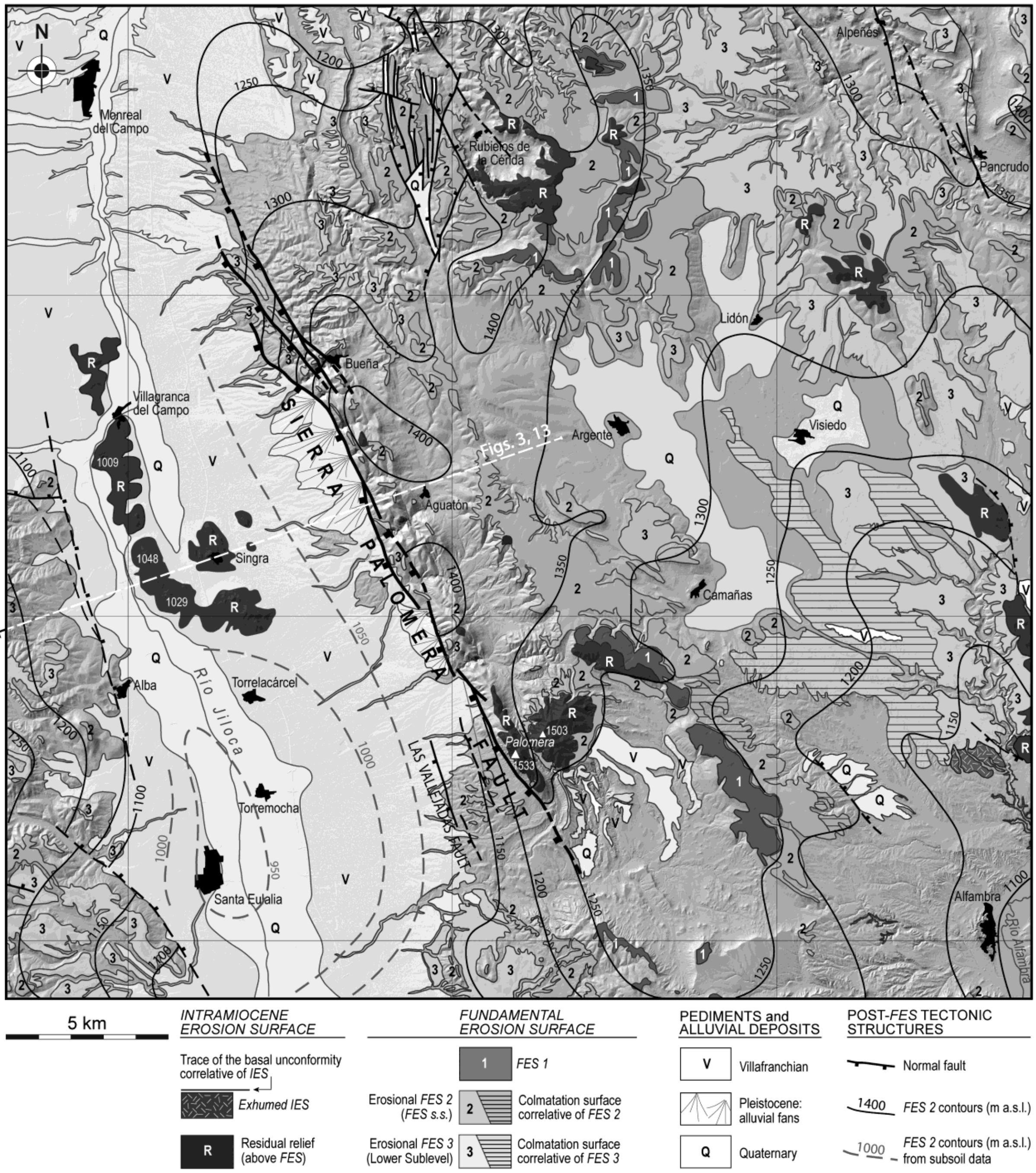
N
Monreal del Campo
Villafranca del Campo
Singra
Alba
Torrelacárcel
Torremocha
Santa Eulalia
Río Jiloca
Bueña
Aguatón
Rubielos de la Cérida
Argente
Visiedo
Lidón
Camañas
Alpeñes
Pancrudo
Alfambra
Río Alfambra
Palomera
1533
1503
1009
1048
1029
SIERRA PALOMERA FAULT
LAS VALLEJADAS FAULT
Figs. 3, 13
5 km
INTRAMIOCENE EROSION SURFACE
Trace of the basal unconformity correlative of IES
Exhumed IES
Residual relief (above FES)
FUNDAMENTAL EROSION SURFACE
FES 1
Erosional FES 2 (FES s.s.)
Colmatation surface correlative of FES 2
Erosional FES 3 (Lower Sublevel)
Colmatation surface correlative of FES 3
PEDIMENTS and ALLUVIAL DEPOSITS
Villafranchian
Pleistocene: alluvial fans
Quaternary
POST-FES TECTONIC STRUCTURES
Normal fault
FES 2 contours (m a.s.l.)
FES 2 contours (m a.s.l.) from subsoil data

Figure 6:

Morphotectonic map of the Sierra Palomera area.

Figure 7:

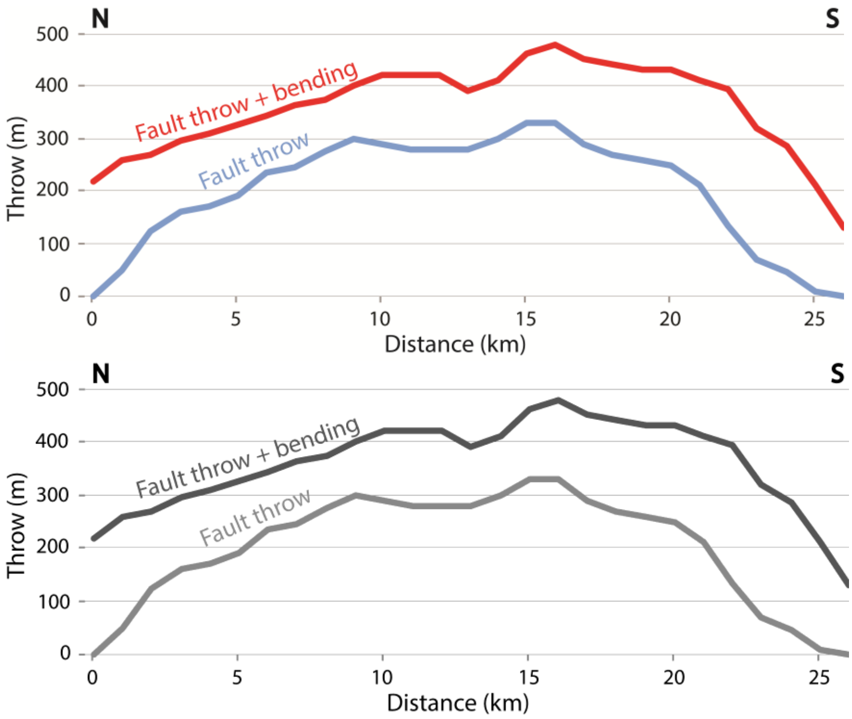
N
S
Fault throw + bending
Fault throw
Throw (m)
Distance (km)
0
100
200
300
400
500
0
5
10
15
20
25
N
S
Fault throw + bending
Fault throw
Throw (m)
Distance (km)

Figure 7:

Throw *vs.* distance (T-D) graph along the Sierra Palomera fault. Lower curve: fault throw *s.s.* recorded by the *FES2* marker. Upper curve: total tectonic offset of *FES2* including the bending component.

Figure 8:

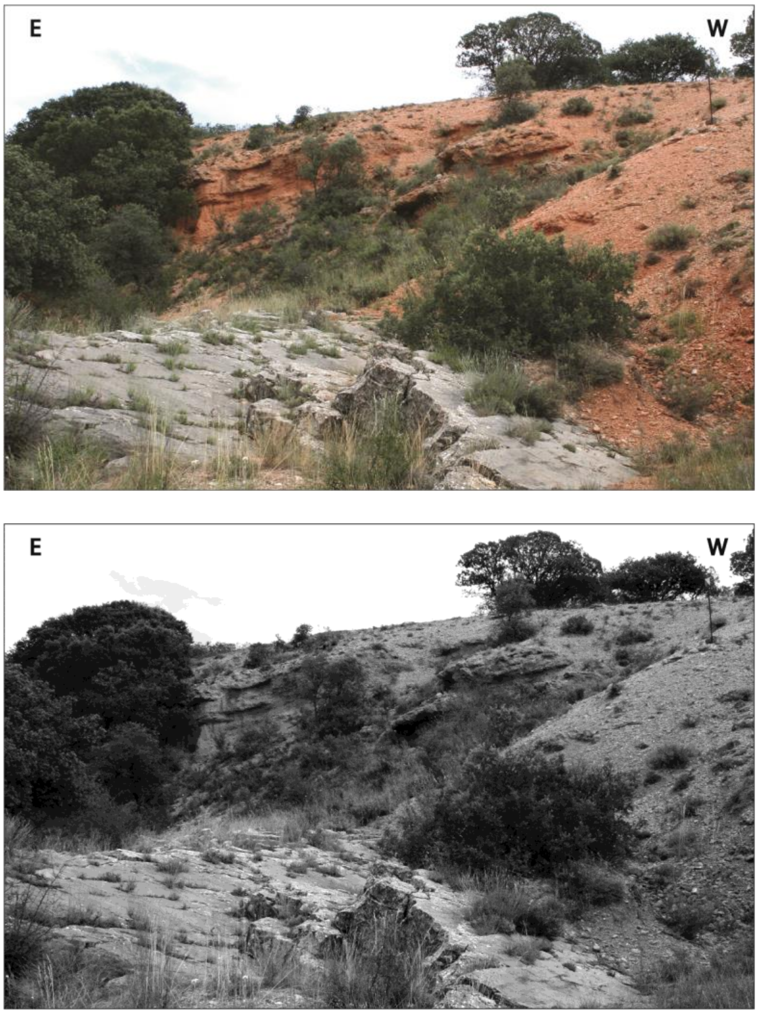

Figure 8:

Villafranchian alluvial deposits deformed by an accommodation monocline in the footwall block of La Peñuela fault. See location in Figure 2.

Figure 9:

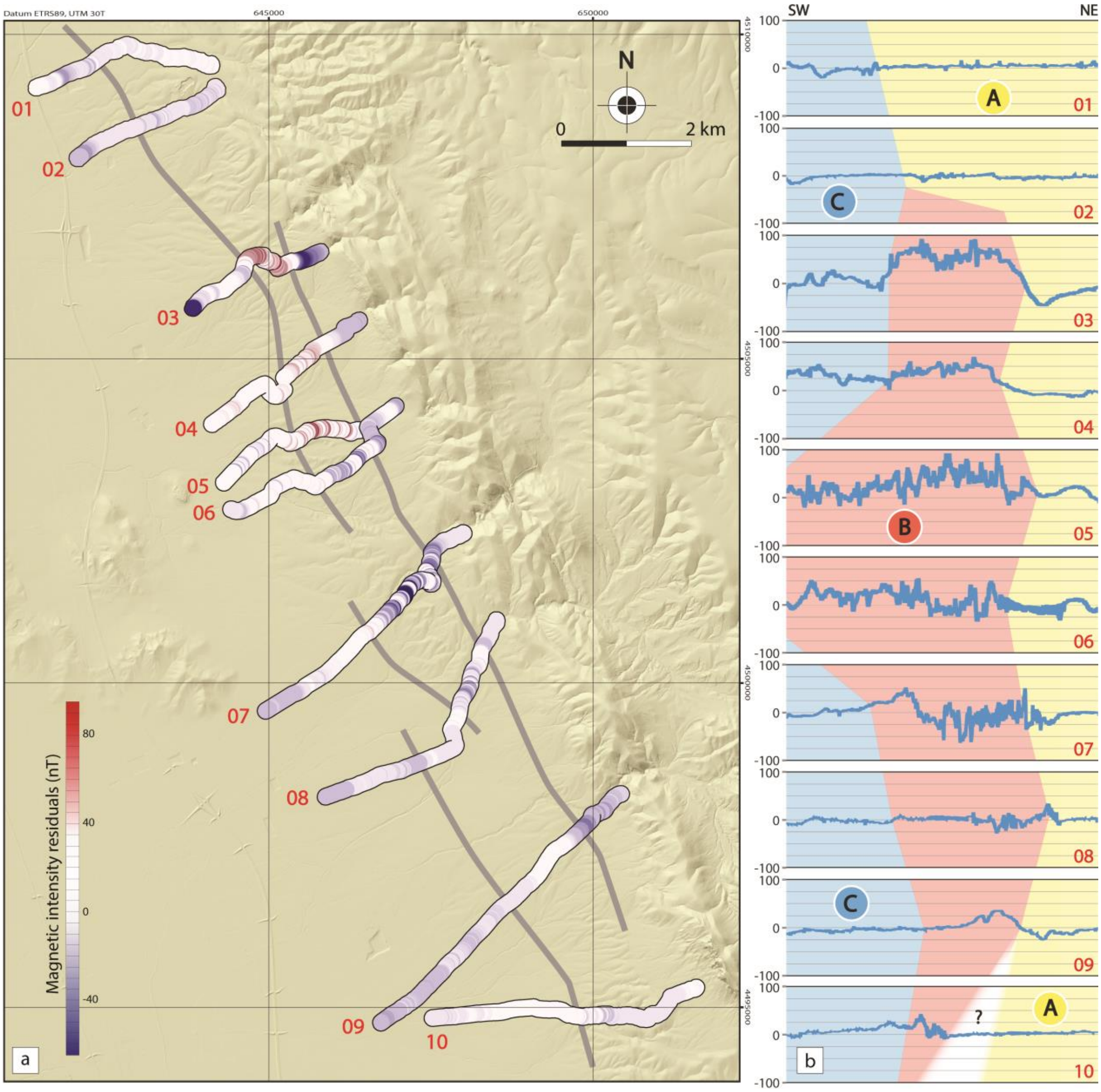

Datum ETRS89, UTM 30T
645000
650000
4510000
4505000
4500000
4495000
N
0
2 km
01
02
03
04
05
06
07
08
09
10
Magnetic intensity residuals (nT)
80
40
0
-40
a
SW
NE
100
0
-100
A
B
C
?
b

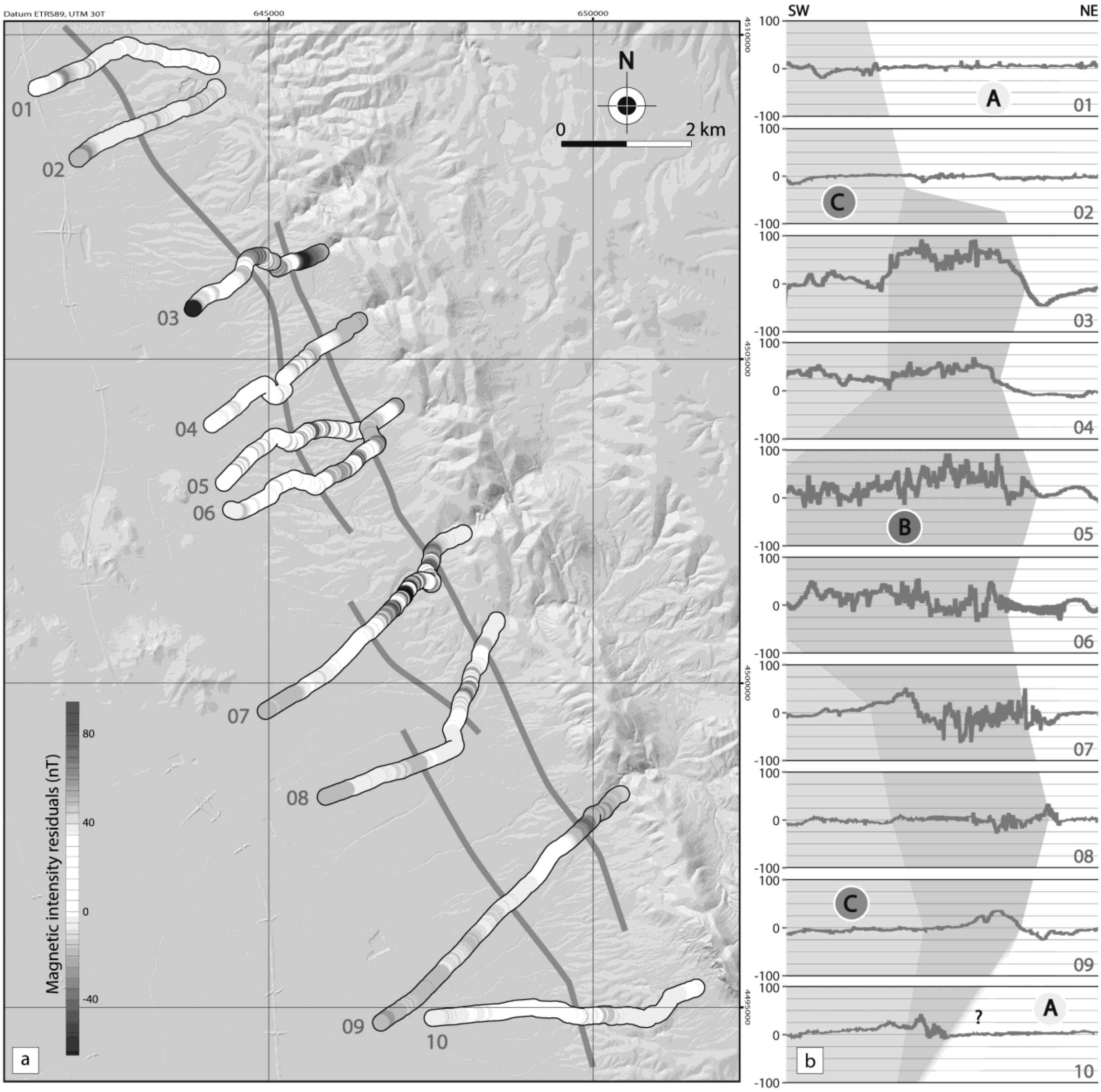
Datum ETRS89, UTM 30T
645000
650000
4510000
4505000
4500000
4495000
N
0
2 km
01
02
03
04
05
06
07
08
09
10
Magnetic intensity residuals (nT)
80
40
0
-40
a
SW
NE
100
0
-100
A
B
C
?
b

Figure 9:

Results of the geomagnetic survey covering the Sierra Palomera piedmont. (a) Location of magnetic profiles 01 to 10, with the residual values of field intensity (nT) plotted as a colour palette. (b) Magnetic profiles plotted with a normalized horizontal length, in which domains A, B and C roughly parallel to the Sierra Palomera fault are defined (see text for details).

Figure 10:

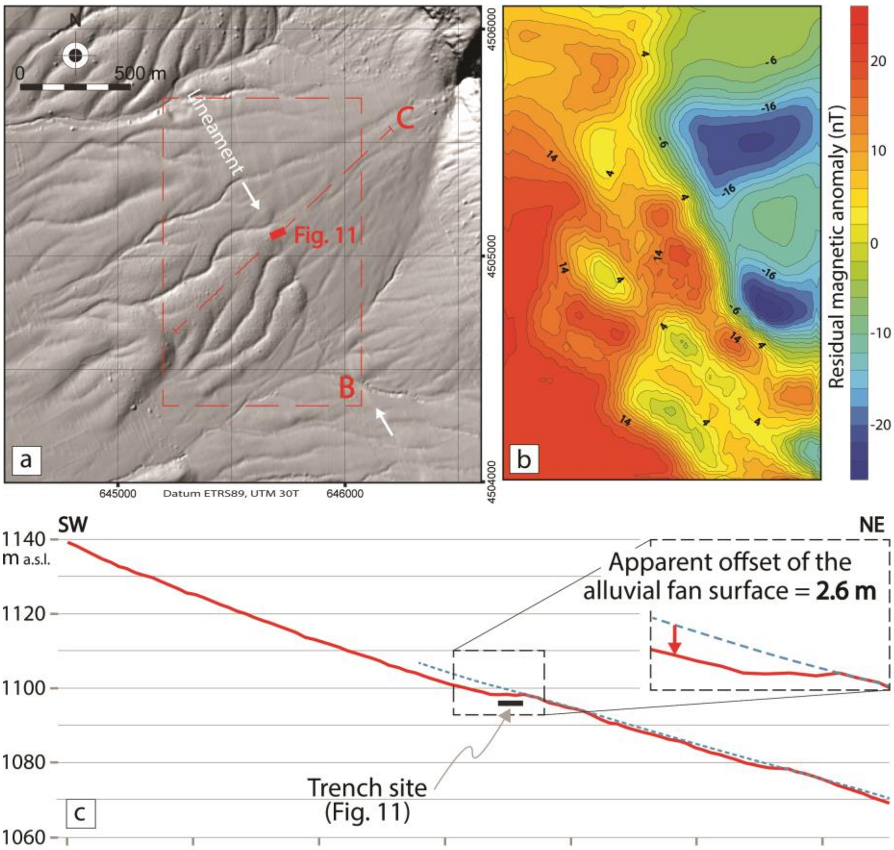
N
0
500 m
Lineament
C
Fig. 11
B
a
645000
Datum ETRS89, UTM 30T
646000
4506000
4505000
4504000
b
Residual magnetic anomaly (nT)
20
10
0
-10
-20
SW
NE
1140
m a.s.l.
1120
1100
1080
1060
Apparent offset of the
alluvial fan surface = 2.6 m
Trench site
(Fig. 11)
c
0
200
400
600
800
1000
1200 m

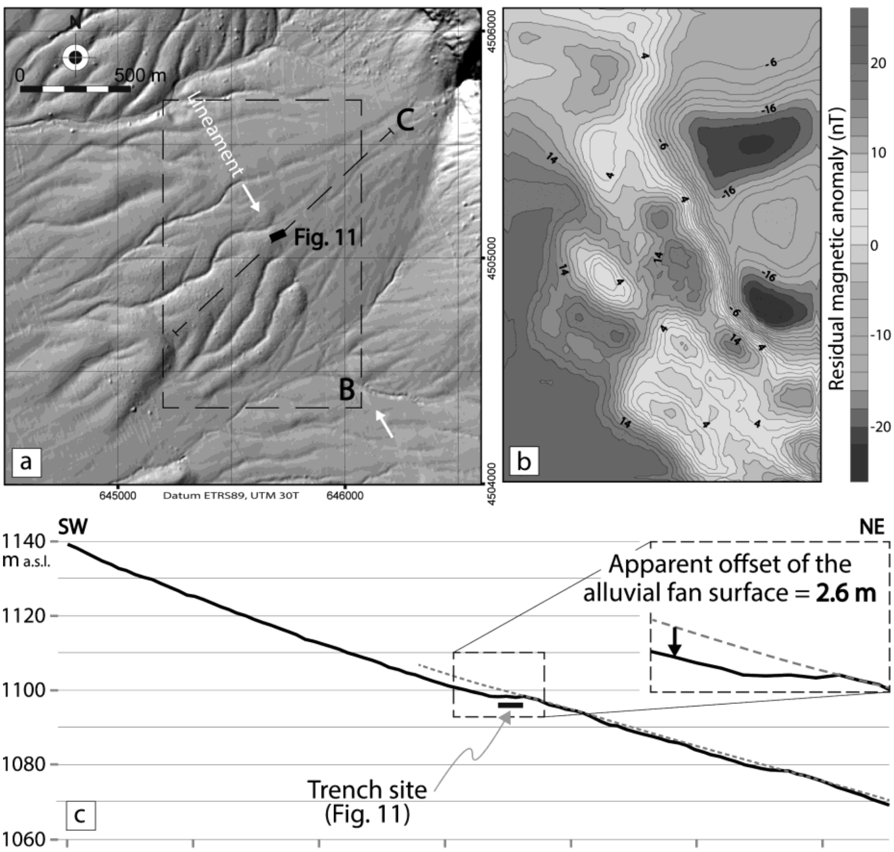
N
0
500 m
Lineament
C
Fig. 11
B
a
645000
Datum ETRS89, UTM 30T
646000
4506000
4505000
4504000
b
Residual magnetic anomaly (nT)
20
10
0
-10
-20
SW
NE
1140
m a.s.l.
1120
1100
1080
1060
Apparent offset of the
alluvial fan surface = 2.6 m
Trench site
(Fig. 11)
c
0
200
400
600
800
1000
1200 m

Figure 10:

(a) Hillshade relief map of the barranco de la Sima alluvial fan rendered from digital elevation model (DEM, 5 m grid) of the Instituto Geográfico Nacional. See location in Figure 2. (b) Residual magnetic field anomalies at the central sector of the alluvial fan. (c) Detailed topographic profile showing a slope anomaly in the longitudinal profile of the alluvial fan surface, from which an apparent antithetic throw of 2,6 m can be inferred.

Figure 11:

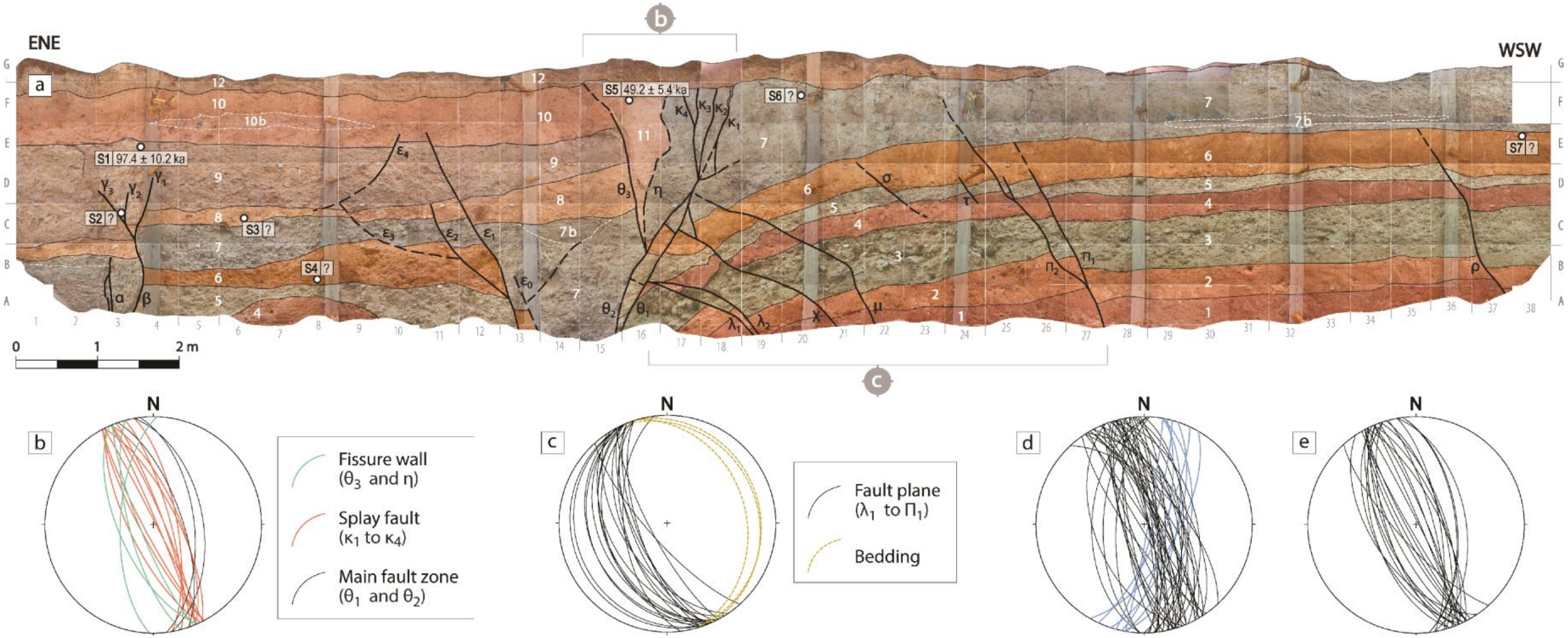
ENE
WSW
a
S1 97.4 ± 10.2 ka
S2 ?
S3 ?
S4 ?
S5 49.2 ± 5.4 ka
S6 ?
S7 ?
0
1
2 m
b
c
d
e
N
Fissure wall
(θ_3 and η)
Splay fault
(κ_1 to κ_4)
Main fault zone
(θ_1 and θ_2)
Fault plane
(λ_1 to Π_1)
Bedding

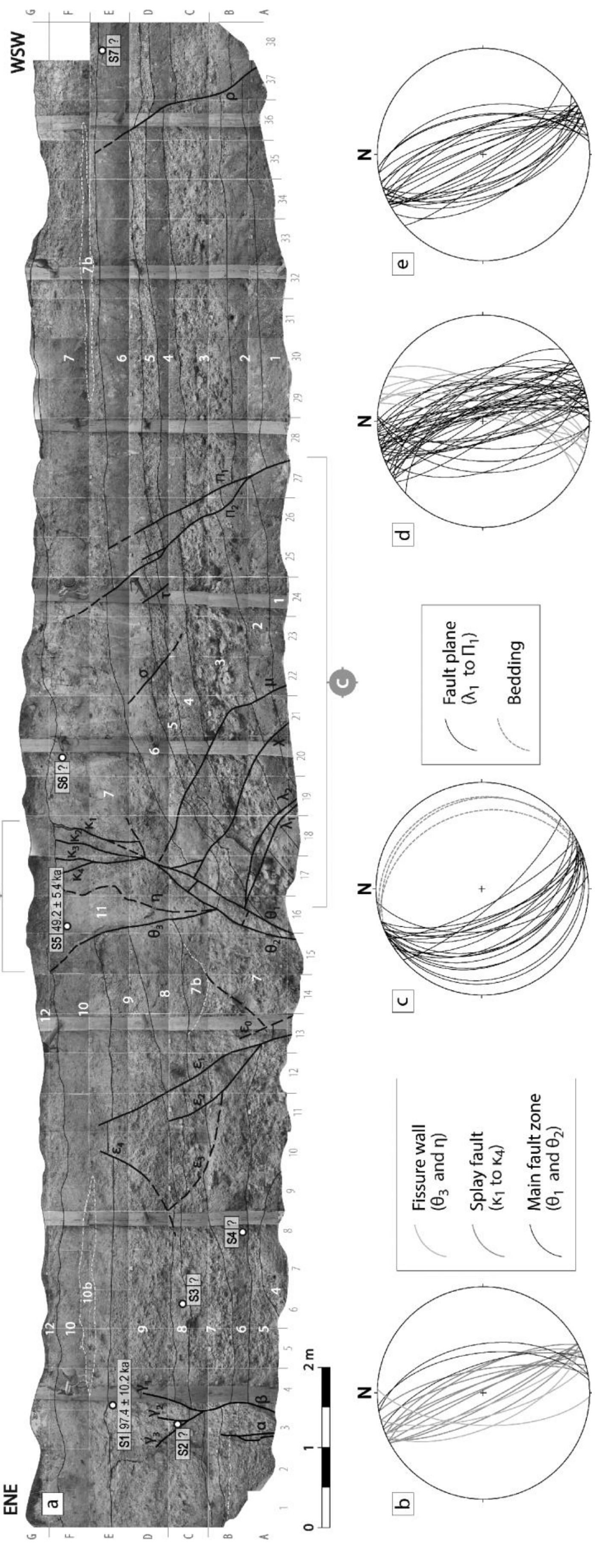
ENE
WSW
2 m
Fissure wall (θ_3 and η)
Splay fault (κ_1 to κ_4)
Main fault zone (θ_1 and θ_2)
Fault plane (λ_1 to Π_1)
Bedding

Figure 11:

(a) Detailed log of La Sima trench. See location in Figure 2. 1 to 12: Quaternary units described in the text. Greek characters: faults referred in the text. The location and age of samples dated by OSL is indicated. Stereoplots (equal area, lower hemisphere) show orientations of faults and fractures measured within the trench: (b) Central fault zone. (c) Footwall block, including monocline. (d) Synthetic stereoplot of fault planes; those rotated at the central monocline have been restored to their original orientation. (e) Synthetic stereoplot of fractures without displacement.

Figure 12:

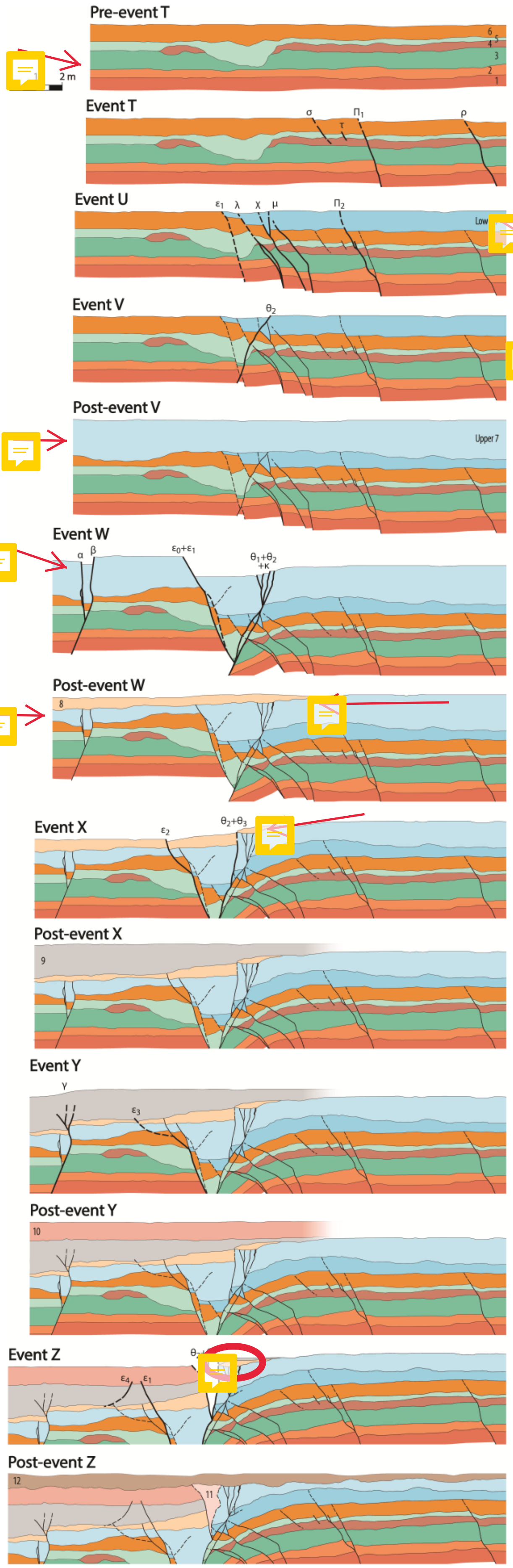

Three first cartoon show that units 1-6 are pre- kinematic and fault activity starts during deposition of unit 7 and most likely fault E1 is the main structure here.

I think this evolutionary model can be simplified into: 1-Pre-kinematic phase (units 1-6); 2-main synthetic (dominantly) fault activity, block rotation and rollover formation (unit 7); 3- Dominantly antithetic fault activity, when faults θ1,2, η, K1-4 and β, α, ϒ1-3 are active (units 8-11, perhaps also latest unit 7) and 4- post-kinematic (unit 12).

Please explain what thin, thick and dashed lines represent in the figure caption.

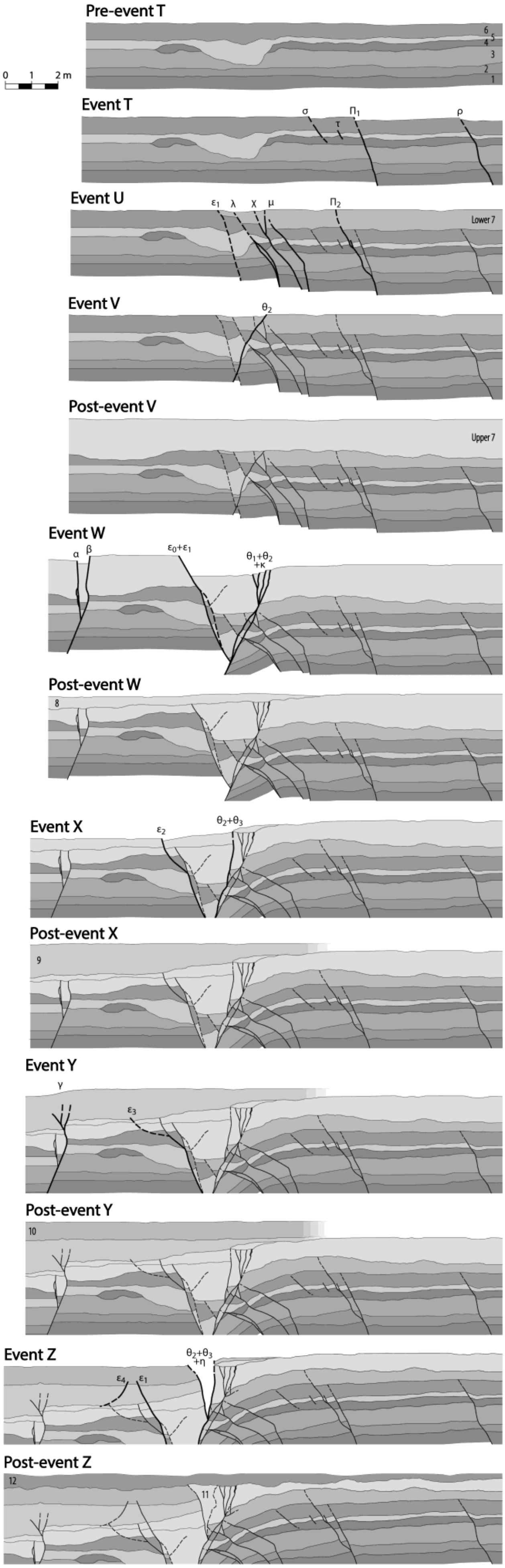

Pre-event T
0 1 2 m
6
5
4
3
2
1
Event T
σ
τ
Π1
ρ
Event U
ε1
λ
χ
μ
Π2
Lower 7
Event V
θ2
Post-event V
Upper 7
Event W
α
β
ε0+ε1
θ1+θ2
+κ
Post-event W
8
Event X
ε2
θ2+θ3
Post-event X
9
Event Y
γ
ε3
Post-event Y
10
Event Z
ε4
ε1
θ2+θ3
+η
Post-event Z
12
11

Figure 12:

Evolutionary model of sedimentation and deformation recorded at the La Sima trench from retrodeformational analysis. Each sketch represents a stage subsequent to the paleoseismic event (and, in some cases, to deposition of sedimentary units) labelled above.

Figure 13:

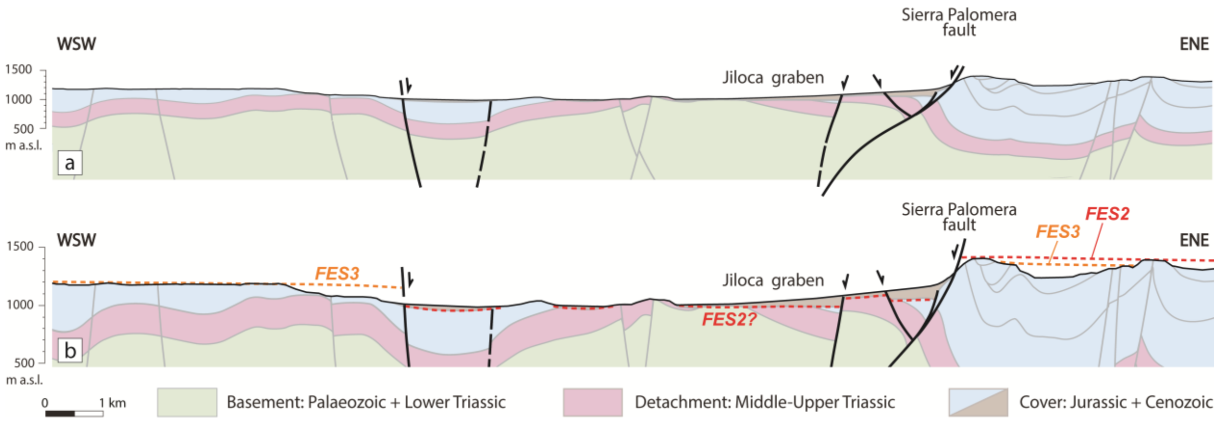

WSW
ENE
Sierra Palomera fault
Jiloca graben
1500
1000
500
m a.s.l.
a
b
FES3
FES2
FES2?
0
1 km
Basement: Palaeozoic + Lower Triassic
Detachment: Middle-Upper Triassic
Cover: Jurassic + Cenozoic

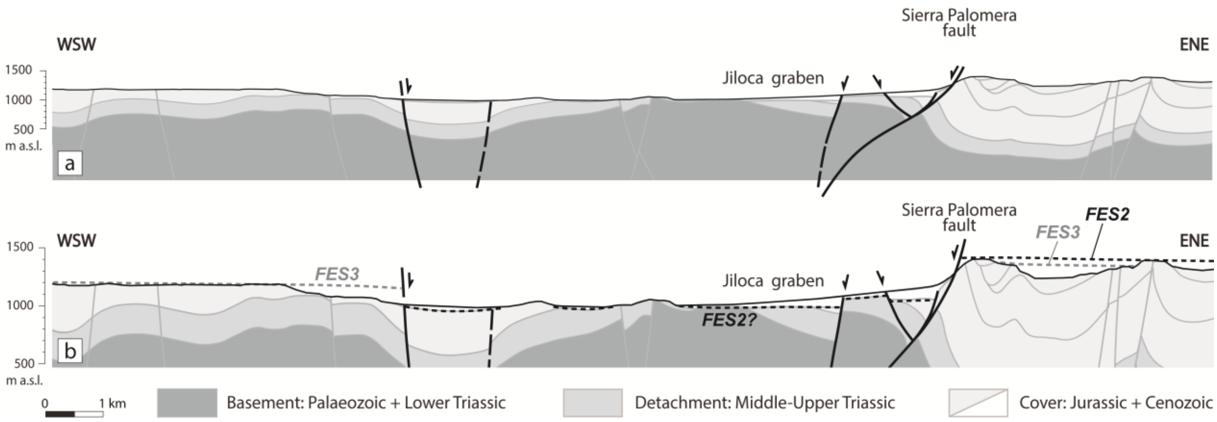

WSW
ENE
Sierra Palomera fault
Jiloca graben
1500
1000
500
m a.s.l.
a
b
FES3
FES2
FES2?
0
1 km
Basement: Palaeozoic + Lower Triassic
Detachment: Middle-Upper Triassic
Cover: Jurassic + Cenozoic

Figure 13:

(a) Refined cross section of the Jiloca graben at its central sector, in which the new inferred, subsidiary faults have been incorporated. (b) Upper fringe of the same cross section (vertical scale x2) showing offset of planation surfaces *FES2* and *FES3*.

Figure 14:

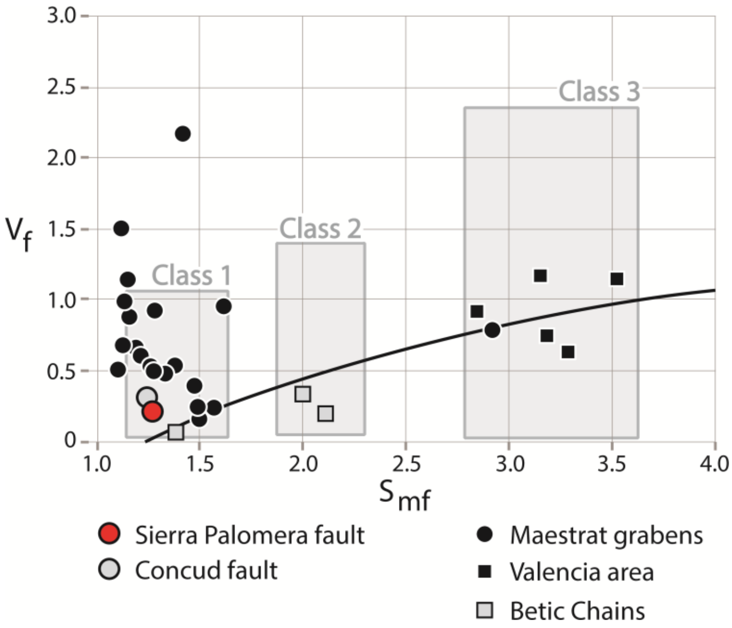
Class 1
Class 2
Class 3
V_f
S_{mf}
3.0
2.5
2.0
1.5
1.0
0.5
0
1.0
1.5
2.0
2.5
3.0
3.5
4.0
Sierra Palomera fault
Concud fault
Maestrat grabens
Valencia area
Betic Chains

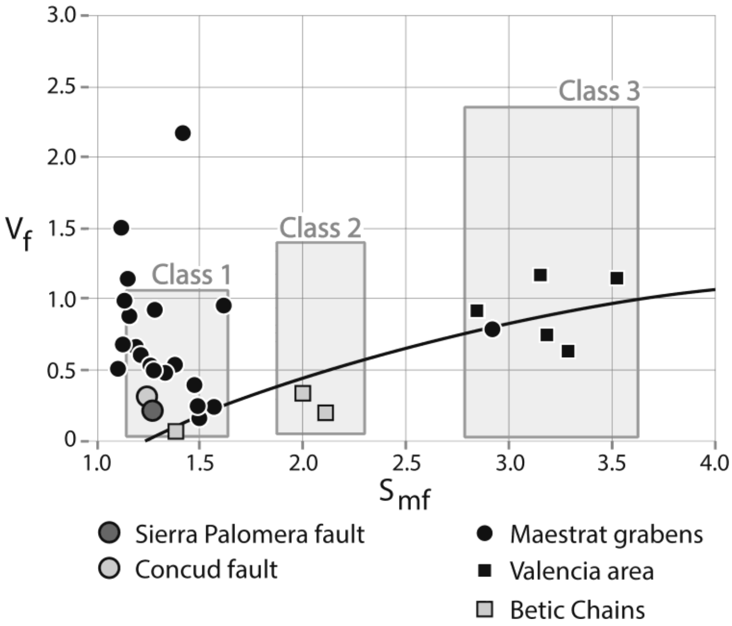
Class 1
Class 2
Class 3
V_f
S_{mf}
3.0
2.5
2.0
1.5
1.0
0.5
0
1.0
1.5
2.0
2.5
3.0
3.5
4.0
Sierra Palomera fault
Concud fault
Maestrat grabens
Valencia area
Betic Chains

Figure 14:

Plot of S_{mf} (mountain-front sinuosity index) *vs.* V_f (valley width/height ratio, measured 250 m upstream from the fault trace), showing the relative position of the Sierra Palomera Fault among extensional fault-generated mountain fronts of eastern Spain. For comparison, the S_{mf} -V_f plots for the neighbouring Concud fault (Lafuente et al, 2011b), faults bounding the Maestrat grabens (eastern Iberian Chain; Perea, 2006), and Valencia region and Betic chains (Silva *et al*., 2003) are also included. Class 1, 2, 3: activity classes (active, moderate and inactive, respectively); the curve represents the tendency for normal faults in SE Spain according to Silva *et al*. (2003).

Figure 15:

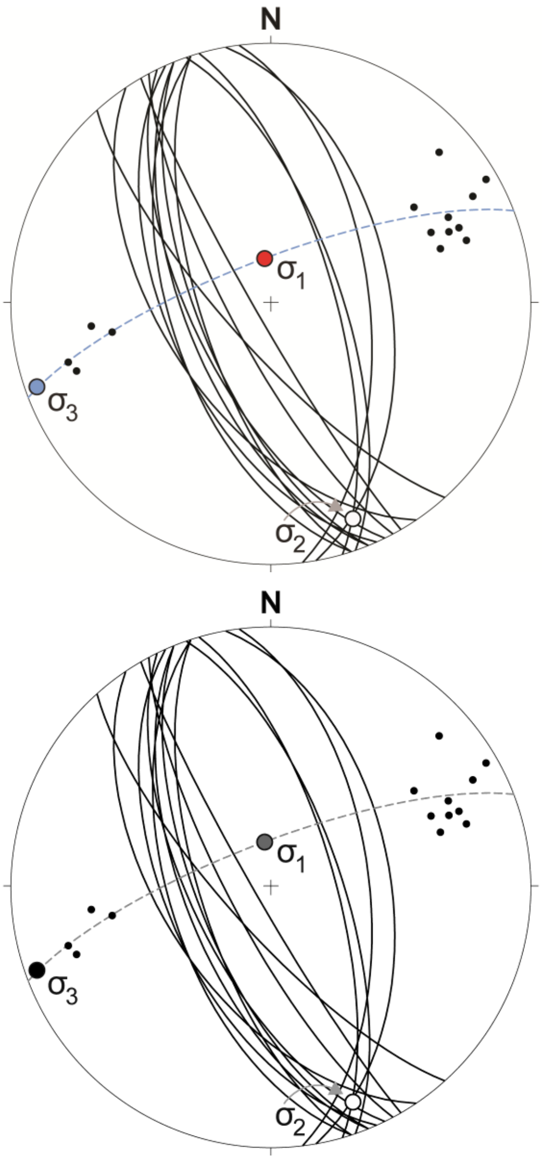

Figure 15:

Interpretation of paleostress axes from orientation of non-rotated, conjugate fault planes measured within La Sima trench. Stress inversion based on model by Anderson (1951).

Table 1:

Sample	Laboratory reference	Stratigraphic location	Depth (m)	H_2O (%)	Quartz Grain (µm)	^{238}U (ppm)	^{232}Th (ppm)	K (%)	Dose rate (Gy/ka)	Equivalent dose (Gy)	Age (ka)
S1	UGA15OSL-1013	Unit 9 (top)	1.0	5±2.5	80-125	1.42±0.33	5.86±1.14	0.6±0.1	1.50±0.15	146.0±3.9	97.4±10.2
S2	UGA15OSL-1014	Unit 9b	2.1	5±2.5	80-250	0.73±0.12	2.24±0.46	0.2±0.1	0.68±0.10	>256	>378
S3	UGA15OSL-1015	Unit 8	1.6	5±2.5	125-250	0.95±0.15	2.45±0.54	0.3±0.1	0.84±0.11	>300	>355
S4	UGA15OSL-1017	Unit 6 (base)	2.8	5±2.5	150-250	1.35±0.25	5.42±0.88	0.5±0.1	1.27±0.13	>300	>236
S5	UGA15OSL-1018	Unit 11	0.4	5±2.5	125-250	1.29±0.20	4.15±0.71	0.5±0.1	1.26±0.12	62.0±3.4	49.2±5.4
S6	UGA15OSL-1019	Unit 7 (top)	0.7	5±2.5	125-250	0.96±0.20	4.73±0.71	0.5±0.1	1.21±0.12	>300	>248
S7	UGA15OSL-1020	Unit 6 (top)	1.2	5±2.5	80-125	1.41±0.21	4.54±0.75	0.8±0.1	1.56±0.13	>300	>193
La Cecilia	MAD-6326BIN	Alluvial fan	3.0	2.31	2-10	2.97	1.54	0.01±0.1	1.63	47.1±2.5	28.9±2.0
La Sima	MAD-6327BIN	Alluvial fan	0.4	6.25	2-10	3.73	1.90	0.18±0.1	2.31	44.3±1.4	19.2±1.1

Table 1:

Parameters and results of OSL dating of samples collected at the La Sima trench (S1 to S7; Luminiscence Dating Laboratory of University of Georgia, USA), and La Cecilia and La Sima alluvial fans (Laboratorio de Datación y Radioquímica de la Universidad Autónoma de Madrid, Spain).

Table 2:

Event	Active faults	Net slip (cm)	Horizontal extension (cm)	Net slip by event[1] (cm)	Horizontal extension by event [2]
T	σ	+ 10	5	+ 45	20 cm (1%)
	τ	+ 5	5		
	π1	+ 15	5		
	ρ	+ 15	5		
U	ε1	+ 15	5	+ 110	45 cm (2%)
	λ1	+ 25	10		
	λ2	+ 20	5		
	χ	+ 20	10		
	μ	+ 15	10		
	π2	+ 15	5		
V	θ2	- 5	5	- 5	5 cm (0%)
W	α	+ 10	0	- 5	85 cm (5%)
	ε0	+ 45	15		
	ε1	+ 45	25		
	β	- 30	5		
	θ1 + θ2 + κ1 to κ4	- 75	40		
X	ε2	+ 5	5	- 90	65 cm (3%)
	θ2+θ3	- 95	60		
Y	ε0	0	0	- 40	
	γ1	- 20	10		10 cm (1%)
	γ2 + γ3	- 20	0		
Z	ε1	+ 10	5	- 125	85 cm (5%)
	ε4	- 10	5		
	θ2 + θ3 + η (open fissure)	- 125	75		
Total synthetic faults		+270			115 cm (6.1%)
Total antithetic faults		-380			200 cm (10.6%)
Monocline		-120			≈70 cm (3.7%)
Total structures		**-230**			≈**385** cm (20.4%)

[1] Fault net slip *s.s.*, excluding vertical displacement associated to the monocline.
[2] Initial (restored) log length= 1890 cm.

Table 2:

Synthesis of deformation events inferred at La Sima trench: faults activated during each event, net slip values calculated from the trench log (positive: synthetic with the Sierra Palomera fault; negative: antithetic), and associated values of horizontal extension.

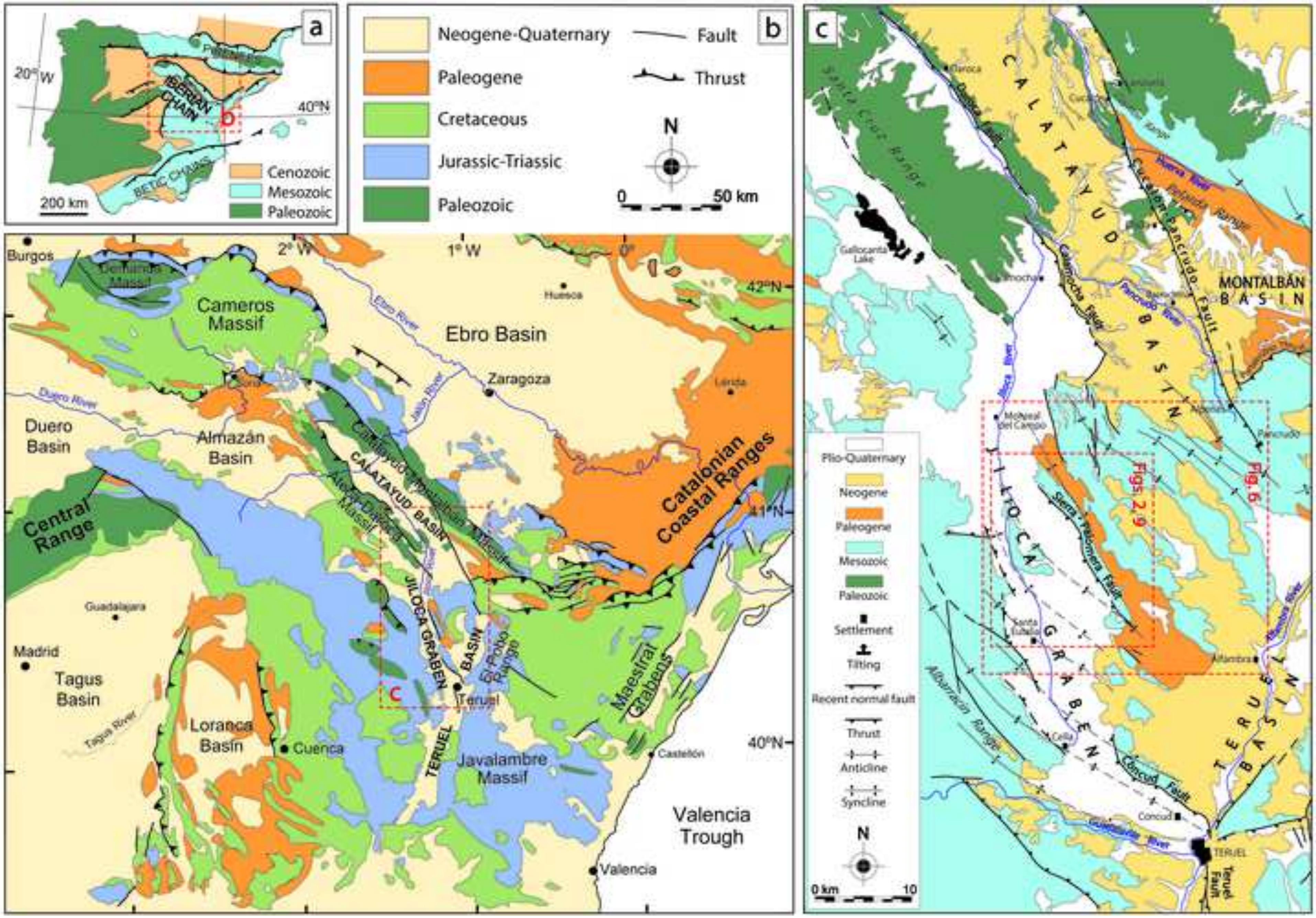
a
20° W
40°N
IBERIAN CHAIN
b
BETIC CHAINS
Cenozoic
Mesozoic
Paleozoic
200 km
b
Neogene-Quaternary
Paleogene
Cretaceous
Jurassic-Triassic
Paleozoic
Fault
Thrust
N
0
50 km
Burgos
2° W
1° W
0°
42°N
Cameros Massif
Ebro Basin
Huesca
Ebro River
Zaragoza
Lérida
Duero River
Duero Basin
Almazán Basin
Catalonian Coastal Ranges
Central Range
CALATAYUD BASIN
JILOCA GRABEN
TERUEL BASIN
El Pobo Range
41°N
Guadalajara
Madrid
Tagus Basin
Tagus River
Loranca Basin
Cuenca
c
Teruel
Javalambre Massif
Maestrat Grabens
Castellón
40°N
Valencia Trough
Valencia
c
CALATAYUD BASIN
MONTALBÁN BASIN
Santa Cruz Range
Gallocanta Lake
Jiloca River
Monreal del Campo
JILOCA GRABEN
Sierra Palomera Fault
Figs. 2, 9
Fig. 6
Santa Eulalia
Albarracín Range
Cella
Concud Fault
Concud
Guadalaviar River
TERUEL
Teruel Fault
TERUEL BASIN
Alfambra
Plio-Quaternary
Neogene
Paleogene
Mesozoic
Paleozoic
Settlement
Tilting
Recent normal fault
Thrust
Anticline
Syncline
N
0 km
10

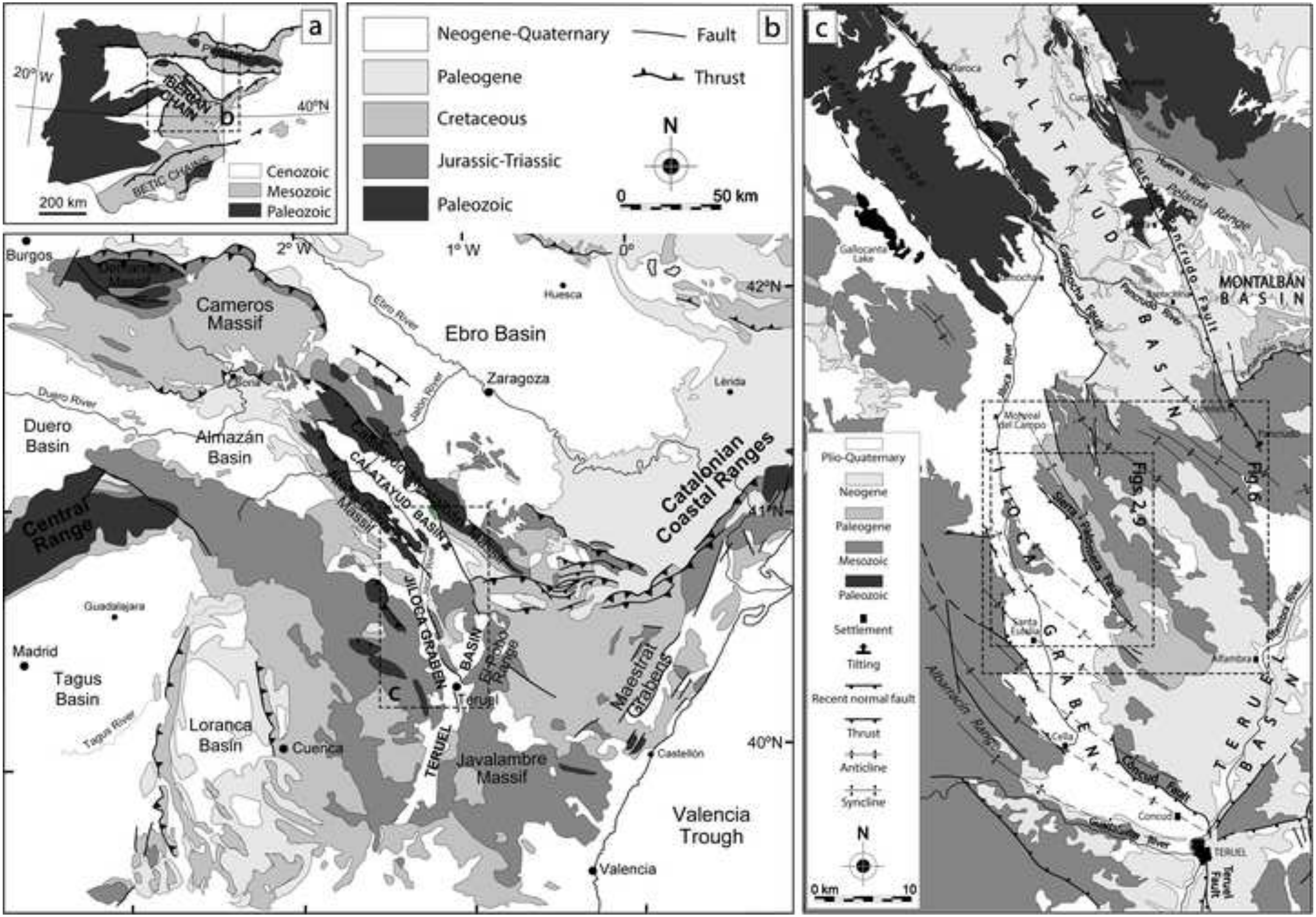
a
20° W
40°N
IBERIAN CHAIN
b
BETIC CHAINS
200 km
Cenozoic
Mesozoic
Paleozoic
b
Neogene-Quaternary
Paleogene
Cretaceous
Jurassic-Triassic
Paleozoic
Fault
Thrust
N
0
50 km
Burgos
2° W
1° W
0°
Huesca
42°N
Cameros Massif
Ebro River
Ebro Basin
Zaragoza
Lerida
Duero River
Duero Basin
Almazán Basin
CALATAYUD BASIN
Catalonian Coastal Ranges
41°N
Central Range
Guadalajara
Madrid
Tagus Basin
Tagus River
Loranca Basin
Cuenca
JILOCA GRABEN
BASIN
El Pobo Range
Teruel
c
TERUEL
Javalambre Massif
Maestrat Grabens
Castellón
40°N
Valencia Trough
Valencia
c
CALATAYUD BASIN
MONTALBÁN BASIN
Gallocanta Lake
Jiloca River
Monreal del Campo
Plio-Quaternary
Neogene
Paleogene
Mesozoic
Paleozoic
Settlement
Tilting
Recent normal fault
Thrust
Anticline
Syncline
N
0 km
10
Figs 2, 9
Fig 6
JILOCA GRABEN
Santa Eulalia
Cella
Albarracín Range
Concud Fault
Alfambra
TERUEL BASIN
Guadalaviar River
TERUEL
Teruel Fault

Figure (with caption below and on the same page)

Click here to access/download;Figure (with caption below and on the same page);Fig 2.tif

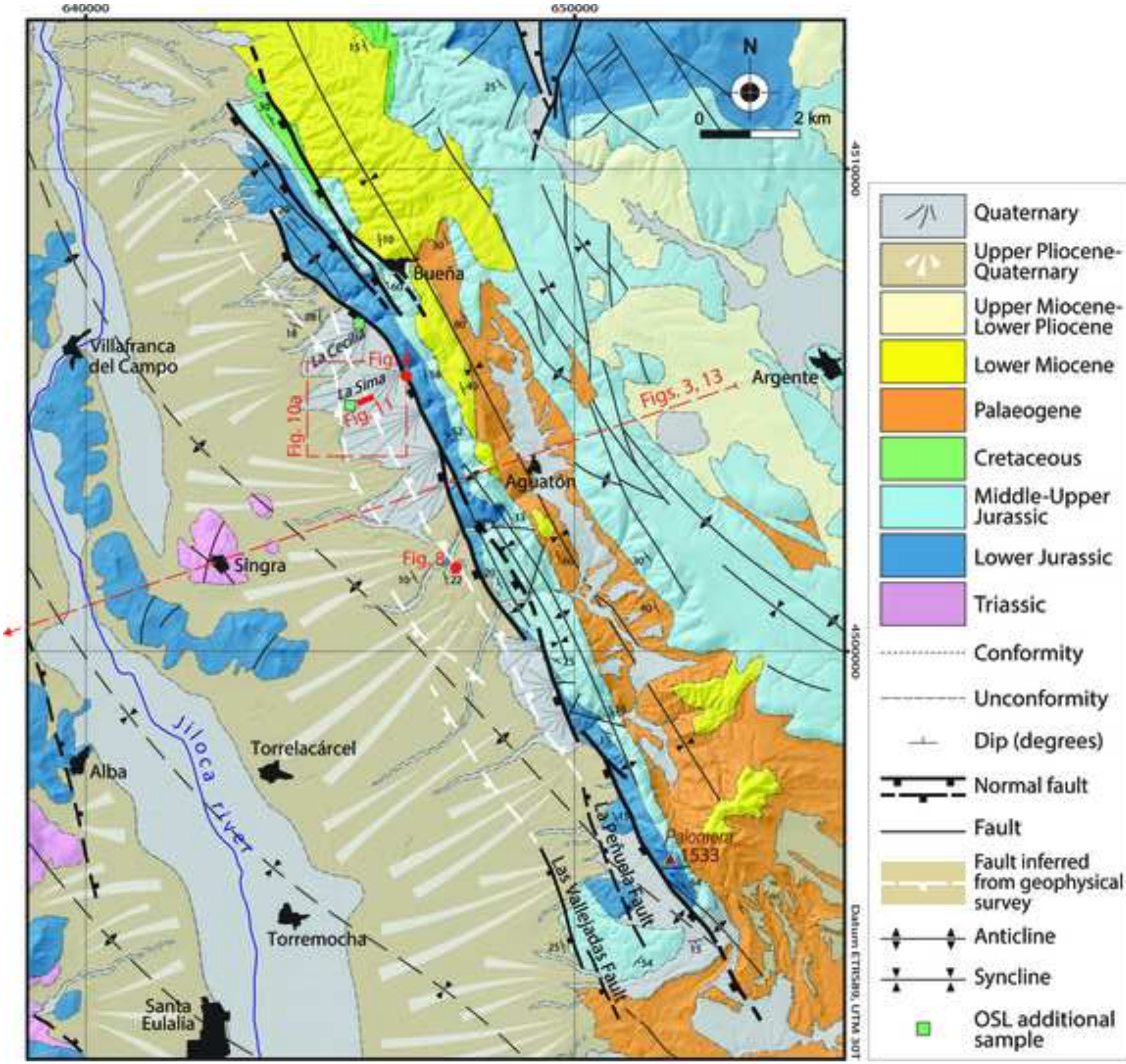

Figure (with caption below and on the same page)

Click here to access/download;Figure (with caption below and on the same page);Fig 2bn.tif

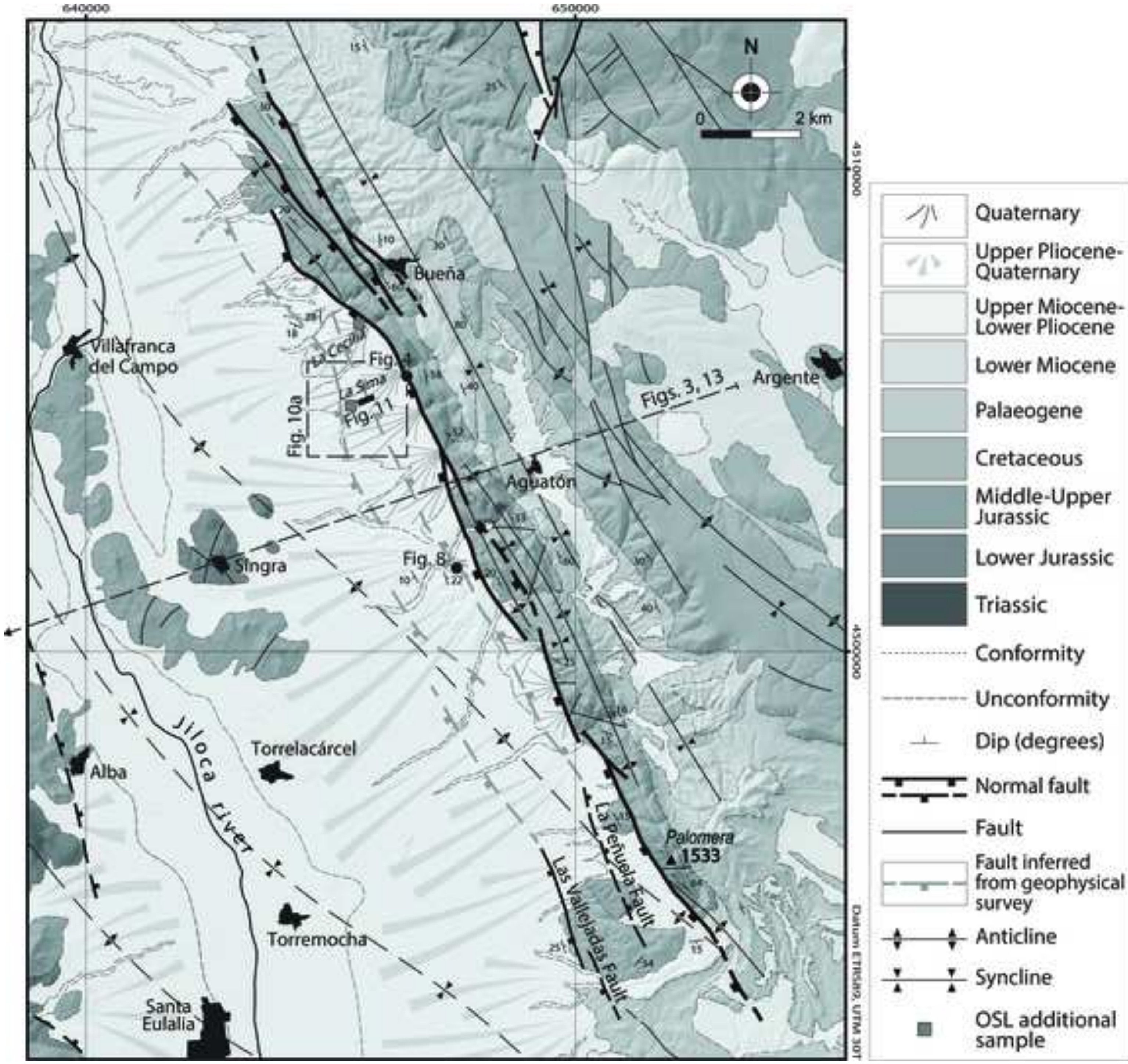

Figure (with caption below and on the same page)

Click here to access/download;Figure (with caption below and on the same page);Fig 3.tif

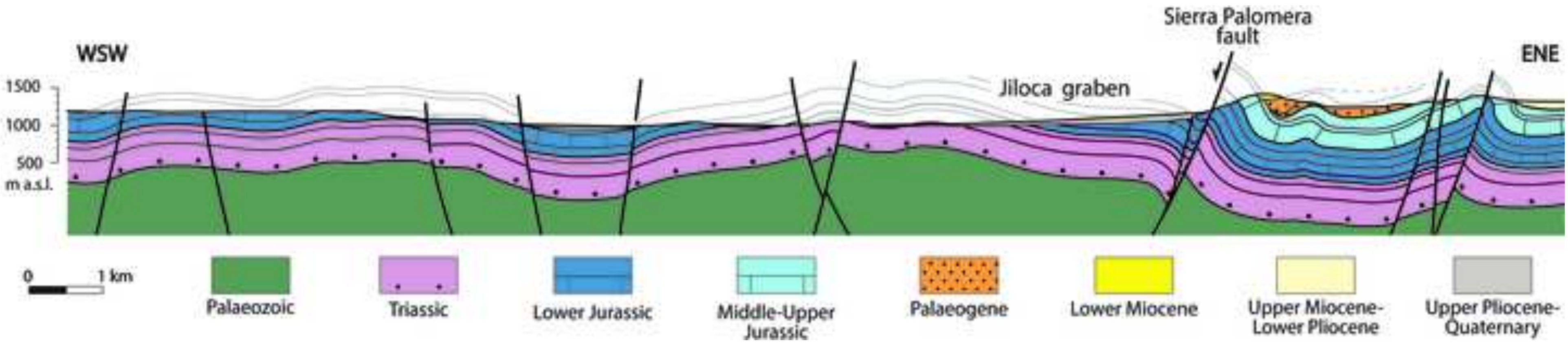

Figure (with caption below and on the same page)

Click here to access/download;Figure (with caption below and on the same page);Fig 3bn.tif

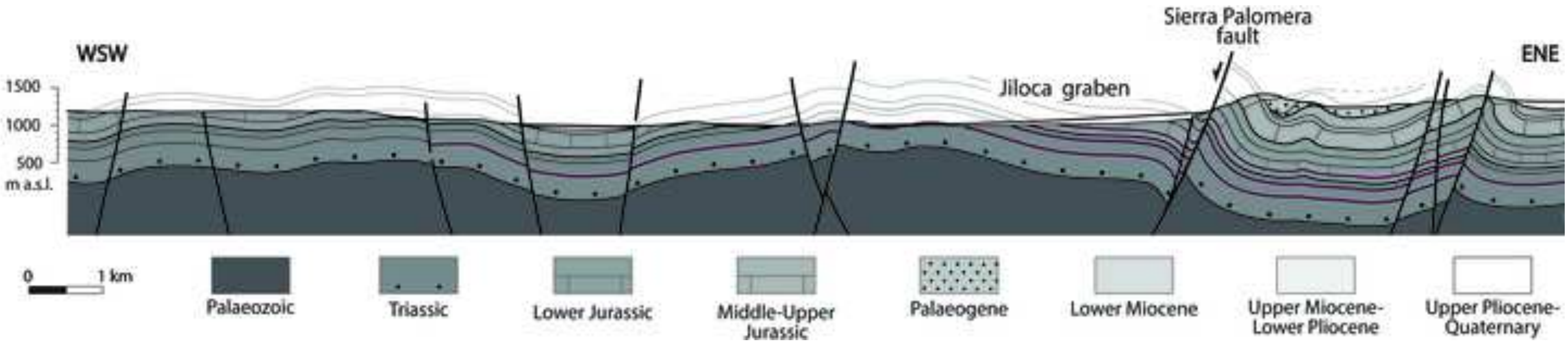

Figure

Click here to access/download;Figure (with caption below and on the same page);Fig 4.tif

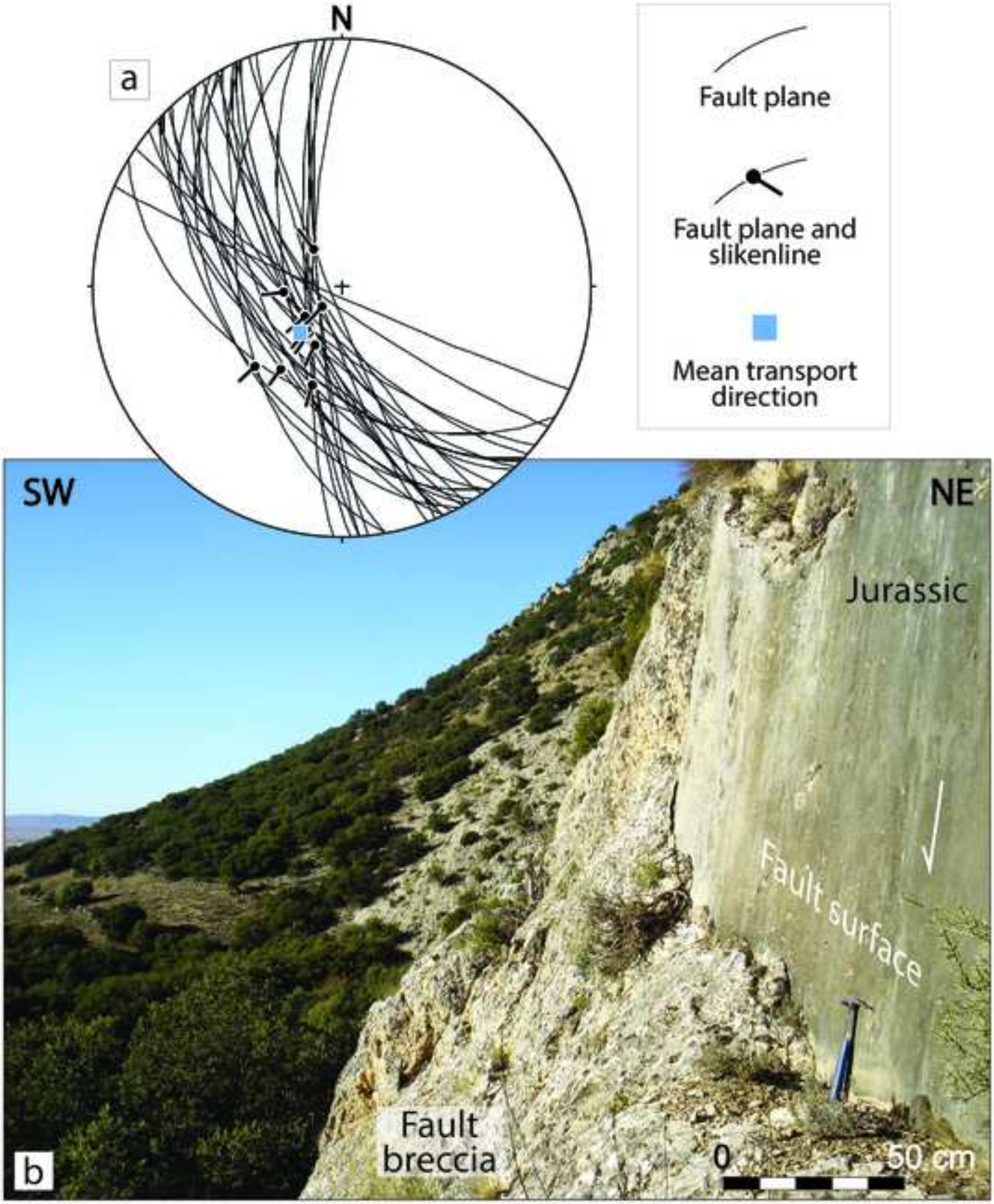

Figure

Click here to access/download;Figure (with caption below and on the same page);Fig 4bn.tif

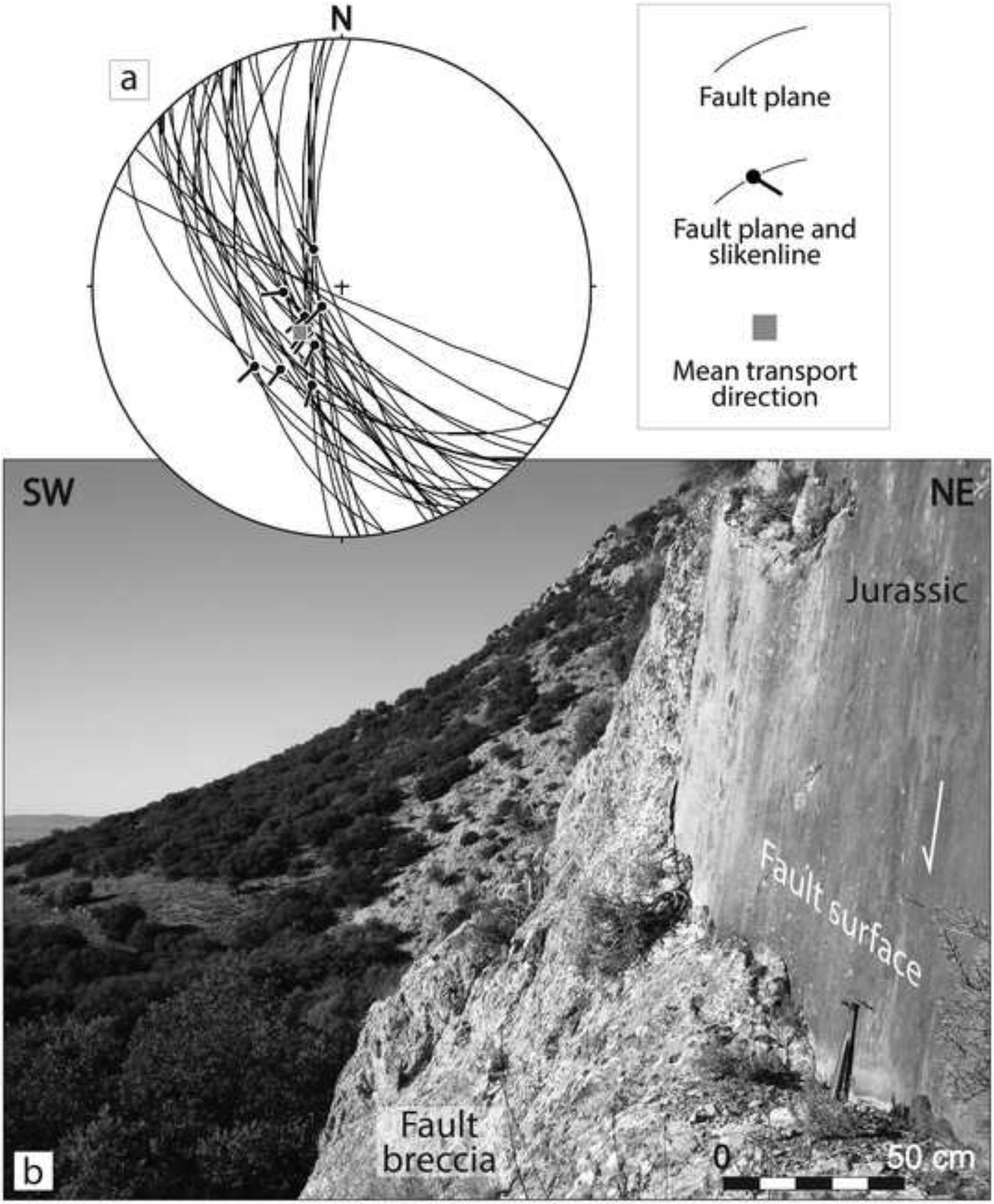

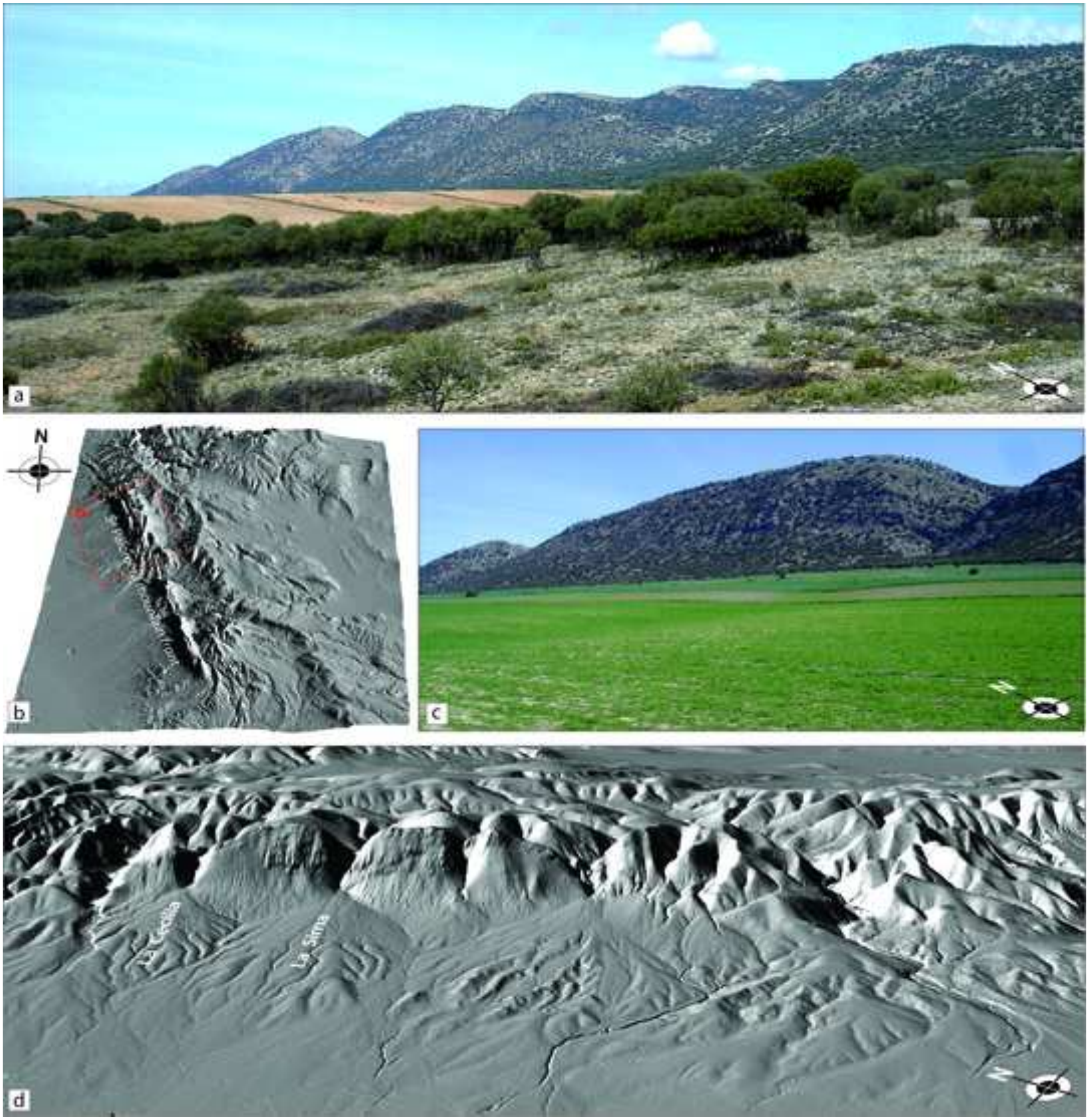
a
N
b
c
d
La Cecilia
La Sima

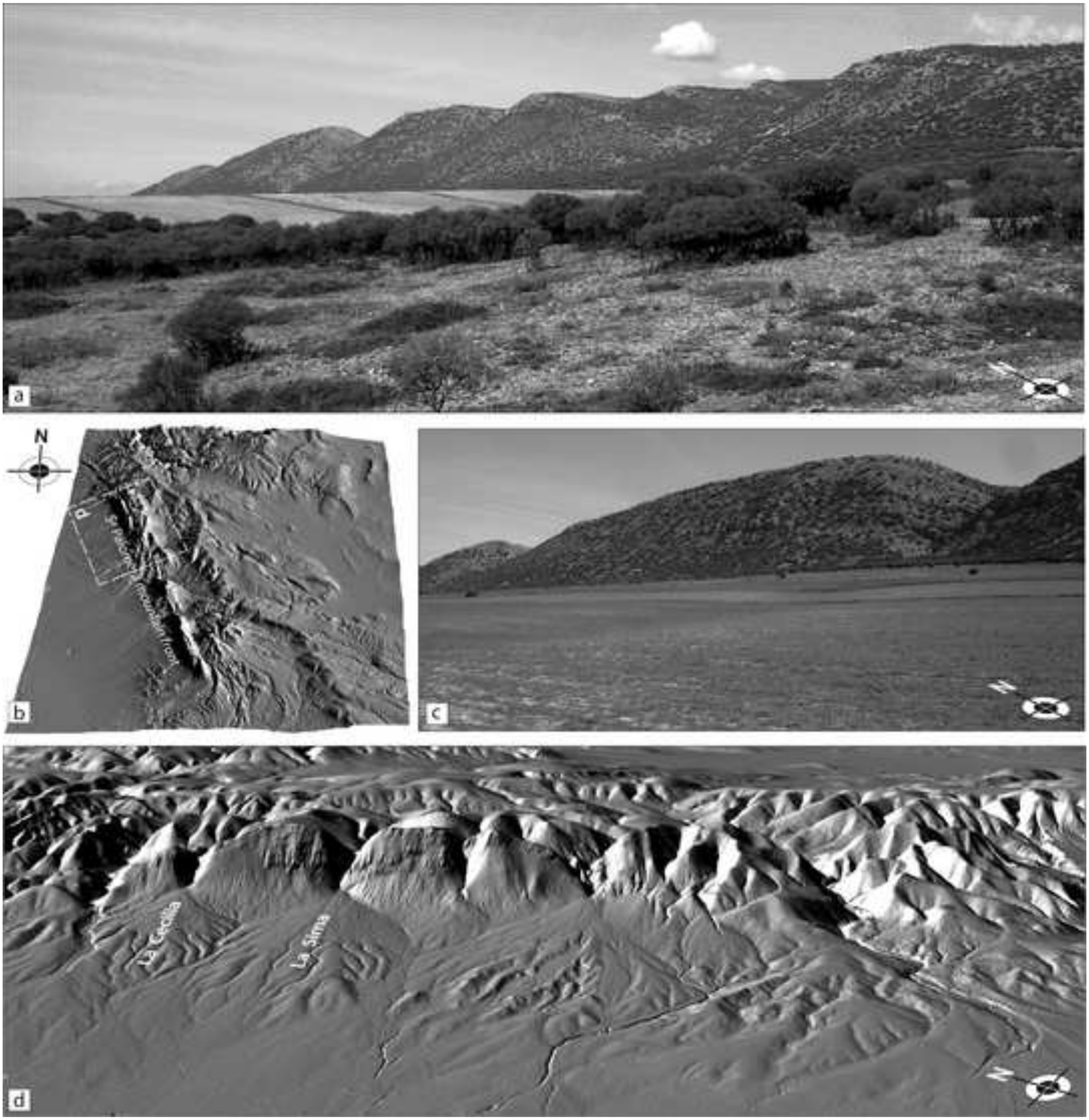
a
N
d
b
c
La Cecilia
La Sima
d

Figure

Click here to access/download;Figure (with caption below and on the same page);Fig 6.tif

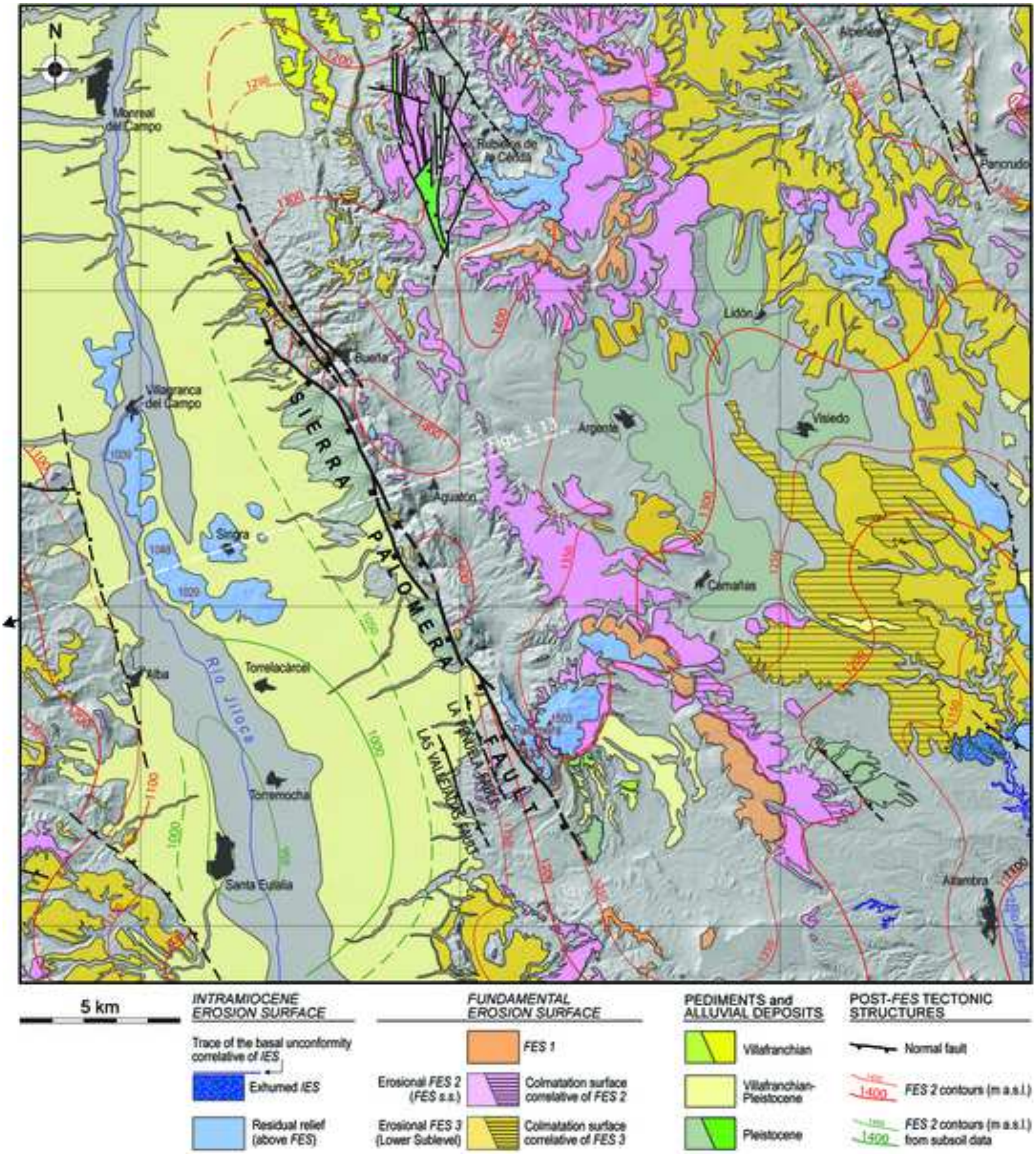

Figure

Click here to access/download;Figure (with caption below and on the same page);Fig 6bn.tif

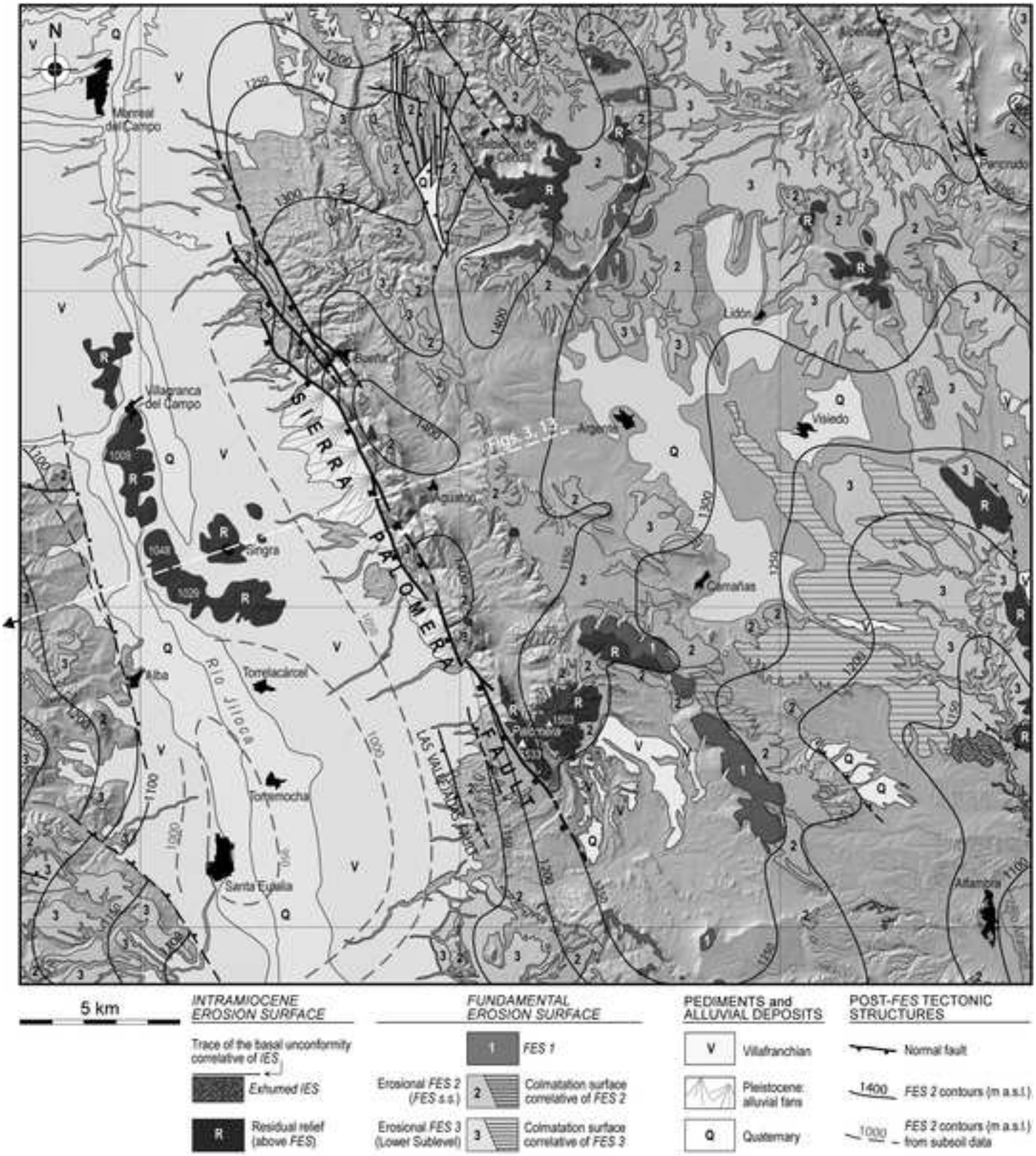

Figure

Click here to access/download;Figure (with caption below and on the same page);Fig 7.tif

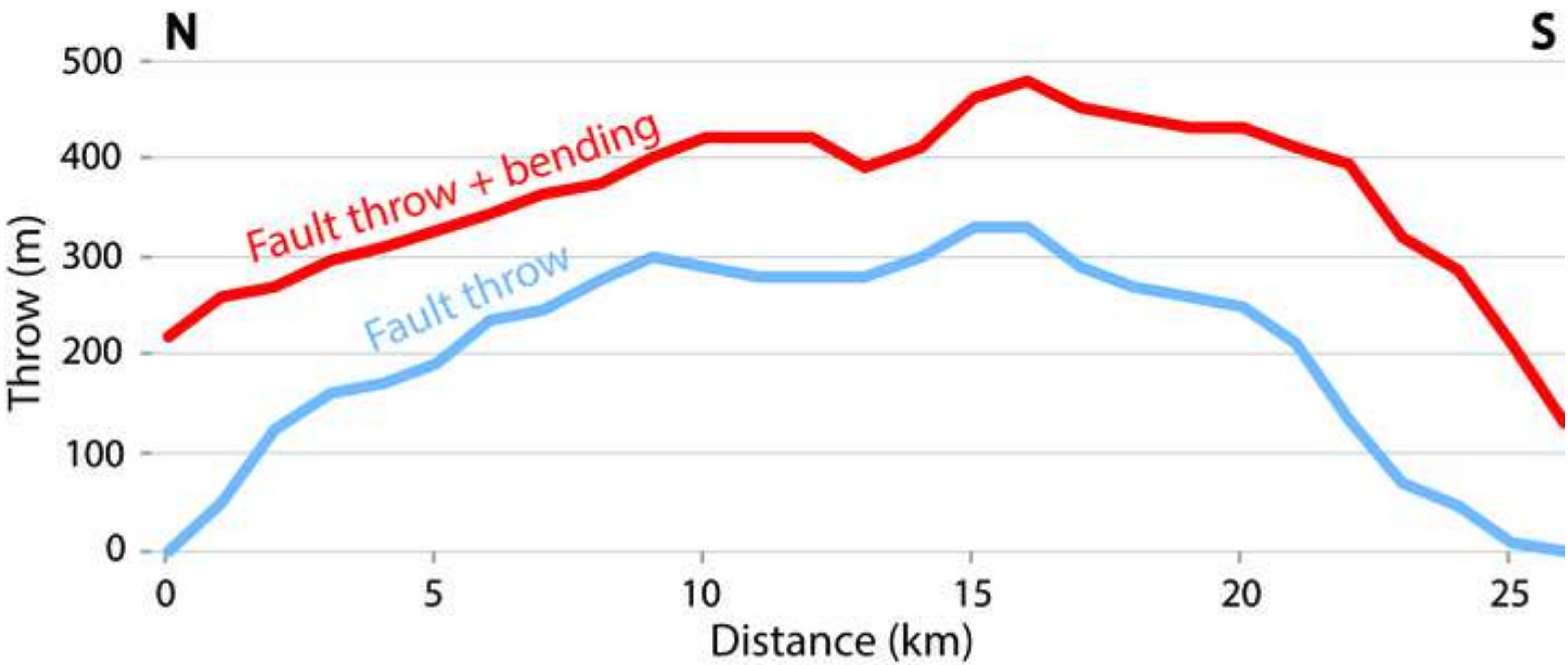

Figure

Click here to access/download;Figure (with caption below and on the same page);Fig 7bn.tif

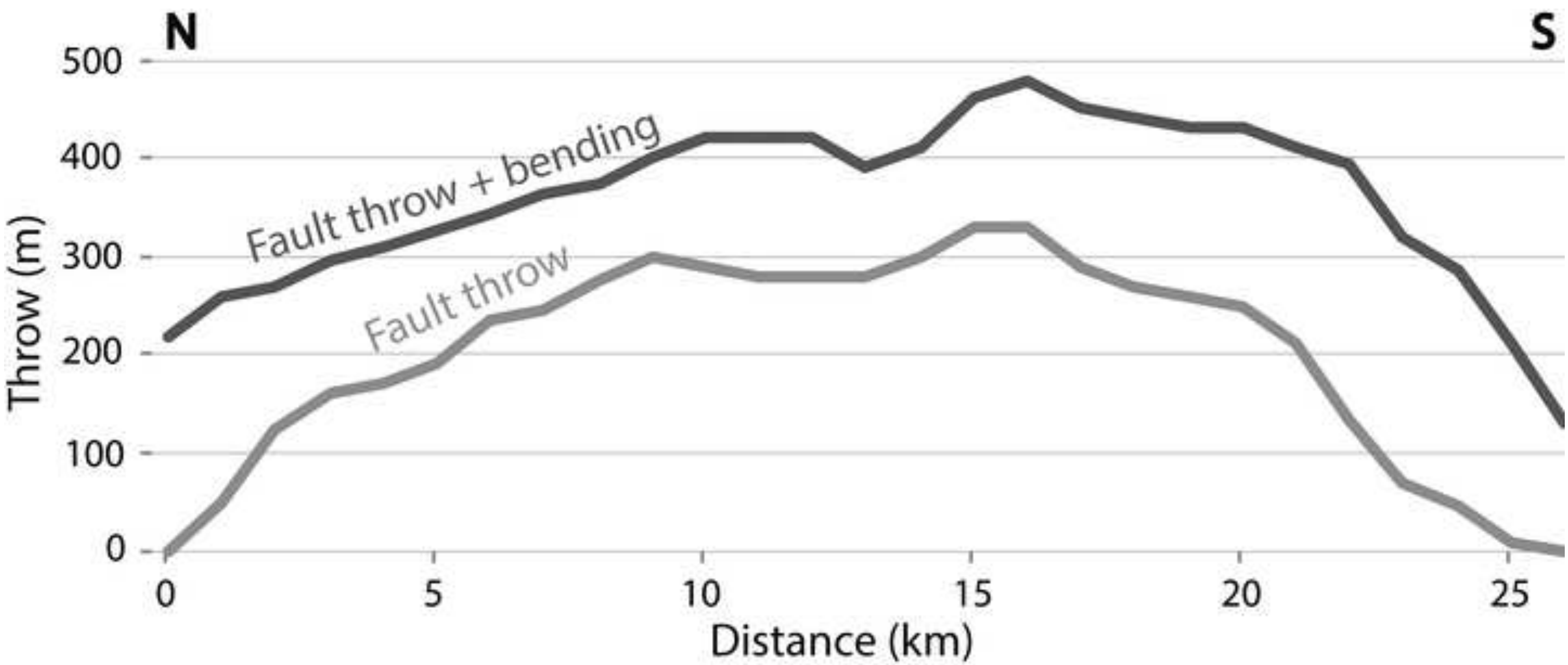


E
W


E
W

Figure

Click here to access/download;Figure (with caption below and on the same page);Fig 9.tif

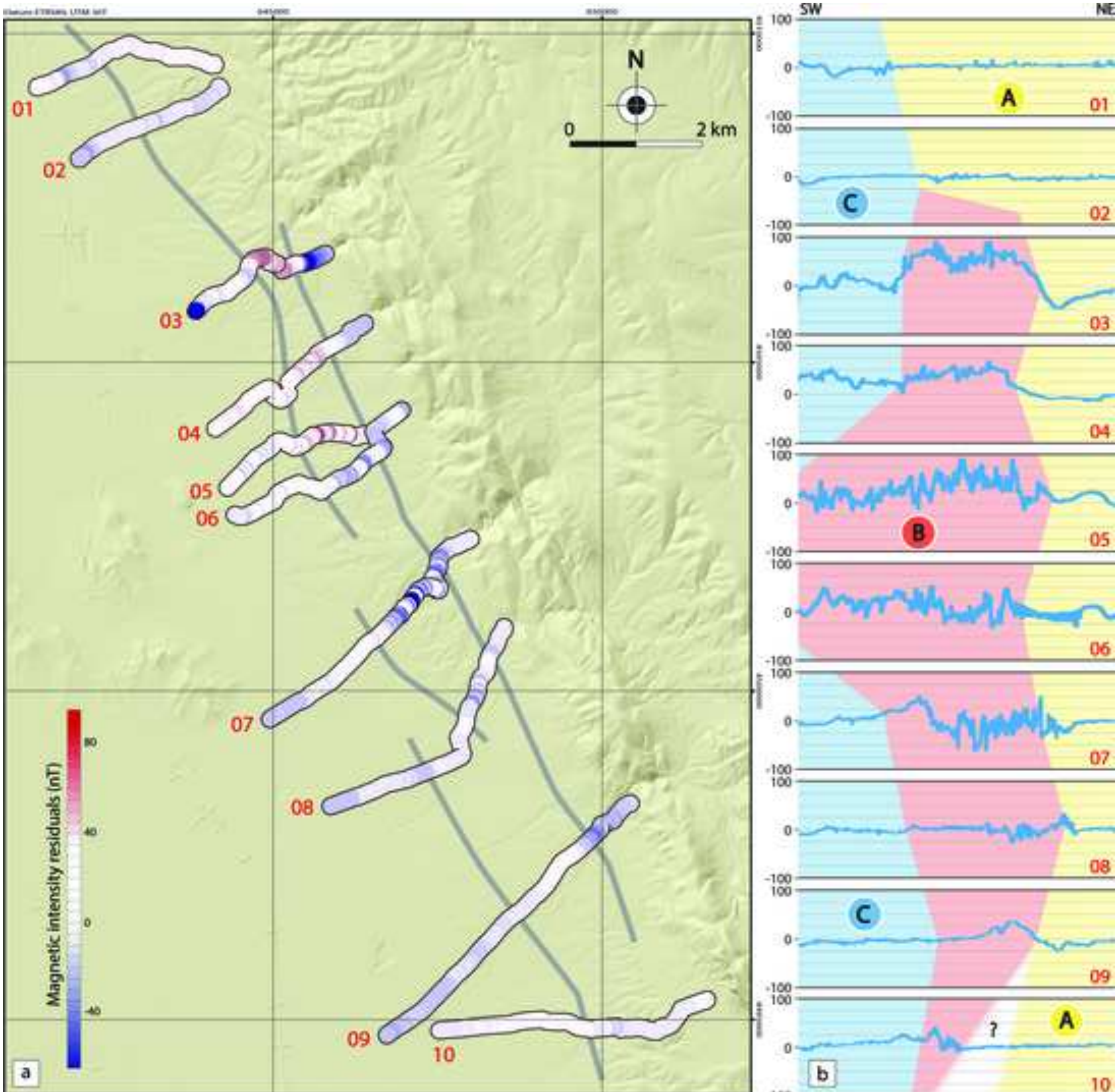

Figure

Click here to access/download;Figure (with caption below and on the same page);Fig 9bn.tif

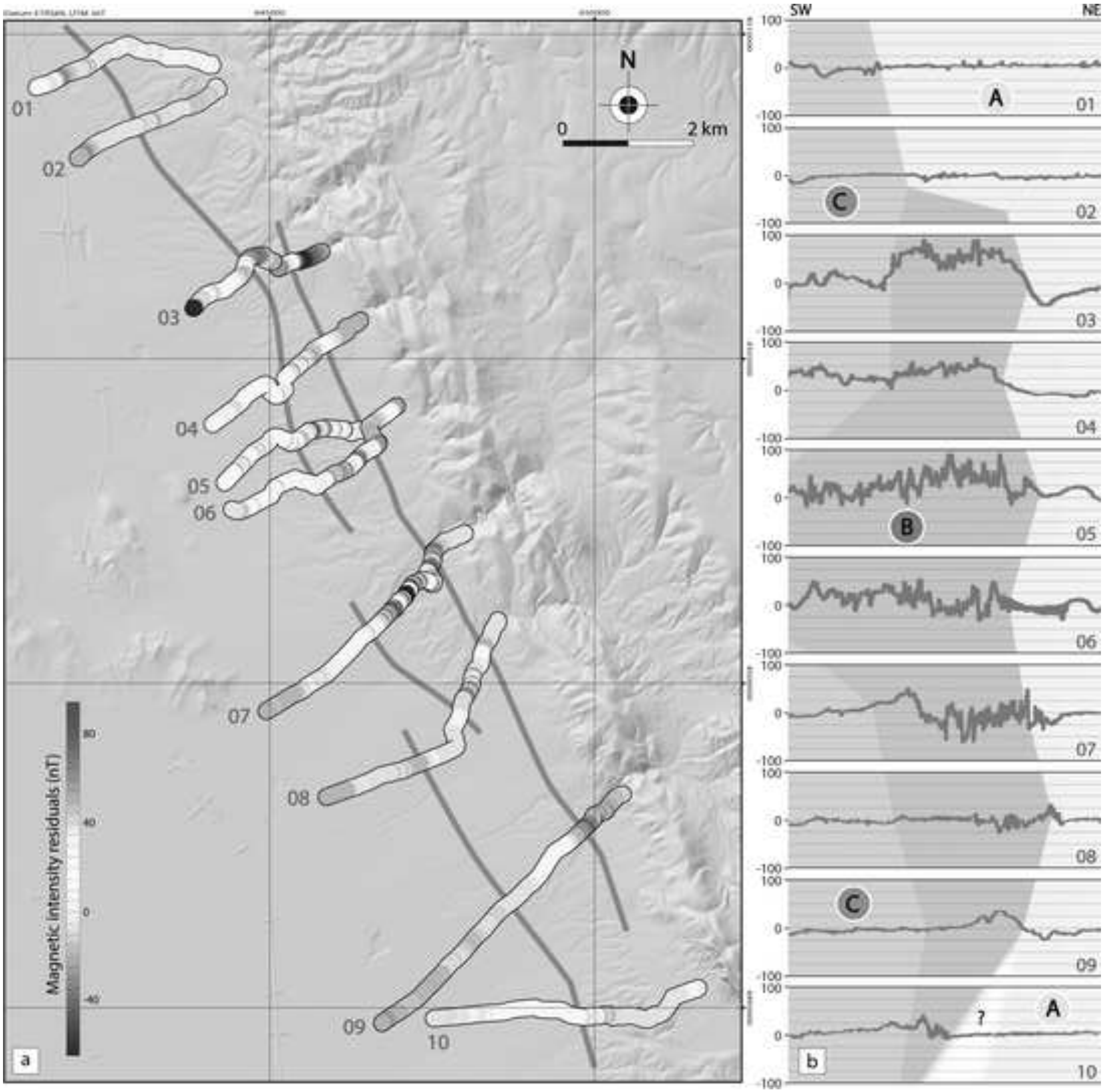

Figure

Click here to access/download;Figure (with caption below and on the same page);Fig 10.tif

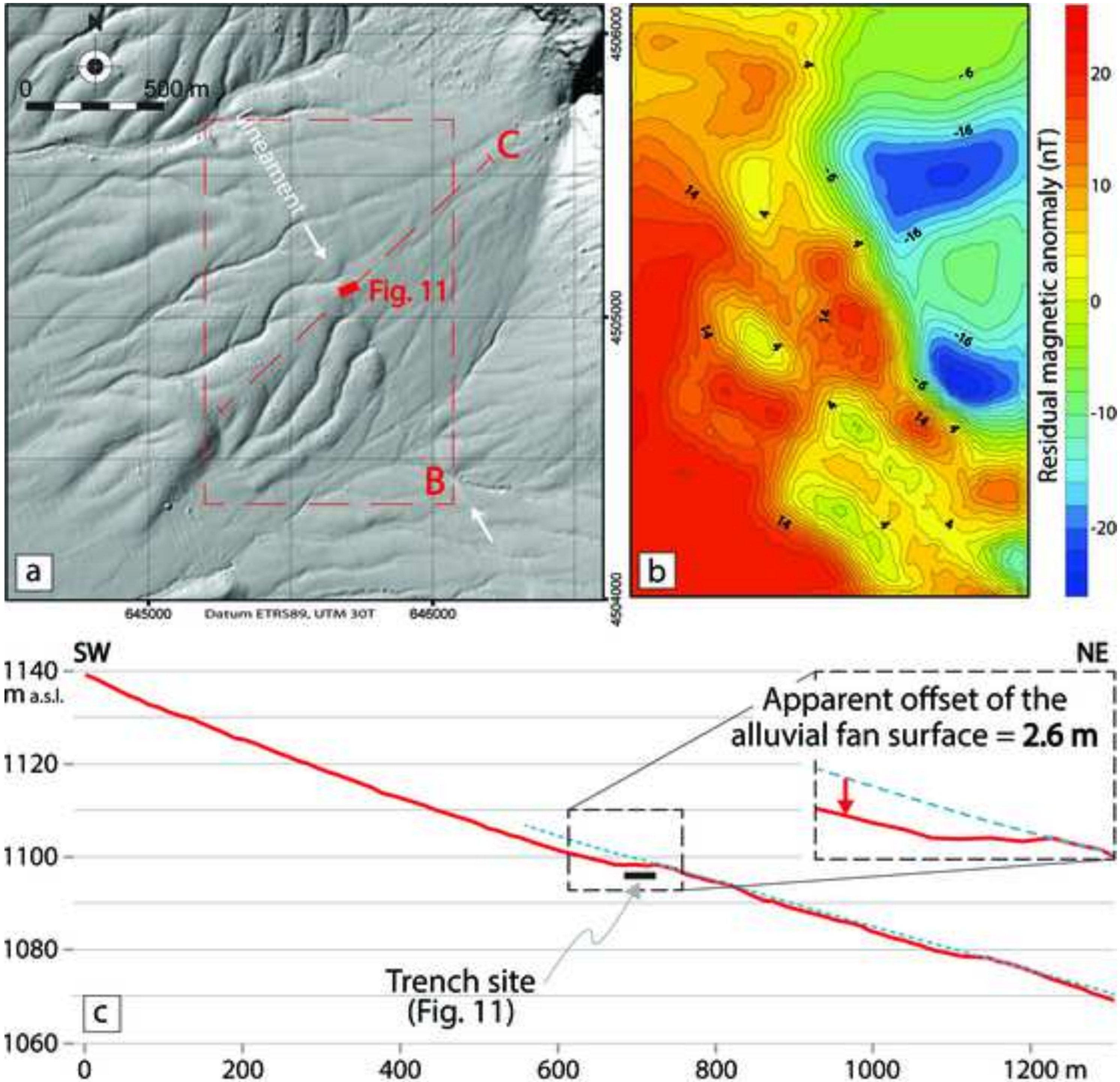

Figure

Click here to access/download;Figure (with caption below and on the same page);Fig 10bn.tif

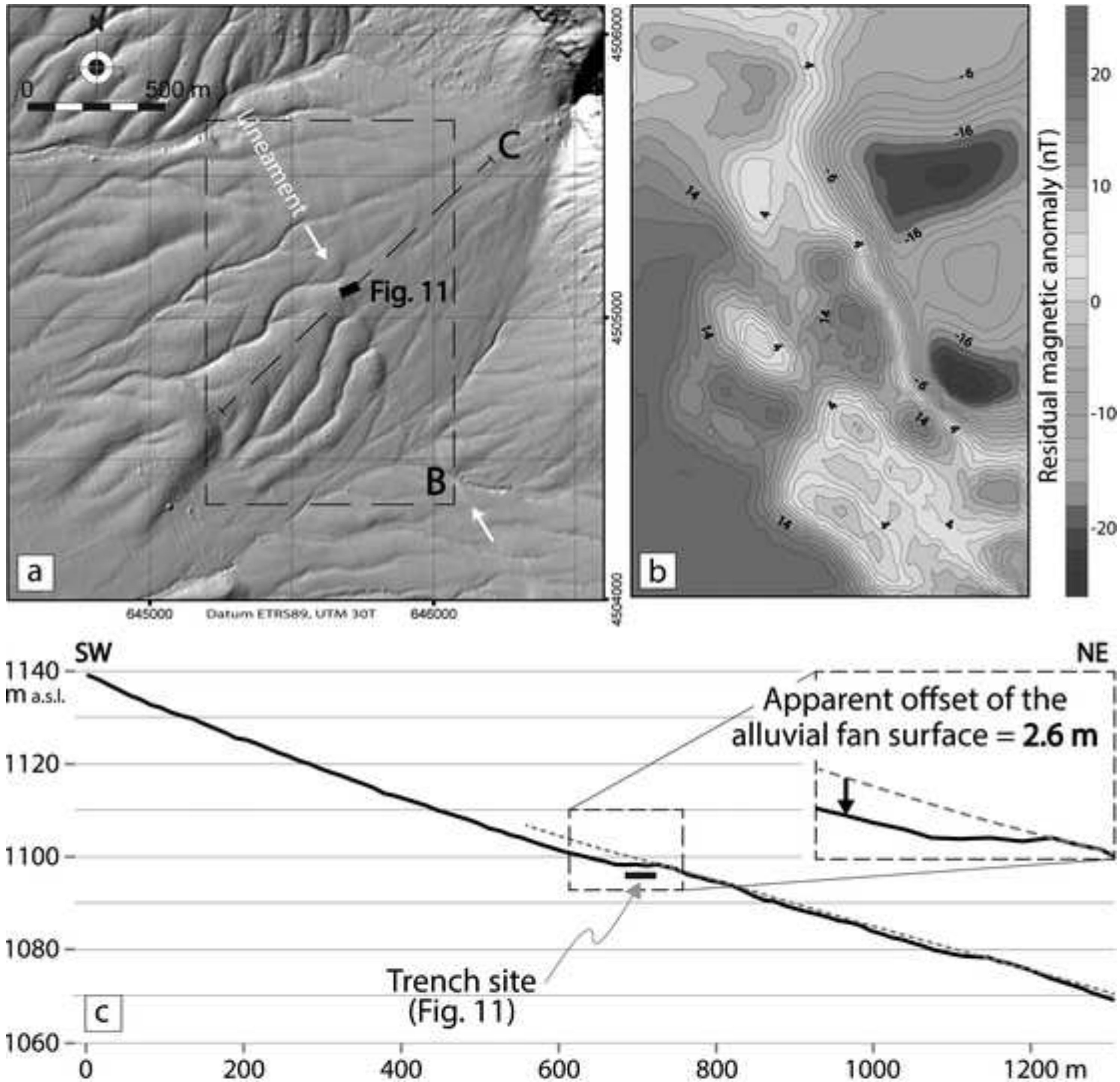

Figure

Click here to access/download;Figure (with caption below and on the same page);Fig 11.tif

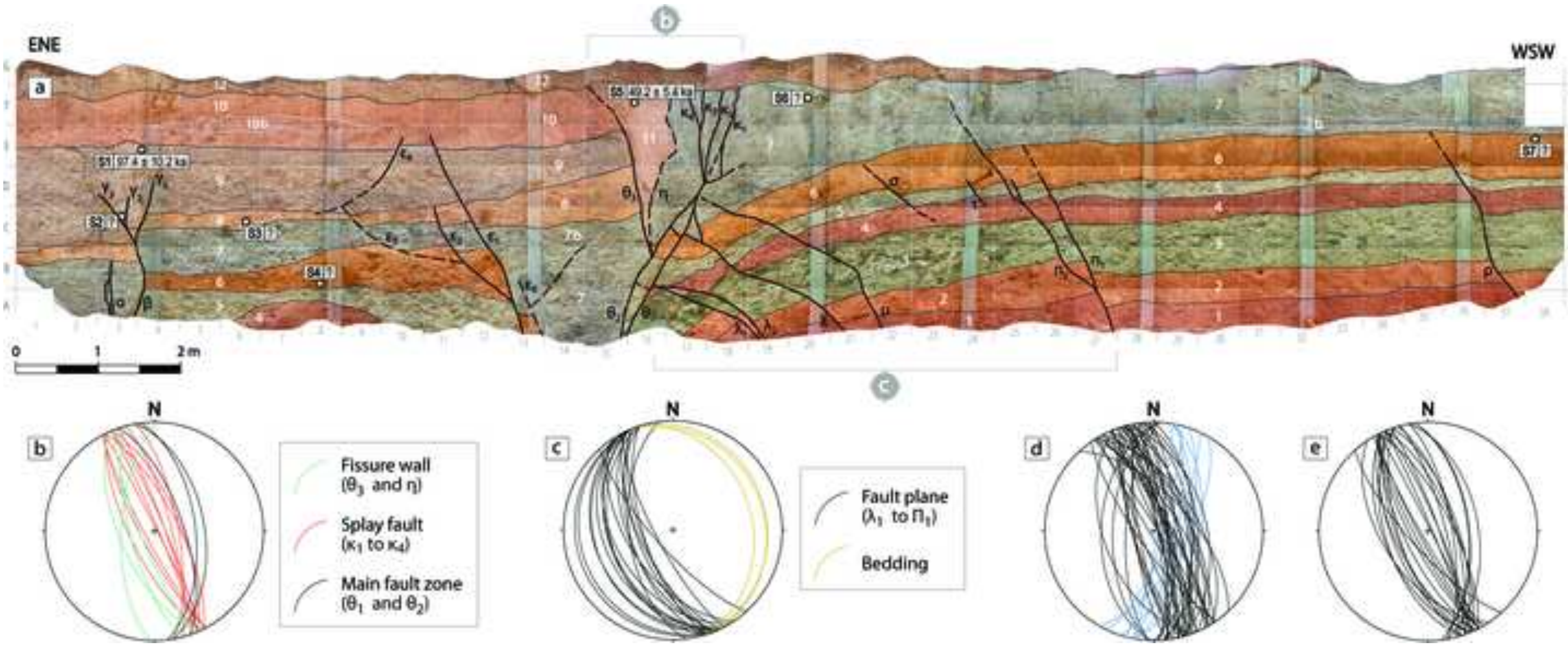

Figure

Click here to access/download;Figure (with caption below and on the same page);Fig 11bn.tif

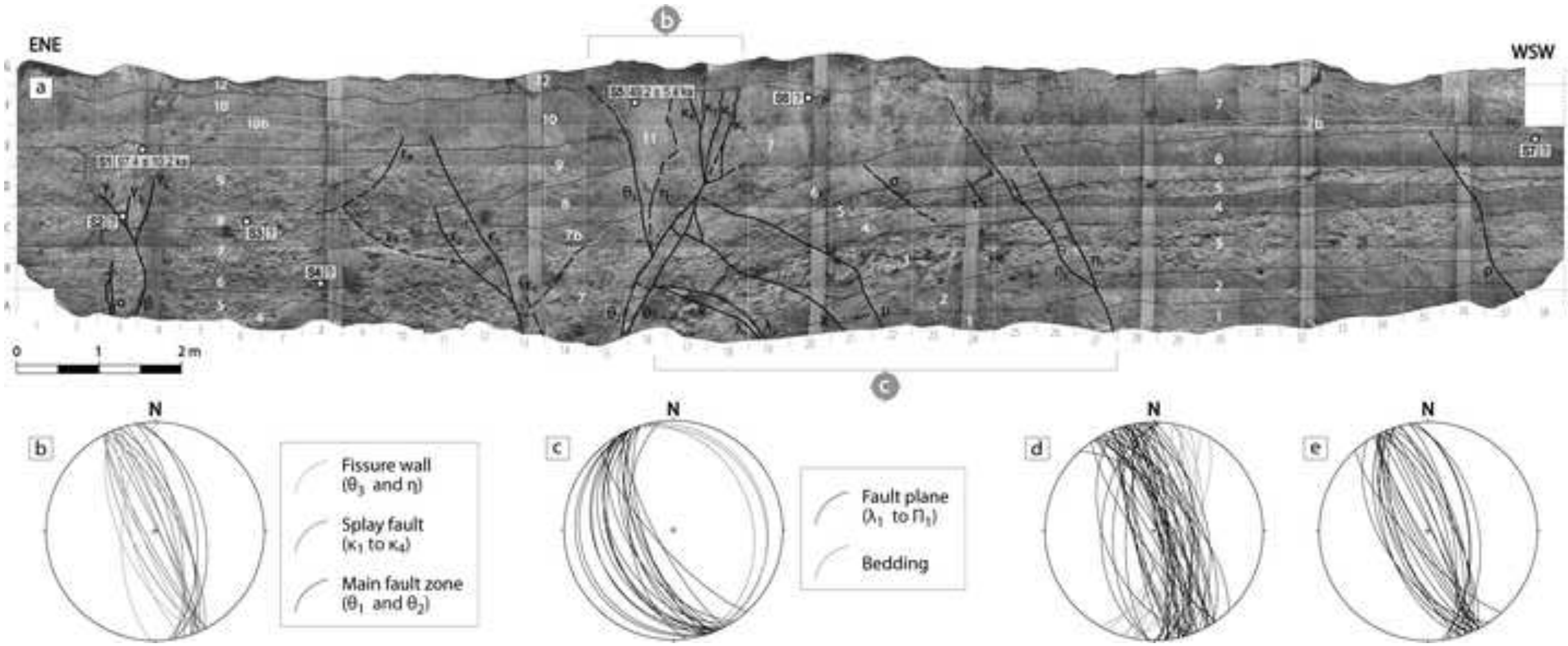

Figure

Click here to access/download;Figure (with caption below and on the same page);Fig 12bn.tif

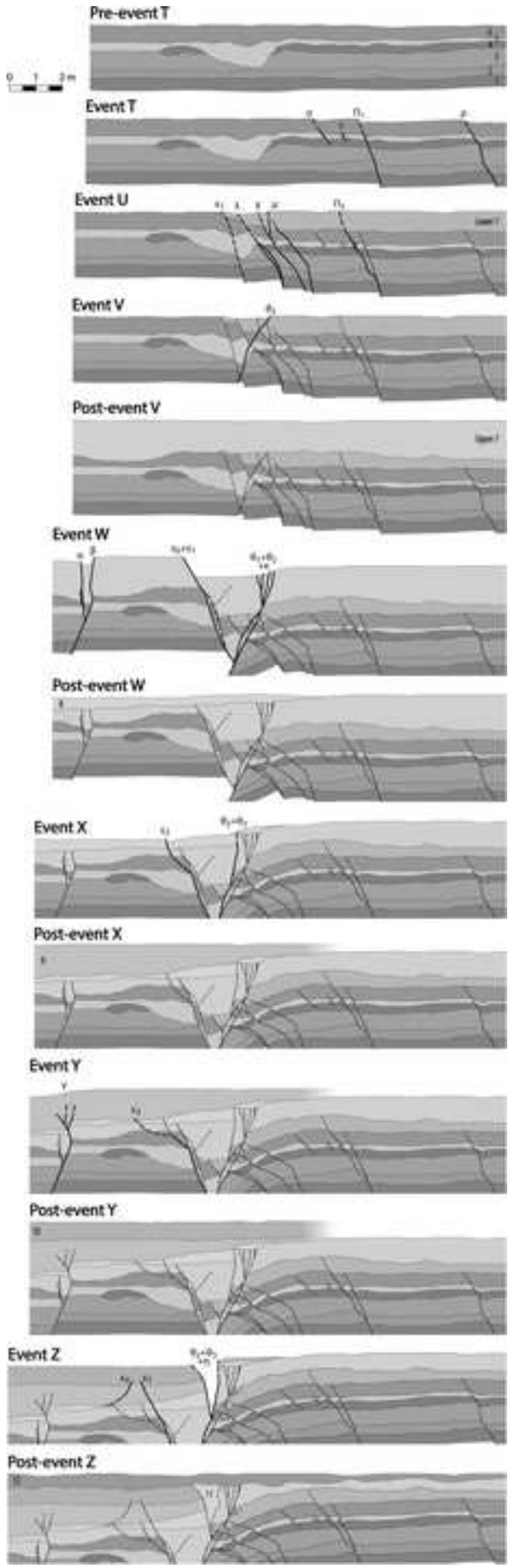

Figure

Click here to access/download;Figure (with caption below and on the same page);Fig 12.tif

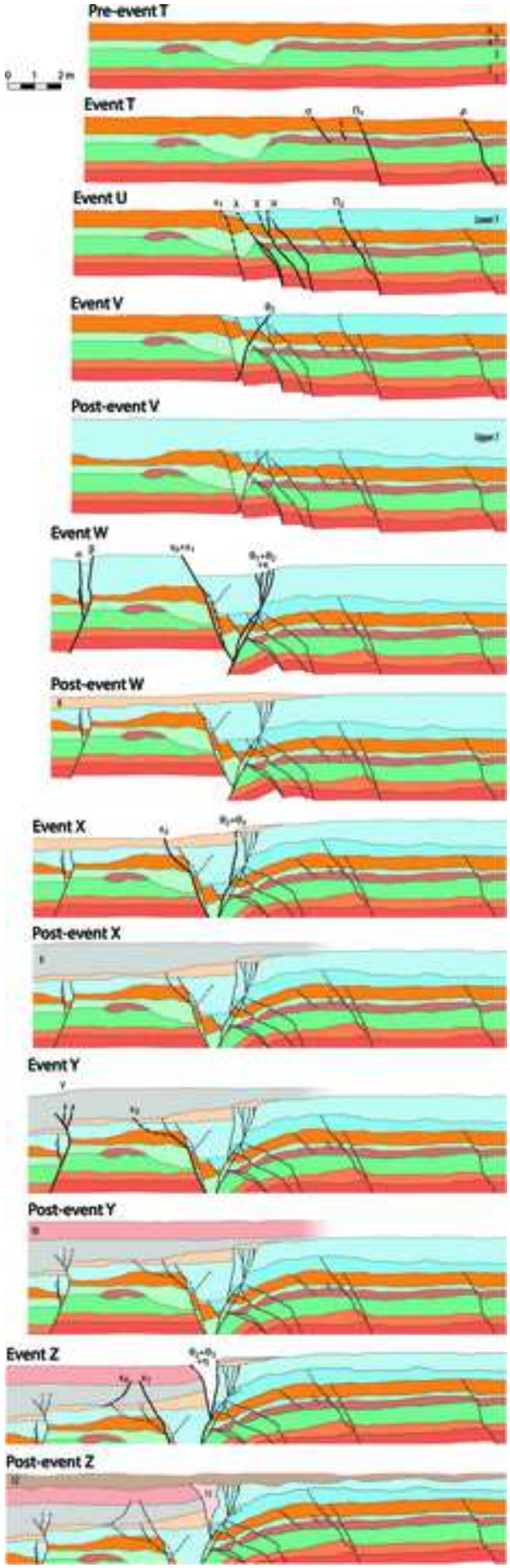

Figure

Click here to access/download;Figure (with caption below and on the same page);Fig 13.tif

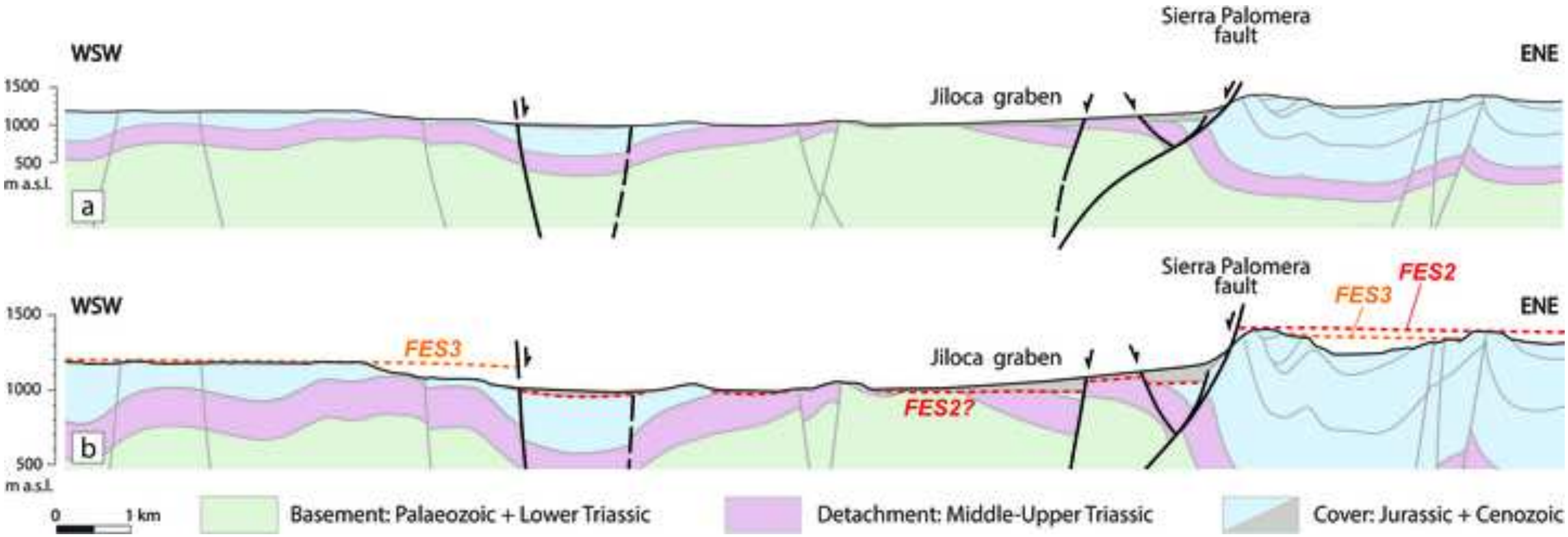

Figure

Click here to access/download;Figure (with caption below and on the same page);Fig 13bn.tif

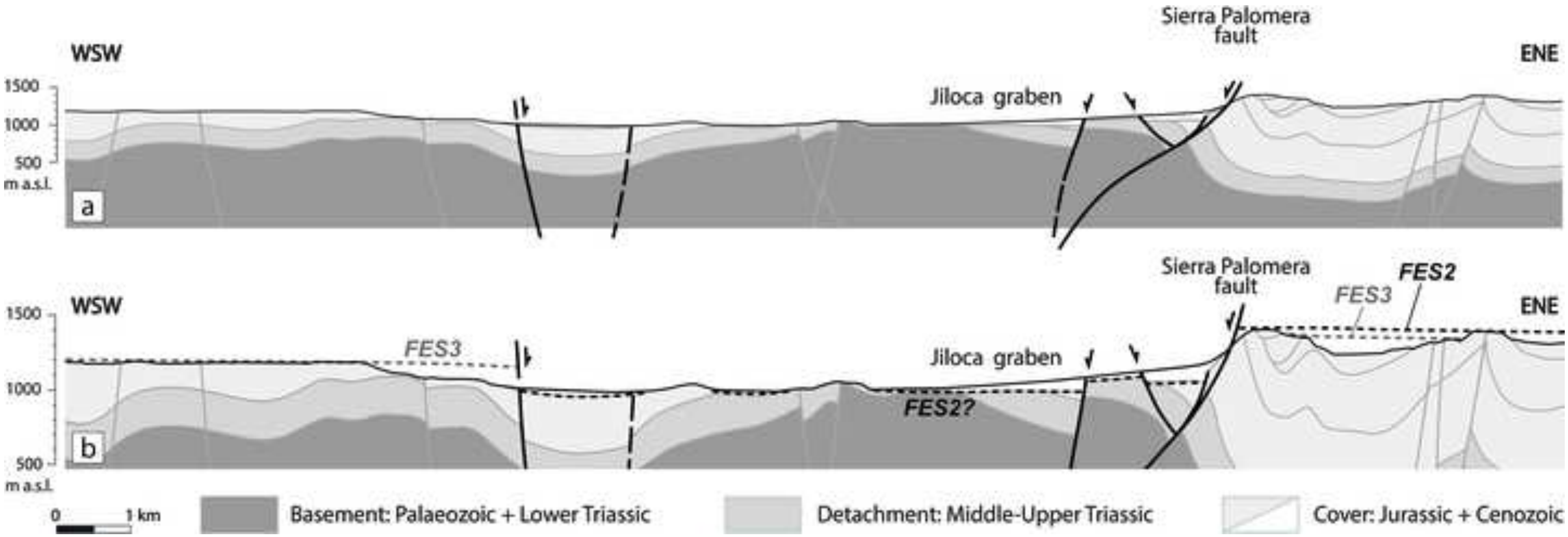

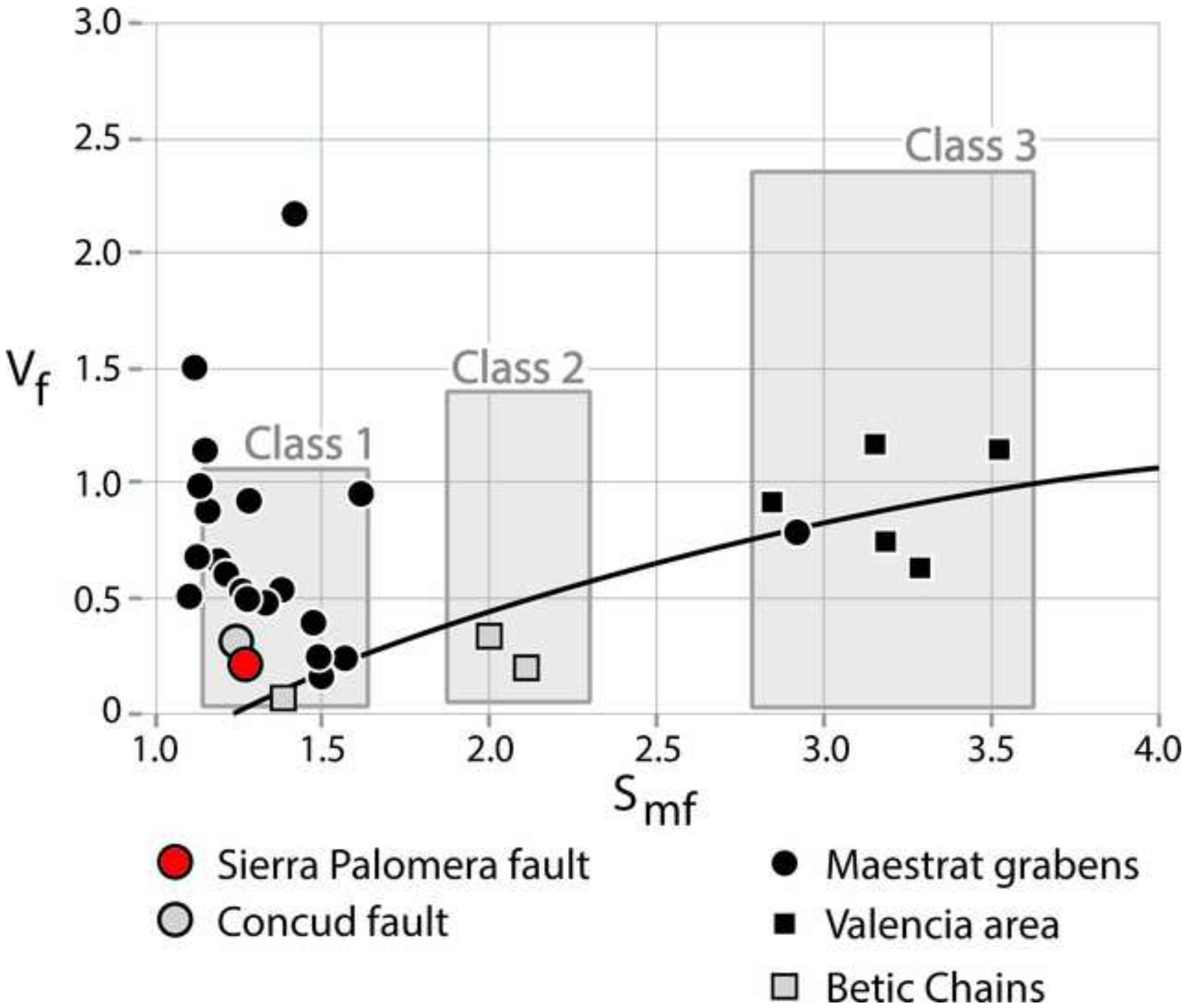

3.0
2.5
2.0
1.5
1.0
0.5
0
Vf
Class 1
Class 2
Class 3
1.0
1.5
2.0
2.5
3.0
3.5
4.0
Smf
Sierra Palomera fault
Concud fault
Maestrat grabens
Valencia area
Betic Chains

Figure

Click here to access/download;Figure (with caption below and on the same page);Fig 14bn.tif

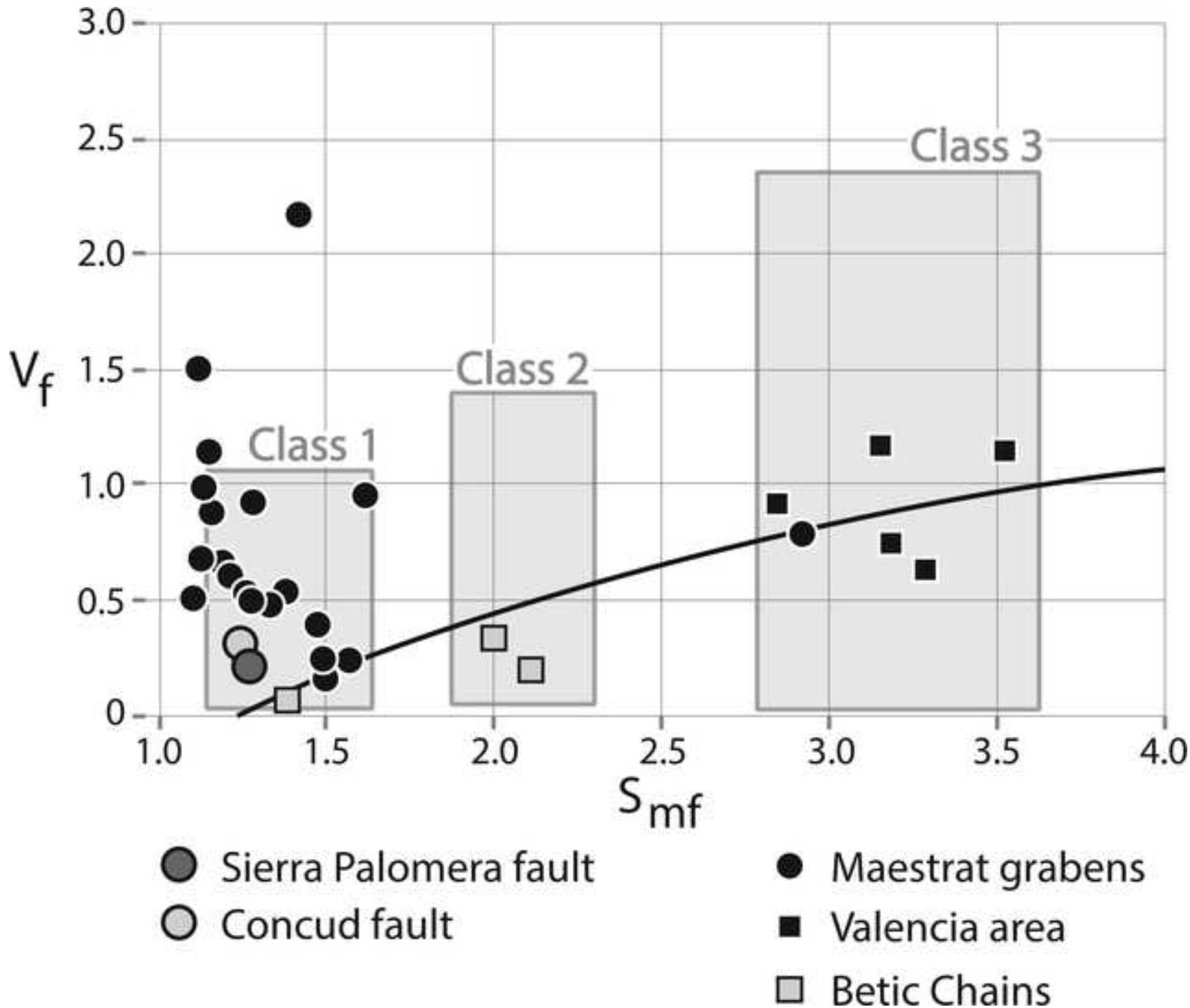

Figure

Click here to access/download;Figure (with caption below and on the same page);Fig 15.tif

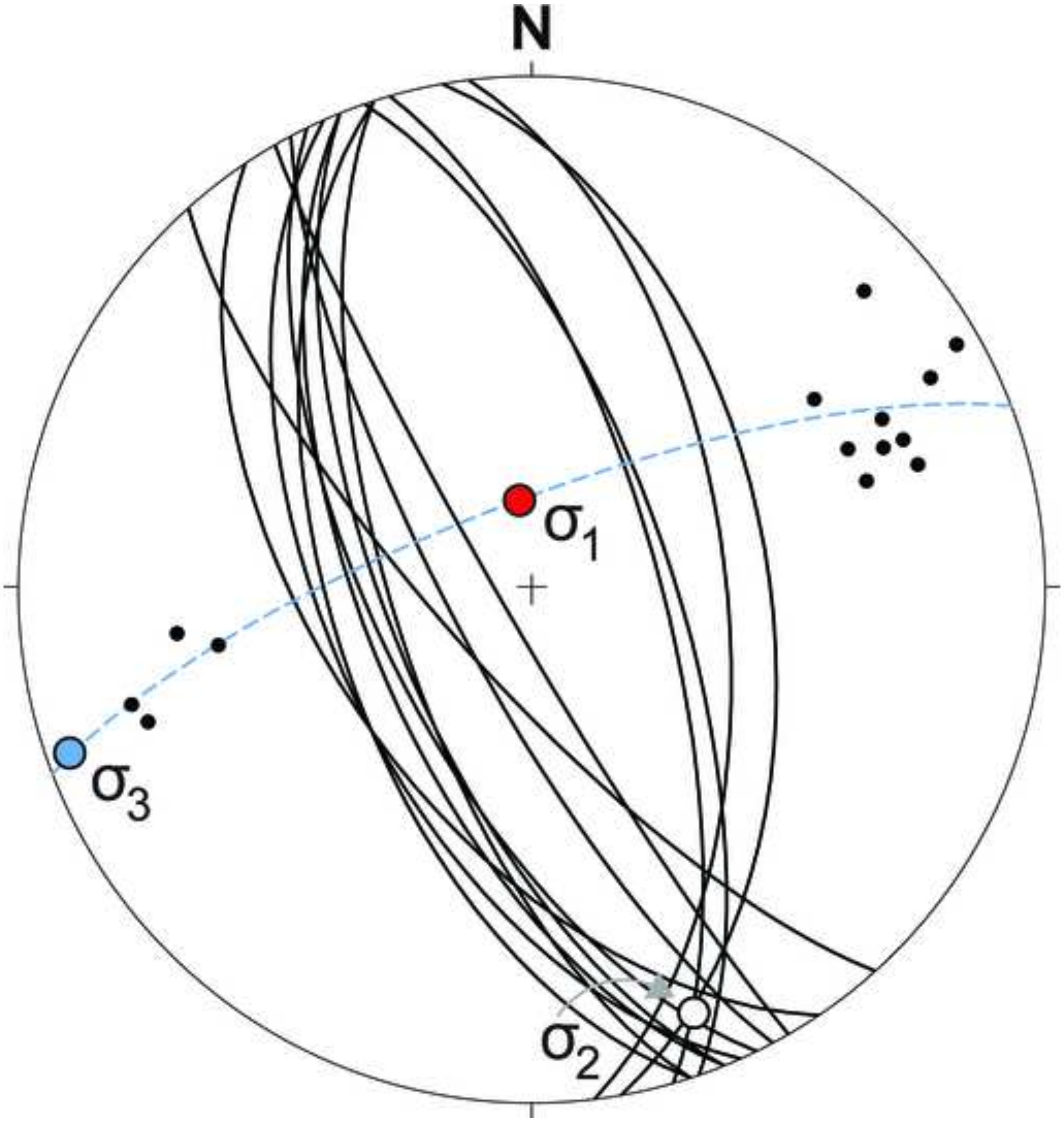

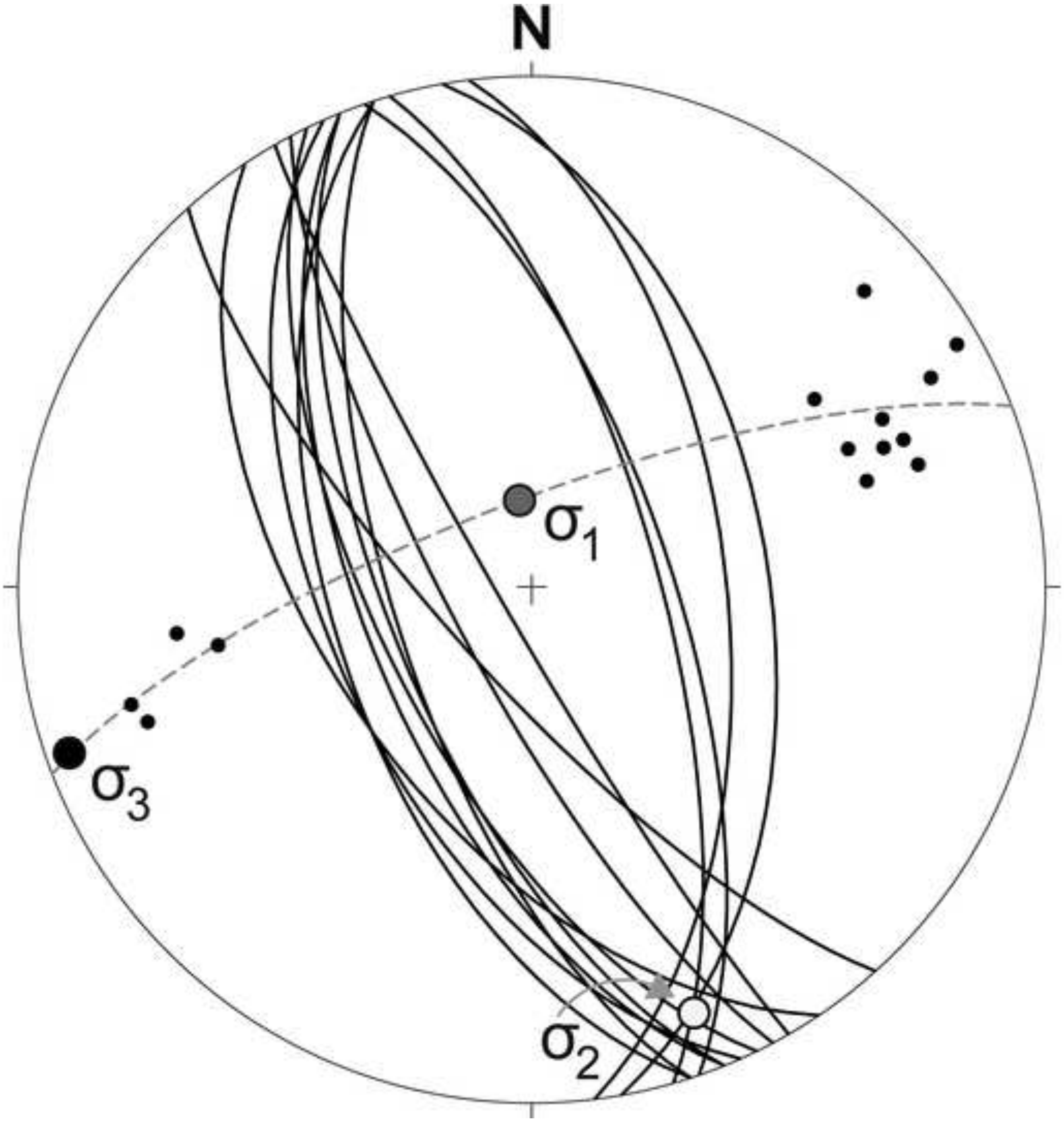

N
σ1
σ2
σ3

HIGHLIGHTS

- The Sierra Palomera fault bounds the central sector of the active Jiloca Graben
- This fault offsets ca. 480 m a mid-Pliocene (3.5 Ma) planation surface
- A large antithetic fault in the hanging-wall block accommodates simple shear associated to roll-over
- The antithetic fault was active during Late Pleistocene time
- Hanging-wall subsidiary faulting is controlled by both roll-over kinematics and the regional extensional stress field

Hanging-wall deformation at the active Sierra Palomera extensional fault (Jiloca basin, Spain) from structural, morphotectonic, geophysical and trench study

~~J.L. Simón[1], ~~A. Peiro[1], J.L. Simón[1]~~L.~~, L.E. Arlegui[1], L. Ezquerro[2], A.I. García-Lacosta[1], M.T. Lamelas[3], C.L. Liesa[1], A. Luzón[1], L. Martín-Bello[1], Ó. Pueyo-Anchuela[1], N. Russo[1]

[1]Departamento de Ciencias de la Tierra and GEOTRANSFER Research Group-IUCA, Universidad de Zaragoza, Pedro Cerbuna, 12, 50009 Zaragoza, Spain. ~~GEOTRANSFER Research Group-IUCA~~. apeiro@unizar.es jsimon@unizar.es~~, apeiro@unizar.es~~, arlegui@unizar.es, anagarcialacosta@hotmail.com, carluis@unizar.es, aluzon@unizar.es, leticia.martin.bello@gmail.com, opueyo@unizar.es, nausicarusso@gmail.com

[2]GEOBIOTEC, Department of Earth Sciences, NOVA School of Science and Technology, Campus de Caparica, P-2829 516 Caparica, Portugal. lopezque~~r~~rro@gmail.com

[3]Centro Universitario de la Defensa, Academia General Militar, Ctra. de Huesca s/n, 50090 Zaragoza, Spain. GEOFOREST Research Group-IUCA. tlamelas@unizar.es

Corresponding author: A. Peiro, apeiro@unizar.es

Abstract

The NNW-SSE trending Sierra Palomera fault is characterized as an active, nearly pure extensional fault with mean transport direction towards N230ºE, consistent with the ENE-WSW extension trajectories of the recent to present-day regional stress field. Its macrostructure is described from surface geology and magnetometric and electromagnetic surveys, which have allowed identifying two subsidiary, nearly parallel normal faults (antithetic and synthetic, respectively). The structural contour map of an extensive planation surface, dated to 3.8 Ma, provides a maximum fault throw *s.s.* of 330 m for the main fault (480 m including bending), and a net slip rate of 0.09 mm/a (0.13 mm/a including bending). Trench study focussed on the subsidiary antithetic fault shows evidence of its activity during Middle-Late Pleistocene times, offsetting ca. 2.5~~6~~ m the slope of a well-preserved alluvial fan. Detailed analysis and retrodeformation of the antithetic fault and other minor ruptures in the trench has allowed defining seven deformation events. The lack of a consistent age model for the involved sedimentary sequence makes them almost meaningless in terms of paleoseismic history. However, geometry and sequential development of meso-scale faults (intermediate between seismic-scale and analogue models) allows unravelling the extensional deformation ~~mechanisms~~ history within the hanging-wall block of the Sierra Palomera fault. Progressive rupture patterns reveal shifting from dominantly synthetic to dominantly antithetic faulting,~~,~~ suggesting both kinematical control linked to rollover growth, and dynamical control by the regional stress field.

Keywords: Active fault, antithetic fault, rollover, magnetometry, Pleistocene, Iberian Chain.

1. Introduction

Our understanding of geometry and kinematics of extensional fault systems has been significantly improved thanks to analytical and scaled analogue models, particularly concerning deformation of the hanging-wall block of listric faults. Such models provide interesting inferences about controls that the shape of the main fault surface exerts on the development of hanging-wall folds and fractures. Fault surfaces with irregular geometry induce antithetic simple shear along a deformation band that nucleates at shallowing fault bends, while synthetic shear is induced at steepening fault bends (McClay and Scott, 1991; Xiao and Suppe, 1992; Withjack *et al.*, 1995; Delogkos *et al.*, 2020). Depending on the mechanical ~~properties~~ behaviour of materials, such overall simple shear mechanism results in either fault-related folding (rollover and drag folds, respectively) or faulting (antithetic and synthetic, respectively). Analogue models provide insights into both differential behaviours, *e.g.*, by comparing experimental materials as clay and sand (*e.g.*, Withjack *et al.*, 1995). Nevertheless, as discussed by Xiao and Suppe (1992), models give limited information about the actual small-scale mechanisms that accommodate deformation. Therefore, contribution of data directly supplied by field examples is necessary for full understanding of kinematics of extensional systems.

~~Methodology of trench analysis, extensively used and standardized for paleoseismological studies (*e.g.*, McCalpin, 1996), offers new insights for detailed analysis of progressive extensional deformation. Each identified paleoseismic event can be considered as an incremental or ‘infinitesimal’ deformation episode, and hence the reconstructed paleoseismic sequence provides a realistic view of extension kinematics (although ineludibly constrained to a given space and time window).~~

The Sierra Palomera fault, at the central sector of the Jiloca basin, is one of the most conspicuous recent, hypothetically active extensional faults in the central Iberian Chain (Spain; Fig. 1), but less known than other neighbouring structures. The Calamocha and

Concud faults, which bound the northern and southern sectors of the Jiloca basin (Fig. 1c), offset early Pliocene lacustrine deposits of the Calatayud and Teruel basins, respectively. This allows calculating their total throws at about 210 m for the Calamocha fault (Martín-Bello *et al.*, 2014), and 260 m for the Concud fault (Ezquerro *et al.*, 2020). On the contrary, no recent stratigraphic marker is available for the Sierra Palomera fault. The tectonic nature of the basin boundary itself, and particularly the relative role of erosive lowering and fault displacement in the creation of the mountain scarp, has been the object of controversy indeed. After Cortés and Casas (2000), its topography is essentially a result of erosive incision in response to orogenic uplift during the Paleogene. Gracia *et al.* (2003) reinterpret the Jiloca depression as a polje developed during the Late Pliocene-Quaternary. Rubio and Simón (2007) and Rubio *et al.* (2007) provide new sedimentary, geomorphological and hydrogeological evidence on the tectonic origin of the Jiloca depression, concluding that the Sierra Palomera fault has a maximum throw approaching 350-400 m.~~. Nevertheless, in contrast with other neighbouring faults (Concud, Teruel, Valdecebro, Calamocha, Munébrega faults), in which numerous trench studies have been carried out in the last two decades (Gutiérrez *et al.*, 2009; Lafuente, 2011; Lafuente *et al.*, 2011a, 2014; Martín-Bello *et al.*, 2014; Simón *et al.*, 2016, 2017, 2019), no paleoseismological analysis has been developed in the Sierra Palomera fault owing to lack of appropriate sites for digging a trench at the main fault zone.~~

~~The Sierra Palomera fault belongs to the Jiloca graben, the youngest Neogene-Quaternary basin of the central-eastern Iberian Chain (eastern Spain; Fig. 1) linked to rifting of the Valencia Trough (Vegas *et al.*, 1979). In overall, it is a half-graben that exhibits a NNW-SSE trend resulting from en-échelon, right-lateral arrangement of NW-SE striking normal faults at its eastern, active border. This basin has developed since Late Pliocene time, under a nearly biaxial or multidirectional extension regime ($\sigma_2 \approx \sigma_3$) with maximum extension trajectories (σ_3) oriented ENE-WSW (Simón, 1983, 1989; Arlegui *et al.*, 2005; Liesa *et al.*, 2019).~~

[PREFERENTIALLY, FIG.1 SHOULD BE INSERTED HERE, AS A 2-COLUMN FIGURE]

~~The northern and southern sectors of the Jiloca basin are bounded by the Calamocha and Concud faults, respectively (Fig. 1c). Both faults cut and offset the uppermost, early Pliocene lacustrine deposits of the neighbouring Calatayud and Teruel basins, respectively. Based on clearly recognized stratigraphic markers, the corresponding maximum throws are calculated at about 210 m for the Calamocha fault (Martín-Bello *et al.*, 2014), and 260 m for the Concud fault (Ezquerro *et al.*, 2020).~~

~~In the central segment of the basin (Fig. 2), the displacement at the Sierra Palomera fault cannot be calculated in the same way since no recent stratigraphic marker is available. The tectonic nature of the boundary itself, and particularly the discrimination between the role of erosive lowering and vertical tectonics in the creation of the mountain scarp has been the object of controversy indeed. After Cortés and Casas (2000), its topography is essentially a result of erosive incision in response to orogenic uplift. Gracia *et al.* (2003) reinterpret the Jiloca depression as a polje, developed during Late Pliocene-Quaternary times on an incipient half graben. Rubio and Simón (2007) and Rubio *et al.* (2007) analyse these arguments and provide new sedimentary, geomorphological and hydrogeological evidence on the tectonic origin of the Jiloca depression, from both surface and subsoil data. These authors conclude that: (i) the basin is a tectonic graben limited by Plio-Quaternary faults; (ii) the Sierra Palomera fault has a maximum throw approaching 350-400 m; and (iii) although the basin is noticeably underfilled, its sedimentary infill shows thickness and facies distribution consistent with such basin model.~~

~~*[PREFERENTIALLY, FIG.2 SHOULD BE INSERTED HERE, AS A 1.5-COLUMN FIGURE]*~~

Concerning the signs of Quaternary activity, these are again conspicuous in the northern and southern sectors of the Jiloca graben but not in the central one. The Concud fault has been object of intense paleoseismological research~~ at both natural outcrops and trenches~~, which ~~have~~ has allowed reconstructing a ~~wide paleoseismic~~ succession of eleven events since ca. 74 ka BP~~ to the present day~~, with average recurrence period of 7.1-8.0 ka, total accumulated net ~~accumulated~~ slip of about 20 m, and average slip rate of 0.29 mm/a (Lafuente, 2011; Lafuente *et al.*, 2011a,b, 2014; Simón *et al.*, 2016). Quaternary activity of the Calamocha fault is revealed by the mechanical contact between Neogene units of the Calatayud basin and Late Pleistocene alluvial deposits that infill the northernmost Jiloca basin~~.~~ ~~Three distinct fault branches are well exposed at the slopes of the A-23 highway and an industrial area in the neighbourhoods of Calamocha town~~ (Martín-Bello *et al.*, 2014). Other neighbouring faults (Munébrega, Teruel, Valdecebro) have also been object of trench studies in the last two decades (Gutiérrez *et al.*, 2009; Simón *et al.*, 2017, 2019).

On the contrary, no exposure of the Sierra Palomera fault cutting Quaternary deposits has been ~~described~~reported, and no paleoseismological analysis has been carried out. This~~It~~ is mainly due to the fact that the Quaternary fluvial incision is virtually absent, and there is a lack of appropriate sites for digging trenches across the main fault. ~~Endorheic conditions in this sector have remained until historical times, with development of a palustrine area at the~~

~~basin centre (ancient Cañizar lake; Rubio and Simón, 2007). Observation of Quaternary surficial ruptures has not been possible, thus their evidence is only indirect.~~

In such a situation, the study of the Sierra Palomera fault should be focussed on obtaining indirect evidence of its recent activity from hanging-wall deformation. This can be achieved by (i) exploring the subsoil of the associated pediment by means of geophysical techniques, (ii) analysing the effects of fault activity on the relief through morphotectonic analysis, and (iii) recognizing deformation of Quaternary materials in trenches. Methodology of trench analysis, extensively used and standardized for paleoseismological studies (*e.g.*, McCalpin, 2009), offers new insights for detailed analysis of progressive extensional deformation. Concerning scale, trenches have the advantage of delivering valuable information on faults at an intermediate scale between seismic profiles and laboratory analogue models. Concerning timing, each identified event can be considered as an incremental or 'infinitesimal' deformation episode, and hence the reconstructed paleoseismic succession provides a detailed and realistic view of extension kinematics (although ineludibly constrained to a given space and time window).

The ~~purpose of the~~ present work has been carried out in that perspective. ~~is contributing to fill this gap, with three~~Our specific objectives are: (~~i~~1) improving our overall knowledge on the structure and evolution of the Sierra Palomera fault and the Jiloca basin; (2~~ii~~) reporting evidence on the activity of the Sierra Palomera fault during the Quaternary, and (3~~iii~~) characterizing the ~~style~~ patterns of progressive extensional deformation within its hanging-wall block. ~~Especial attention will be paid to structural features that indicate recent activity of the Sierra Palomera fault and other structures associated to it, showing how geophysical exploration provides complementary subsoil information with that respect. We will go deeper into the morphotectonics of the area, analysing the effects of fault activity on the relief. In the absence of stratigraphic markers, extensive Late Neogene planation surfaces existing in the region will be especially useful as geomorphological markers of deformation. Finally, we will address a detailed analysis of ruptures within a portion of the hanging-wall block of the Sierra Palomera fault by using trenching techniques.~~

2. Geological setting

The Iberian Chain is a NW-SE trending, 450 km long intraplate mountain range located in the eastern Iberian Peninsula (Fig. 1a). This chain developed in Paleogene to Early Miocene times due to positive inversion of the extensional Mesozoic Iberian basin, under the convergence between the Africa and Eurasia plates. ~~, under which an heterogeneous ensemble of fold-and-thrust belts, depicting a roughly double-vergence structure, was built by positive inversion of the extensional Mesozoic Iberian basin~~ (Álvaro *et al.*, 1979; Guimerà and Álvaro, 1990; Capote *et al.*, 2002; Liesa *et al.*, 2018). After a transition period during the Early Miocene, in which the longitudinal Calatayud basin developed under a transpressional regime (Colomer and Santanach, 1988; Simón *et al.*, 2021), a new extensional stage associated to rifting of the Valencia Trough took place.

Extensional deformation propagated onshore towards the central part of the Iberian Chain (Álvaro *et al.* 1979, Vegas *et al.*, 1979) in two stages, inducing both reactivation of the main inherited Mesozoic faults and formation of new normal faults, and generating a number of diversely oriented intracontinental grabens and half-grabens (Simón, 1982, 1989; Gutiérrez *et al.*, 2008, 2012; Ezquerro, 2017; Liesa *et al.*, 2019).

~~Relationships of extensional macrostructures with geomorphic features and stress evolution in the Iberian Chain allow defining two main extensional phases.~~ During the first ~~phase~~ stage (Late Miocene to Early Pliocene in age), the 90-km-long, NNE-SSW to N-S trending Teruel half-graben basin developed, filled with terrestrial sediments up to 500 m thick (Simón, 1982, 1983; Moissenet, 1983; Anadón and Moissenet, 1996; Ezquerro, 2017; Ezquerro *et al.*, 2019, 2020). ~~Throughout this period, the Teruel basin propagated northwards, acquiring a N-S trend at its northern sector (El Pobo fault zone; Fig. 1b; Ezquerro *et al.*, 2019, 2020), while other N-S trending half-grabens were settled in its footwall block (western and eastern El Pobo basins; Simón-Porcar *et al.*, 2019). The~~ The second extensional ~~phase~~ stage that started by~~in~~ the ~~Late~~ mid-Pliocene ~~and shows~~ has produced a more widespread deformation i~~. I~~n the central Iberian Chain.~~,~~ ~~a~~A large number of ~~compressional and extensional~~inherited structures were reactivated, producing new NNW-SSE trending grabens and half-grabens that are inset or cross-cut the pre-existent Teruel and Calatayud basins (Simón, 1983, 1989; Gutiérrez *et al.*, 2008, 2020; Liesa *et al.*, 2019). They include, among others (Fig. 1c), ~~: (i)~~ the 80-km-long Jiloca graben, which results from en-échelon, right releasing arrangement of the NW-SE striking Concud, Sierra Palomera and Calamocha faults (Simón, 1983; Rubio and Simón, 2007; Simón *et al.*, 2012, 2017; Peiro *et al.*, 2019, 2020).~~; (ii) the 30-km-long Daroca half-graben (Colomer, 1987; Gracia, 1992; Gutiérrez *et al.*, 2008, 2020; Casas *et al.*, 2018); (iii) the 88-km-long Río Grío-Pancrudo Fault Zone, made of two main faults, Río Grío-Lanzuela and Cucalón-Pancrudo (Peiro and Simón, 2021).~~ In the first extensional phase, the direction of maximum extension (σ_3) was E-W to ESE-WNW (under a triaxial extensional regime), ~~whereas~~ while 'multidirectional' extension with ENE-WSW σ_3

trajectories characterizes the second phase (Simón, 1982, 1983, 1989; Cortés, 1999; Capote *et al.*, 2002; Arlegui *et al.*, 2005, 2006; Liesa, 2011; Ezquerro, 2017; Liesa *et al.*, 2019). ~~Regional uplift during the Late Pliocene-Quaternary resulted in: (i) constraining sedimentation to underfilled residual basins, with a modest sedimentary infill (normally less than 100 m thick), and (ii) driving most of the area to exorheic conditions.~~

Geometric construction of normal fault profiles of the Teruel ~~fault~~ half-graben system ~~locates~~ allows locating the sole detachment at a depth of 14-17 km b.s.l., and estimating an average E-W stretching factor ß = 1.1 since its onset (11.2 Ma ago) (Ezquerro *et al.*, 2020).~~, *i.e.*, in an intermediate location within the ~30-km-thick crust of the central Iberian Chain, although it diminishes up to ~14 km in the central part of the Valencia Trough (*e.g.* Roca and Guimerà, 1992). Ezquerro *et al.* (2020) estimate an average E-W stretching factor ß=1.1 since the formation of the Teruel basin (11.2 Ma ago), accommodated by m~~Major faults ~~that have vertical~~accumulated slip ~~between~~ of a few hundred metres ~~and~~ to ca. 1 km (computing both fault throw *s.s.* and associated bending). The ~~total vertical~~resulting slip rate, ~~(considering fault throw and associated bending) shows a similar value (~~around 0.09 mm/a in average, ~~)~~ is very similar for distinct transects across the ~~Teruel half graben~~structure, but shows a clear increase between both extensional phases: ~~(~~from 0.05-0.07 mm/a to 0.12-0.16 mm/a ~~) has been reported~~ (Ezquerro *et al.*, 2020). Such ~~S~~slip rate increase has been attributed to: (i) onshore, westwards propagation of extensional deformation from the inner parts of the Valencia Trough, enhanced by crustal doming that would have affected the eastern Iberian Chain; (ii) ~~change of the regional stress field, which evolved to~~onset of the multidirectional extension stress field driven by ~~a~~ crustal doming mechanism; (iii) progressive fault linkage since the beginning of the Late Miocene (Ezquerro *et al.*, 2020).~~, which is documented from tectono-stratigraphic information.~~

Mountains surrounding the Teruel and Jiloca basins show extensive erosion surfaces modelling Mesozoic-Palaeogene rocks and bevelling compressional structures. Two large planation surfaces, whose remnants appear at different heights either on the upthrown blocks or in the basin floors, have been traditionally defined (Gutiérrez and Peña, 1976; Peña *et al.*, 1984; Sánchez-Fabre *et al.*, 2019): (i) *Intra-Miocene Erosion Surface* (*IES*, middle Miocene), generally recognized in the upper part of the main reliefs, and (ii) *Fundamental Erosion Surface* (*FES*, middle Pliocene), easily recognizable as a vast planation level at lower heights. They approximately correspond to the *Iberian Chain Surface* and the *Lower Pliocene Surface* by Pailhé (1984), and the S1 and S2 by Gutiérrez and Gracia (1997), respectively. Recent detailed studies (Simón-Porcar *et al.*, 2019; Ezquerro *et al.*, 2020) have demonstrated that the

FES splits into three different surfaces: an Upper Sublevel, the *FES s.s.* (the most widely developed), and a Lower Sublevel. In this work, these surfaces will be called as *FES1*, *FES2* and *FES3*, respectively. Planation surfaces have been physically correlated with different coeval sedimentary horizons (lacustrine-palustrine carbonates) within the sedimentary infill of the Teruel basin (Ezquerro, 2017), whose ages are well-constrained ~~B~~on the basis of~~ased~~ ~~on~~ mammal sites ~~as well as on~~and magnetostratigraph~~yic constraints,~~. In this way, the *Intra-Miocene Erosion Surface* has been dated close to the Aragonian-Vallesian limit (~11.2 Ma; Alcalá *et al.*, 2000; Ezquerro, 2017), *FES1* and *FES2* to the Late Ruscinian (both merging around ~3.8 Ma), and *FES3* to the Early Villafranchian (~3,5 Ma) (Ezquerro *et al.*, 2020).

Qualitative and quantitative geomorphological features of the mountain fronts and the associated piedmonts of the eastern margin of the Jiloca graben are those typical of active normal faults. At the Concud fault, Lafuente *et al.* (2011b) described conspicuous triangular facets and short, non-incised alluvial fans, and provided a significantly low value of the mountain-front sinuosity index defined by Bull and McFadden (1977) (S_{mf} = 1.24). At the Sierra Palomera fault, García-Lacosta (2013) described trapezoidal facets and V-shaped gullies, and provided a similar value for the sinuosity index (S_{mf} = 1.27). The fault scarps are connected with the depression bottom by gentle pediments mostly draining towards the Jiloca river, although endorheic conditions have locally remained until historical times, with development of a palustrine area at the basin centre (ancient Cañizar lake; Rubio and Simón, 2007).

Historic and instrumental seismicity of the central-eastern Iberian Chain is low to moderate. In the Teruel region, the epicentres are concentrated at the Jiloca graben margins, the central-southern sector of the Teruel basin, and the Albarracín and Javalambre massifs. Apart from the Albarracín massif, epicentres can be reasonably associated to Neogene-Quaternary known faults. Measured magnitudes (Mb) usually range from 1.5 to 3.5, with maximum Mb = 4.4 in the Teruel Graben and Mb = 3.8 in the Albarracín massif (~~data from seismic database of Instituto Geográfico Nacional, IGN: https://www.ign.es/web/ign/portal/sis-catalogo-terremotos~~IGN, 2021).

3. Methodology

3.1. Structural and morphotectonic study

The structural study is based on recognizing and mapping the main structures on aerial photographs at 1: 18,000 and 1: 33,000 scale, and satellite imagery, complemented with field surveys involving outcrop-scale observations. Data of orientation of rupture surfaces and slickenlines have been collected in a number of sites within the Sierra Palomera fault damage zone, as well as within the trench described below. Stereoplots (equal-area, lower hemisphere) of those data sets have been elaborated using Stereonet 8 software (Allmendinger *et al.*, 2012; Cardozo and Allmendinger, 2013).

To characterize the geometry of recent vertical deformation, the three erosional planation surfaces (*FES1*, *FES2* and *FES3*) described above were used as markers. This required mapping of erosion surfaces and morphotectonic analysis based on aerial photographs (scales 1: 18,000 and 1: 33,000) and orthorectified photographs (1: 5000), as well as on digital elevation models (DEM, pixel = 5 m) and the resulting hillshade images. A structural contour map of *FES2* was elaborated by interpolating the altitude of their remnants, which permits measuring ~~vertical displacement~~ throw across the main fault and hence calculating slip rate. Changes of throw ~~vertical displacement~~ along the fault zone were ~~inferred~~ calculated from 1-km-spaced transects orthogonal to the fault trace and analysed on a throw *vs.* distance (T-D) graph.

Once constrained the age of a planation surface (see Section 2), the main challenge to be addressed ~~when using it as a marker~~ is ensuring its degree of flatness, being aware of the degree of error involved in height ~~treatment~~management. Continental planation surfaces can show gentle (short- to middle-wavelength) unevenness, or locally connect with residual, non-flattened reliefs through pediment slopes. Amplitude of the~~ir~~ unevenness advises to use an adequate ~~spacing for~~ contour intervals for *FES2* in order to represent its present-day geometry with the suitable precision. Both the local difference in height between *FES2* and *FES3* and the local unevenness within each one usually lies within the range of 10-40 m. Therefore, we assume that: (i) ~~vertical~~ fault throws calculated from them implicitly include a maximum error bar of ±40 m, and (ii) a 50-m-spaced contour map can be considered as reasonable for assessing recent movements (as previously proposed by Ezquerro *et al.*, 2020). Such level of uncertainty in the calculated fault throws results in errors for slip rates around 0.01 mm/a.

3.2. Subsoil exploration

Subsurface information was acquired by means of geophysical exploration. Two different techniques were utilised, which had rendered interesting results in other neighbouring sectors (*e.g.*, Pueyo *et al.*, 2016): magnetometry and electromagnetic (EM) multifrequency survey. A twofold approach was taken: first, a regional analysis by means of ten transects approximately orthogonal to the Sierra Palomera mountain front; second, a detailed analysis of a sector where the highest geophysical anomalies were identified and also where geomorphological evidences hinted at the presence of a previously unknown antithetic fault. For the magnetometry survey, a GSM-19 equipment with built-in GPS was used to measure both Earth magnetic field intensity and vertical magnetic gradient (sensors separation of 0.5 m). Diurnal correction was performed from a second, stationary, magnetometer (PMG-01) that permitted to exclude natural earth magnetic field changes during the survey and to compare the results performed during different days. Then, the regional general trend was identified and subtracted to earth magnetic data to highlight anomalies in the form of residual values. The EM multifrequency survey was performed by a GEM-02 device for a range of frequencies between 65 and 0.5 kHz.

Subsoil information has been complemented with borehole data extensively compiled by Rubio (2004), whose synthetic results were presented by Rubio and Simón (2007). ~~Such subsoil information,~~ T~~t~~ogether with surface geology, it was used for constructing geological cross sections that have allowed characterizing the general geometry of macrostructure. Moreover, they were used for extending the contour map of FES2 to the centre of the Jiloca basin.

3.3. Trench analysis

A trench study focussed on the northwards prolongation of the La Peñuela fault, antithetic to the main Sierra Palomera fault, has been carried out following the classical methodology (see, *e.g.*, ~~McCalpin, 1996~~McCalpin, 2009): excavating and shoring; cleansing and gridding the most suitable wall; identifying and marking sedimentary boundaries and deformation structures; drawing a detailed log and taking photographs of each grid cell; analysing the relationship between units and faults to identify individual events; and sampling materials for dating. Sedimentary units were defined on the basis of lithology, bed geometry, texture, colour and sedimentary structures.

Individual deformation events identified within the trench have been carefully verified by retrodeformational analysis, following the common practice in paleoseismological reconstruction (McCalpin, 2009). Several post-event sedimentary stages have also been included for a better understanding and representation of the evolutionary model. A number of identifiable faults were either formed, propagated or reactivated during successive deformation events. For each fault involved in each event, dip separation has been measured and equated to net slip (with precision of 5 cm). In addition, the resulting horizontal extension has been calculated taking into account the average dip of each fault. Further details are given in Section 7.4.

Dating of trench samples was achieved by the Luminiscence Dating Laboratory of

University of Georgia, USA, using the Optically Stimulated Luminiscence (OSL) technique. Unfortunately, five of them were saturated samples that only provided minimum ages, which drastically decreased the consistency of the age model. Additional, preliminary OSL dating of shallow alluvial fan sediments had been achieved by Laboratorio de Datación y Radioquímica de la Universidad Autónoma de Madrid.

4. Structure and morphotectonics of the Sierra Palomera area

The NNW-SSE trending Sierra Palomera extensional fault makes the eastern boundary of the Jiloca graben at its central sector (Figs. 1b, 2). In the footwall block, Jurassic marine carbonates are unconformably covered by Paleogene continental clastics ~~materials~~ (Figs. 2, 3). In the ~~western,~~ hanging-wall block, *i.e.*, the central sector of the Jiloca basin, the sedimentary infill is made of: (i) Late Pliocene (Villafranchian) to Pleistocene alluvial and episodic palustrine deposits, all of them exposed at the ~~land~~ surface; (ii) an underlying carbonate unit, only observed in boreholes, that could represent an early lacustrine stage of Late Miocene-Early Pliocene age (Rubio and Simón, 2007). ~~Isopach maps elaborated from b~~Borehole information ~~show how~~indicates that the maximum thickness of the total infill approaches ~~one hundred metres, and its geometry is partially controlled by NW-SE to NNW-SSE striking normal faults~~100 m (Rubio and Simón, 2007).

[PREFERENTIALLY, FIG.2 SHOULD BE INSERTED HERE, AS A 1.5-COLUMN FIGURE]

[PREFERENTIALLY, FIG.3 SHOULD BE INSERTED HERE, AS A 2-COLUMN FIGURE]

The Jiloca basin runs slightly oblique to previous Paleogene, NW-SE trending folds (Fig. 1b; ~~). Their hinges can be tentatively interpolated beneath the Neogene-Quaternary infilling from geology of the basin margins, borehole data and hydrogeological criteria (~~Rubio and Simón, 2007; Rubio *et al.*, 2007). In particular, the Sierra Palomera ~~extensional~~ fault follows the eastern limb, nearly vertical, of an eastwards verging anticline (Fig. 3)~~, suggesting that it could result from negative inversion of a previous reverse fault linked to that fold~~. Its core is represented by ~~the~~ Lower-~~ and~~ Middle Triassic rocks that crop out in the neighbourhoods of Singra village, ~~making two gentle reliefs not completely buried by the basin filling. I~~and its periclinal closure is partially preserved close to the southern tip of Sierra Palomera fault (Fig. 2). ~~-~~Such structural setting suggests that the main extensional fault resulted from negative inversion, during Late Pliocene-Pleistocene times, of a previous reverse fault linked to that anticline and developed during the Paleogene compression (Rubio and Simón, 2007).

The Sierra Palomera fault trace is ca. 26 km long and trends N152ºE in average. The main fault surface only crops out in a few~~, very~~ small exposures (1 to 4 m^2 in area). A number of rupture surfaces observed within the damage zone show orientations consistent with the map trend: ~~they~~ strike between NW-SE and N-S, and dip between 54º and 87º W (mean orientation: N155ºE, 70º W; Fig. 4). Slickenlines show pitch ranging from 75ºN to 70ºS, therefore indicating almost pure normal movement, with mean transport direction towards N230ºE.

[PREFERENTIALLY, FIG.4 SHOULD BE INSERTED HERE, AS A 1-COLUMN FIGURE]

Two wide right relay zones separate the Sierra Palomera fault from the Calamocha and Concud faults. The dominant trend of recent, extensional faults and fractures distributed within both relay zones is similar to that of the main fault or slightly deviates to approach the N-S direction. These relay zones dominated by along-strike fractures were described in detail by Peiro *et al.* (2019, 2020).

The Sierra Palomera fault is expressed in the landscape by a conspicuous, 20-km-long fault mountain front (Fig. 5a,b), which attains heights of 200 to 300 m above its toe, 450 to 550 with respect to the bottom of the Jiloca ~~basin~~depression. The mountain front~~It~~ ~~is quite rectilinear, with~~shows a significantly low value of the sinuosity index (S_{mf} = 1.27; García-Lacosta, 2013). A number of gullies (most of them exhibiting V-shaped transverse profiles) run across the fault scarp and delimit some well-preserved trapezoidal facets (Fig. 5c). Gullies feed short, high-slope alluvial fans (Fig. 5d) that are barely incised, only partially connected to the axial fluvial system, and exhibit signs of present-day functionality (*e.g.*, gravel aggradation affecting bush vegetation).

[PREFERENTIALLY, FIG.5 SHOULD BE INSERTED HERE, AS A 2-COLUMN FIGURE]

The difference in height of the geomorphological markers *FES2* and *FES3* between the footwall and the hanging-wall blocks reasonably allows approaching the Sierra Palomera fault throw. The envelope of relief at the footwall block is largely represented by the *FES2* planation surface cutting~~, which cuts~~ ~~Triassic, Jurassic and Paleogene~~pre-Neogene units, ~~and~~ which attains a maximum height of 1430 m close to the edge (Fig. 6). The summit of Sierra Palomera (1533 m a.s.l.) and its surrounding area constitutes a residual relief that stands out from ~~the~~ *FES2* ~~erosion level~~, while remains of an upper erosion sublevel (*FES1*) extend at the eastern foothills. A lower sublevel (*FES3*, usually lying 10-40 m below *FES2*) is also present: (i) eastwards of Sierra Palomera, over large areas of the northern Teruel basin; (ii) northwards and southwards, at the relay zones with the Calamocha and Concud faults, respectively; and (iii) along a narrow band westwards of the Sierra Palomera divide.

[PREFERENTIALLY, FIG.6 SHOULD BE INSERTED HERE, AS A 2-COLUMN FIGURE]

~~Within the sedimentary infill of the Teruel basin, these planation surfaces can be physically correlated with different coeval sedimentary horizons (lacustrine-palustrine carbonates) that were precisely characterized and dated by Ezquerro (2017) based on both paleontological and magnetostratigraphic data. As stated above, the age of *FES1* and *FES2* is constrained at about 3.8 Ma (Late Ruscinian, mammal zone MN15), while *FES3* is dated to 3.5 Ma (Early Villafranchian, MN16) (Ezquerro *et al*., 2020).~~

The height of *FES2* and *FES3* ~~surfaces~~ within the Jiloca depression can only be inferred indirectly. Both have been mapped at the eastern margin of the Jiloca depression, W of Santa Eulalia town, where they descend to ca. 1100 and 1050 m, respectively (Fig. 6). Then they are supposed to be covered by the Plio-Pleistocene infill, while gentle residual reliefs at the Singra-Villafranca del Campo area (made of Triassic and Jurassic rocks belonging to the core of the Sierra Palomera anticline) stand out above the depression bottom. ~~Having in mind the morpho-sedimentary setting at the nearby Teruel basin, t~~The subsoil data provided by Rubio and Simón (2007; Fig. 6) for the central Jiloca basin ~~can be used for~~ constrainin~~g~~ the heights of those planation surfaces. T~~In this way, t~~he boundary between Plio-Pleistocene alluvial deposits and the underlying carbonate unit, lying at about 950 m a.s.l. in the Santa Eulalia area, could be correlated with either *FES2* or *FES3*. ~~This piece of data will allow reasonably approaching the total tectonic offset at the Sierra Palomera fault zone since 3.8-3.5 Ma.~~

Within the Sierra Palomera block, *FES2* and its correlative Late Ruscinian carbonates ~~of the Teruel basin systematically lose height towards east. Both~~ are in continuity with each other and show a quite homogeneous slope of about 1.5-2% along a distance of 20 km, in which the altitude of this morpho~~-~~sedimentary marker diminishes from 1400-1430 m (central sector of Sierra Palomera) to 1090-1120 m (Alfambra area) (Fig. 6). This morphotectonic setting defines a conspicuously tilted block whose edge has undergone a tectonic uplift of about 300 m relative to the bottom of the Teruel depression, as can be visualized from structural contours in Figure 6.

The latter value closely approaches the topographic amplitude of the Sierra Palomera scarp itself, and ~~also~~ is comparable to the ~~maximum~~ fault throw inferred from offset of the *FES2* marker. Such fault throw, and its variation along the Sierra Palomera fault, have been analysed on a series of 1-km-spaced transects across the fault trace on the contour map of Figure 6, assuming that *FES2* within the Jiloca basin coincides with the base of the Plio-Pleistocene infill. The result is shown in the throw *vs.* distance (T-D) graph of Figure 7, where two distinct curves depict values of (i) fault throw *s.s.*, and (ii) total tectonic ~~offset~~ throw of *FES2* between the Sierra Palomera summits and the Jiloca depression bottom (including the bending component). The T-D curves show an overall bell-shape, ~~while exhibiting~~although slightly bimodal~~ity~~ in detail. The maximum values, 330 m and 480 m, respectively, are found at the central sector. Considering the age of the *FES2* morpho~~-~~sedimentary marker (3.8 Ma), and assuming an average dip of 70º for the fault plane and a pure normal movement, a maximum net slip rate of 0.09 mm/a can be inferred (0.13 mm/a for the total rate between Sierra Palomera and the Jiloca bottom).

[PREFERENTIALLY, FIG.7 SHOULD BE INSERTED HERE, AS A 1-COLUMN FIGURE]

~~Although~~ Despite the initial appearance of the Sierra Palomera fault is that of a single major rupture that accommodates the entire ~~vertical~~ throw, there ~~are indications~~is evidence of a parallel, synthetic fault (Las Vallejadas fault) located west of the main escarpment at its southern sector (Fig. 2). Both delimit an intermediate step within the mountain front, in which *FES2* lies at an altitude of 1140-1220 m, furthermore offset (ca. 10 m) by a minor antithetic rupture (La Peñuela fault). Recent activation of both subsidiary faults is revealed by local deformation of Villafranchian alluvial deposits: (i) back tilting (up to 25ºE), due to rollover kinematics, observed at the foot of the morphological escarpment of Las Vallejadas fault (Fig. 2); (ii) accommodation monocline (dip up to 22ºE) in the case of La Peñuela fault (Fig. 8; see location in Fig. 2).

[PREFERENTIALLY, FIG.8 SHOULD BE INSERTED HERE, AS A 1-COLUMN FIGURE]

5. Geophysical exploration of the overall Sierra Palomera piedmont

Data of magnetic intensity field and vertical magnetic gradient were extensively collected along ten transects, roughly orthogonal to the Sierra Palomera fault trace along its hanging-wall block and ranging from 2.0 to 5.2 km in length (Fig. 9a). Spacing between successive measurement points was about 0.8 m. The two northernmost transects (profiles 01 and 02) and the southernmost one (profile 10) show a narrow distribution of residuals due to their lesser contrast with respect to the general, regional trend (Fig. 9b). The central transects (03 to 09) have spikes and lows that depart considerably from the general trend, and therefore, when data of the ten transects are considered as a whole, they define the range of the distribution (more specifically, profile 03 has the lowest and the highest values of residual magnetic intensity). Nonetheless, transects 01, 02 and 10 show a similar (albeit reduced in magnitude) outline to the rest.

[PREFERENTIALLY, FIG.9 SHOULD BE INSERTED HERE, AS A 2-COLUMN FIGURE]

The variation pattern of residuals in magnetometric ~~magnetic and EM~~ profiles (also corroborated by EM profiles) allows ~~follow a common pattern of variation of residuals,~~ portraying three domains (A, B and C) that are broadly parallel the Sierra Palomera fault (Fig. 9b). In the northern section of the studied area, the boundary between domains A and B is largely evident, due to the sudden change and amplitude of the anomaly. Moreover, these profiles show a more direct correlation between them than the southern ones, where the contact progresses through a magnetic dipole (Fig 9a, b). These three domains are characterised by:~~:~~

a) Close~~st~~r to the Sierra Palomera fault, domain A is an area where residual values of magnetic intensity are close to zero and barely change, except for a subtle decrease to the west.

b) Westwards, a sharp change of attitude marks the onset of domain B, a zone of anomalies expressed as variations of residuals up to 20-30 nT over decametric distances. Such anomalies reflect the presence of small magnetic dipoles and~~,~~ a slightly higher mean value of Earth magnetic field. Values for~~,~~ apparent conductivity ~~while~~ are still homogeneous~~ values for apparent conductivity~~.

c) Finally, domain C is separated from domain B by a sharp decrease in magnetic intensity (it goes down about 100 nT) with lower relative values of Earth magnetic field~~,~~ and presence of a lower density of magnetic dipoles (including those of higher wavelength).~~,~~ Apparent conductivity and magnetic susceptibility ~~and~~ are higher~~ apparent conductivity and magnetic susceptibility~~.

~~In map view, Figure 9a shows the location of transects, on which the residual values of field intensity (nT) are plotted as a colour palette. The spatial correlation of the described~~

~~domains on successive transects is depicted. While the boundary between A and B domains is largely evident, the northern profiles show a more direct correlation than the southern ones, where the contact progresses through a magnetic dipole.~~

The reported geophysical results (Earth magnetic field, together with apparent conductivity~~,~~ and susceptibility) suggest the presence of a body of relatively higher magnetic susceptibility underlying domain A, which gets shallower under domain B, and gets again deeper under domain C. Boundaries between those domains are sharp and clear. This setting can be interpreted as an uplifted block (made of Paleozoic and Triassic materials belonging to the core of the Sierra Palomera anticline) bounded by faults nearly parallel to the Sierra Palomera fault trace.

6. ~~Detailed study at~~ La Sima alluvial fan: linear topographic anomaly and its geomagnetic expression

In the absence of any visible surficial rupture across Quaternary sediments of the Sierra Palomera piedmont, ~~the need to excavate and survey a trench arose~~evidence of recent tectonic activity should be obtained from trenching. ~~After careful field survey in search of a suitable location for such trench, no locality could be selected on the Sierra Palomera fault trace itself,~~ O~~o~~wing to non-favourable topographic, lithologic and access conditions at the Sierra Palomera fault trace itself,~~.~~ o~~O~~ur search was ~~then~~ focused on the surface of two ~~of the recent~~ alluvial fans sourced at the mountain front, at La Cecilia and La Sima areas (see location in Figs. 2 and 5d). Both exhibit well-preserved alluvial fan morphology at its proximal sectors, with evidence of present-day aggradation at the apex. Shallow sand and silty sedimentary horizons in those alluvial fans have provided ages of 28.9 ± 2.0 ka BP (La Cecilia) and 19.2 ± 1.1 ka BP (La Sima) (see Table 1; location in Fig. 2).

[PREFERENTIALLY, TABLE 1 SHOULD BE INSERTED HERE AS A 2-COLUMN FIGURE]

In the middle sector of La Sima alluvial fan, a sharp NNW-SSE trending lineament is clearly visible on aerial photographs and DEM images, beyond which the fan surface is more deeply incised by the local drainage network (Fig. 10a). That lineament involves a morphological anomaly, a break in the fan slope, which becomes null or even negative up to take locally the appearance of a gentle, degraded uphill-facing scarplet (Fig. 10c). ~~In view of t~~These features~~, it came to mind~~ suggest the ~~hypothesis~~ occurrence of an antithetic fault that would have ~~raised~~ sunk the ~~middle~~ proximal sector of the fan with respect to the ~~proximal~~ middle one by about 2.5~~6~~ m. This ~~e described~~ lineament coincides with the boundary between domains A and B defined from geophysical results (Fig. 9b), ~~. Moreover, it~~and is virtually prolonged towards SSE up to connect with the antithetic La Peñuela fault (Fig. 2).

[PREFERENTIALLY, FIG.10 SHOULD BE INSERTED HERE AS A 1.5-COLUMN FIGURE]

In order to test the hypothesis of an antithetic fault cutting the La Sima alluvial fan, the subsoil in the neighbourhoods of the morphological lineament was intensively explored by means of a magnetic and electromagnetic survey. ~~Seeing at the geophysical domains described in Section 5, the~~The coincidence of the lineament ~~coincides~~ with the A/B boundary~~,~~ ~~which~~ is clearly expressed in the detailed map of residual magnetic anomalies shown in Figure 10b. The area east of the sharp linear~~,~~ NNW-SSE trending limit, clearly visible on this map, shows low residual values with wide (hectometre-scale) wavelength variations. To the west of this limit, an increase of more than 30 nT is observed, as well as a decrease of more than 50 mS/m in the total conductivity; moreover, the texture of the residual map changes noticeably, showing sharper magnetic dipoles of decametric wavelength.

The amplitude and morphology of the linear anomaly is not consistent with the susceptibility values of surficial sediments, and suggest the contrast, at shallow levels, between a high-susceptibility rock body to the west (domain B, as defined in section 5) and the domain A to the east. In addition, Figure 10b shows other NW-SE trending linear anomalies in domain B, which involve a lower contrast of magnetic field values. Both the main anomaly and the secondary ones show high gradient and sharpness of the observed dipoles, suggesting near-surface, high dipping discontinuities or rock boundaries compatible with recent faults.

7. Trench study at La Sima alluvial fan

Once verified that geophysical and topographic analysis of La Sima lineament reinforced our preliminary hypothesis about the northwards prolongation of the antithetic La Peñuela fault, we selected an easily accessible site for trench study. A 40 m long, 1.4 m wide trench was dug along a N067ºE direction, roughly orthogonal to the linear anomaly that separates domains A and B. A segment of 19 m on its southern wall, with depth ranging from 3.0 to 3.5 m, was logged and analysed in detail (Fig. 11a,b).

[PREFERENTIALLY, FIG.11 SHOULD BE INSERTED HERE IN VERTICAL IF POSSIBLE]

7.1. Sedimentary units

The materials exposed at La Sima trench essentially correspond to relatively well-bedded Pleistocene alluvial sediments (Fig. 11a). Sedimentary features indicate alternating energetic flows, sometimes flash floods, recorded by gravel channel and bar deposits, and waning discharges that settled fines over the gravel deposits. All the succession includes clear signs of calcrete development and periods of time with negligible sedimentation. Bioturbation signs and carbonate precipitation are related to pedogenesis, ~~and~~ suggesting wetting and drying episodes of the sedimentary surface. The sedimentary succession has been subdivided into twelve lithological units (Fig. 11b~~a~~):

Unit 1 (up to 50 cm in thickness): Massive reddish mudstone with isolated, mm- to cm-sized angular limestone clasts (more abundant at the base), with bioturbation traces and smooth carbonate nodules.

Unit 2 (25 to 55 cm): Orange massive sandy mudstone with floating angular-subangular grey limestone granules and pebbles, and some irregular cm-thick gravel bed. Grey mudstones laminae towards the top.

Unit 3 (55 to 75 cm): Tabular laminated, indurated and brecciated, carbonate crust with some cm-thick interbedded silts with carbonate clasts. Carbonate fragments are smaller in the upper part; laminated fragments are less abundant towards W.

Unit 4 (20 to 35 cm): Reddish massive silty sand and mudstone in a tabular level with vertical root traces filled by fine sands. Some carbonate nodules, plant remains and scattered grey, angular limestone and caliche clasts up to 10 cm in size can be recognized.

Unit 5 (15 to >50 cm): Clast-supported gravel with silty to sandy matrix in a tabular, locally channelized sedimentary body with crude horizontal stratification. Gravel is made of angular-subrounded limestone clasts (up to 8 cm) and smaller caliche clasts.

Unit 6 (25-55 cm): Orange to brownish massive silt and mudstone with greyish limestone angular clasts and floating whitish caliche rounded nodules (up to 2 cm). Clast content increases locally. Root traces, plant remains and organic matter patches can be recognized in the western sector.

Unit 7 (30 to >150 cm): Heterogeneous unit mainly made of grain-supported gravel, locally cemented, with angular-subrounded limestone clasts (up to 15 cm in size) and caliche nodules. It includes red mudstone discontinuous intercalations, up to 20 cm in thickness, with floating cm-sized angular clasts~~ (labelled as 7a in Fig. 11a)~~. The overall geometry of the unit is tabular in the footwall block and channelized in the hanging-wall block. A level of calcrete gravel, >50 cm in thickness, appears at the top of this unit within the footwall block.

Unit 8 (10-60 cm): Reddish silt with floating limestone angular granules and pebbles (up to 8 cm) with evidence of bioturbation.

Unit 9 (45-120 cm): Grey gravel in a channeled body with limestone angular clasts (up to 12-14 cm in size) and rounded caliche ~~rounded~~ clasts. Crude finning upwards cycles can be recognized. Pedogenic features increase towards the top, where brecciated limestones locally appear.

Unit 10 (55 to 70 cm): Reddish massive silts with floating subangular limestone clasts (up to 7 cm), whitish carbonate nodules and an interbedded discontinuous clast-supported gravel level~~ (10b)~~ with subangular clasts up to 10 cm in size.

Unit 11: Wedge-shaped body of orange and whitish massive, highly cemented silt, with carbonate floating subangular limestone clasts (up to 10 cm) and caliche clasts arranged with the A-axis subvertical.

Unit 12 (20 to 50 cm): Surface regolith made of silt with angular to subangular clasts, reworked by agricultural labours.

7.2. OSL dating

~~Dating of a total of s~~Seven samples (S1 to S7) of alluvial sediments within the trench (see Fig. 11b~~a~~ for location) have been dated, ~~has allowed approaching their age distribution,~~ although~~,~~ unfortunately~~,~~ the results show a high level of uncertainty (see Table 1). Other three collected samples did not contain enough sand grains for providing a representative dose distribution and therefore OSL dates were not reliable in this case. These samples are not located in Fig. 11b~~a~~.

Samples S2, S3, S4, S6 and S7 have presented signal saturation, *i.e.*, their natural luminescence signal lies beyond the saturation of the OSL response with dose, making it impossible to provide adequate results. According to laboratory results, their ages should be older than 193 to 378 ka, although such figures should not be taken *sensu stricto*. Only one of the alluvial sedimentary units is directly dated: S1 provides an age 97.4±10.2 ka for the top of unit 9. Unit 11 (sample S5), which will be next interpreted as a fissure infill, is dated to 49.2±5.4 ka. As a result, the chronology of unit 10, overlapping unit 9 and being cut by the fissure, can be broadly constrained between both numerical ages.

Without the support of further anchors, building an age model for the overall alluvial succession exposed in the trench is not feasible. In any case, the ensemble of OSL dating results and geomorphological observations in the study area suggest that: (i) most of that alluvial succession belongs to the Middle Pleistocene; (ii) a rapid decrease of sedimentation rate occurs by the Middle-Late Pleistocene transition; and (iii) sedimentation persisting in proximal and middle sectors of the alluvial fans during Late Pleistocene to present-day times only represents a small contribution to the surficial aggradation and landscape modelling.

7.3. Deformation structures

~~In a first approach, t~~The trench log shows a main extensional fault zone at the central sector, dipping eastward and hence antithetic with respect to the Sierra Palomera fault (Fig. 11~~a~~b), and full consistent with the uphill-facing scarplet described in section 6. These features allow identifying such antithetic fault zone with the map-scale La Peñuela fault (Fig. 2).~~-~~ The footwall block of that fault zone shows a gentle monocline, while other normal (both synthetic and antithetic) faults, cutting most of the sedimentary succession, are distributed along the entire section. The orientations of all these structures are overall consistent, as depicted in stereoplots of Figure~~.~~ 11~~b,~~c,d,e,f.~~-~~

The central fault zone is made of three significant structural elements:

1~~(i~~) Main ~~rupture~~fault, expressed by θ_1 and θ_2 ~~fault~~ individual rupture surfaces.

2~~(ii~~) Splay faults κ1, κ2, κ3 and κ4, associated to the tip of the main rupture and propagated through unit 7. Both the main, westwards dipping rupture surfaces and the nearly vertical splay faults consistently strike NNW-SSE (Fig. 11c~~b~~). Such structural arrangement suggests that, at certain stage of its development, the main rupture θ_1-θ_2 was covered by the upper part of unit 7, and then reactivated in the form of splay faults related to refraction at the extensional tip (horse-tail structure, in the sense of Granier, 1985). That is the key, purely instrumental criterium for separating lower and upper unit 7 in Figure 12; therefore, such separation is not based on a visible lithological boundary (we have defined a single unit 7 indeed).

3~~(iii~~) Open fissure bounded by fault θ_3 ~~and η~~and another irregular surface, and filled with unit 11. The interpretation is based on its wedge shape, the massive internal structure of the infill, and the occurrence of clasts with nearly vertical A-axes. According to this interpretation, both bounding surfaces ~~θ_3 (smooth) and η (more irregular)~~ would have represented both walls of a single, also NNW-SSE striking fault, then disengaged from each other when the fissure opened up and , in the case of η, partially crumbled before infilling took place.

The footwall block is deformed by the monocline and cut by a number of NNW-SSE striking normal faults (Fig. 11cd), all of them synthetic with the Sierra Palomera fault and exhibiting dip separations in the range of 10 to 20 cm (Fig. 11ba). Faults ρ, π_1 and π_2 cut the horizontal limb of the monocline, and have apparently kept their original, high dip. The rest of faults (τ, σ, μ, χ, λ_1 and λ_2) appear at the hinge and the abrupt limb of the monocline. They show a progressive decrease in dip towards the east as the bedding dip increases, and some individual faults (μ, λ_1, λ_2) exhibit conspicuously arched traces, so that the angle between faults and bedding remains broadly constant (mostly within the range of 55-65º). Such geometrical setting strongly suggests that they were folded by the monocline. Concerning the relationships between faults and sedimentary units, ρ and π_1 uniformly offset (15-20 cm) the base of units 2 to 6, while they suddenly vanish and does not affect the base of unit 7. Also fault σ shows similar relationships, although in this case it does not propagated through the lower units, probably detached within low-viscosity materials of unit 4. As a consequence, ρ, π_1 and σ produce a noticeable thickening of unit 6 in their respective hanging-wall blocks. Faults π_2, τ, μ, χ, λ_1 and λ_2) also offset rather uniformly the sedimentary boundaries, and at least two of them (π_2 and μ) propagated across unit 7.

The hanging-wall block shows two ensembles of intersecting faults that cut younger units that are younger than the ones from the footwall block (Fig. 11ba). Individual faults show distinct offsets slip for different sedimentary markers, which indicates diachronic development. The ε_0-ε_1 couple offsets more than 1.42 m the base of unit 7, while it produces a rather uniform dip separation of 8-10 cm in the bases of units 8, 9 and 10. We should therefore interpret that ε_0-ε_1 underwent most of its present-date displacement (>1.3 m) before sedimentation of unit 8, and was then reactivated after the lower part (at least) of unit 10 was deposited. Splaying from ε_1, fault ε_2 cuts units 7 and 8, and is covered by unit 9, while ε_3 cuts the base of unit 9, thus making the three faults a footwall rupture sequence. The antithetic ε_4 propagated up thorough unit 9 andto the lowermost unit 10. At the easternmost trench sector we find a similar pattern in the NNW-SSE striking faults α and β. Fault β offsets more than 0.7 m the base of unit 7, while (together with its splay faults γ_1, γ_2 and γ_3) produces a smaller separation (0.4 m) in the bases of units 8 and 9. We interpret that β underwent displacement ≈ 0.3 m before sedimentation of unit 8, and was then reactivated after deposition of unit 9. Fault α propagated through unit 7, previous to sedimentation of unit 8, and did not undergo further reactivation.

~~We should emphasize the strict consistence of~~The orientations of the described structures have a strict consistence. All faults systematically strike NNW-SSE (Fig. 11f~~e~~), and so does the limb of the monocline (Fig. 11d~~e~~). There is no doubt that the latter is (i) genetically linked to faults, and (ii) responsible for the decrease in dip of faults σ, μ, χ, λ_1 and λ_2. Bedding and fault surfaces are rotated around a common, well-defined horizontal axis ca. N160ºE (Fig. 11d~~e~~). Strikes of minor fractures measured along the trench are also clustered around NNW-SSE, although a small number among them are oriented NNE-SSW (in blue in Fig. 11e~~d~~). A brief discussion about the dynamic framework (stress fields) in which such fault and fracture pattern developed will be made in Section 8.5~~7.6~~.

7.4. Retrodeformational analysis and ~~E~~evolutionary model: deformation events

~~According~~ Based onto the former structural description, in particular ~~to~~ on the relationships between structures ~~themselves~~ and ~~with~~ the sedimentary units, a careful retrodeformational analysis has been achieved, with a double purpose: (i) building an evolutionary model, i.e. a systematic succession of deformation events, and (ii) testing its kinematic consistence ~~we propose the evolutionary model explained below, tested by means of careful retrodeformation analysis~~ (Fig. 12).

~~The evolution has been conventionally divided into a succession of "deformation events", following the common practice in paleoseismological reconstruction. Several post-event sedimentary stages have been also included for better understanding.~~ A number of identifiable faults were either formed, propagated of reactivated during each deformation event (Fig. 12 and Table 2). Dip separation directly measured on the trench log is taken as practically representing the net slip on each fault, since: (i) bedding is roughly horizontal, (ii) the trench, oriented N067ºE, is nearly orthogonal to the prevailing strike of faults, and (iii) the only kinematical indicator observed during trench survey (slickenlines with pitch 82ºS on fault μ; Fig. 11d), as well as those collected at the Sierra Palomera fault zone itself (see Fig. 4b), suggest nearly pure normal slip for the overall extensional fault system.

Net slip for every individual fault (with positive sign for synthetic faults and negative sign for antithetic ones), together with the resulting horizontal extension (considering the average fault dip), are depicted in Table 2. Such measurements exclude offset accommodated by the bending monocline. The latter has been only considered for computing the total accumulated deformation, since it is not possible to accurately calculate which fraction of bending occurred during each event. The total slip per event, taken as the algebraic sum of slip values on individual faults, is also shown. The total horizontal extension per event considers the aggregate of extension values on individual faults, but also includes an estimate of the contribution of bending, in order to jointly accommodate the horizontal extension visually expressed in the successive cross sections of Fig. 12.

[PREFERENTIALLY, FIG.12 SHOULD BE INSERTED HERE, AS A 1-COLUMN FIGURE]

[PREFERENTIALLY, TABLE 2 SHOULD BE INSERTED HERE AS A 2-COLUMN FIGURE]

~~A number of identifiable faults were either formed, propagated of reactivated during each deformation event (Fig. 12 and Table 2). Dip separation directly measured on the trench log is taken as the first approach to the net slip on each fault, since: (i) bedding is roughly horizontal, (ii) the trench, oriented N067ºE, is nearly orthogonal to the prevailing strike of faults, and (iii) the only kinematical indicator observed during trench survey (slickenlines with pitch 82ºS on fault μ), as well as those collected at the Sierra Palomera fault zone itself (see Fig. 4b), suggest nearly pure normal movement for the overall extensional fault system. A precision of 5 cm has been adopted for net slip measurements; those that are synthetic to the Sierra Palomera fault (downthrown block to the west) are compiled as positive in Table 2, while those antithetic are compiled as negative.~~

Below we summarize the main features of each of the seven deformation events (T to Z) ~~distinguished~~ defined at~~in~~ the La Sima trench (Fig. 12; see measurements in Table 2):

Event T: Slip on faults ρ, π_1, τ and σ after deposition of unit 6 and previous to unit 7. Accumulated net slip: +45 cm.

Event U: Slip on faults π_2,~~ τ,~~ μ, χ, λ_1, λ_2 and ε_1, subsequent or coeval with deposition of the lower part of unit 7. Accumulated net slip: +105~~10~~ cm.

Event V: Slip on fault θ_2, subsequent to deposition of lower unit 7, then covered by upper unit 7. Development of the monocline begins; according to our progressive deformation model depicted in Fig. 12, in which the main rupture had always propagated through units 1 to 6, this monocline should be interpreted as a drag fold. Net slip: −10~~5~~ cm.

Event W: Reactivation of the main, central fault through the rupture surfaces θ_1-θ_2, which propagates across upper unit 7 splitting into κ1, κ2, κ3 and κ4. Progress of the monocline produces rotation of faults τ, σ, μ, χ, λ_1 and λ_2. Slip on faults ε_0-ε_1, α and β, all of them subsequent to top of unit 7 and previous to unit 8. Accumulated net slip: +125~~00~~ −6~~10~~5 = +60~~−5~~ cm.

Event X: Propagation of the main fault zones, θ and ε, through new rupture surfaces: θ_2-θ_3 and ε_2, respectively. Both are younger than unit 8 and older than unit 9. Accumulated net slip: +~~0~~5 −50~~95~~ = −45~~90~~ cm.

Event Y: Activation of fault ε_3, and propagation of β splitting into γ_1, γ_2 and γ_3. Both processes are subsequent to deposition of unit 9 and probably previous to unit 10, therefore close to (or slightly younger than) the numerical age provided by sample S1 (97.4 ± 10.2 ka). Accumulated net slip: −35~~40~~ cm.

Event Z: Formation of fault ε_4 and propagation of ε_1 cutting the lower part of unit 10. Slip on θ_2 that induces extensional movement on ~~passively activates~~ the θ_3 surface~~ with extensional component~~, giving rise to an open fissure ~~(from fault η)~~ that tears apart units 7 to 10 and is subsequently filled with unit 11. This event should be dated just prior to the numerical age provided by sample S5 (49.2 ± 5.4 ka). Accumulated net slip: +10 −120~~35~~ = −110~~25~~ cm.

8. The Sierra Palomera fault: synthesis~~Overall interpretation~~ and discussion

8.1. Geometry and kinematics of macrostructures

Structural information from field survey has allowed characterizing geometry and kinematics of the Sierra Palomera fault itself (Figs. 4, 6, 13). The attitude of the main fault surface is N155ºE, 70º W in average, while most ruptures visible along and close to it are systematically parallel. The fault shows pure normal movement, with mean transport direction towards N230ºE. In addition, the use of two geomorphological markers (mid-Pliocene *FES2* and *FES3* planation surfaces; Fig 13b) has permitted measuring the fault throw *s.s.* (330 m) and the total tectonic throw (480 m, including bending) at the Sierra Palomera fault, resulting in slip rates of 0.09 and 0.13 mm/a, respectively.

[PREFERENTIALLY, FIG.13 SHOULD BE INSERTED HERE, AS A 2-COLUMN FIGURE]

~~We have seen how g~~Geophysical results reported in Section 5, defining three adjacent, NNW-SSE trending elongated domains (A, B, C) suggest the existence of an uplifted block bounded by faults nearly parallel to the Sierra Palomera fault trace. At the southern sector of the study area, local coincidence of the A/B and B/C domain boundaries with La Peñuela and Las Vallejadas faults, respectively, strongly supports such interpretation. The antithetic rupture exposed in La Sima trench, revealed in the landscape by a gentle uphill-facing scarplet across the La Sima alluvial fan (section 6), unequivocally represents that map-scale antithetic La Peñuela fault and corroborates the extensional character of such structure.

In this way, the results of subsoil exploration by geophysical methods and trench survey, together with structural and morphotectonic data, allow refining the structural model of the central Jiloca graben, beyond the apparently flat appearance of the Sierra Palomera pediment. ~~*i.e.*, deformation style of the hanging-wall block of the Sierra Palomera fault. These new inferred faults separating domains A, B and C have been incorporated to the geological map of Fig. 2.~~

~~The Sierra Palomera fault probably resulted from negative inversion, during the Late Pliocene-Quaternary extensional phase, of a previous contractive structure developed under the Paleogene-Early Miocene compression. Such origin is suggested by its spatial coincidence with the eastern, nearly vertical limb of an eastwards verging anticline. Evidence of the same inversion setting has been described for the other master faults bounding the Jiloca graben, namely the Concud fault (Lafuente *et al.*, 2011a) and the Calamocha fault (Liesa *et al.*, 2021).~~

~~The attitude of the main fault surface is N155ºE, 70º W in average, while most ruptures visible along and close to it are systematically parallel to it. The fault shows pure normal movement, with mean transport direction towards N230ºE. These features are similar to those of the Concud and Calamocha faults, the other structures that make the eastern boundary of the Jiloca graben. In particular, the average transport direction of those faults is N220ºE (Lafuente *et al.*, 2014) and W to SW (Martín-Bello *et al.*, 2014), respectively, thus jointly making a geometrically and kinematically consistent major extensional fault system.~~

~~Two wide right relay zones separate the Sierra Palomera fault from the Calamocha and Concud faults. The dominant trend of recent, extensional faults and fractures distributed within both relay zones is similar to that of the main fault or slightly deviates to approach the N-S direction. Close to the southern tip, such fractures mainly affect Upper Miocene and Villafranchian sediments, while close to the northern tip they cut Jurassic carbonates giving rise to narrow N-S trending grabens filled with Pleistocene alluvial sediments (Capote *et al.*, 1981). These relay zones dominated by along-strike fractures were described in detail and~~

~~interpreted by Peiro *et al*. (2019, 2020) with the help of analogue modelling. Fracturing in this new type of fault relay is controlled by both the structural inherited grain and the remote stress field, and efficiently contribute to slip transfer and dynamical interaction between adjacent faults. It strongly contrasts with the classical models reported in the literature (*e.g.*, Peacock and Sanderson, 1994; Young *et al.*, 2001; Fossen and Rotevatn, 2016), in which transverse connecting faults controlled by the own relay kinematics prevail. According to Peiro *et al*. (2020), the overall fault system at the eastern boundary of the Jiloca basin is at an intermediate stage between complete independence and coalescence, and will probably evolve to an along-strike propagation of the master faults through the distributed longitudinal fracture ensembles. The slightly bimodal throw *vs*. distance (T-D) curve depicted in Fig. 7 suggests that the Sierra Palomera fault itself resulted from coalescence of two distinct fault segments, although their overall bell-shape indicates full linkage between them. Moreover, the persistence of an important bending component beyond both tips of the fault trace reveals that the total length of the Sierra Palomera fault is larger than that exposed at the surface, thus being propagated towards NNW and SSE as a blind fault.~~

~~Geophysical and morphotectonic data have allowed characterizing the overall structure of the hanging-wall block beyond the apparently flat appearance of the Sierra Palomera pediment. We have explained (sections 5 and 6) how magnetic field linear anomalies parallel to the Sierra Palomera fault trace suggest a distribution of subsoil lithological domains consistent with a gentle horst-and-graben setting.~~

~~The most conspicuous linear anomaly coincides with a morphological lineament (a gentle uphill-facing scarplet) across the middle sector of La Sima alluvial fan (section 6), and with the uphill-facing fault scarp east of Las Vallejadas fault. The hypothesis that all of these elements represent an antithetic fault has been corroborated by the exposure of that antithetic rupture in La Sima trench. In summary, the available information reveals a more complex structure in the Sierra Palomera hanging-wall block than the one assumed so far, including: (i) a synthetic fault, located at about 1.5 km basinwards, which at its southern sector emerges at surface (Las Vallejadas fault); (ii) a recent antithetic fault, at a distance of 0.7-1.0 km, which would have displaced the surface of the La Sima alluvial fan and would extend southwards up to La Peñuela fault.~~

~~In order to depict the refined structural model of the Sierra Palomera hanging-wall block,~~ The synthetic Las Vallejadas fault and the antithetic La Peñuela fault ~~both faults~~ have been incorporated to the geological map of Figure 2, as well as to a new version of the cross section (Fig. 13a). Furthermore, the latter depicts a reinterpretation of the geometry of the master fault. It is known that the shape of the main fault surface strongly controls the style of accommodation folding and subsidiary faulting in the hanging-wall block of extensional faults. Rollover folds and antithetic faults develop above concave-upward fault bends, whereas drag folds and synthetic faults form above convex-upward fault bends, their propagation being facilitated by high curvature of such fault bends (McClay and Scott, 1991; Xiao and Suppe, 1992; Withjack *et al.*, 1995; Delogkos *et al.*, 2020). In our case, the occurrence of the antithetic and the synthetic inferred subsidiary faults strongly suggests the presence, at a depth of less than 1 km, of a relative flat in the main fault surface (*i.e.*, a double, convex-concave bend), probably located at the Middle-Upper Triassic lutite and evaporite units (Middle Muschelkalk and Keuper facies).

Concerning the along-strike propagation of the Sierra Palomera fault, the slightly bimodal throw *vs.* distance (T-D) curve depicted in Fig. 7 suggests that it could result from coalescence of two distinct fault segments (although the amplitude of the relative minimum between both maxima, close to the error bar adopted for throw estimations, casts doubt on the significance of this detail). In any case, the overall bell-shape of the T-D curve indicates full linkage along the fault zone. Moreover, the persistence of a bending component beyond both tips of the fault trace reveals that the total length of the Sierra Palomera fault is larger than that exposed at the surface, thus being propagated towards NNW and SSE as a blind fault.

According to Peiro *et al.* (2020), the overall fault system at the eastern boundary of the Jiloca basin is at a transient stage towards coalescence, and will probably evolve to an along-strike propagation of the master faults through distributed longitudinal fractures. The relay zones between Sierra Palomera, Calamocha and Concud faults, dominated by longitudinal fractures, represent a type of fault relay controlled by both inherited structures and the remote stress field (Peiro *et al.*, 2019, 2020). It strongly contrasts with the classical models reported in the literature (*e.g.*, Peacock and Sanderson, 1994; Young *et al.*, 2001; Fossen and Rotevatn, 2016), in which transverse connecting faults controlled by the own relay kinematics prevail.

Such fault system makes a geometrically and kinematically consistent, genetically related major extensional fault system. The N230ºE mean transport direction at the Sierra Palomera fault is similar to those of Concud (N220ºE; Lafuente *et al.*, 2014) and Calamocha (W to SW; Martín-Bello *et al.*, 2014). Moreover, all them probably resulted from negative inversion, during the Late Pliocene-Quaternary times, of previous contractive structures developed under the Paleogene-Early Miocene compression (Rubio and Simón, 2007; Lafuente et al., 2011a; Liesa et al., 2021).

~~[PREFERENTIALLY, FIG.13 SHOULD BE INSERTED HERE, AS A 2-COLUMN FIGURE]~~

8.2. Morphotectonic approach to assessing recent fault activity within the context of eastern Spain ~~Planation surfaces as structural markers: inferred offsets and slip rates~~

In the absence of stratigraphic markers recognized in both fault blocks, the ~~In contrast to the other master faults bounding the Jiloca graben, namely the Calamocha and Concud faults, no dated stratigraphic marker is available at the Sierra Palomera fault in order to precisely calculate its total offset and slip rate. In such context, the use of planation surfaces (in our case, the mid-Pliocene *FES2* and *FES3* surfaces; Fig 13b) is necessary for characterizing the macrostructure and measuring fault throws. As explained in Section 4,~~ fault throw *s.s.* and the total tectonic ~~offset of *FES2*~~throw at the Sierra Palomera graben margin ~~attain maximum values of~~(up to 330 m and 480 m, respectively) have been reasonably estimated from offset of Late Neogene planation surfaces. Nevertheless, uncertainties linked to such geomorphological markers should be highlighted.~~, resulting in slip rates of 0.09 and 0.13 mm/a.~~

~~We should draw attention to the fact that o~~Our main geomorphological marker, *FES2*, is poorly represented within the Jiloca bottom, *i.e.*, the hanging-all block of the Sierra Palomera fault, which makes difficult to calculate the actual throw. We interpret that the boundary between Plio-Pleistocene alluvial deposits and the underlying carbonate unit probably represents the ~~first approach to the~~ position of *FES2* (Fig. 13b), although it also could be correlated with *FES3*. According to the results provided by Ezquerro *et al.* (2020), such uncertainty introduces a potential error of either 10-40 m in the height of the marker (equivalent to the thickness of Villafranchian palustrine carbonates ≈ M8 megasequence of Ezquerro, 2017), or 0.3 Ma in its age. If the top of the buried carbonate unit would be Early Villafranchian in age (3.5 Ma, therefore correlative of *FES3*): (i) the fault throw *s.s.* and the total tectonic ~~offset~~ throw calculated in section 4 (330 m and 480 m, respectively) should be applied to a 3.5 Ma time span, therefore resulting in slightly higher slip rates (0.10 *vs*. 0.09 mm/a, 0.15 *vs*. 0.13 mm/a, respectively); (ii) *FES2* would lie 10-40 m lower within the downthrown block, and hence the fault throw *s.s.* and the maximum total tectonic ~~offset~~ throw could increase up to 370 m and 520 m, respectively, giving rise to slip rates of 0.10 and 0.15 mm/a for the last 3.8 Ma. In any case, such height uncertainty is of the same order as the unevenness of the planation surfaces themselves, and results in a very small error in slip rate (0.01~~-0.02~~ mm/a).

The consistency of this interpretation is further reinforced if ~~a broader morphotectonic perspective is adopted, considering~~ the whole morphotectonic setting ~~of footwall and~~

~~hanging wall blocks of the Sierra Palomera fault and neighbouring structures~~is considered. We have explained how the morpho~~-~~sedimentary *FES2* marker defines a tilted Sierra Palomera-Alfambra block whose edge is tectonically uplifted ca. 300 m relative to the bottom of the Teruel basin. A similar morphostructural outline can be drawn for the Sierra de Albarracín-Jiloca block, in which the *FES2* ~~shows a~~altitude progressively decreases eastwards ~~decrease in altitude~~, from 1400-1500 m to <1100 m. Therefore, the inference that the fault separating such tilted blocks has a throw in the range of 300-400 m seems well-founded. On the other hand, the notion of recent ~~vertical displacement~~throw on the Sierra Palomera fault being larger than those on Calamocha and Concud faults (210 and 260 m, respectively; Martín-Bello *et al.*, 2014; Ezquerro *et al.*, 2020) fits a common structural feature of segmented extensional fault zones, in which maximum throws are found in central segments (self-similar pattern as that of individual faults; Cowie and Roberts, 2001). Gracia *et al.* (2003) aimed to minimize the role of tectonic slip on the Sierra Palomera fault ~~subsidence~~ in benefit of erosional lowering in the development of the central Jiloca depression, ~~and hence to underestimate the throw of the Sierra Palomera fault (see further discussion by Rubio and Simón, 2007; Rubio *et al.*, 2007; Gracia *et al.*, 2008). Nevertheless, such~~but that controversy is currently out of place.

~~It is also pertinent to~~We should compare the displacement and slip rates on the Sierra Palomera fault with those in the neighbouring Teruel graben. During the last 3.8 Ma (Late Pliocene-Quaternary extensional phase), fault zones making the eastern margin of the Teruel basin underwent total ~~vertical displacement~~throw (including bending component) in the range of 440 to 620 m, and hence long-term vertical slip rates of 0.12 to 0.16 mm/a (Ezquerro *et al.*, 2020). Assuming an average dip of 70º for the fault plane and a pure normal movement, the resulting total net slip rates for this period are 0.13 to 0.17 mm/a, similar to that calculated for the Sierra Palomera fault (0.15 mm/a) and higher than those for the Concud (0.07-0.08 mm/a; Lafuente *et al.*, 2011a), Calamocha (0.06-0.09 mm/a; Martín-Bello *et al.*, 2014), and Teruel (0.075 mm/a; Simón *et al.*, 2017) faults.

~~***8.3. Geomorphic indices of the mountain front: assessing fault activity***~~

It is also pertinent to consider g~~G~~eomorphic indices ~~constitute an~~as auxiliary tools for assessing fault activity~~, as enhanced by,~~ (*e.g.*, Bull and McFadden, ~~(~~1977;~~),~~ McCalpin, ~~(1996~~2009;~~),~~ Silva *et al.*, ~~(~~2003;~~),~~ ~~or~~ Burbank and Anderson, ~~(~~2012)~~. With this respect, it is interesting to~~ , and compare the values ~~proposed~~ obtained for the Sierra Palomera mountain front with those of other faults in the same geodynamic framework.

At Sierra Palomera, García-Lacosta (2013) calculated ~~values of two significant~~

~~geomorphic indices defined by Bull and McFadden (1977), *i.e.*,~~the mountain-front sinuosity (S_{mf} = 1.27), and valley width/height ratio (V_f = 0.22). ~~The value of S_{mf} is 1.27. The average width/height ratio calculated for 10 gullies crossing the fault is V_f = 0.22 (measured 250 m upstream from the fault trace).~~ These values, together with ~~other mentioned~~ qualitative attributes ~~of the mountain front (~~as trapezoidal facets, V-shaped gullies, and~~,~~ small alluvial fans not connected to the regional fluvial system~~)~~, indicate 'rapid' fault slip according to the classification by McCalpin (2009~~1996~~), and 'active' (according to Silva *et al.*, 2003) (Fig. 14). The range of slip rates that those authors estimate for such categories in their respective classifications (0.08 to 0.5 mm/a) encloses the value calculated for the Sierra Palomera ~~our~~ fault from offset of the *FES2* marker (0.09-0.13 mm/a).

[PREFERENTIALLY, FIG.14 SHOULD BE INSERTED HERE, AS A 1-COLUMN FIGURE]

The sinuosity index S_{mf} at the Sierra Palomera mountain front is very similar to those published for ~~that at~~ the Concud fault (S_{mf} =1.24; Lafuente *et al.*, 2011b),~~ and to those calculated by Perea (2006) for twenty fault-generated mountain fronts at the~~ Maestrat grabens in~~,~~ eastern Iberian Chain (S_{mf} = 1.04-1.60; mean = 1.27; Perea, 2006), or ~~. They also resemble those obtained at well-known active faults of the Betic Chains (SE Spain), such as the~~ Carboneras, Lorca-Alhama ~~or~~ and Baza faults in the Betic Chains~~,~~ (~~in which~~ S_{mf} usually ranging~~es~~ from 1.05 to 1.4; ~~(~~Silva *et al.*, 2003; García-Tortosa *et al.*, 2008).

The ~~average value of the~~ V_f index computed ~~at a distance of 250 m upstream from~~for the Sierra Palomera fault ~~trace (V_f = 0.22)~~ does not differ ~~very much~~ from that of the Concud fault (V_f = 0.30; Lafuente *et al.*, 2011b), while higher and more variable values have been reported in the Maestrat grabens (Silva *et al.*, 2003;~~V_f = 0.12-1.5;~~ Perea, 2006~~), and Betic Chains: Baza fault (V_f = 0.28-0.86;~~ ; García-Tortosa *et al.*, 2008)~~; Carboneras and Lorca-Alhama faults (0.38 to 0.59; Silva *et al.*, 2003)~~.

Plotting S_{mf} *vs.* V_f values on the diagram proposed by Silva *et al.* (2003) allows ~~us~~ assessing the relative position of the Sierra Palomera fault among extensional fault-generated mountain fronts of eastern Spain (Fig. 14). The relatively low values of both S_{mf} and V_f indices found at the Sierra Palomera mountain front (1.27 and 0.22, respectively) represent a morphotectonic signal similar to that of the Concud fault, and also consistent with the tendency of extensional faults studied by Silva *et al.* (2003) in the Valencia area and Betic Chains~~, which draw the tendency curve plotted in Fig. 14. The position of our geomorphic~~

~~indices on that diagram: (i) demonstrates that the Sierra Palomera fault fits the same tendency, and (ii) corroborates that it lies within Class 1 (active).~~.

8.~~3~~4. Pleistocene fault activity and its paleoseismological relevance

~~Although m~~Morphotectonic data indicate that the Sierra Palomera fault has a significant degree of activity, but no outcrop observation on the main trace has unequivocally evidenced ~~its~~ Quaternary ~~activity~~displacement on it. Therefore, it is very relevant the finding, in La Sima trench, of Pleistocene faults that accommodate extensional deformation associated to the hanging-wall rollover, since they indirectly confirm, for the first time, Pleistocene activity of the ~~main~~ Sierra Palomera fault.

As explained in section 6.4, seven deformation events (T to Z) have been recognized after detailed trench analysis, which could be conventionally considered as paleoseismic events according to usual criteria in Paleoseismology. Individual faults activated in each event have been recognized, and~~;~~ ~~their displacements have~~slip on them has been quantified (individual net slip in the range of 5 to 1125 cm; ~~mean = 28 cm;~~ Table 2). Finally, t~~, and t~~he overall faulting history has been carefully reconstructed by means of retrodeformational analysis (Fig. 12). Nevertheless, we should critically admit that the meaning of these results in relation to paleoseismicity of the Sierra Palomera fault is very imprecise, since:

(i) Instead of crossing the main fault, the trench only represents a short transect within the hanging-wall block, at a distance of 1.0 km from the ~~Sierra Palomera~~ fault trace.

(ii) During each event, faults widely distributed along the surveyed transect underwent both synthetic slip with Sierra Palomera fault (downthrown block to the west; positive values in Table 2) and antithetic slip (negative). The algebraic sum of those values does not necessarily haves ~~no~~ any meaning in relation to the real slip on the main fault.

(iii) The poor quality of OSL results precludes us from having an age model of the exposed sedimentary succession; therefore, the age constraints of the individual events are very limited. Only the last two events, Y and Z, could be dated to ca. 97±10 ka and 49±5 ka, respectively.

Concerning the net slip accumulated by faults (see Table 2), three among~~: (i)~~ the first ~~two~~ four events (T, ~~and~~ U and W) involve significant synthetic slip (+45, +105 and +60~~110~~ cm, respectively), while ~~; (ii) for V and W, synthetic and antithetic movements almost counterbalanced each other; (iii)~~ the last three ~~events~~ ones (X, Y, Z) involve significant antithetic slip (−45~~90~~, −35~~40~~ and −110~~25~~ cm, respectively). The ~~cumulative~~ global aggregate fault slip for the ensemble of deformation events~~,~~ is virtually null (+10 cm). Nevertheless, a total accumulated ~~=110 cm, considering an average fault dip of 65°, represents an antithetic~~

~~throw of ca. 100 cm. We should add the vertical offset accommodated as continuous deformation in the bending monocline (amplitude: ca. 120 cm), not included when computing fault slip *s.s.* The total tectonic,~~ antithetic throw ~~throw at the transect should be therefore estimated at~~of 21~~2~~0 cm ~~(net slip ≈ 230 cm). This value reasonably approaches the total throw (190 cm) that~~ can be directly measured on the log from offset of the top of unit 6, the ~~(~~youngest sedimentary marker previous to the recorded faulting episodes (compare the first and the last picture in Fig. 12)~~)~~. Consequently, that resulting throw should be entirely attributed to the bending monocline (i.e., accommodated in the form of continuous deformation, not computed within fault slip measurements depicted in Table 2). That value reasonably approaches the apparent vertical offset of~~It is also consistent with the apparent height of the gentle uphill-facing scarplet that breaks~~ the natural slope of La Sima alluvial fan (ca. 2.5~~260 c~~m; Fig. 10c). In summary, the morphological expression (up-facing scarplet) of the fault zone exposed in the trench fits well the antithetic sign of the accumulated ~~displacements~~slip during the ~~most recent~~youngest faulting episodes.

These~~e~~ youngest, antithetic faulting events (X, Y and Z) have associated net slip values (-35~~40~~ to -110~~25~~ cm) that should be accommodated on faults several km long (in the range of 10~~1~~ to 40~~23~~ km, according to the empirical relationships proposed by Wells and Coppersmith, 1994). This inference plays in favour of: (i) the interpretation of the antithetic fault exposed at La Sima trench as a large structure, comparable in length to the Sierra Palomera fault itself, as the macrostructural and geophysical data suggested (see sections 5, 6 and 8~~7~~.1); (ii) the notion that faulting events recorded at the trench, in particular those dated to ca. 97±10 ka and 49±5 ka, ~~very probably~~should respond to coseismic ~~slip~~ events on the main fault.

Could the timing of those younger events be taken as a reference for approaching seismic recurrence periods and slip rates of the Sierra Palomera fault during Pleistocene times? ~~This is a very difficult question to answer from the available information.~~ The tempting hypothesis that the two aforementioned ages correspond to the last two major paleoearthquakes would suggest a single interseismic period of around 48 ka. According to ~~the empirical relationship by~~ Villamor and Berryman (1999), ~~such a recurrence period is~~this would be reliable for faults ~~moving at an~~showing average slip rate around 0.1 mm/a~~; therefore, it fits well the long-term slip rate estimated for~~, as the Sierra Palomera fault does~~(in the range of 0.09 to 0.15 mm/a)~~.

Nevertheless, ~~we do not consider this as the most reliable scenario. T~~the space and time window examined in our trench is too narrow for providing a representative paleoseismological record. Subsidiary faults similar to those exposed at La Sima could have form at other sites within the hanging-wall block in response to other ~~slip~~ events on the ~~Sierra~~

~~Palomera~~main fault. Furthermore, each ~~slip~~ event on this main fault did not necessarily reactivate the antithetic~~al~~ fault exposed at La Sima trench. Accordingly, the actual slip rate on the ~~main~~ Sierra Palomera fault during Late Pleistocene times could be significantly higher than the long-term one~~, as evinced in other active faults of the region. Slip rate increased during Late Pleistocene times with respect to its average value since Late Pliocene times in the most documented structures south of Sierra Palomera: the Concud fault (0.29 *vs.* 0.07-0.08 mm/a) and Teruel fault (0.19 *vs.* 0.07 mm/a) (Lafuente *et al.*, 2014; Simón *et al.*, 2016, 2017). The same tendency has been revealed for other large faults of the neighbouring Teruel basin (Ezquerro *et al.*, 2020; see Section 2) and Calatayud basin (Peiro and Simón, 2021). We therefore consider that the Sierra Palomera fault, larger than the Concud and Teruel faults, very probably underwent a slip rate higher than 0.09-0.15 mm/a, and an average recurrence period shorter than 48 ka, since Late Pleistocene time.~~ (0.09-0.15 mm/a since mid-Pliocene times; see sections 8.1 and 8.2), following the same tendency found in other active structures of the region, such as the Concud fault (Lafuente *et al.*, 2014; Simón *et al.*, 2016), Teruel fault (Simón *et al.*, 2017), Teruel basin (Ezquerro *et al.*, 2020; see Section 2) and Calatayud basin (Peiro and Simón, 2021).

~~With this respect, the estimation of short-term slip rate that can be made for the antithetic La Peñuela fault from offset of Unit 9 in the studied trench is irrelevant. The top of that unit is dated to 97.4 ± 10.2 ka, and has been displaced by the last two deformation events defined (Y and Z), totalizing a cumulative antithetic net slip of 165 cm. This results in a slip rate of 0.015-0.019 mm/a, which only reflects the local deformation rate on a subsidiary fault for a very narrow, non-representative time window.~~

8.~~5~~4. Internal deformation of the hanging-wall fault block: a close look from trench analysis

Although the succession of deformation events identified at La Sima trench have a very limited paleoseismic meaning, it allows understanding progressive stretching within the hanging-wall block of the Sierra Palomera fault. In particular, sequential activation of synthetic and antithetic individual faults has been carefully reconstructed by means of retrodeformational analysis (Fig. 12) and can be precisely compared with faulting patterns linked to rollover deformation at both smaller and larger scales (~~observed in published~~ analogue models and field or seismic-profile examples, respectively)~~ of rollover deformation~~.

Usually, the hanging-wall rollover geometry is not entirely achieved through ductile ~~continuous~~ deformation. Examples from analogue models (*e.g.*, Withjack and Schlische, 2006), outcrops and high-resolution seismic profiles (*e.g.*, Song and Cawood, 2001; Delogkos *et al.*, 2020) indicate that a portion of ~~the hanging-wall~~ deformation is accommodated by smaller-scale faults. Antithetic faults directly materialize the antithetic simple shear ~~band~~ that nucleates at the transition ~~zone~~ from the main ramp to the basal detachment (Withjack *et al.*, 1995)~~. Therefore, they occur above, and~~ , frequently abutting~~,~~ the connection line between the steep and flat segments of the main fault surface (Bruce, 1973; Song and Cawood, 2001; Withjack and Schlische, 2006). In addition, together with subsidiary synthetic faults, they can accommodate layer-parallel extension along the rollover~~. Such extension mainly operates at the hinge zone of the rollover~~, giving rise to crestal collapse grabens ~~that are well documented from~~in both analogue models (*e.g.*, McClay, 1990; McClay and Scott, 1991; Buchanan and McClay, 1991; Soto *et al.*, 2007) and field examples (*e.g.*, Imber *et al.*, 2003; Back and Morley, 2016; Fazli K~~k~~hani *et al.*, 2017).

The locus of active hanging-wall antithetic faulting, as well as that of crestal graben formation, have the appearance of having migrated landwards during development of extensional systems: e~~. E~~ach individual antithetic fault ~~(or fault fan) forms near the fault bend,~~ moves passively ~~within the hanging-wall block~~ beyond the fault bend~~,~~ and becomes inactive, while a new fault ~~zone~~ propagating from the same ~~fault~~ bend replaces it. Thus, secondary faults tend to be progressively older basinwards (Christiansen, 1983; McClay, 1990; Withjack *et al.*, 1995; Withjack and Schlische, 2006). ~~That tendency can be enhanced by repeated footwall collapse (footwall faulting sequence) at the main structure (Imber *et al.*, 2003).~~

In any case, periods of activity of the hanging-wall growth faults can overlap ~~such overall time polarity of hanging-wall growth faults does not exclude significant overlap in their periods of activity~~ (Imber *et al.*, 2003)~~, as well as variations in the relative occurrence of synthetic and antithetic faults~~. The great majority of analogue models of rollovers show a faulting sequence that begins with an antithetic fault, then alternating synthetic and antithetic ones eventually joining and reciprocally offsetting at depth (McClay, 1990; McClay *et al.*, 1991; T. Román-Berdiel, personal communication). The same pattern has been reported in actual examples (e.g., Fazli Khani and Back, 2015, fig. 10). Nevertheless, sandbox experiments have also been ~~reported~~ described in which alternating activation of synthetic and antithetic faults is initiated with a synthetic one (*e.g.*, Buchanan and McClay, 1991).

The fault sequence interpreted at La Sima trench share some of the former evolutionary patterns typical of rollover deformation, such as the~~: (i)~~ relevance and persistence of a subsidiary antithetic fault, the~~; (ii)~~ activation of ~~additional,~~ younger antithetic ruptures closer to the main fault, and~~; (iii)~~ overall alternating onset of synthetic and antithetic ruptures. ~~On the other hand~~However, we have also found a non-typical feature: the oldest recorded meso-scale faults are synthetic with the Sierra Palomera fault, despite having formed in the same area where the persistent antithetic fault will later appear. The first ~~two~~ deformational events (T to W~~and U~~) mainly involve accumulation of significant synthetic net slip (+200~~155~~ cm), while ~~in the following two (V and W) synthetic and antithetic movements almost counterbalanced each other, and~~ the last three ones (X, Y, Z) involve substantial antithetic net slip (−190~~255~~ cm). Briefly, progressive deformation in the hanging-wall block is shifted from dominantly synthetic faulting to dominantly antithetic faulting. Such particular deformation pattern~~“irregularity”~~ suggests the existence of other controls on the hanging-wall deformation in addition to the rollover kinematics itself, as discussed in the next section.~~.~~

~~On the other hand~~Finally, the accumulated net slip has an associated component of horizontal extension that enables ~~another~~ a further quantitative kinematical approach (see Table 2). The total extension recorded at La Sima trench is ≈310~~85~~ cm, which represents about 19~~20~~% of the ~~total~~ restored length of the logged transect (local β factor = 1.19~~2~~). Horizontal extension accommodated by faults totalizes ca. 210 cm (125 cm by synthetic ones and 86 cm by antithetic ones). Development of the bending monocline involves additional extension of about 100 cm.~~The antithetic faults accommodate much more extension (200 cm) than the synthetic ones (115 cm). Considering that the bending monocline represents additional antithetic offset, it also involves additional horizontal extension, which can be estimated at 70 cm assuming a fault dip of 65º. Two main events (W, equally represented by synthetic and antithetic faults, and Z, mostly antithetic) accumulate about one half of the total extension (85 cm, ca. 4.5%, each one).~~

Overall considered, our results represent a high-resolution, sub-seismic-scale picture of hanging-wall deformation that complements natural case studies based on seismic profiles and ‘fills the gap’ with the scale of laboratory analogue models. It documents both (i) earlier stages of a process of hanging-wall deformation (those mostly governed by synthetic faulting) that usually are not recognized from seismic reflection data, and (ii) later stages governed by antithetic faulting that better correlate with seismic-reflection-based models.

8.5~~6~~. Kinematic and dynamic controls on deformation of the hanging-wall block: relevance of the tectonic ~~S~~stress ~~regime and tectonic~~ framework

It is not easy to discriminate whether faults propagated through the hanging-wall block are kinematically or dynamically controlled, *i.e.*, they essentially accommodate extensional deformation associated to the rollover monocline, or they are directly linked to regional stress.

Geometry and kinematics of faults ~~exposed in the~~surveyed at both map and trench scales~~, as well as of those inferred at a macrostructural scale from surface mapping and geophysical exploration, ~~overall fits the expected deformation within the hanging-wall block of the Sierra Palomera fault. But~~, at the same time, it is~~ they are also consistent with the regional extensional stress field, whose σ_3 trajectories trend ENE-WSW (Simón, 1982, 1989; Arlegui *et al.*, 2005, 2006; Liesa *et al.*, 2019), orthogonal to the overall trend of the Jiloca graben, and only slightly oblique to the Sierra Palomera fault trace itself. Stress inversion from the most representative, non-rotated conjugate faults measured within the trench, according to Anderson (1951)~~'s model~~, provides local stress axes matching those regional trajectories (Fig. 15).

[PREFERENTIALLY, FIG.15 SHOULD BE INSERTED HERE, AS A 1-COLUMN FIGURE]

~~It is not easy to discriminate whether the faults propagated through the hanging-wall block are kinematically or dynamically controlled, *i.e.*, they essentially accommodate extensional deformation associated to the rollover monocline, or they are directly linked to regional stress conditions. ~~The extension direction expectable for the ~~first ~~kinematical scenario could be constrained between N065ºE (orthogonal to the average strike of the Sierra Palomera fault; an inherited feature indeed) and N050ºE (transport direction). The extension trend expectable for the ~~second ~~dynamical scenario would approach N075ºE (seeing at the average trend of the Jiloca graben), or would range from N055ºE to N080ºE (seeing at paleostress results reported by Arlegui *et al.*, 2005, and Liesa *et al.*, 2019). The similarity between both inferences prevents us from discriminating among those hypothetical controls based solely on the orientation of structures (stereoplots of Fig. 11 show how the strongly clustered directions of normal faults in La Sima trench fit equally well the two scenarios). Nevertheless, some details of the faulting succession suggest that both controls probably coexist. The kinematical control has been attested and discussed in sections 8.1 and 8.5. The dynamical one could explain the ~~early ~~occurrence of early synthetic meso-scale faults (an unusual feature in kinematically-driven models) at La Sima site.

Additionally, there also seems to be a certain degree of control by a recent ESE-WNW extension direction. B~~the imprint of the regional stress field is revealed by certain fracture features directly linked to characteristic heterogeneities of the extensional Plio-Quaternary stress field in the eastern Iberian Chain. First, under the biaxial or multidirectional extension regime characterizing such stress field, a strong tendency for the σ_2 and σ_3 axes to switch~~

~~typically results in secondary faults striking at right angles to the master faults (Simón *et al.*, 1988; Simón, 1989; Arlegui *et al.* 2005, 2006). Second, b~~oth E-W to ESE-WNW, and ENE-WSW extension directions (characterizing the Late Miocene-Early Pliocene and the Plio-Quaternary rift episodes, respectively) are recorded during the entire extensional period indeed (Liesa *et al.*, 2019)~~,~~. This suggests~~ing~~ stress partitioning (in the sense of Simón *et al.*, 2008) of the composite extensional field that results from combination of intraplate NNW-SSE compression (Africa-Iberia convergence) and WNW-ESE extension (rifting of the Valencia trough) (Simón, 1989; Herraiz *et al.*, 2000; Capote *et al.*, 2002). Among f~~F~~ractures observed at La Sima trench that do not show any sign of displacement,~~only reveal the second type of stress heterogeneity. There is no orthogonal fault or fracture, and hence no evidence of permutation of~~ ~~σ_2~~ ~~and~~ ~~σ_3~~ ~~axes. Nevertheless,~~ a minority NNE-SSW trending set can be distinguished ~~among fractures that do not show any sign of displacement~~ (Fig. 11f~~e~~), which records the WNW-ESE extensional component of the regional, locally and episodically partitioned stress field.

9. Conclusions

~~1) The NNW-SSE trending, 26 km long Sierra Palomera extensional fault probably resulted from negative inversion of a previous contractive structure developed under the Paleogene-Early Miocene compression of the Iberian Chain.~~

~~2)~~ The NNW-SSE trending, 26 km long Sierra Palomera extensional fault has been active during Late Pliocene-Quaternary times. It~~n~~ has undergone nearly pure normal movement with mean transport direction towards N230ºE, consistent with the ENE-WSW extension trajectories of the recent to present-day regional stress field.

~~3) Magnetic and electromagnetic profiles, together with local geological and geomorphological evidence, suggest that t~~The hanging-wall block of the Sierra Palomera fault is cut by two subsidiary parallel ruptures: (i) the synthetic Las Vallejadas fault, located at about 1.5 km basinwards, and (ii) the antithetic La Peñuela fault, at a distance of 0.7-1.0 km, which apparently offsets ca. 2.5 m the surface of the La Sima alluvial fan giving rise to a gentle uphill-facing scarplet.

~~4)~~ In the absence of recent stratigraphic markers~~ visible in the both fault blocks~~, the *FES2* planation surface (3.8 Ma) ~~has constituted a useful marker for estimating the extensional net slip on the main fault. The corresponding contour map~~ has allowed calculating a maximum value of 330 ± 40 m for the fault throw *s.s.*, and ca. 480 ± 40 m for the total tectonic ~~offset~~

throw at the half-graben margin (including the bending component). Assuming an average dip of 70º for the fault plane and a pure normal movement,, resulting in a net slip rate of 0.09 ± 0.01 mm/a is inferred (0.13 ± 0.01 mm/a including bending). Based on the natural unevenness of the *FES2* marker, the error bar for the calculated throws and net slip values is ±40 m, which results in errors for slip rates around 0.01 mm/a.

5) The Sierra Palomera fault is expressed in the landscape by a conspicuous fault mountain front. Qualitative geomorphological features (trapezoidal facets; V-shaped gullies; small, steep alluvial fans not fully connected to the axial drainage), as well as values of geomorphic indices, are consistent with a significant degree of recent fault activity.

6) Trench study hasResults from La Sima trench have demonstrated the existence of the above-mentioned antithetic subsidiary La Peñuela fault, accompanied by a number of minor synthetic and antithetic ones, and its activity during Middle-Late Pleistocene times. Their detailed kinematical analysis has allowed building an evolutionary model made of seven deformation events recorded in Middle-Late Pleistocene alluvial deposits. Net slip on individual faults ranges from 5 to 1125 cm (mean = 28 cm). The cumulative global antithetic throw at the antithetic exposed fault zone, including fault slip *s.s.* and bending, is estimated at 2120 cm, which reasonably approaches the apparent offset of the natural slope of La Sima alluvial fan. at the uphill-facing scarplet (260 cm).

The significance of the paleoseismic results is certainly limited. The surveyed trench within the hanging-wall block does not cross the main fault itself. In addition7) Unfortunately, it was not feasible to achieve a consistent age model for the entire sedimentary sequence, since the majority of samples dated by Optically Stimulated Luminiscence (OSL) presented signal saturation. O; only the last two deformation events have been dated to ca. 97±10 ka and 49±5 ka, respectively. In addition, the surveyed trench only represents a short transect within the hanging-wall block, not across the main fault itself, so that its paleoseismic significance is limited. Nevertheless, it is worth highlighting the fact that, for the first time, Pleistocene activity of the Sierra Palomera fault has been unequivocally (although indirectly) proved for the first time, although indirectly from hanging-wall deformation.from outcrop observation.

8) Despite its poor paleoseismic meaning, tThe succession of faulting events identified at La Sima trench study allows unravelling the progressive extensional deformation mechanisms within the hanging-wall block of the Sierra Palomera fault. The total horizontal extension recorded at La Sima trench is ≈31085 cm (local β factor = 1.192). The evolutionary modelfaulting succession built from retrodeformation analysis indicates that synthetic slip

prevailing in early deformation events was ~~gradually substituted by~~shifted to antithetic slip ~~,~~ ~~the latter being clearly predominant~~ during the younger ones. Geometry and sequential development of meso-scale faults suggest the concurrence of: (1) a kinematic control, *i.e.*, antithetic simple shear linked to rollover kinematics (mostly resulting in the main antithetic fault zone), eventually accompanied by layer-parallel extension orthogonal to the rollover axis, and (2) a dynamic control, *i.e.*, response to the ~~regional~~ remote extensional stress field, characterized by ENE-WSW (occasionally ESE-WSW) extension trajectories.

Acknowledgments

The research has been financed by projects LMP127_18 (Gobierno de Aragón-Programa Operativo del Fondo Europeo de Desarrollo Regional Aragón 2014-2020), and PID2019-108705-GB-I00 of the Agencia Estatal de Investigación (AEI/10.13039/501100011033) of the Spanish Government~~the Spanish Government (Ministerio de Ciencia e Innovación)~~. This work is a contribution of the Geotransfer Research Group (E32_20R) funded by Gobierno de Aragón. A. Peiro benefits from an FPU contract (FPU17/02470) of the Spanish Government. We thank G. Brook~~,~~ (Luminiscence Dating Laboratory of University of Georgia, ~~(~~USA), and P. Beneítez~~,~~ (Laboratorio de Datación y Radioquímica of the Universidad Autónoma de Madrid, ~~(~~Spain)~~,~~ for OSL dating. A. Medialdea advised us on issues related to OSL dating, and T. Román-Berdiel helped us comparing the results with analogue models. Finally, we sincerely thank the thorough reviews and valuable comments of Hamed Fazli Khani and an anonymous reviewer, which have greatly improved the paper.

References

Alcalá, L., Alonso-Zarza, A.M., Álvarez, M.A., Azanza, B., Calvo, J.P., Cañaveras, J. C., van Dam, J.A., Garcés, M., Krijgsman, W., van der Meulen, A.J., Morales, J., Peláez, P., Pérez-González, A., Sánchez, S., Sancho, R., Sanz, E., 2000. El registro sedimentario y faunístico de las cuencas de Calatayud-Daroca y Teruel. Evolución paleoambiental y paleoclimática durante el Neógeno. Revista Sociedad Geológica España. 13, 323-343.

Allmendinger, R.W., Cardozo, N., Fisher, D., 2012. Structural geology algorithms: Vectors and tensors in structural geology. Cambridge University Press.

Álvaro, M., Capote, R., Vegas, R., 1979. Un modelo de evolución geotectónica para la Cadena Celtibérica. Acta Geológica Hispánica. 14, 172-177.

Anadón, P., Moissenet, E., 1996. Neogene basins in the Eastern Iberian Range, in: Friend, P.F., Dabrio, C.F. (Eds.), Tertiary basins of Spain. The stratigraphic Record of Crustal kinematics. World and Regional Geology series 6, Cambridge University press, Cambridge, pp. 68-76.

Anderson, E.M., 1951. The dynamics of faulting and dyke formation with application to Britain. Oliver & Boyd, Edinburgh.

Arlegui, L.E., Simón, J.L., Lisle, R.J., Orife, T., 2005. Late Pliocene-Pleistocene stress field in the Teruel and Jiloca grabens (eastern Spain): contribution of a new method of stress inversion. Journal of Structural Geology. 27, 693-705. https://doi.org/10.1016/j.jsg.2004.10.013.

Arlegui, L.E., Simón, J.L., Lisle, R.J., Orife, T., 2006. Analysis of non-striated faults in a recent extensional setting: the Plio-Pleistocene Concud fault (Jiloca graben, eastern Spain). Journal of Structural Geology. 28, 1019-1027. https://doi.org/10.1016/j.jsg.2006.03.009.

Back, S., Morley, C.K., 2016. Growth faults above shale–Seismic-scale outcrop analogues from the Makran foreland, SW Pakistan. Marine and Petroleum Geology. 70, 144-162. https://doi.org/10.1016/j.marpetgeo.2015.11.008

Bruce, C.H., 1973. Pressured shale and related sediment deformation: mechanism for development of regional contemporaneous faults. AAPG Bulletin. 57, 878-886. https://doi.org/10.1306/819A4352-16C5-11D7-8645000102C1865D.

Buchanan, P.G., McClay, K.R., 1991. Sandbox experiments of inverted listric and planar fault systems. Tectonophysics. 188, 97-115. https://doi.org/10.1016/0040-1951(91)90317-L.

Bull, W.B., McFadden, L.D., 1977. Tectonic Geomorphology north and south of the Garlock fault California, in: Doehring, D.O. (Ed.), Geomorphology in arid regions. Allen & Unwin, London, pp. 115-138.

Burbank, D.W., Anderson, R.S., 2012. Tectonic Geomorphology. Wiley-Blackwell, Oxford.

~~Capote, R., Gutiérrez, M., Hernández, A., Olivé A., 1981. Movimientos recientes de la fosa del Jiloca (Cordillera Ibérica). Proceedings V Reunión del Grupo Español de Trabajo del Cuaternario, Sevilla, pp. 245-257.~~

Capote, R., Muñoz, J.A., Simón, J.L., Liesa, C.L., Arlegui, L.E., 2002. Alpine tectonics I: The Alpine system north of the Betic Cordillera, in: Gibbons, W., Moreno, T., (Eds.), Geology of Spain. The Geological Society, London, pp. 367-400.

Cardozo, N., Allmendinger, R.W., 2013. Spherical projections with OSXStereonet: Computers & Geosciences. 51, 193-205, https://doi.org/10.1016/j.cageo.2012.07.021.

~~Casas-Sainz, A.M., Gil-Imaz, A., Simón, J.L., Izquierdo-Llavall, E., Aldega, L., Román-Berdiel, T., Osácar, M.C., Pueyo-Anchuela, Ó., Ansón, M., García-Lasanta, C., Corrado, S., Invernicci, C., Caricchi, C., 2018. Strain indicators and magnetic fabric in intraplate fault zones: Case study of Daroca thrust, Iberian Chain, Spain. Tectonophysics. 730, 29-47. https://doi.org/10.1016/j.tecto.2018.02.013.~~

Christiansen, A.F., 1983. An example of a major syndepositional listric fault, in: Bally, A.W. (Ed.), Seismic expression of structural styles. AAPG Studies in Geology. 15 (2.3.1), 36-40.

~~Colomer, M., 1987. Estudi geològic de la vora sud-oest de la Fossa de Calataiud-Daroca, entre Villafeliche i Calamocha. BSc thesis, Univ. Barcelona.~~

Colomer, M., Santanach, P., 1988. Estructura y evolución del borde sur-occidental de la Fosa de Calatayud-Daroca. Geogaceta. 4, 29-31.

Cortés, A.L., Casas, A.M., 2000. ¿Tiene el sistema de fosas de Teruel origen extensional? Revista de la Sociedad Geológica de España. 13(3-4), 445-470.

Cortés, A.L., 1999. Evolución tectónica reciente de la Cordillera Ibérica, Cuenca del Ebro y Pirineo centro-occidental. Unpublished PhD thesis. Univ. Zaragoza.

Cowie, P., Roberts, G.P., 2001. Constraining slip rates and spacings for active normal faults. Journal of Structural Geology. 23, 1901-1915. https://doi.org/10.1016/S0191-8141(01)00036-0.

Delogkos, E., Saqab, M.M., Walsh, J.J., Roche, V., Childs, C., 2020. Throw variations and strain partitioning associated with fault-bend folding along normal faults. Solid Earth. 11, 935-945. https://doi.org/10.5194/se-11-935-2020.

Ezquerro, L., 2017. El sector norte de la cuenca neógena de Teruel: tectónica, clima y sedimentación. PhD thesis, Univ. Zaragoza, http://zaguan.unizar.es/record/77098#

Ezquerro, L., Simón, J.L., Luzón, A., Liesa, C.L., 2019. Alluvial sedimentation and tectono-stratigraphic evolution in a narrow extensional zigzag basin margin (northern Teruel Basin, Spain). Journal of Palaeogeography.~~,~~ 8, 1-25. https://doi.org/10.1186/s42501-019-0044-4

Ezquerro, L., Simón, J.L., Luzón, A., Liesa, C.L., 2020. Segmentation and increasing activity in the Neogene-Quaternary Teruel Basin rift (Spain) revealed by morphotectonic approach. Journal of Structural Geology. 135, 104043. https://doi.org/10.1016/j.jsg-2020.104403.

Fazli Khani, H., Back, S. 2015. The influence of pre-existing structure on the growth of syn-sedimentary normal faults in a deltaic setting, Niger Delta. Journal of Structural Geology. 73, 18-32. https://doi.org/10.1016/j.jsg.2015.01.011

Fazli ~~k~~Khani, H., Back, S., Kukla, P. A., Fossen, H., 2017. Interaction between gravity-driven listric normal fault linkage and their hanging-wall rollover development: a case study from the western Niger Delta, Nigeria. Geological Society. London, Special Publications. 439(1), 169-186. https://doi.org/10.1144/SP439.20.

Fossen, H., Rotevatn, A., 2016. Fault linkage and relay structures in extensional settings-A review. Earth-Science Reviews. 154, 14-28. https://doi.org/10.1016/j.earscirev.2015.11.014.

García-Lacosta, A.I., 2013. La falla de Sierra Palomera: evolución estructural y actividad reciente. Unpublished MSc thesis, Univ. Zaragoza.

García-Tortosa, F.J., Sanz de Galdeano, C., Sánchez-Gómez, M., Alfaro, P., 2008. Geomorphologic evidence of the active Baza Fault (Betic Cordillera, South Spain), Geomorphology. 97, 374-391. https://doi.org/10.1016/j.geomorph.2007.08.007.

~~Gracia, J., 1992. Tectónica pliocena de la Fosa de Daroca (prov. de Zaragoza). Geogaceta, 11, 127-129.~~

Gracia, F.J., Gutiérrez, F., Gutiérrez, M., 2003. The Jiloca karst polje-tectonic graben (Iberian Range, NE Spain). Geomorphology. 52, 215-231. https://doi.org/10.1016/S0169-

555X(02)00257-X.

Gracia, F.J., Gutiérrez, F., Gutiérrez, M., Rubio, J.C., Simón, J.L., 2008. Discussion of ‘Tectonic subsidence vs erosional lowering in a controversial intramontane depression: the Jiloca basin (Iberian Chain, Spain)’. Geological Magazine. 145, 591-597.

Granier, T., 1985. Origin, damping, and pattern of development of faults in granite. Tectonics. 4, 721-737. https://doi.org/10.1029/TC004i007p00721.

Guimerà, J., Alvaro, M., 1990. Structure et evolution de la compression alpine dans la Chaine Cotiere Catalane (Espagne). Bulletin Société Géologique France. 8, 339-348. https://doi.org/10.2113/gssgfbull.VI.2.339.

Gutiérrez, M., Gracia, F.J., 1997. Environmental interpretation and evolution of the Tertiary erosion surfaces in the lberian Range (Spain), in: Widdowson, M. (Ed.), Palaeosurfaces: Recognition, Reconstruction and Palaeoenvironmental Interpretation. Geological Society. London, Special Publications. 120, 147-158.

Gutiérrez, M., Peña, J.L., 1976. Glacis y terrazas en el curso medio del río Alfambra (provincia de Teruel). Boletín Geológico y Minero. 87, 561-570.

Gutiérrez, F., Gutiérrez, M., Gracia, F.J., McCalpin, J.P., Lucha, P., Guerrero, J., 2008. Plio-Quaternary extensional seismotectonics and drainage network development in the central sector of the Iberian Range (NE Spain). Geomorphology. 102, 21-42. https://doi.org/10.1016/j.geomorph.2007.07.020.

Gutiérrez, F., Masana, E., González, Á., Lucha, P., Guerrero, J., McCalpin, J.P., 2009. Late Quaternary paleoseismic evidence on the Munébrega half-graben fault (Iberian Range, Spain). International Journal of Earth Sciences. 98, 1691-1703. https://doi.org/10.1007/s00531-008-0319-y.

Gutiérrez, F., Gracia, F.J., Gutiérrez, M., Lucha, P., Guerrero, J., Carbonel, D., Galve, J.P., 2012. A review on Quaternary tectonic and nontectonic faults in the central sector of the Iberian Chain, NE Spain. Journal of Iberian Geology. 38, 145-160. https://doi.org/10.5209/revJIGE.2012.v38.n1.39210.

Gutiérrez, F., Carbonel, D., Sevil, J., Moreno, D., Linares, R., Comas, X., Zarroca, M., Roqué, C., McCalpin, J.P., 2020. Neotectonics and late Holocene paleoseismic evidence in the Plio-Quaternary Daroca Half-graben, Iberian Chain, NE Spain. Implications for fault source characterization. Journal of Structural Geology. 131, 103933. https://doi.org/10.1016/j.jsg.2019.103933.

Herraiz, M., De Vicente, G., Lindo, R., Giner, J., Simón, J.L., González, J.M., Vadillo, O., Rodríguez, M.A., Cicuéndez, J.I., Casas, A., Rincón, P., Cortés, A.L., Lucini, M., 2000. The recent (Upper Miocene to Quaternary) and present tectonics stress distributions in the Iberian Peninsula. Tectonics. 19, 762-786. https://doi.org/10.1029/2000TC900006.

IGN, 2021. Catálogo de terremotos. https://www.ign.es/web/ign/portal/sis-catalogo-terremotos (accessed August 2021).

Imber, J., Childs, C., Nell, P.A.R., Walsh, J.J., Hodgetts, D., Flint, S., 2003. Hanging wall fault kinematics and footwall collapse in listric growth fault systems. Journal of Structural Geology. 25(2), 197-208. https://doi.org/10.1016/S0191-8141(02)00034-2.

Lafuente, P., 2011. Tectónica activa y paleosismicidad de la falla de Concud (Cordillera Ibérica central). Unpublished PhD thesis, Univ. Zaragoza.

Lafuente, P., Arlegui, L.E., Liesa, C.L., Simón, J.L., 2011a. Paleoseismological analysis of an intraplate extensional structure: the Concud fault (Iberian Chain, Eastern Spain). International Journal of Earth Sciences. 100, 1713-1732. https://doi.org/10.1007/s00531-010-0542-1.

Lafuente, P., Lamelas, T., Simón, J.L., Soriano, M.A., 2011b. Comparing geomorphic and geologic indices of activity in an intraplate extensional structure: the Concud fault (central Iberian Chain, Spain). Geodinamica Acta. 24, 107-122. https://doi.org/10.1007/S00531-010-0542-1.

Lafuente, P., Arlegui, L.E., Liesa, C.L., Pueyo, O., Simón, J.L., 2014. Spatial and temporal variation of paleoseismic activity at an intraplate, historically quiescent structure: the Concud fault (Iberian Chain, Spain). Tectonophysics. 632, 167-187. https://doi.org/10.1016/j.tecto.2014.06.012.

Liesa, C.L. 2011. Evolución de campos de esfuerzos en la Sierra del Pobo (Cordillera Ibérica, España). Revista Sociedad Geológica España. 24, 49-68.

Liesa, C.L., Simón, J.L., Casas, A.M., 2018. La tectónica de inversión en una región intraplaca: La Cordillera Ibérica. Revista Sociedad Geológica España. 31, 23-50.

Liesa, C.L., Simon, J.L., Ezquerro, L., Arlegui, L.E., Luzón, A., 2019. Stress evolution and structural inheritance controlling an intracontinental extensional basin: The central-northern sector of the Neogene Teruel Basin. Journal of Structural Geology. 118, 362-376. https://doi.org/10.1016/j.jsg.2018.11.011.

Liesa, C.L., Corral, M.B., Arlegui, L.A., Peiro, A., Simón, J.L., 2021. Inversión tectónica negativa y estructuración de la zona de relevo entre las fallas normales plio-cuaternarias de Calamocha y Daroca. X Congreso de Geología de España, Sociedad Geológica de España, Vitoria, Spain.

Martín-Bello, L., Arlegui, L.E., Ezquerro, L., Liesa, C.L., Simón, J.L., 2014. La falla de Calamocha (fosa del Jiloca, Cordillera Ibérica): estructura y actividad pleistocena, in: Álvarez-Gomez, J.A., Martín González, F. (Eds.), Una aproximación multidisciplinar al estudio de las fallas activas, los terremotos y el riesgo sísmico. Segunda reunión ibérica sobre fallas activas y paleosismología, Lorca, (Murcia, España), pp. 55-85.

McCalpin, J.P., 1996. Paleoseismology, 2nd Edition. Academic Press. International Geophysics Series., New York.

McClay, K.R., 1990. Extensional fault systems in sedimentary basins: a review of analogue model studies. Marine and Petroleum Geology. 7, 206-233. https://doi.org/10.1016/0264-8172(90)90001-W.

McClay, K.R., Scott, A.D., 1991. Experimental models of hangingwall deformation in ramp-flat listric extensional fault systems. Tectonophysics. 188, 85-96. https://doi.org/10.1016/0040-1951(91)90316-K.

McClay, K.R., Waltham, D.A., Scott, A.D., Abousetta, A., 1991. Physical and seismic modelling of listric normal fault geometries. Geological Society. London, Special Publications. 56, 231-239. https://doi.org/10.1144/GSL.SP.1991.056.01.16.

Moissenet, E., 1983. Aspectos de la Neotectónica en la fosa de Teruel, in: Comba, J.A. (Ed.), Geología de España. Libro Jubilar J.M. Ríos. 2, IGME, Madrid, pp. 427-446.

Pailhé, P., 1984. La Chaîne Ibérique Orientale. Étude géomorphologique, PhD thesis. Univ. Bordeaux.

Peacock, D.C.P., Sanderson, D.J., 1994. Geometry and development of relay ramps in normal fault systems. Bull. Am. Ass. Petrol. Geol. 78, 147-165. https://doi.org/10.1306/BDFF9046-1718-11D7-8645000102C1865D.

Peiro, A., Simón, J.L., 2021. The Río Grío-Pancrudo Fault Zone (central Iberian Chain, Spain): recent extensional activity revealed by drainage reversal. Geological Magazine. 159(1), 21-36(in press). https://doi.org/10.1017/S0016756821000790

Peiro, A., Simón, J.L., Román-Berdiel, T., 2019. Zonas de relevo de falla en el margen oriental de la fosa del Jiloca (Cordillera Ibérica): geometría, cinemática y modelización analógica. Boletín Geológico y Minero. 130 (3),~~:~~ 393-416. https://doi.org/10.21701/bolgeomin.130.3.002.

Peiro, A., Simón, J.L., Román-Berdiel, T., 2020. Fault relay zones evolving through distributed longitudinal fractures: the case of the Teruel graben system (Iberian Chain, Spain). Journal of Structural Geology. 131, 103942. https://doi.org/10.1016/j.jsg.2019.103942.

Peña, J.L., Gutiérrez, M., Ibáñez, M., Lozano, M.V., Rodríguez, J., Sánchez, M., Simón, J.L., Soriano, M.A., Yetano, L.M., 1984. Geomorfología de la provincia de Teruel. Instituto de Estudios Turolenses. Teruel.

Perea, H., 2006. Falles actives i perillositat sísmica al marge nord-occidental del solc de Valencia. Unpublished PhD thesis, Univ. Barcelona.

Pueyo, Ó., Lafuente, P., Arlegui, L.E., Liesa, C.L., Simón, J.L., 2016. Geophysical characterization of buried active faults: the Concud Fault (Iberian Chain, NE Spain). International Journal of Earth Sciences. 105, 2221-2239. https://doi.org/10.1007/s00531-015-1283-y.

~~Roca, E.; Guimerà, J., 1992. The Neogene structure of the eastern Iberian margin: structural constraints on the crustal evolution of the Valencia trough (western Mediterranean). Tectonophysics. 203, 203-218. https:// doi.org/10.1016/0040-1951(92)90224-T.~~

Rubio, J.C., 2004. Los humedales del Alto Jiloca: estudio hidrogeológico e histórico-arqueológico. Unpublished PhD thesis, Univ. Zaragoza.

Rubio, J.C., Simón, J.L., 2007. Tectonic subsidence vs. erosional lowering in a controversial intramontane depression: the Jiloca basin (Iberian Chain, Spain). Geological Magazine. 144, 1-15. https://doi.org/10.1017/S0016756806002949.

Rubio, J.C., Simón, J.L., Soriano, A., 2007. Interacting tectonics, hydrogeology and karst processes in an intramontane basin: the Jiloca graben (NE Spain). Hydrological Journal. 15, 1565-1576. https://doi.org/10.1007/s10040-007-0190-0.

Sánchez-Fabre, M., Peña-Monné, J.L., Sampietro-Vattuone, M.M., 2019. Geomorphology of the northern sector of the Alfambra-Teruel depression (Iberian ranges, NE Spain). Journal of Maps. 15, 112-121. https://doi.org/10.1080/17445647.2018.1551157.

Silva, P.G.; Goy, J.L.; Zazo, C., Bardají, T., 2003. Fault-generated mountain fronts in southeast Spain: geomorphologic assessment of tectonic and seismic activity. Geomorphology. 50, 203-225. https://doi.org/10.1016/S0169-555X(02)00215-5.

Simón, J.L., 1982. Compresión y distensión alpinas en la Cadena Ibérica oriental. PhD thesis. Universidad de Zaragoza, Instituto de Estudios Turolenses, Teruel.

Simón, J.L., 1983. Tectónica y neotectónica del sistema de fosas de Teruel. Teruel. 69, 21-97.

Simón, J.L., 1989. Late Cenozoic stress field and fracturing in the Iberian Chain and Ebro Basin (Spain). Journal of Structural Geology. 11, 285-294. https://doi.org/10.1016/0191-8141(89)90068-0.

~~Simón, J.L., Serón, F.J., Casas, A.M., 1988. Stress deflection and fracture development in a multidirectional extension regime. Mathematical and experimental approach with field examples. Annales Tectonicae. 2, 21-32.~~

Simón, J.L., Arlegui, L.E., Lafuente, P., Liesa, C.L., 2012. Active extensional faults in the central-eastern Iberian Chain, Spain. Journal of Iberian Geology. 38, 127-144. https://doi.org/10.5209/rev_JIGE.2012.v38.n1.39209.

Simón, J. L., Arlegui, L. E., Ezquerro, L., Lafuente, P., Liesa, C. L., Luzón, A., 2016. Enhanced palaeoseismic succession at the Concud Fault (Iberian Chain, Spain): new insights for seismic hazard assessment. Natural Hazards. 80, 1967-1993. https://doi.org/10.1007/s11069-015-2054-6.

Simón, J.L., Arlegui, L.E., Ezquerro, L., Lafuente, P., Liesa, C.L. Luzón, A. 2017. Assessing interaction of active extensional faults from structural and paleoseismological analysis: The Teruel and Concud faults (eastern Spain). Journal of Structural Geology. 103, 100-119. https://doi.org/10.1016/j.jsg.2017.08.003.

Simón, J.L., Ezquerro, L., Arlegui, L.E., Liesa, C.L., Luzón, A., Medialdea, A., García, A., Zarazaga, D., 2019. Role of transverse structures in paleoseismicity and drainage rearrangement in rift systems: the case of the Valdecebro fault zone (Teruel graben, eastern Spain). International Journal of Earth Sciences. 108, 1429-1449. https://doi.org/10.1007/s00531-019-01707-9.

Simón, J. L., Casas-Sainz, A. M., Gil-Imaz, A., 2021. Controversial epiglyptic thrust sheets: The case of the Daroca Thrust (Iberian Chain, Spain). Journal of Structural Geology. 145, 104298. https://doi.org/10.1016/j.jsg.2021.104298.

Simón-Porcar, G., Simón, J.L., Liesa, C.L., 2019. La cuenca neógena extensional de El Pobo (Teruel, Cordillera Ibérica): sedimentología, estructura y relación con la evolución del relieve. Revista Sociedad Geológica España. 32, 17-42.

Song, T., Cawood, P.A., 2001. Effects of subsidiary faults on the geometric construction of listric normal fault systems. AAPG Bulletin. 85(2), 221-232. https://doi.org/10.1306/8626C7A3-173B-11D7-8645000102C1865D.

Soto, R., Casas-Sainz, A. M., Del Río, P., 2007. Geometry of half-grabens containing a mid-level viscous décollement. Basin Research. 19(3), 437-450. https://doi.org/10.1111/j.1365-2117.2007.00328.x.

Vegas, R., Fontboté, J.M., Banda, E., 1979. Widespread neogene rifting superimposed on alpine regions of the Iberian Peninsula. Proceedings Symposium Evolution and Tectonics of the Western Mediterranean and Surrounding Areas, EGS, Viena. Instituto Geográfico Nacional, Madrid, Special Publication. 201, 109-128.

Villamor, P., Berryman, K.R., 1999. La tasa de desplazamiento de una falla como aproximación de primer orden en las estimaciones de peligrosidad sísmica. I Congreso Nacional de Ingeniería Sísmica, Asociación Española de Ingeniería Sísmica~~, Abstracts, 1~~. 153-163.

Wells, D.L., Coppersmith, K.J., 1994. New Empirical Relationships among Magnitude, Rupture Length, Rupture Width, Rupture Area, and Surface Displacement. Bull. Seismol. Soc. Am. 84, 974-1002.

Withjack, M.O., Schlische, R.W., 2006. Geometric and experimental models of extensional fault-bend folds. Geological Society, London, Special Publications. 253(1), 285-305.

Withjack, M.O., Islam, Q.T., La Pointe, P.R., 1995. Normal faults and their hanging-wall deformation: An experimental study. AAPG Bulletin. 79, 1-18. https://doi.org/10.1144/GSL.SP.2006.253.01.15.

Young, M.J., Gawthorpe, R.L., Hardy, S., 2001. Growth and linkage of a segmented normal fault zone; the Late Jurassic Murchison-Statfjord North Fault, northern North Sea. Journal of Structural Geology. 23, 1933-1952. https://doi.org/10.1016/S0191-8141(01)00038-4.

The authors declare that they have no known competing financial interests or personal relationships that could have appeared to influence the work reported in this paper.

FIGURE CAPTIONS:

Figure 1:

(a) Location of the Iberian Chain within the Iberian Peninsula. (b) Geological sketch of the Iberian Chain, with location of the main Neogene-Quaternary extensional basins. (c) Simplified geological map of the Jiloca graben, with location of Figures 2, 6 and 9.

Figure 2:

Geological map of the Sierra Palomera area (on DEM image from Instituto Geográfico Nacional) showing the main structures associated to the Sierra Palomera fault. Location of Figures 3, 4, 8, 10a, 11 is indicated, as well as that of OSL samples in La Cecilia and La Sima alluvial fans (see Table 1).

Figure 3:

Cross section of the Jiloca Graben at its central sector, initially reconstructed from surface geology and shallow borehole data (modified from Rubio and Simón, 2007). See location in Figure 2.

Figure 4:

(a) Field view of one of the rupture surfaces within the damage zone of the Sierra Palomera fault; it cuts Lower Jurassic limestones and shows associated fault breccia. (b) Stereoplot (equal area, lower hemisphere) showing orientations of fault planes and slickenlines collected in that zone.

Figure 5:

The Sierra Palomera mountain front. (a) Field panoramic view. (b) Hillshade oblique image rendered from Digital Elevation Model (5 m grid) of Instituto Geográfico Nacional (IGN). (c) Detail of a trapezoidal facet within the fault scarp. (d) Hillshade oblique image (5-m-grid DEM, IGN) showing a close view to the alluvial fans sourced at the mountain front; La Cecilia and La Sima alluvial fans are identified.

Figure 6:

Morphotectonic map of the Sierra Palomera area.

Figure 7:

Throw *vs.* distance (T-D) graph along the Sierra Palomera fault. Lower curve: fault throw *s.s.* recorded by the *FES2* marker. Upper curve: total tectonic ~~offset~~ throw of *FES2* including the bending component.

Figure 8:

Villafranchian alluvial deposits (V) ~~deformed~~ tilted by an accommodation monocline above ~~in the footwall block of~~ La Peñuela fault. Jurassic limestones (J) of the footwall block crops out at the bottom of the gully. See location in Figure 2.

Figure 9:

Results of the ~~geomagnetic~~ magnetometric survey covering the Sierra Palomera piedmont. (a) Location of ~~magnetic~~ profiles 01 to 10 (which is the same as for the electromagnetic survey), with the residual values of field intensity (nT) plotted as a colour palette. Black thin lines depict the Sierra Palomera fault trace. Grey thick lines depict the spatial correlation of trending changes on the successive transects, and therefore of the described domains (A, B and C). (b) ~~Magnetic~~ Residual earth magnetic field profiles plotted with a normalized horizontal length, in which domains A, B and C roughly parallel to the Sierra Palomera fault are defined (data are in nT; see text for details).

Figure 10:

(a) Hillshade relief map of the barranco de la Sima alluvial fan rendered from digital elevation model (DEM, 5 m grid) of the Instituto Geográfico Nacional. See location in Figure 2. (b) Residual magnetic field anomalies at the central sector of the alluvial fan, at the contact between domains A and B. (c) Detailed topographic profile showing a slope anomaly in the longitudinal profile of the alluvial fan surface, from which an apparent antithetic throw of ca. 2.~~,~~5~~6~~ m can be inferred.

Figure 11:

(a) Uninterpreted photomosaic of La Sima trench, see location in Figure 2. (b) Detailed log ~~of La Sima trench~~. ~~See location in Figure 2.~~ 1 to 12: Quaternary units described in the text. Greek characters: faults referred in the text. The location and age of samples dated by OSL is indicated. Stereoplots (equal area, lower hemisphere) show orientations of faults and fractures measured within the trench: (c~~b~~) Central fault zone. (d~~c~~) Footwall block, including monocline. (~~d~~e) Synthetic stereoplot of fault planes, including a main set parallel to the prevailing structural trend (NNW-SSE, black great circles) and a subsidiary set oriented NNE-SSW (blue great circles); fault planes rotated at the~~;~~ ~~those rotated at the central~~ monocline have been restored to their original orientation. (~~e~~f) Synthetic stereoplot of fractures without displacement.

Figure 12:

Evolutionary model of sedimentation and deformation recorded at the La Sima trench from retrodeformational analysis. Each sketch represents a stage subsequent to the paleoseismic event (and, in some cases, to deposition of sedimentary units) labelled above. Unexposed sectors below the trench have been locally reconstructed in the sketches in order to complete the evolutionary model. Bold traces indicate which faults are active during each event. Total horizontal extension and throw calculated in Table 2 are shown.

Figure 13:

(a) Refined cross section of the Jiloca graben at its central sector, in which the new inferred, subsidiary faults have been incorporated. (b) Upper fringe of the same cross section (vertical scale x2) showing offset of planation surfaces *FES2* and *FES3*.

Figure 14:

Plot of S_{mf} (mountain-front sinuosity index) *vs.* V_f (valley width/height ratio, measured 250 m upstream from the fault trace), showing the relative position of the Sierra Palomera Fault among extensional fault-generated mountain fronts of eastern Spain. For comparison, the S_{mf} -V_f plots for the neighbouring Concud fault (Lafuente et al, 2011b), faults bounding the Maestrat grabens (eastern Iberian Chain; Perea, 2006), and Valencia region and Betic chains (Silva *et al*., 2003) are also included. Class 1, 2, 3: activity classes (active, moderate and inactive, respectively); the curve represents the tendency for normal faults in SE Spain according to Silva *et al*. (2003).

Figure 15:

Interpretation of paleostress axes from orientation of non-rotated, conjugate fault planes measured within La Sima trench. Stress inversion based on model by Anderson (1951).

Table 1:

Parameters and results of OSL dating of samples collected at the La Sima trench (S1 to S7; Luminiscence Dating Laboratory of University of Georgia, USA), and La Cecilia and La Sima alluvial fans (Laboratorio de Datación y Radioquímica de la Universidad Autónoma de Madrid, Spain).

Table 2:

Synthesis of deformation events inferred at La Sima trench: faults activated during each event;, net slip values calculated from the trench log and the retrodeformational analysis (positive: synthetic with the Sierra Palomera fault; negative: antithetic; Figs. 11, 12), and associated values of horizontal extension. Further explanation in text.

Hanging-wall deformation at the active Sierra Palomera extensional fault (Jiloca basin, Spain) from structural, morphotectonic, geophysical and trench study

A. Peiro[1], J.L. Simón[1], L.E. Arlegui[1], L. Ezquerro[2], A.I. García-Lacosta[1], M.T. Lamelas[3], C.L. Liesa[1], A. Luzón[1], L. Martín-Bello[1], Ó. Pueyo-Anchuela[1], N. Russo[1]

[1]Departamento de Ciencias de la Tierra and GEOTRANSFER Research Group-IUCA, Universidad de Zaragoza, Pedro Cerbuna, 12, 50009 Zaragoza, Spain.. apeiro@unizar.es jsimon@unizar.es, arlegui@unizar.es, anagarcialacosta@hotmail.com, carluis@unizar.es, aluzon@unizar.es, leticia.martin.bello@gmail.com, opueyo@unizar.es, nausicarusso@gmail.com

[2]GEOBIOTEC, Department of Earth Sciences, NOVA School of Science and Technology, Campus de Caparica, P-2829 516 Caparica, Portugal. lopezquerro@gmail.com

[3]Centro Universitario de la Defensa, Academia General Militar, Ctra. de Huesca s/n, 50090 Zaragoza, Spain. GEOFOREST Research Group-IUCA. tlamelas@unizar.es

Corresponding author: A. Peiro, apeiro@unizar.es

Abstract

The NNW-SSE trending Sierra Palomera fault is characterized as an active, nearly pure extensional fault with mean transport direction towards N230ºE, consistent with the ENE-WSW extension trajectories of the recent to present-day regional stress field. Its macrostructure is described from surface geology and magnetometric and electromagnetic surveys, which have allowed identifying two subsidiary, nearly parallel normal faults (antithetic and synthetic, respectively). The structural contour map of an extensive planation surface, dated to 3.8 Ma, provides a maximum fault throw *s.s.* of 330 m for the main fault (480 m including bending), and a net slip rate of 0.09 mm/a (0.13 mm/a including bending). Trench study focussed on the subsidiary antithetic fault shows evidence of its activity during Middle-Late Pleistocene times, offsetting ca. 2.5 m the slope of a well-preserved alluvial fan. Detailed analysis and retrodeformation of the antithetic fault and other minor ruptures in the trench has allowed defining seven deformation events. The lack of a consistent age model for the involved sedimentary sequence makes them almost meaningless in terms of paleoseismic history. However, geometry and sequential development of meso-scale faults (intermediate between seismic-scale and analogue models) allows unravelling the extensional deformation history within the hanging-wall block of the Sierra Palomera fault. Progressive rupture patterns reveal shifting from dominantly synthetic to dominantly antithetic faulting, suggesting both kinematical control linked to rollover growth, and dynamical control by the regional stress field.

Keywords: Active fault, antithetic fault, rollover, magnetometry, Pleistocene, Iberian Chain.

1. Introduction

Our understanding of geometry and kinematics of extensional fault systems has been significantly improved thanks to analytical and scaled analogue models, particularly concerning deformation of the hanging-wall block of listric faults. Such models provide interesting inferences about controls that the shape of the main fault surface exerts on the development of hanging-wall folds and fractures. Fault surfaces with irregular geometry induce antithetic simple shear along a deformation band that nucleates at shallowing fault bends, while synthetic shear is induced at steepening fault bends (McClay and Scott, 1991; Xiao and Suppe, 1992; Withjack *et al.*, 1995; Delogkos *et al.*, 2020). Depending on the mechanical behaviour of materials, such overall simple shear mechanism results in either fault-related folding (rollover and drag folds, respectively) or faulting (antithetic and synthetic, respectively). Analogue models provide insights into both differential behaviours, *e.g.*, by comparing experimental materials as clay and sand (*e.g.*, Withjack *et al.*, 1995). Nevertheless, as discussed by Xiao and Suppe (1992), models give limited information about the actual small-scale mechanisms that accommodate deformation. Therefore, contribution of data directly supplied by field examples is necessary for full understanding of kinematics of extensional systems.

The Sierra Palomera fault, at the central sector of the Jiloca basin, is one of the most conspicuous recent, hypothetically active extensional faults in the central Iberian Chain (Spain; Fig. 1), but less known than other neighbouring structures. The Calamocha and Concud faults, which bound the northern and southern sectors of the Jiloca basin (Fig. 1c), offset early Pliocene lacustrine deposits of the Calatayud and Teruel basins, respectively. This allows calculating their total throws at about 210 m for the Calamocha fault (Martín-Bello *et al.*, 2014), and 260 m for the Concud fault (Ezquerro *et al.*, 2020). On the contrary, no recent stratigraphic marker is available for the Sierra Palomera fault. The tectonic nature of the basin boundary itself, and particularly the relative role of erosive lowering and fault displacement in the creation of the mountain scarp, has been the object of controversy indeed. After Cortés and Casas (2000), its topography is essentially a result of erosive incision in response to orogenic uplift during the Paleogene. Gracia *et al.* (2003) reinterpret the Jiloca depression as a polje developed during the Late Pliocene-Quaternary. Rubio and Simón (2007) and Rubio *et al.* (2007) provide new sedimentary, geomorphological and hydrogeological evidence on the tectonic origin of the Jiloca depression, concluding that the Sierra Palomera fault has a maximum throw approaching 350-400 m.

Concerning the signs of Quaternary activity, these are again conspicuous in the northern and southern sectors of the Jiloca graben but not in the central one. The Concud fault has been object of intense paleoseismological research, which has allowed reconstructing a succession of eleven events since ca. 74 ka BP, with average recurrence period of 7.1-8.0 ka, total accumulated net slip of about 20 m, and average slip rate of 0.29 mm/a (Lafuente, 2011; Lafuente *et al.*, 2011a,b, 2014; Simón *et al.*, 2016). Quaternary activity of the Calamocha fault is revealed by the mechanical contact between Neogene units of the Calatayud basin and Late Pleistocene alluvial deposits that infill the northernmost Jiloca basin (Martín-Bello *et al.*, 2014). Other neighbouring faults (Munébrega, Teruel, Valdecebro) have also been object of trench studies in the last two decades (Gutiérrez *et al.*, 2009; Simón *et al.*, 2017, 2019). On the contrary, no exposure of the Sierra Palomera fault cutting Quaternary deposits has been reported, and no paleoseismological analysis has been carried out. This is mainly due to the fact that the Quaternary fluvial incision is virtually absent, and there is a lack of appropriate sites for digging trenches across the main fault.

In such a situation, the study of the Sierra Palomera fault should be focussed on obtaining indirect evidence of its recent activity from hanging-wall deformation. This can be achieved by (i) exploring the subsoil of the associated pediment by means of geophysical techniques, (ii) analysing the effects of fault activity on the relief through morphotectonic analysis, and (iii) recognizing deformation of Quaternary materials in trenches. Methodology of trench analysis, extensively used and standardized for paleoseismological studies (*e.g.*, McCalpin, 2009), offers new insights for detailed analysis of progressive extensional deformation. Concerning scale, trenches have the advantage of delivering valuable information on faults at an intermediate scale between seismic profiles and laboratory analogue models. Concerning timing, each identified event can be considered as an incremental or ‘infinitesimal’ deformation episode, and hence the reconstructed paleoseismic succession provides a detailed and realistic view of extension kinematics (although ineludibly constrained to a given space and time window).

The present work has been carried out in that perspective. Our specific objectives are: (1) improving our overall knowledge on the structure and evolution of the Sierra Palomera fault and the Jiloca basin; (2) reporting evidence on the activity of the Sierra Palomera fault during the Quaternary, and (3) characterizing the patterns of progressive extensional deformation within its hanging-wall block.

2. Geological setting

The Iberian Chain is a NW-SE trending, 450 km long intraplate mountain range located in the eastern Iberian Peninsula (Fig. 1a). This chain developed in Paleogene to Early Miocene times due to positive inversion of the extensional Mesozoic Iberian basin, under the convergence between the Africa and Eurasia plates (Álvaro *et al.*, 1979; Guimerà and Álvaro, 1990; Capote *et al.*, 2002; Liesa *et al.*, 2018). After a transition period during the Early Miocene, in which the longitudinal Calatayud basin developed under a transpressional regime (Colomer and Santanach, 1988; Simón *et al.*, 2021), a new extensional stage associated to rifting of the Valencia Trough took place.

Extensional deformation propagated onshore towards the central part of the Iberian Chain (Álvaro *et al.* 1979, Vegas *et al.*, 1979) in two stages, inducing both reactivation of the main inherited Mesozoic faults and formation of new normal faults, and generating a number of diversely oriented intracontinental grabens and half-grabens (Simón, 1982, 1989; Gutiérrez *et al.*, 2008, 2012; Ezquerro, 2017; Liesa *et al.*, 2019). During the first stage (Late Miocene to Early Pliocene in age), the 90-km-long, NNE-SSW to N-S trending Teruel half-graben basin developed, filled with terrestrial sediments up to 500 m thick (Simón, 1982, 1983; Moissenet, 1983; Anadón and Moissenet, 1996; Ezquerro, 2017; Ezquerro *et al.*, 2019, 2020). The second extensional stage that started by the mid-Pliocene has produced a more widespread deformation in the central Iberian Chain. A large number of inherited structures were reactivated, producing new NNW-SSE trending grabens and half-grabens that are inset or cross-cut the pre-existent Teruel and Calatayud basins (Simón, 1983, 1989; Gutiérrez *et al.*, 2008, 2020; Liesa *et al.*, 2019). They include, among others (Fig. 1c), the 80-km-long Jiloca graben, which results from en-échelon, right releasing arrangement of the NW-SE striking Concud, Sierra Palomera and Calamocha faults (Simón, 1983; Rubio and Simón, 2007; Simón *et al.*, 2012, 2017; Peiro *et al.*, 2019, 2020). In the first extensional phase, the direction of maximum extension (σ_3) was E-W to ESE-WNW (under a triaxial extensional regime), while 'multidirectional' extension with ENE-WSW σ_3 trajectories characterizes the second phase (Simón, 1982, 1983, 1989; Cortés, 1999; Capote *et al.*, 2002; Arlegui *et al.*, 2005, 2006; Liesa, 2011; Ezquerro, 2017; Liesa *et al.*, 2019).

Geometric construction of normal fault profiles of the Teruel half-graben system allows locating the sole detachment at a depth of 14-17 km b.s.l., and estimating an average E-W stretching factor ß = 1.1 since its onset (11.2 Ma ago) (Ezquerro *et al.*, 2020). Major faults accumulated slip of a few hundred metres to ca. 1 km (computing both fault throw *s.s.* and associated bending). The resulting slip rate, around 0.09 mm/a in average, is very similar for distinct transects across the structure, but shows a clear increase between both extensional phases: from 0.05-0.07 mm/a to 0.12-0.16 mm/a (Ezquerro *et al.*, 2020). Such slip rate increase has been attributed to: (i) onshore, westwards propagation of extensional deformation from the inner parts of the Valencia Trough, enhanced by crustal doming that would have affected the eastern Iberian Chain; (ii) onset of the multidirectional extension stress field driven by crustal doming mechanism; (iii) progressive fault linkage since the beginning of the Late Miocene (Ezquerro *et al.*, 2020).

Mountains surrounding the Teruel and Jiloca basins show extensive erosion surfaces modelling Mesozoic-Palaeogene rocks and bevelling compressional structures. Two large planation surfaces, whose remnants appear at different heights either on the upthrown blocks or in the basin floors, have been traditionally defined (Gutiérrez and Peña, 1976; Peña *et al.*, 1984; Sánchez-Fabre *et al.*, 2019): (i) *Intra-Miocene Erosion Surface* (*IES*, middle Miocene), generally recognized in the upper part of the main reliefs, and (ii) *Fundamental Erosion Surface* (*FES*, middle Pliocene), easily recognizable as a vast planation level at lower heights. They approximately correspond to the *Iberian Chain Surface* and the *Lower Pliocene Surface* by Pailhé (1984), and the S1 and S2 by Gutiérrez and Gracia (1997), respectively. Recent detailed studies (Simón-Porcar *et al.*, 2019; Ezquerro *et al.*, 2020) have demonstrated that the *FES* splits into three different surfaces: an Upper Sublevel, the *FES s.s.* (the most widely developed), and a Lower Sublevel. In this work, these surfaces will be called as *FES1*, *FES2* and *FES3*, respectively. Planation surfaces have been physically correlated with different coeval sedimentary horizons (lacustrine-palustrine carbonates) within the sedimentary infill of the Teruel basin (Ezquerro, 2017), whose ages are well-constrained on the basis of mammal sites and magnetostratigraphy. In this way, the *Intra-Miocene Erosion Surface* has been dated close to the Aragonian-Vallesian limit (~11.2 Ma; Alcalá *et al.*, 2000; Ezquerro, 2017), *FES1* and *FES2* to the Late Ruscinian (both merging around ~3.8 Ma), and *FES3* to the Early Villafranchian (~3,5 Ma) (Ezquerro *et al.*, 2020).

Qualitative and quantitative geomorphological features of the mountain fronts and the associated piedmonts of the eastern margin of the Jiloca graben are those typical of active normal faults. At the Concud fault, Lafuente *et al.* (2011b) described conspicuous triangular facets and short, non-incised alluvial fans, and provided a significantly low value of the mountain-front sinuosity index defined by Bull and McFadden (1977) (S_{mf} = 1.24). At the Sierra Palomera fault, García-Lacosta (2013) described trapezoidal facets and V-shaped gullies, and provided a similar value for the sinuosity index (S_{mf} = 1.27). The fault scarps are connected with the depression bottom by gentle pediments mostly draining towards the Jiloca river, although endorheic conditions have locally remained until historical times, with development of a palustrine area at the basin centre (ancient Cañizar lake; Rubio and Simón, 2007).

Historic and instrumental seismicity of the central-eastern Iberian Chain is low to moderate. In the Teruel region, the epicentres are concentrated at the Jiloca graben margins, the central-southern sector of the Teruel basin, and the Albarracín and Javalambre massifs. Apart from the Albarracín massif, epicentres can be reasonably associated to Neogene-Quaternary known faults. Measured magnitudes (Mb) usually range from 1.5 to 3.5, with maximum Mb = 4.4 in the Teruel Graben and Mb = 3.8 in the Albarracín massif (IGN, 2021).

3. Methodology

3.1. Structural and morphotectonic study

The structural study is based on recognizing and mapping the main structures on aerial photographs at 1: 18,000 and 1: 33,000 scale, and satellite imagery, complemented with field surveys involving outcrop-scale observations. Data of orientation of rupture surfaces and slickenlines have been collected in a number of sites within the Sierra Palomera fault damage zone, as well as within the trench described below. Stereoplots (equal-area, lower hemisphere) of those data sets have been elaborated using Stereonet 8 software (Allmendinger *et al.*, 2012; Cardozo and Allmendinger, 2013).

To characterize the geometry of recent vertical deformation, the three erosional planation surfaces (*FES1*, *FES2* and *FES3*) described above were used as markers. This required mapping of erosion surfaces and morphotectonic analysis based on aerial photographs (scales 1: 18,000 and 1: 33,000) and orthorectified photographs (1: 5000), as well as on digital elevation models (DEM, pixel = 5 m) and the resulting hillshade images. A structural contour map of *FES2* was elaborated by interpolating the altitude of their remnants, which permits measuring throw across the main fault and hence calculating slip rate. Changes of throw along the fault zone were calculated from 1-km-spaced transects orthogonal to the fault trace and analysed on a throw *vs.* distance (T-D) graph.

Once constrained the age of a planation surface (see Section 2), the main challenge to be addressed is ensuring its degree of flatness, being aware of the degree of error involved in height management. Continental planation surfaces can show gentle (short- to middle-wavelength) unevenness, or locally connect with residual, non-flattened reliefs through pediment slopes. Amplitude of the unevenness advises to use an adequate contour interval for *FES2* in order to represent its present-day geometry with the suitable precision. Both the local difference in height between *FES2* and *FES3* and the local unevenness within each one usually lies within the range of 10-40 m. Therefore, we assume that: (i) fault throws calculated from them implicitly include a maximum error bar of ±40 m, and (ii) a 50-m-spaced contour map can be considered as reasonable for assessing recent movements (as previously proposed by Ezquerro *et al.*, 2020). Such level of uncertainty in the calculated fault throws results in errors for slip rates around 0.01 mm/a.

3.2. Subsoil exploration

Subsurface information was acquired by means of geophysical exploration. Two different techniques were utilised, which had rendered interesting results in other neighbouring sectors (*e.g.*, Pueyo *et al.*, 2016): magnetometry and electromagnetic (EM) multifrequency survey. A twofold approach was taken: first, a regional analysis by means of ten transects approximately orthogonal to the Sierra Palomera mountain front; second, a detailed analysis of a sector where the highest geophysical anomalies were identified and also where geomorphological evidences hinted at the presence of a previously unknown antithetic fault. For the magnetometry survey, a GSM-19 equipment with built-in GPS was used to measure both Earth magnetic field intensity and vertical magnetic gradient (sensors separation of 0.5 m). Diurnal correction was performed from a second, stationary, magnetometer (PMG-01) that permitted to exclude natural earth magnetic field changes during the survey and to compare the results performed during different days. Then, the regional general trend was identified and subtracted to earth magnetic data to highlight anomalies in the form of residual values. The EM multifrequency survey was performed by a GEM-02 device for a range of frequencies between 65 and 0.5 kHz.

Subsoil information has been complemented with borehole data extensively compiled by Rubio (2004), whose synthetic results were presented by Rubio and Simón (2007). Together with surface geology, it was used for constructing geological cross sections that have allowed characterizing the general geometry of macrostructure. Moreover, they were used for extending the contour map of FES2 to the centre of the Jiloca basin.

3.3. Trench analysis

A trench study focussed on the northwards prolongation of the La Peñuela fault, antithetic to the main Sierra Palomera fault, has been carried out following the classical methodology (see, *e.g*., McCalpin, 2009): excavating and shoring; cleansing and gridding the most suitable wall; identifying and marking sedimentary boundaries and deformation structures; drawing a detailed log and taking photographs of each grid cell; analysing the relationship between units and faults to identify individual events; and sampling materials for dating. Sedimentary units were defined on the basis of lithology, bed geometry, texture, colour and sedimentary structures.

Individual deformation events identified within the trench have been carefully verified by retrodeformational analysis, following the common practice in paleoseismological reconstruction (McCalpin, 2009). Several post-event sedimentary stages have also been included for a better understanding and representation of the evolutionary model. A number of identifiable faults were either formed, propagated or reactivated during successive deformation events. For each fault involved in each event, dip separation has been measured and equated to net slip (with precision of 5 cm). In addition, the resulting horizontal extension has been calculated taking into account the average dip of each fault. Further details are given in Section 7.4.

Dating of trench samples was achieved by the Luminiscence Dating Laboratory of University of Georgia, USA, using the Optically Stimulated Luminiscence (OSL) technique. Unfortunately, five of them were saturated samples that only provided minimum ages, which drastically decreased the consistency of the age model. Additional, preliminary OSL dating of shallow alluvial fan sediments had been achieved by Laboratorio de Datación y Radioquímica de la Universidad Autónoma de Madrid.

4. Structure and morphotectonics of the Sierra Palomera area

The NNW-SSE trending Sierra Palomera extensional fault makes the eastern boundary of the Jiloca graben at its central sector (Figs. 1b, 2). In the footwall block, Jurassic marine carbonates are unconformably covered by Paleogene continental clastics (Figs. 2, 3). In the hanging-wall block, *i.e*., the central sector of the Jiloca basin, the sedimentary infill is made of: (i) Late Pliocene (Villafranchian) to Pleistocene alluvial and episodic palustrine deposits, all of them exposed at the surface; (ii) an underlying carbonate unit, only observed in boreholes, that could represent an early lacustrine stage of Late Miocene-Early Pliocene age

(Rubio and Simón, 2007). Borehole information indicates that the maximum thickness of the total infill approaches 100 m (Rubio and Simón, 2007).

The Jiloca basin runs slightly oblique to previous Paleogene, NW-SE trending folds (Fig. 1b; Rubio and Simón, 2007; Rubio *et al.*, 2007). In particular, the Sierra Palomera fault follows the eastern limb, nearly vertical, of an eastwards verging anticline (Fig. 3). Its core is represented by Lower-Middle Triassic rocks that crop out in the neighbourhoods of Singra village, and its periclinal closure is partially preserved close to the southern tip of Sierra Palomera fault (Fig. 2). Such structural setting suggests that the main extensional fault resulted from negative inversion, during Late Pliocene-Pleistocene times, of a previous reverse fault linked to that anticline and developed during the Paleogene compression (Rubio and Simón, 2007).

The Sierra Palomera fault trace is ca. 26 km long and trends N152ºE in average. The main fault surface only crops out in a few small exposures (1 to 4 m^2 in area). A number of rupture surfaces observed within the damage zone show orientations consistent with the map trend: strike between NW-SE and N-S, and dip between 54º and 87º W (mean orientation: N155ºE, 70º W; Fig. 4). Slickenlines show pitch ranging from 75ºN to 70ºS, therefore indicating almost pure normal movement, with mean transport direction towards N230ºE.

Two wide right relay zones separate the Sierra Palomera fault from the Calamocha and Concud faults. The dominant trend of recent, extensional faults and fractures distributed within both relay zones is similar to that of the main fault or slightly deviates to approach the N-S direction. These relay zones dominated by along-strike fractures were described in detail by Peiro *et al.* (2019, 2020).

The Sierra Palomera fault is expressed in the landscape by a conspicuous, 20-km-long fault mountain front (Fig. 5a,b), which attains heights of 200 to 300 m above its toe, 450 to 550 with respect to the bottom of the Jiloca depression. The mountain front shows a significantly low value of the sinuosity index (S_{mf} = 1.27; García-Lacosta, 2013). A number of gullies (most of them exhibiting V-shaped transverse profiles) run across the fault scarp and delimit some well-preserved trapezoidal facets (Fig. 5c). Gullies feed short, high-slope alluvial fans (Fig. 5d) that are barely incised, only partially connected to the axial fluvial system, and exhibit signs of present-day functionality (*e.g.*, gravel aggradation affecting bush vegetation).

The difference in height of the geomorphological markers *FES2* and *FES3* between the footwall and the hanging-wall blocks reasonably allows approaching the Sierra Palomera fault throw. The envelope of relief at the footwall block is largely represented by the *FES2* planation surface cutting pre-Neogene units, which attains a maximum height of 1430 m close to the edge (Fig. 6). The summit of Sierra Palomera (1533 m a.s.l.) and its surrounding area constitutes a residual relief that stands out from *FES2*, while remains of an upper erosion sublevel (*FES1*) extend at the eastern foothills. A lower sublevel (*FES3*, usually lying 10-40 m below *FES2*) is also present: (i) eastwards of Sierra Palomera, over large areas of the northern Teruel basin; (ii) northwards and southwards, at the relay zones with the Calamocha and Concud faults, respectively; and (iii) along a narrow band westwards of the Sierra Palomera divide.

The height of *FES2* and *FES3* within the Jiloca depression can only be inferred indirectly. Both have been mapped at the eastern margin of the Jiloca depression, W of Santa Eulalia town, where they descend to ca. 1100 and 1050 m, respectively (Fig. 6). Then they are supposed to be covered by the Plio-Pleistocene infill, while gentle residual reliefs at the Singra-Villafranca del Campo area (made of Triassic and Jurassic rocks belonging to the core of the Sierra Palomera anticline) stand out above the depression bottom. The subsoil data provided by Rubio and Simón (2007; Fig. 6) for the central Jiloca basin constrain the heights of those planation surfaces. The boundary between Plio-Pleistocene alluvial deposits and the underlying carbonate unit, lying at about 950 m a.s.l. in the Santa Eulalia area, could be correlated with either *FES2* or *FES3*.

Within the Sierra Palomera block, *FES2* and its correlative Late Ruscinian carbonates are in continuity with each other and show a quite homogeneous slope of about 1.5-2% along a distance of 20 km, in which the altitude of this morphosedimentary marker diminishes from 1400-1430 m (central sector of Sierra Palomera) to 1090-1120 m (Alfambra area) (Fig. 6). This morphotectonic setting defines a conspicuously tilted block whose edge has undergone a tectonic uplift of about 300 m relative to the bottom of the Teruel depression, as can be visualized from structural contours in Figure 6.

The latter value closely approaches the topographic amplitude of the Sierra Palomera scarp itself, and is comparable to the fault throw inferred from offset of the *FES2* marker. Such fault throw, and its variation along the Sierra Palomera fault, have been analysed on a series of 1-km-spaced transects across the fault trace on the contour map of Figure 6, assuming that *FES2* within the Jiloca basin coincides with the base of the Plio-Pleistocene infill. The result is shown in the throw *vs.* distance (T-D) graph of Figure 7, where two distinct curves depict values of (i) fault throw *s.s.*, and (ii) total tectonic throw of *FES2* between the Sierra Palomera summits and the Jiloca depression bottom (including the bending component). The T-D curves show an overall bell-shape, although slightly bimodal in detail.

The maximum values, 330 m and 480 m, respectively, are found at the central sector. Considering the age of the *FES2* morphosedimentary marker (3.8 Ma), and assuming an average dip of 70º for the fault plane and a pure normal movement, a maximum net slip rate of 0.09 mm/a can be inferred (0.13 mm/a for the total rate between Sierra Palomera and the Jiloca bottom).

Despite the initial appearance of the Sierra Palomera fault is that of a single major rupture that accommodates the entire throw, there is evidence of a parallel, synthetic fault (Las Vallejadas fault) located west of the main escarpment at its southern sector (Fig. 2). Both delimit an intermediate step within the mountain front, in which *FES2* lies at an altitude of 1140-1220 m, furthermore offset (ca. 10 m) by a minor antithetic rupture (La Peñuela fault). Recent activation of both subsidiary faults is revealed by local deformation of Villafranchian alluvial deposits: (i) back tilting (up to 25ºE), due to rollover kinematics, observed at the foot of the morphological escarpment of Las Vallejadas fault (Fig. 2); (ii) accommodation monocline (dip up to 22ºE) in the case of La Peñuela fault (Fig. 8; see location in Fig. 2).

5. Geophysical exploration of the overall Sierra Palomera piedmont

Data of magnetic intensity field and vertical magnetic gradient were extensively collected along ten transects, roughly orthogonal to the Sierra Palomera fault trace along its hanging-wall block and ranging from 2.0 to 5.2 km in length (Fig. 9a). Spacing between successive measurement points was about 0.8 m. The two northernmost transects (profiles 01 and 02) and the southernmost one (profile 10) show a narrow distribution of residuals due to their lesser contrast with respect to the general, regional trend (Fig. 9b). The central transects (03 to 09) have spikes and lows that depart considerably from the general trend, and therefore, when data of the ten transects are considered as a whole, they define the range of the distribution (more specifically, profile 03 has the lowest and the highest values of residual magnetic intensity). Nonetheless, transects 01, 02 and 10 show a similar (albeit reduced in magnitude) outline to the rest.

The variation pattern of residuals in magnetometric profiles (also corroborated by EM profiles) allows portraying three domains (A, B and C) that are broadly parallel the Sierra Palomera fault (Fig. 9b). In the northern section of the studied area, the boundary between domains A and B is largely evident, due to the sudden change and amplitude of the anomaly. Moreover, these profiles show a more direct correlation between them than the southern ones, where the contact progresses through a magnetic dipole (Fig 9a, b). These three domains are characterised by:

a) Closer to the Sierra Palomera fault, domain A is an area where residual values of magnetic intensity are close to zero and barely change, except for a subtle decrease to the west.

b) Westwards, a sharp change of attitude marks the onset of domain B, a zone of anomalies expressed as variations of residuals up to 20-30 nT over decametric distances. Such anomalies reflect the presence of small magnetic dipoles and a slightly higher mean value of Earth magnetic field. Values for apparent conductivity are still homogeneous.

c) Finally, domain C is separated from domain B by a sharp decrease in magnetic intensity (it goes down about 100 nT) with lower relative values of Earth magnetic field and presence of a lower density of magnetic dipoles (including those of higher wavelength). Apparent conductivity and magnetic susceptibility are higher.

The reported geophysical results (Earth magnetic field, together with apparent conductivity and susceptibility) suggest the presence of a body of relatively higher magnetic susceptibility underlying domain A, which gets shallower under domain B, and gets again deeper under domain C. Boundaries between those domains are sharp and clear. This setting can be interpreted as an uplifted block (made of Paleozoic and Triassic materials belonging to the core of the Sierra Palomera anticline) bounded by faults nearly parallel to the Sierra Palomera fault trace.

6. La Sima alluvial fan: linear topographic anomaly and its geomagnetic expression

In the absence of any visible surficial rupture across Quaternary sediments of the Sierra Palomera piedmont, evidence of recent tectonic activity should be obtained from trenching. Owing to non-favourable topographic, lithologic and access conditions at the Sierra Palomera fault trace itself, our search was focused on the surface of two alluvial fans sourced at the mountain front, at La Cecilia and La Sima areas (see location in Figs. 2 and 5d). Both exhibit well-preserved alluvial fan morphology at its proximal sectors, with evidence of present-day aggradation at the apex. Shallow sand and silty sedimentary horizons in those alluvial fans have provided ages of 28.9 ± 2.0 ka BP (La Cecilia) and 19.2 ± 1.1 ka BP (La Sima) (see Table 1; location in Fig. 2).

In the middle sector of La Sima alluvial fan, a sharp NNW-SSE trending lineament is clearly visible on aerial photographs and DEM images, beyond which the fan surface is more deeply incised by the local drainage network (Fig. 10a). That lineament involves a morphological anomaly, a break in the fan slope, which becomes null or even negative up to take locally the appearance of a gentle, degraded uphill-facing scarplet (Fig. 10c). These features suggest the occurrence of an antithetic fault that would have sunk the proximal sector of the fan with respect to the middle one by about 2.5 m. This lineament coincides with the boundary between domains A and B defined from geophysical results (Fig. 9b), and is virtually prolonged towards SSE up to connect with the antithetic La Peñuela fault (Fig. 2).

In order to test the hypothesis of an antithetic fault cutting the La Sima alluvial fan, the subsoil in the neighbourhoods of the morphological lineament was intensively explored by means of a magnetic and electromagnetic survey. The coincidence of the lineament with the A/B boundary is clearly expressed in the detailed map of residual magnetic anomalies shown in Figure 10b. The area east of the sharp linear NNW-SSE trending limit, clearly visible on this map, shows low residual values with wide (hectometre-scale) wavelength variations. To the west of this limit, an increase of more than 30 nT is observed, as well as a decrease of more than 50 mS/m in the total conductivity; moreover, the texture of the residual map changes noticeably, showing sharper magnetic dipoles of decametric wavelength.

The amplitude and morphology of the linear anomaly is not consistent with the susceptibility values of surficial sediments, and suggest the contrast, at shallow levels, between a high-susceptibility rock body to the west (domain B, as defined in section 5) and the domain A to the east. In addition, Figure 10b shows other NW-SE trending linear anomalies in domain B, which involve a lower contrast of magnetic field values. Both the main anomaly and the secondary ones show high gradient and sharpness of the observed dipoles, suggesting near-surface, high dipping discontinuities or rock boundaries compatible with recent faults.

7. Trench study at La Sima alluvial fan

Once verified that geophysical and topographic analysis of La Sima lineament reinforced our preliminary hypothesis about the northwards prolongation of the antithetic La Peñuela fault, we selected an easily accessible site for trench study. A 40 m long, 1.4 m wide trench was dug along a N067ºE direction, roughly orthogonal to the linear anomaly that separates domains A and B. A segment of 19 m on its southern wall, with depth ranging from 3.0 to 3.5 m, was logged and analysed in detail (Fig. 11a,b).

7.1. Sedimentary units

The materials exposed at La Sima trench essentially correspond to relatively well-bedded Pleistocene alluvial sediments (Fig. 11a). Sedimentary features indicate alternating energetic flows, sometimes flash floods, recorded by gravel channel and bar deposits, and waning discharges that settled fines over the gravel deposits. All the succession includes clear signs of calcrete development and periods of time with negligible sedimentation. Bioturbation signs and carbonate precipitation are related to pedogenesis, suggesting wetting and drying episodes of the sedimentary surface. The sedimentary succession has been subdivided into twelve lithological units (Fig. 11b):

Unit 1 (up to 50 cm in thickness): Massive reddish mudstone with isolated, mm- to cm-sized angular limestone clasts (more abundant at the base), with bioturbation traces and smooth carbonate nodules.

Unit 2 (25 to 55 cm): Orange massive sandy mudstone with floating angular-subangular grey limestone granules and pebbles, and some irregular cm-thick gravel bed. Grey mudstones laminae towards the top.

Unit 3 (55 to 75 cm): Tabular laminated, indurated and brecciated, carbonate crust with some cm-thick interbedded silts with carbonate clasts. Carbonate fragments are smaller in the upper part; laminated fragments are less abundant towards W.

Unit 4 (20 to 35 cm): Reddish massive silty sand and mudstone in a tabular level with vertical root traces filled by fine sands. Some carbonate nodules, plant remains and scattered grey, angular limestone and caliche clasts up to 10 cm in size can be recognized.

Unit 5 (15 to >50 cm): Clast-supported gravel with silty to sandy matrix in a tabular, locally channelized sedimentary body with crude horizontal stratification. Gravel is made of angular-subrounded limestone clasts (up to 8 cm) and smaller caliche clasts.

Unit 6 (25-55 cm): Orange to brownish massive silt and mudstone with greyish limestone angular clasts and floating whitish caliche rounded nodules (up to 2 cm). Clast content increases locally. Root traces, plant remains and organic matter patches can be recognized in the western sector.

Unit 7 (30 to >150 cm): Heterogeneous unit mainly made of grain-supported gravel, locally cemented, with angular-subrounded limestone clasts (up to 15 cm in size) and caliche nodules. It includes red mudstone discontinuous intercalations, up to 20 cm in thickness, with floating cm-sized angular clasts. The overall geometry of the unit is tabular in the footwall block and channelized in the hanging-wall block. A level of calcrete gravel, >50 cm in thickness, appears at the top of this unit within the footwall block.

Unit 8 (10-60 cm): Reddish silt with floating limestone angular granules and pebbles (up to 8 cm) with evidence of bioturbation.

Unit 9 (45-120 cm): Grey gravel in a channeled body with limestone angular clasts (up to 12-14 cm in size) and rounded caliche clasts. Crude finning upwards cycles can be recognized. Pedogenic features increase towards the top, where brecciated limestones locally appear.

Unit 10 (55 to 70 cm): Reddish massive silts with floating subangular limestone clasts (up to 7 cm), whitish carbonate nodules and an interbedded discontinuous clast-supported gravel level with subangular clasts up to 10 cm in size.

Unit 11: Wedge-shaped body of orange and whitish massive, highly cemented silt, with carbonate floating subangular limestone clasts (up to 10 cm) and caliche clasts arranged with the A-axis subvertical.

Unit 12 (20 to 50 cm): Surface regolith made of silt with angular to subangular clasts, reworked by agricultural labours.

7.2. OSL dating

Seven samples (S1 to S7) of alluvial sediments within the trench (see Fig. 11b for location) have been dated, although unfortunately the results show a high level of uncertainty (see Table 1). Other three collected samples did not contain enough sand grains for providing a representative dose distribution and therefore OSL dates were not reliable in this case. These samples are not located in Fig. 11b.

Samples S2, S3, S4, S6 and S7 have presented signal saturation, *i.e.*, their natural luminescence signal lies beyond the saturation of the OSL response with dose, making it impossible to provide adequate results. According to laboratory results, their ages should be older than 193 to 378 ka, although such figures should not be taken *sensu stricto*. Only one of the alluvial sedimentary units is directly dated: S1 provides an age 97.4±10.2 ka for the top of unit 9. Unit 11 (sample S5), which will be next interpreted as a fissure infill, is dated to 49.2±5.4 ka. As a result, the chronology of unit 10, overlapping unit 9 and being cut by the fissure, can be broadly constrained between both numerical ages.

Without the support of further anchors, building an age model for the overall alluvial succession exposed in the trench is not feasible. In any case, the ensemble of OSL dating results and geomorphological observations in the study area suggest that: (i) most of that alluvial succession belongs to the Middle Pleistocene; (ii) a rapid decrease of sedimentation rate occurs by the Middle-Late Pleistocene transition; and (iii) sedimentation persisting in proximal and middle sectors of the alluvial fans during Late Pleistocene to present-day times only represents a small contribution to the surficial aggradation and landscape modelling.

7.3. Deformation structures

The trench log shows a main extensional fault zone at the central sector, dipping eastward and hence antithetic with respect to the Sierra Palomera fault (Fig. 11b), and full consistent with the uphill-facing scarplet described in section 6. These features allow identifying such antithetic fault zone with the map-scale La Peñuela fault (Fig. 2). The footwall block of that fault zone shows a gentle monocline, while other normal (both synthetic and antithetic) faults, cutting most of the sedimentary succession, are distributed along the entire section. The orientations of all these structures are overall consistent, as depicted in stereoplots of Figure 11c,d,e,f.

The central fault zone is made of three significant structural elements:

1) Main fault, expressed by θ_1 and θ_2 individual rupture surfaces.

2) Splay faults κ1, κ2, κ3 and κ4, associated to the tip of the main rupture and propagated through unit 7. Both the main, westwards dipping rupture surfaces and the nearly vertical splay faults consistently strike NNW-SSE (Fig. 11c). Such structural arrangement suggests that, at certain stage of its development, the main rupture θ_1-θ_2 was covered by the upper part of unit 7, and then reactivated in the form of splay faults related to refraction at the extensional tip (horse-tail structure, in the sense of Granier, 1985). That is the key, purely instrumental criterium for separating lower and upper unit 7 in Figure 12; therefore, such separation is not based on a visible lithological boundary (we have defined a single unit 7 indeed).

3) Open fissure bounded by fault θ_3 and another irregular surface, and filled with unit 11. The interpretation is based on its wedge shape, the massive internal structure of the infill, and the occurrence of clasts with nearly vertical A-axes. According to this interpretation, both bounding surfaces would have represented both walls of a single, also NNW-SSE striking fault, then disengaged from each other when the fissure opened up and partially crumbled before infilling took place.

The footwall block is deformed by the monocline and cut by a number of NNW-SSE striking normal faults (Fig. 11d), all of them synthetic with the Sierra Palomera fault and exhibiting dip separations in the range of 10 to 20 cm (Fig. 11b). Faults ρ, π_1 and π_2 cut the horizontal limb of the monocline, and have apparently kept their original, high dip. The rest of faults (τ, σ, μ, χ, λ_1 and λ_2) appear at the hinge and the abrupt limb of the monocline. They show a progressive decrease in dip towards the east as the bedding dip increases, and some individual faults (μ, λ_1, λ_2) exhibit conspicuously arched traces, so that the angle between faults and bedding remains broadly constant (mostly within the range of 55-65º). Such geometrical setting strongly suggests that they were folded by the monocline. Concerning the relationships between faults and sedimentary units, ρ and π_1 uniformly offset (15-20 cm) the base of units 2 to 6, while they suddenly vanish and does not affect the base of unit 7. Also fault σ shows similar relationships, although in this case it does not propagated through the lower units, probably detached within low-viscosity materials of unit 4. As a consequence, ρ, π_1 and σ produce a noticeable thickening of unit 6 in their respective hanging-wall blocks. Faults π_2, τ, μ, χ, λ_1 and λ_2) also offset rather uniformly the sedimentary boundaries, and at least two of them (π_2 and μ) propagated across unit 7.

The hanging-wall block shows two ensembles of intersecting faults that cut units that are younger than the ones from the footwall block (Fig. 11b). Individual faults show distinct slip for different sedimentary markers, which indicates diachronic development. The ε_0-ε_1 couple offsets more than 1.2 m the base of unit 7, while it produces a rather uniform dip separation of 8-10 cm in the bases of units 8, 9 and 10. We should therefore interpret that ε_0-ε_1 underwent most of its present-date displacement (>1.3 m) before sedimentation of unit 8, and was then reactivated after the lower part (at least) of unit 10 was deposited. Splaying from ε_1, fault ε_2 cuts units 7 and 8, and is covered by unit 9, while ε_3 cuts the base of unit 9, thus making the three faults a footwall rupture sequence. The antithetic ε_4 propagated thorough unit 9 and the lowermost unit 10. At the easternmost trench sector we find a similar pattern in the NNW-SSE striking faults α and β. Fault β offsets more than 0.7 m the base of unit 7, while (together with its splay faults γ_1, γ_2 and γ_3) produces a smaller separation (0.4 m) in the bases of units 8 and 9. We interpret that β underwent displacement $\approx$ 0.3 m before sedimentation of unit 8, and was then reactivated after deposition of unit 9. Fault α propagated through unit 7, previous to sedimentation of unit 8, and did not undergo further reactivation.

The orientations of the described structures have a strict consistence. All faults systematically strike NNW-SSE (Fig. 11f), and so does the limb of the monocline (Fig. 11d). There is no doubt that the latter is (i) genetically linked to faults, and (ii) responsible for the decrease in dip of faults σ, μ, χ, λ_1 and λ_2. Bedding and fault surfaces are rotated around a common, well-defined horizontal axis ca. N160ºE (Fig. 11d). Strikes of minor fractures measured along the trench are also clustered around NNW-SSE, although a small number among them are oriented NNE-SSW (in blue in Fig. 11e). A brief discussion about the dynamic framework (stress fields) in which such fault and fracture pattern developed will be made in Section 8.5.

7.4. Retrodeformational analysis and evolutionary model: deformation events

Based on the former structural description, in particular on the relationships between structures and the sedimentary units, a careful retrodeformational analysis has been achieved, with a double purpose: (i) building an evolutionary model, i.e. a systematic succession of deformation events, and (ii) testing its kinematic consistence (Fig. 12).

A number of identifiable faults were either formed, propagated of reactivated during each deformation event (Fig. 12 and Table 2). Dip separation directly measured on the trench log is taken as practically representing the net slip on each fault, since: (i) bedding is roughly horizontal, (ii) the trench, oriented N067ºE, is nearly orthogonal to the prevailing strike of faults, and (iii) the only kinematical indicator observed during trench survey (slickenlines with pitch 82ºS on fault μ; Fig. 11d), as well as those collected at the Sierra Palomera fault zone itself (see Fig. 4b), suggest nearly pure normal slip for the overall extensional fault system.

Net slip for every individual fault (with positive sign for synthetic faults and negative sign for antithetic ones), together with the resulting horizontal extension (considering the average fault dip), are depicted in Table 2. Such measurements exclude offset accommodated by the bending monocline. The latter has been only considered for computing the total accumulated deformation, since it is not possible to accurately calculate which fraction of bending occurred during each event. The total slip per event, taken as the algebraic sum of slip values on individual faults, is also shown. The total horizontal extension per event considers the aggregate of extension values on individual faults, but also includes an estimate of the contribution of bending, in order to jointly accommodate the horizontal extension visually expressed in the successive cross sections of Fig. 12.

Below we summarize the main features of each of the seven deformation events (T to Z) defined at the La Sima trench (Fig. 12; see measurements in Table 2):

Event T: Slip on faults ρ, $\pi_{1,}$ τ and σ after deposition of unit 6 and previous to unit 7. Accumulated net slip: +45 cm.

Event U: Slip on faults π_2, μ, χ, λ_1, λ_2 and ε_1, subsequent or coeval with deposition of the lower part of unit 7. Accumulated net slip: +105 cm.

Event V: Slip on fault θ_2, subsequent to deposition of lower unit 7, then covered by upper unit 7. Development of the monocline begins; according to our progressive deformation model depicted in Fig. 12, in which the main rupture had always propagated through units 1 to 6, this monocline should be interpreted as a drag fold. Net slip: −10 cm.

Event W: Reactivation of the main, central fault through the rupture surfaces θ_1-θ_2, which propagates across upper unit 7 splitting into κ1, κ2, κ3 and κ4. Progress of the monocline produces rotation of faults τ, σ, μ, χ, λ_1 and λ_2. Slip on faults ε_0-ε_1, α and β, all of them subsequent to top of unit 7 and previous to unit 8. Accumulated net slip: +125 −65 = +60 cm.

Event X: Propagation of the main fault zones, θ and ε, through new rupture surfaces: θ_2-θ_3 and ε_2, respectively. Both are younger than unit 8 and older than unit 9. Accumulated net slip: +5 −50 = −45 cm.

Event Y: Activation of fault ε_3, and propagation of β splitting into γ_1, γ_2 and γ_3. Both processes are subsequent to deposition of unit 9 and probably previous to unit 10, therefore close to (or slightly younger than) the numerical age provided by sample S1 (97.4 ± 10.2 ka). Accumulated net slip: −35 cm.

Event Z: Formation of fault ε_4 and propagation of ε_1 cutting the lower part of unit 10. Slip on θ_2 that induces extensional movement on the θ_3 surface, giving rise to an open fissure that tears apart units 7 to 10 and is subsequently filled with unit 11. This event should be dated just prior to the numerical age provided by sample S5 (49.2 ± 5.4 ka). Accumulated net slip: +10 −120 = −110 cm.

8. The Sierra Palomera fault: synthesis and discussion

8.1. Geometry and kinematics of macrostructures

Structural information from field survey has allowed characterizing geometry and kinematics of the Sierra Palomera fault itself (Figs. 4, 6, 13). The attitude of the main fault surface is N155ºE, 70º W in average, while most ruptures visible along and close to it are systematically parallel. The fault shows pure normal movement, with mean transport direction towards N230ºE. In addition, the use of two geomorphological markers (mid-Pliocene *FES2* and *FES3* planation surfaces; Fig 13b) has permitted measuring the fault throw *s.s.* (330 m) and the total tectonic throw (480 m, including bending) at the Sierra Palomera fault, resulting in slip rates of 0.09 and 0.13 mm/a, respectively.

Geophysical results reported in Section 5, defining three adjacent, NNW-SSE trending elongated domains (A, B, C) suggest the existence of an uplifted block bounded by faults nearly parallel to the Sierra Palomera fault trace. At the southern sector of the study area, local coincidence of the A/B and B/C domain boundaries with La Peñuela and Las Vallejadas faults, respectively, strongly supports such interpretation. The antithetic rupture exposed in La Sima trench, revealed in the landscape by a gentle uphill-facing scarplet across the La Sima alluvial fan (section 6), unequivocally represents that map-scale antithetic La Peñuela fault and corroborates the extensional character of such structure.

In this way, the results of subsoil exploration by geophysical methods and trench survey, together with structural and morphotectonic data, allow refining the structural model of the central Jiloca graben, beyond the apparently flat appearance of the Sierra Palomera pediment. The synthetic Las Vallejadas fault and the antithetic La Peñuela fault have been incorporated to the geological map of Figure 2, as well as to a new version of the cross section (Fig. 13a). Furthermore, the latter depicts a reinterpretation of the geometry of the master fault. It is known that the shape of the main fault surface strongly controls the style of accommodation folding and subsidiary faulting in the hanging-wall block of extensional faults. Rollover folds and antithetic faults develop above concave-upward fault bends, whereas drag folds and synthetic faults form above convex-upward fault bends, their propagation being facilitated by high curvature of such fault bends (McClay and Scott, 1991; Xiao and Suppe, 1992; Withjack *et al.*, 1995; Delogkos *et al.*, 2020). In our case, the occurrence of the antithetic and the synthetic inferred subsidiary faults strongly suggests the presence, at a depth of less than 1 km, of a relative flat in the main fault surface (*i.e.*, a double, convex-concave bend), probably located at the Middle-Upper Triassic lutite and evaporite units (Middle Muschelkalk and Keuper facies).

Concerning the along-strike propagation of the Sierra Palomera fault, the slightly bimodal throw *vs.* distance (T-D) curve depicted in Fig. 7 suggests that it could result from coalescence of two distinct fault segments (although the amplitude of the relative minimum between both maxima, close to the error bar adopted for throw estimations, casts doubt on the significance of this detail). In any case, the overall bell-shape of the T-D curve indicates full linkage along the fault zone. Moreover, the persistence of a bending component beyond both tips of the fault trace reveals that the total length of the Sierra Palomera fault is larger than that exposed at the surface, thus being propagated towards NNW and SSE as a blind fault.

According to Peiro *et al.* (2020), the overall fault system at the eastern boundary of the Jiloca basin is at a transient stage towards coalescence, and will probably evolve to an along-strike propagation of the master faults through distributed longitudinal fractures. The relay zones between Sierra Palomera, Calamocha and Concud faults, dominated by longitudinal fractures, represent a type of fault relay controlled by both inherited structures and the remote stress field (Peiro *et al.*, 2019, 2020). It strongly contrasts with the classical models reported in the literature (*e.g.*, Peacock and Sanderson, 1994; Young *et al.*, 2001; Fossen and Rotevatn, 2016), in which transverse connecting faults controlled by the own relay kinematics prevail.

Such fault system makes a geometrically and kinematically consistent, genetically related major extensional fault system. The N230ºE mean transport direction at the Sierra Palomera fault is similar to those of Concud (N220ºE; Lafuente *et al.*, 2014) and Calamocha (W to SW; Martín-Bello *et al.*, 2014). Moreover, all them probably resulted from negative inversion, during the Late Pliocene-Quaternary times, of previous contractive structures developed under the Paleogene-Early Miocene compression (Rubio and Simón, 2007; Lafuente et al., 2011a; Liesa et al., 2021).

8.2. Morphotectonic approach to assessing recent fault activity within the context of eastern Spain

In the absence of stratigraphic markers recognized in both fault blocks, the fault throw *s.s.* and the total tectonic throw at the Sierra Palomera graben margin (up to 330 m and 480 m, respectively) have been reasonably estimated from offset of Late Neogene planation surfaces. Nevertheless, uncertainties linked to such geomorphological markers should be highlighted.

Our main geomorphological marker, *FES2*, is poorly represented within the Jiloca bottom, *i.e.*, the hanging-all block of the Sierra Palomera fault, which makes difficult to calculate the actual throw. We interpret that the boundary between Plio-Pleistocene alluvial deposits and the underlying carbonate unit probably represents the position of *FES2* (Fig. 13b), although it also could be correlated with *FES3*. According to the results provided by Ezquerro *et al.* (2020), such uncertainty introduces a potential error of either 10-40 m in the height of the marker (equivalent to the thickness of Villafranchian palustrine carbonates ≈ M8 megasequence of Ezquerro, 2017), or 0.3 Ma in its age. If the top of the buried carbonate unit would be Early Villafranchian in age (3.5 Ma, therefore correlative of *FES3*): (i) the fault throw *s.s.* and the total tectonic throw calculated in section 4 (330 m and 480 m, respectively) should be applied to a 3.5 Ma time span, therefore resulting in slightly higher slip rates (0.10 *vs*. 0.09 mm/a, 0.15 *vs*. 0.13 mm/a, respectively); (ii) *FES2* would lie 10-40 m lower within the downthrown block, and hence the fault throw *s.s.* and the maximum total tectonic throw could increase up to 370 m and 520 m, respectively, giving rise to slip rates of 0.10 and 0.15 mm/a for the last 3.8 Ma. In any case, such height uncertainty is of the same order as the unevenness of the planation surfaces themselves, and results in a very small error in slip rate (0.01 mm/a).

The consistency of this interpretation is further reinforced if the whole morphotectonic setting is considered. We have explained how the morphosedimentary *FES2* marker defines a tilted Sierra Palomera-Alfambra block whose edge is tectonically uplifted ca. 300 m relative to the bottom of the Teruel basin. A similar morphostructural outline can be drawn for the Sierra de Albarracín-Jiloca block, in which the *FES2* altitude progressively decreases eastwards, from 1400-1500 m to <1100 m. Therefore, the inference that the fault separating such tilted blocks has a throw in the range of 300-400 m seems well-founded. On the other hand, the notion of recent throw on the Sierra Palomera fault being larger than those on Calamocha and Concud faults (210 and 260 m, respectively; Martín-Bello *et al.*, 2014; Ezquerro *et al.*, 2020) fits a common structural feature of segmented extensional fault zones, in which maximum throws are found in central segments (self-similar pattern as that of individual faults; Cowie and Roberts, 2001). Gracia *et al.* (2003) aimed to minimize the role of tectonic slip on the Sierra Palomera fault in benefit of erosional lowering in the development of the central Jiloca depression, but that controversy is currently out of place.

We should compare the displacement and slip rates on the Sierra Palomera fault with those in the neighbouring Teruel graben. During the last 3.8 Ma (Late Pliocene-Quaternary extensional phase), fault zones making the eastern margin of the Teruel basin underwent total throw (including bending component) in the range of 440 to 620 m, and hence long-term vertical slip rates of 0.12 to 0.16 mm/a (Ezquerro *et al.*, 2020). Assuming an average dip of 70º for the fault plane and a pure normal movement, the resulting total net slip rates for this period are 0.13 to 0.17 mm/a, similar to that calculated for the Sierra Palomera fault (0.15 mm/a) and higher than those for the Concud (0.07-0.08 mm/a; Lafuente *et al.*, 2011a), Calamocha (0.06-0.09 mm/a; Martín-Bello *et al.*, 2014), and Teruel (0.075 mm/a; Simón *et al.*, 2017) faults.

It is also pertinent to consider geomorphic indices as auxiliary tools for assessing fault activity (*e.g.*, Bull and McFadden, 1977; McCalpin, 2009; Silva *et al.*, 2003; Burbank and Anderson, 2012), and compare the values obtained for the Sierra Palomera mountain front with those of other faults in the same geodynamic framework. At Sierra Palomera, García-Lacosta (2013) calculated the mountain-front sinuosity (S_{mf} = 1.27), and valley width/height ratio (V_f = 0.22). These values, together with qualitative attributes as trapezoidal facets, V-shaped gullies, and small alluvial fans not connected to the regional fluvial system, indicate 'rapid' fault slip according to the classification by McCalpin (2009), and 'active' (according to Silva *et al.*, 2003) (Fig. 14). The range of slip rates that those authors estimate for such categories in their respective classifications (0.08 to 0.5 mm/a) encloses the value calculated for the Sierra Palomera fault from offset of the *FES2* marker (0.09-0.13 mm/a).

The sinuosity index S_{mf} at the Sierra Palomera mountain front is very similar to those published for the Concud fault (S_{mf} =1.24; Lafuente *et al.*, 2011b), Maestrat grabens in eastern Iberian Chain (S_{mf} = 1.04-1.60; mean = 1.27; Perea, 2006), or Carboneras, Lorca-Alhama and Baza faults in the Betic Chains (S_{mf} usually ranging from 1.05 to 1.4; Silva *et al.*, 2003; García-Tortosa *et al.*, 2008). The V_f index computed for the Sierra Palomera fault does not differ from that of the Concud fault (V_f = 0.30; Lafuente *et al.*, 2011b), while higher and more variable values have been reported in the Maestrat grabens (Silva *et al.*, 2003; Perea, 2006; García-Tortosa *et al.*, 2008).

Plotting S_{mf} *vs*. V_f values on the diagram proposed by Silva *et al.* (2003) allows assessing the relative position of the Sierra Palomera fault among extensional fault-generated mountain fronts of eastern Spain (Fig. 14). The relatively low values of both S_{mf} and V_f indices found at the Sierra Palomera mountain front (1.27 and 0.22, respectively) represent a morphotectonic signal similar to that of the Concud fault, and also consistent with the tendency of extensional faults studied by Silva *et al.* (2003) in the Valencia area and Betic Chains.

8.3. Pleistocene fault activity and its paleoseismological relevance

Morphotectonic data indicate that the Sierra Palomera fault has a significant degree of activity, but no outcrop observation on the main trace has unequivocally evidenced Quaternary displacement on it. Therefore, it is very relevant the finding, in La Sima trench, of Pleistocene faults that accommodate extensional deformation associated to the hanging-wall rollover, since they indirectly confirm, for the first time, Pleistocene activity of the Sierra Palomera fault.

As explained in section 6.4, seven deformation events (T to Z) have been recognized after detailed trench analysis, which could be conventionally considered as paleoseismic events according to usual criteria in Paleoseismology. Individual faults activated in each event have been recognized, and slip on them has been quantified (individual net slip in the range of 5 to 115 cm; Table 2). Finally, the overall faulting history has been carefully reconstructed by means of retrodeformational analysis (Fig. 12). Nevertheless, we should critically admit that the meaning of these results in relation to paleoseismicity of the Sierra Palomera fault is very imprecise, since:

(i) Instead of crossing the main fault, the trench only represents a short transect within the hanging-wall block, at a distance of 1.0 km from the fault trace.

(ii) During each event, faults widely distributed along the surveyed transect underwent both synthetic slip with Sierra Palomera fault (downthrown block to the west; positive values in Table 2) and antithetic slip (negative). The algebraic sum of those values does not necessarily have any meaning in relation to the real slip on the main fault.

(iii) The poor quality of OSL results precludes us from having an age model of the exposed sedimentary succession; therefore, the age constraints of the individual events are very limited. Only the last two events, Y and Z, could be dated to ca. 97±10 ka and 49±5 ka, respectively.

Concerning the net slip accumulated by faults (see Table 2), three among the first four events (T, U and W) involve significant synthetic slip (+45, +105 and +60 cm, respectively), while the last three ones (X, Y, Z) involve significant antithetic slip (−45, −35 and −110 cm, respectively). The global aggregate fault slip for the ensemble of deformation events is virtually null (+10 cm). Nevertheless, a total accumulated antithetic throw of 210 cm can be directly measured on the log from offset of the top of unit 6, the youngest sedimentary marker previous to the recorded faulting episodes (compare the first and the last picture in Fig. 12). Consequently, that resulting throw should be entirely attributed to the bending monocline (i.e., accommodated in the form of continuous deformation, not computed within fault slip measurements depicted in Table 2). That value reasonably approaches the apparent vertical offset of the natural slope of La Sima alluvial fan (ca. 2.5 m; Fig. 10c). In summary, the morphological expression (up-facing scarplet) of the fault zone exposed in the trench fits well the antithetic sign of the accumulated slip during the youngest faulting episodes.

These youngest, antithetic faulting events (X, Y and Z) have associated net slip values (-35 to -110 cm) that should be accommodated on faults several km long (in the range of 10 to 40 km, according to the empirical relationships proposed by Wells and Coppersmith, 1994). This inference plays in favour of: (i) the interpretation of the antithetic fault exposed at La Sima trench as a large structure, comparable in length to the Sierra Palomera fault itself, as the macrostructural and geophysical data suggested (see sections 5, 6 and 8.1); (ii) the notion that faulting events recorded at the trench, in particular those dated to ca. 97±10 ka and 49±5 ka, should respond to coseismic events on the main fault.

Could the timing of those younger events be taken as a reference for approaching seismic recurrence periods and slip rates of the Sierra Palomera fault during Pleistocene times? The tempting hypothesis that the two aforementioned ages correspond to the last two major paleoearthquakes would suggest a single interseismic period of around 48 ka. According to Villamor and Berryman (1999), this would be reliable for faults showing average slip rate around 0.1 mm/a, as the Sierra Palomera fault does. Nevertheless, the space and time window examined in our trench is too narrow for providing a representative paleoseismological record. Subsidiary faults similar to those exposed at La Sima could have form at other sites within the hanging-wall block in response to other events on the main fault. Furthermore, each event on this main fault did not necessarily reactivate the antithetic fault exposed at La Sima trench. Accordingly, the actual slip rate on the Sierra Palomera fault during Late Pleistocene times could be significantly higher than the long-term one (0.09-0.15 mm/a since mid-Pliocene times; see sections 8.1 and 8.2), following the same tendency found in other active structures of the region, such as the Concud fault (Lafuente *et al.*, 2014; Simón *et al.*, 2016), Teruel fault (Simón *et al.*, 2017), Teruel basin (Ezquerro *et al.*, 2020; see Section 2) and Calatayud basin (Peiro and Simón, 2021).

8.4. Internal deformation of the hanging-wall fault block: a close look from trench analysis

Although the succession of deformation events identified at La Sima trench have a very limited paleoseismic meaning, it allows understanding progressive stretching within the hanging-wall block of the Sierra Palomera fault. In particular, sequential activation of synthetic and antithetic individual faults has been carefully reconstructed by means of retrodeformational analysis (Fig. 12) and can be precisely compared with faulting patterns linked to rollover deformation at both smaller and larger scales (analogue models and field or seismic-profile examples, respectively).

Usually, the hanging-wall rollover geometry is not entirely achieved through ductile deformation. Examples from analogue models (*e.g.*, Withjack and Schlische, 2006), outcrops and high-resolution seismic profiles (*e.g.*, Song and Cawood, 2001; Delogkos *et al.*, 2020) indicate that a portion of deformation is accommodated by smaller-scale faults. Antithetic faults directly materialize the antithetic simple shear that nucleates at the transition from the main ramp to the basal detachment (Withjack *et al.*, 1995), frequently abutting the connection line between the steep and flat segments of the main fault surface (Bruce, 1973; Song and Cawood, 2001; Withjack and Schlische, 2006). In addition, together with subsidiary synthetic faults, they can accommodate layer-parallel extension along the rollover, giving rise to crestal collapse grabens in both analogue models (*e.g.*, McClay, 1990; McClay and Scott, 1991; Buchanan and McClay, 1991; Soto *et al.*, 2007) and field examples (*e.g.*, Imber *et al.*, 2003; Back and Morley, 2016; Fazli Khani *et al.*, 2017). The locus of active hanging-wall antithetic faulting, as well as that of crestal graben formation, have the appearance of having migrated landwards during development of extensional systems: each individual antithetic fault moves passively beyond the fault bend and becomes inactive, while a new fault propagating from the same bend replaces it. Thus, secondary faults tend to be progressively older basinwards

(Christiansen, 1983; McClay, 1990; Withjack *et al.*, 1995; Withjack and Schlische, 2006). In any case, periods of activity of the hanging-wall growth faults can overlap (Imber *et al.*, 2003). The great majority of analogue models of rollovers show a faulting sequence that begins with an antithetic fault, then alternating synthetic and antithetic ones eventually joining and reciprocally offsetting at depth (McClay, 1990; McClay *et al.*, 1991; T. Román-Berdiel, personal communication). The same pattern has been reported in actual examples (e.g., Fazli Khani and Back, 2015, fig. 10). Nevertheless, sandbox experiments have also been described in which alternating activation of synthetic and antithetic faults is initiated with a synthetic one (*e.g.*, Buchanan and McClay, 1991).

The fault sequence interpreted at La Sima trench share some of the former evolutionary patterns typical of rollover deformation, such as the relevance and persistence of a subsidiary antithetic fault, the activation of younger antithetic ruptures closer to the main fault, and overall alternating onset of synthetic and antithetic ruptures. However, we have also found a non-typical feature: the oldest recorded meso-scale faults are synthetic with the Sierra Palomera fault, despite having formed in the same area where the persistent antithetic fault will later appear. The first deformational events (T to W) mainly involve accumulation of significant synthetic net slip (+200 cm), while the last three ones (X, Y, Z) involve substantial antithetic net slip (−190 cm). Briefly, progressive deformation in the hanging-wall block is shifted from dominantly synthetic faulting to dominantly antithetic faulting. Such particular deformation pattern suggests the existence of other controls on the hanging-wall deformation in addition to the rollover kinematics itself, as discussed in the next section.

Finally, the accumulated net slip has an associated component of horizontal extension that enables a further quantitative kinematical approach (see Table 2). The total extension recorded at La Sima trench is ≈310 cm, which represents about 19% of the restored length of the logged transect (local β factor = 1.19). Horizontal extension accommodated by faults totalizes ca. 210 cm (125 cm by synthetic ones and 86 cm by antithetic ones). Development of the bending monocline involves additional extension of about 100 cm.

Overall considered, our results represent a high-resolution, sub-seismic-scale picture of hanging-wall deformation that complements natural case studies based on seismic profiles and ‘fills the gap’ with the scale of laboratory analogue models. It documents both (i) earlier stages of a process of hanging-wall deformation (those mostly governed by synthetic faulting) that usually are not recognized from seismic reflection data, and (ii) later stages governed by antithetic faulting that better correlate with seismic-reflection-based models.

8.5. Kinematic and dynamic controls on deformation of the hanging-wall block: relevance of the tectonic stress framework

It is not easy to discriminate whether faults propagated through the hanging-wall block are kinematically or dynamically controlled, *i.e.*, they essentially accommodate extensional deformation associated to the rollover monocline, or they are directly linked to regional stress. Geometry and kinematics of faults surveyed at both map and trench scales overall fits the expected deformation within the hanging-wall block of the Sierra Palomera fault. But they are also consistent with the regional extensional stress field, whose σ_3 trajectories trend ENE-WSW (Simón, 1982, 1989; Arlegui *et al.*, 2005, 2006; Liesa *et al.*, 2019), orthogonal to the overall trend of the Jiloca graben, and only slightly oblique to the Sierra Palomera fault trace itself. Stress inversion from the most representative, non-rotated conjugate faults measured within the trench, according to Anderson (1951), provides local stress axes matching those regional trajectories (Fig. 15).

The extension direction expectable for the kinematical scenario could be constrained between N065ºE (orthogonal to the average strike of the Sierra Palomera fault; an inherited feature indeed) and N050ºE (transport direction). The extension trend expectable for the dynamical scenario would approach N075ºE (seeing at the average trend of the Jiloca graben), or would range from N055ºE to N080ºE (seeing at paleostress results reported by Arlegui *et al.*, 2005, and Liesa *et al.*, 2019). The similarity between both inferences prevents us from discriminating among those hypothetical controls based solely on the orientation of structures (stereoplots of Fig. 11 show how the strongly clustered directions of normal faults in La Sima trench fit equally well the two scenarios). Nevertheless, some details of the faulting succession suggest that both controls probably coexist. The kinematical control has been attested and discussed in sections 8.1 and 8.5. The dynamical one could explain the occurrence of early synthetic meso-scale faults (an unusual feature in kinematically-driven models) at La Sima site.

Additionally, there also seems to be a certain degree of control by a recent ESE-WNW extension direction. Both E-W to ESE-WNW, and ENE-WSW extension directions (characterizing the Late Miocene-Early Pliocene and the Plio-Quaternary rift episodes, respectively) are recorded during the entire extensional period indeed (Liesa *et al.*, 2019). This suggests stress partitioning (in the sense of Simón *et al.*, 2008) of the composite extensional field that results from combination of intraplate NNW-SSE compression (Africa-Iberia convergence) and WNW-ESE extension (rifting of the Valencia trough) (Simón, 1989; Herraiz *et al.*, 2000; Capote *et al.*, 2002). Among fractures observed at La Sima trench that do not show any sign of displacement, a minority NNE-SSW trending set can be distinguished (Fig. 11f), which records the WNW-ESE extensional component of the regional, locally and episodically partitioned stress field.

9. Conclusions

The NNW-SSE trending, 26 km long Sierra Palomera extensional fault has been active during Late Pliocene-Quaternary times. It has undergone nearly pure normal movement with mean transport direction towards N230ºE, consistent with the ENE-WSW extension trajectories of the recent to present-day regional stress field.

The hanging-wall block of the Sierra Palomera fault is cut by two subsidiary parallel ruptures: (i) the synthetic Las Vallejadas fault, located at about 1.5 km basinwards, and (ii) the antithetic La Peñuela fault, at a distance of 0.7-1.0 km, which apparently offsets ca. 2.5 m the surface of the La Sima alluvial fan giving rise to a gentle uphill-facing scarplet.

In the absence of recent stratigraphic markers, the *FES2* planation surface (3.8 Ma) has allowed calculating a maximum value of 330 ± 40 m for the fault throw *s.s.*, and ca. 480 ± 40 m for the total tectonic throw at the half-graben margin (including the bending component), resulting in a net slip rate of 0.09 ± 0.01 mm/a (0.13 ± 0.01 mm/a including bending).

Results from La Sima trench have demonstrated the existence of the antithetic La Peñuela fault, accompanied by a number of minor synthetic and antithetic ones, and its activity during Middle-Late Pleistocene times. Their detailed kinematical analysis has allowed building an evolutionary model made of seven deformation events. Net slip on individual faults ranges from 5 to 115 cm. The cumulative antithetic throw at the exposed fault zone, including fault slip *s.s*. and bending, is estimated at 210 cm, which reasonably approaches the apparent offset of the natural slope of La Sima alluvial fan.

The significance of the paleoseismic results is certainly limited. The surveyed trench within the hanging-wall block does not cross the main fault itself. In addition, it was not feasible to achieve a consistent age model for the entire sedimentary sequence; only the last two deformation events have been dated to ca. 97±10 ka and 49±5 ka, respectively. Nevertheless, Pleistocene activity of the Sierra Palomera fault has been proved for the first time, although indirectly from hanging-wall deformation.

The succession of faulting events at La Sima trench study allows unravelling the progressive extensional deformation within the hanging-wall block of the Sierra Palomera fault. The total horizontal extension recorded at La Sima trench is ≈310 cm (local β factor =

1.19). The faulting succession indicates that synthetic slip prevailing in early deformation events was shifted to antithetic slip during the younger ones. Geometry and sequential development of meso-scale faults suggest the concurrence of: (1) a kinematic control, *i.e.*, antithetic simple shear linked to rollover kinematics (mostly resulting in the main antithetic fault zone), eventually accompanied by layer-parallel extension orthogonal to the rollover axis, and (2) a dynamic control, *i.e.*, response to the remote extensional stress field, characterized by ENE-WSW (occasionally ESE-WSW) extension trajectories.

Acknowledgments

The research has been financed by projects LMP127_18 (Gobierno de Aragón-Programa Operativo del Fondo Europeo de Desarrollo Regional Aragón 2014-2020), and PID2019-108705-GB-I00 of the Agencia Estatal de Investigación (AEI/10.13039/501100011033) of the Spanish Government. This work is a contribution of the Geotransfer Research Group (E32_20R) funded by Gobierno de Aragón. A. Peiro benefits from an FPU contract (FPU17/02470) of the Spanish Government. We thank G. Brook (Luminiscence Dating Laboratory of University of Georgia, USA), and P. Beneítez (Laboratorio de Datación y Radioquímica of the Universidad Autónoma de Madrid, Spain) for OSL dating. A. Medialdea advised us on issues related to OSL dating, and T. Román-Berdiel helped us comparing the results with analogue models. Finally, we sincerely thank the thorough reviews and valuable comments of Hamed Fazli Khani and an anonymous reviewer, which have greatly improved the paper.

References

Alcalá, L., Alonso-Zarza, A.M., Álvarez, M.A., Azanza, B., Calvo, J.P., Cañaveras, J. C., van Dam, J.A., Garcés, M., Krijgsman, W., van der Meulen, A.J., Morales, J., Peláez, P., Pérez-González, A., Sánchez, S., Sancho, R., Sanz, E., 2000. El registro sedimentario y faunístico de las cuencas de Calatayud-Daroca y Teruel. Evolución paleoambiental y paleoclimática durante el Neógeno. Revista Sociedad Geológica España. 13, 323-343.

Allmendinger, R.W., Cardozo, N., Fisher, D., 2012. Structural geology algorithms: Vectors and tensors in structural geology. Cambridge University Press.

Álvaro, M., Capote, R., Vegas, R., 1979. Un modelo de evolución geotectónica para la Cadena Celtibérica. Acta Geológica Hispánica. 14, 172-177.

Anadón, P., Moissenet, E., 1996. Neogene basins in the Eastern Iberian Range, in: Friend, P.F., Dabrio, C.F. (Eds.), Tertiary basins of Spain. The stratigraphic Record of Crustal kinematics. World and Regional Geology series 6, Cambridge University press, Cambridge, pp. 68-76.

Anderson, E.M., 1951. The dynamics of faulting and dyke formation with application to Britain. Oliver & Boyd, Edinburgh.

Arlegui, L.E., Simón, J.L., Lisle, R.J., Orife, T., 2005. Late Pliocene-Pleistocene stress field in the Teruel and Jiloca grabens (eastern Spain): contribution of a new method of stress inversion. Journal of Structural Geology. 27, 693-705. https://doi.org/10.1016/j.jsg.2004.10.013.

Arlegui, L.E., Simón, J.L., Lisle, R.J., Orife, T., 2006. Analysis of non-striated faults in a recent extensional setting: the Plio-Pleistocene Concud fault (Jiloca graben, eastern Spain). Journal of Structural Geology. 28, 1019-1027. https://doi.org/10.1016/j.jsg.2006.03.009.

Back, S., Morley, C.K., 2016. Growth faults above shale–Seismic-scale outcrop analogues from the Makran foreland, SW Pakistan. Marine and Petroleum Geology. 70, 144-162. https://doi.org/10.1016/j.marpetgeo.2015.11.008

Bruce, C.H., 1973. Pressured shale and related sediment deformation: mechanism for development of regional contemporaneous faults. AAPG Bulletin. 57, 878-886. https://doi.org/10.1306/819A4352-16C5-11D7-8645000102C1865D.

Buchanan, P.G., McClay, K.R., 1991. Sandbox experiments of inverted listric and planar fault systems. Tectonophysics. 188, 97-115. https://doi.org/10.1016/0040-1951(91)90317-L.

Bull, W.B., McFadden, L.D., 1977. Tectonic Geomorphology north and south of the Garlock fault California, in: Doehring, D.O. (Ed.), Geomorphology in arid regions. Allen & Unwin, London, pp. 115-138.

Burbank, D.W., Anderson, R.S., 2012. Tectonic Geomorphology. Wiley-Blackwell, Oxford.

Capote, R., Muñoz, J.A., Simón, J.L., Liesa, C.L., Arlegui, L.E., 2002. Alpine tectonics I: The Alpine system north of the Betic Cordillera, in: Gibbons, W., Moreno, T., (Eds.), Geology of Spain. The Geological Society, London, pp. 367-400.

Cardozo, N., Allmendinger, R.W., 2013. Spherical projections with OSXStereonet: Computers & Geosciences. 51, 193-205, https://doi.org/10.1016/j.cageo.2012.07.021.

Christiansen, A.F., 1983. An example of a major syndepositional listric fault, in: Bally, A.W. (Ed.), Seismic expression of structural styles. AAPG Studies in Geology. 15 (2.3.1), 36-40.

Colomer, M., Santanach, P., 1988. Estructura y evolución del borde sur-occidental de la Fosa de Calatayud-Daroca. Geogaceta. 4, 29-31.

Cortés, A.L., Casas, A.M., 2000. ¿Tiene el sistema de fosas de Teruel origen extensional? Revista de la Sociedad Geológica de España. 13(3-4), 445-470.

Cortés, A.L., 1999. Evolución tectónica reciente de la Cordillera Ibérica, Cuenca del Ebro y Pirineo centro-occidental. Unpublished PhD thesis. Univ. Zaragoza.

Cowie, P., Roberts, G.P., 2001. Constraining slip rates and spacings for active normal faults. Journal of Structural Geology. 23, 1901-1915. https://doi.org/10.1016/S0191-8141(01)00036-0.

Delogkos, E., Saqab, M.M., Walsh, J.J., Roche, V., Childs, C., 2020. Throw variations and strain partitioning associated with fault-bend folding along normal faults. Solid Earth. 11, 935-945. https://doi.org/10.5194/se-11-935-2020.

Ezquerro, L., 2017. El sector norte de la cuenca neógena de Teruel: tectónica, clima y sedimentación. PhD thesis, Univ. Zaragoza, http://zaguan.unizar.es/record/77098#

Ezquerro, L., Simón, J.L., Luzón, A., Liesa, C.L., 2019. Alluvial sedimentation and tectono-stratigraphic evolution in a narrow extensional zigzag basin margin (northern Teruel Basin, Spain). Journal of Palaeogeography. 8, 1-25. https://doi.org/10.1186/s42501-019-0044-4

Ezquerro, L., Simón, J.L., Luzón, A., Liesa, C.L., 2020. Segmentation and increasing activity in the Neogene-Quaternary Teruel Basin rift (Spain) revealed by morphotectonic approach. Journal of Structural Geology. 135, 104043. https://doi.org/10.1016/j.jsg-2020.104403.

Fazli Khani, H., Back, S. 2015. The influence of pre-existing structure on the growth of syn-sedimentary normal faults in a deltaic setting, Niger Delta. Journal of Structural Geology. 73, 18-32. https://doi.org/10.1016/j.jsg.2015.01.011

Fazli Khani, H., Back, S., Kukla, P. A., Fossen, H., 2017. Interaction between gravity-driven listric normal fault linkage and their hanging-wall rollover development: a case study from the western Niger Delta, Nigeria. Geological Society. London, Special Publications. 439(1), 169-186. https://doi.org/10.1144/SP439.20.

Fossen, H., Rotevatn, A., 2016. Fault linkage and relay structures in extensional settings-A review. Earth-Science Reviews. 154, 14-28. https://doi.org/10.1016/j.earscirev.2015.11.014.

García-Lacosta, A.I., 2013. La falla de Sierra Palomera: evolución estructural y actividad reciente. Unpublished MSc thesis, Univ. Zaragoza.

García-Tortosa, F.J., Sanz de Galdeano, C., Sánchez-Gómez, M., Alfaro, P., 2008. Geomorphologic evidence of the active Baza Fault (Betic Cordillera, South Spain), Geomorphology. 97, 374-391. https://doi.org/10.1016/j.geomorph.2007.08.007.

Gracia, F.J., Gutiérrez, F., Gutiérrez, M., 2003. The Jiloca karst polje-tectonic graben (Iberian Range, NE Spain). Geomorphology. 52, 215-231. https://doi.org/10.1016/S0169-555X(02)00257-X.

Granier, T., 1985. Origin, damping, and pattern of development of faults in granite. Tectonics. 4, 721-737. https://doi.org/10.1029/TC004i007p00721.

Guimerà, J., Alvaro, M., 1990. Structure et evolution de la compression alpine dans la Chaine Cotiere Catalane (Espagne). Bulletin Société Géologique France. 8, 339-348. https://doi.org/10.2113/gssgfbull.VI.2.339.

Gutiérrez, M., Gracia, F.J., 1997. Environmental interpretation and evolution of the Tertiary erosion surfaces in the lberian Range (Spain), in: Widdowson, M. (Ed.), Palaeosurfaces: Recognition, Reconstruction and Palaeoenvironmental Interpretation. Geological Society. London, Special Publications. 120, 147-158.

Gutiérrez, M., Peña, J.L., 1976. Glacis y terrazas en el curso medio del río Alfambra (provincia de Teruel). Boletín Geológico y Minero. 87, 561-570.

Gutiérrez, F., Gutiérrez, M., Gracia, F.J., McCalpin, J.P., Lucha, P., Guerrero, J., 2008. Plio-Quaternary extensional seismotectonics and drainage network development in the central sector of the Iberian Range (NE Spain). Geomorphology. 102, 21-42. https://doi.org/10.1016/j.geomorph.2007.07.020.

Gutiérrez, F., Masana, E., González, Á., Lucha, P., Guerrero, J., McCalpin, J.P., 2009. Late Quaternary paleoseismic evidence on the Munébrega half-graben fault (Iberian Range, Spain). International Journal of Earth Sciences. 98, 1691-1703. https://doi.org/10.1007/s00531-008-0319-y.

Gutiérrez, F., Gracia, F.J., Gutiérrez, M., Lucha, P., Guerrero, J., Carbonel, D., Galve, J.P., 2012. A review on Quaternary tectonic and nontectonic faults in the central sector of the Iberian Chain, NE Spain. Journal of Iberian Geology. 38, 145-160. https://doi.org/10.5209/revJIGE.2012.v38.n1.39210.

Gutiérrez, F., Carbonel, D., Sevil, J., Moreno, D., Linares, R., Comas, X., Zarroca, M., Roqué, C., McCalpin, J.P., 2020. Neotectonics and late Holocene paleoseismic evidence in the Plio-Quaternary Daroca Half-graben, Iberian Chain, NE Spain. Implications for fault source characterization. Journal of Structural Geology. 131, 103933. https://doi.org/10.1016/j.jsg.2019.103933.

Herraiz, M., De Vicente, G., Lindo, R., Giner, J., Simón, J.L., González, J.M., Vadillo, O., Rodríguez, M.A., Cicuéndez, J.I., Casas, A., Rincón, P., Cortés, A.L., Lucini, M., 2000. The recent (Upper Miocene to Quaternary) and present tectonics stress distributions in the Iberian Peninsula. Tectonics. 19, 762-786. https://doi.org/10.1029/2000TC900006.

IGN, 2021. Catálogo de terremotos. https://www.ign.es/web/ign/portal/sis-catalogo-terremotos (accessed August 2021).

Imber, J., Childs, C., Nell, P.A.R., Walsh, J.J., Hodgetts, D., Flint, S., 2003. Hanging wall fault kinematics and footwall collapse in listric growth fault systems. Journal of Structural Geology. 25(2), 197-208. https://doi.org/10.1016/S0191-8141(02)00034-2.

Lafuente, P., 2011. Tectónica activa y paleosismicidad de la falla de Concud (Cordillera Ibérica central). Unpublished PhD thesis, Univ. Zaragoza.

Lafuente, P., Arlegui, L.E., Liesa, C.L., Simón, J.L., 2011a. Paleoseismological analysis of an intraplate extensional structure: the Concud fault (Iberian Chain, Eastern Spain). International Journal of Earth Sciences. 100, 1713-1732. https://doi.org/10.1007/s00531-010-0542-1.

Lafuente, P., Lamelas, T., Simón, J.L., Soriano, M.A., 2011b. Comparing geomorphic and geologic indices of activity in an intraplate extensional structure: the Concud fault (central Iberian Chain, Spain). Geodinamica Acta. 24, 107-122. https://doi.org/10.1007/S00531-010-0542-1.

Lafuente, P., Arlegui, L.E., Liesa, C.L., Pueyo, O., Simón, J.L., 2014. Spatial and temporal variation of paleoseismic activity at an intraplate, historically quiescent structure: the Concud fault (Iberian Chain, Spain). Tectonophysics. 632, 167-187. https://doi.org/10.1016/j.tecto.2014.06.012.

Liesa, C.L. 2011. Evolución de campos de esfuerzos en la Sierra del Pobo (Cordillera Ibérica, España). Revista Sociedad Geológica España. 24, 49-68.

Liesa, C.L., Simón, J.L., Casas, A.M., 2018. La tectónica de inversión en una región intraplaca: La Cordillera Ibérica. Revista Sociedad Geológica España. 31, 23-50.

Liesa, C.L., Simon, J.L., Ezquerro, L., Arlegui, L.E., Luzón, A., 2019. Stress evolution and structural inheritance controlling an intracontinental extensional basin: The central-northern sector of the Neogene Teruel Basin. Journal of Structural Geology. 118, 362-376. https://doi.org/10.1016/j.jsg.2018.11.011.

Liesa, C.L., Corral, M.B., Arlegui, L.A., Peiro, A., Simón, J.L., 2021. Inversión tectónica negativa y estructuración de la zona de relevo entre las fallas normales plio-cuaternarias de Calamocha y Daroca. X Congreso de Geología de España, Sociedad Geológica de España, Vitoria, Spain.

Martín-Bello, L., Arlegui, L.E., Ezquerro, L., Liesa, C.L., Simón, J.L., 2014. La falla de Calamocha (fosa del Jiloca, Cordillera Ibérica): estructura y actividad pleistocena, in: Álvarez-Gomez, J.A., Martín González, F. (Eds.), Una aproximación multidisciplinar al estudio de las fallas activas, los terremotos y el riesgo sísmico. Segunda reunión ibérica sobre fallas activas y paleosismología, Lorca, (Murcia, España), pp. 55-85.

McCalpin, J.P., 1996. Paleoseismology, 2nd Edition. Academic Press. International Geophysics Series.

McClay, K.R., 1990. Extensional fault systems in sedimentary basins: a review of analogue model studies. Marine and Petroleum Geology. 7, 206-233. https://doi.org/10.1016/0264-8172(90)90001-W.

McClay, K.R., Scott, A.D., 1991. Experimental models of hangingwall deformation in ramp-flat listric extensional fault systems. Tectonophysics. 188, 85-96. https://doi.org/10.1016/0040-1951(91)90316-K.

McClay, K.R., Waltham, D.A., Scott, A.D., Abousetta, A., 1991. Physical and seismic modelling of listric normal fault geometries. Geological Society. London, Special Publications. 56, 231-239. https://doi.org/10.1144/GSL.SP.1991.056.01.16.

Moissenet, E., 1983. Aspectos de la Neotectónica en la fosa de Teruel, in: Comba, J.A. (Ed.), Geología de España. Libro Jubilar J.M. Ríos. 2, IGME, Madrid, pp. 427-446.

Pailhé, P., 1984. La Chaîne Ibérique Orientale. Étude géomorphologique, PhD thesis. Univ. Bordeaux.

Peacock, D.C.P., Sanderson, D.J., 1994. Geometry and development of relay ramps in normal fault systems. Bull. Am. Ass. Petrol. Geol. 78, 147-165. https://doi.org/10.1306/BDFF9046-1718-11D7-8645000102C1865D.

Peiro, A., Simón, J.L., 2021. The Río Grío-Pancrudo Fault Zone (central Iberian Chain, Spain): recent extensional activity revealed by drainage reversal. Geological Magazine. 159(1), 21-36. https://doi.org/10.1017/S0016756821000790

Peiro, A., Simón, J.L., Román-Berdiel, T., 2019. Zonas de relevo de falla en el margen oriental de la fosa del Jiloca (Cordillera Ibérica): geometría, cinemática y modelización analógica. Boletín Geológico y Minero. 130 (3), 393-416. https:// doi.org/10.21701/bolgeomin.130.3.002.

Peiro, A., Simón, J.L., Román-Berdiel, T., 2020. Fault relay zones evolving through distributed longitudinal fractures: the case of the Teruel graben system (Iberian Chain, Spain). Journal of Structural Geology. 131, 103942. https://doi.org/10.1016/j.jsg.2019.103942.

Peña, J.L., Gutiérrez, M., Ibáñez, M., Lozano, M.V., Rodríguez, J., Sánchez, M., Simón, J.L., Soriano, M.A., Yetano, L.M., 1984. Geomorfología de la provincia de Teruel. Instituto de Estudios Turolenses. Teruel.

Perea, H., 2006. Falles actives i perillositat sísmica al marge nord-occidental del solc de Valencia. Unpublished PhD thesis, Univ. Barcelona.

Pueyo, Ó., Lafuente, P., Arlegui, L.E., Liesa, C.L., Simón, J.L., 2016. Geophysical characterization of buried active faults: the Concud Fault (Iberian Chain, NE Spain).

International Journal of Earth Sciences. 105, 2221-2239. https://doi.org/10.1007/s00531-015-1283-y.

Rubio, J.C., 2004. Los humedales del Alto Jiloca: estudio hidrogeológico e histórico-arqueológico. Unpublished PhD thesis, Univ. Zaragoza.

Rubio, J.C., Simón, J.L., 2007. Tectonic subsidence vs. erosional lowering in a controversial intramontane depression: the Jiloca basin (Iberian Chain, Spain). Geological Magazine. 144, 1-15. https://doi.org/10.1017/S0016756806002949.

Rubio, J.C., Simón, J.L., Soriano, A., 2007. Interacting tectonics, hydrogeology and karst processes in an intramontane basin: the Jiloca graben (NE Spain). Hydrological Journal. 15, 1565-1576. https://doi.org/10.1007/s10040-007-0190-0.

Sánchez-Fabre, M., Peña-Monné, J.L., Sampietro-Vattuone, M.M., 2019. Geomorphology of the northern sector of the Alfambra-Teruel depression (Iberian ranges, NE Spain). Journal of Maps. 15, 112-121. https://doi.org/10.1080/17445647.2018.1551157.

Silva, P.G.; Goy, J.L.; Zazo, C., Bardají, T., 2003. Fault-generated mountain fronts in southeast Spain: geomorphologic assessment of tectonic and seismic activity. Geomorphology. 50, 203-225. https://doi.org/10.1016/S0169-555X(02)00215-5.

Simón, J.L., 1982. Compresión y distensión alpinas en la Cadena Ibérica oriental. PhD thesis. Universidad de Zaragoza, Instituto de Estudios Turolenses, Teruel.

Simón, J.L., 1983. Tectónica y neotectónica del sistema de fosas de Teruel. Teruel. 69, 21-97.

Simón, J.L., 1989. Late Cenozoic stress field and fracturing in the Iberian Chain and Ebro Basin (Spain). Journal of Structural Geology. 11, 285-294. https://doi.org/10.1016/0191-8141(89)90068-0.

Simón, J.L., Arlegui, L.E., Lafuente, P., Liesa, C.L., 2012. Active extensional faults in the central-eastern Iberian Chain, Spain. Journal of Iberian Geology. 38, 127-144. https://doi.org/10.5209/rev_JIGE.2012.v38.n1.39209.

Simón, J. L., Arlegui, L. E., Ezquerro, L., Lafuente, P., Liesa, C. L., Luzón, A., 2016. Enhanced palaeoseismic succession at the Concud Fault (Iberian Chain, Spain): new insights for seismic hazard assessment. Natural Hazards. 80, 1967-1993. https://doi.org/10.1007/s11069-015-2054-6.

Simón, J.L., Arlegui, L.E., Ezquerro, L., Lafuente, P., Liesa, C.L. Luzón, A. 2017. Assessing interaction of active extensional faults from structural and paleoseismological analysis:

The Teruel and Concud faults (eastern Spain). Journal of Structural Geology. 103, 100-119. https://doi.org/10.1016/j.jsg.2017.08.003.

Simón, J.L., Ezquerro, L., Arlegui, L.E., Liesa, C.L., Luzón, A., Medialdea, A., García, A., Zarazaga, D., 2019. Role of transverse structures in paleoseismicity and drainage rearrangement in rift systems: the case of the Valdecebro fault zone (Teruel graben, eastern Spain). International Journal of Earth Sciences. 108, 1429-1449. https://doi.org/10.1007/s00531-019-01707-9.

Simón, J. L., Casas-Sainz, A. M., Gil-Imaz, A., 2021. Controversial epiglyptic thrust sheets: The case of the Daroca Thrust (Iberian Chain, Spain). Journal of Structural Geology. 145, 104298. https://doi.org/10.1016/j.jsg.2021.104298.

Simón-Porcar, G., Simón, J.L., Liesa, C.L., 2019. La cuenca neógena extensional de El Pobo (Teruel, Cordillera Ibérica): sedimentología, estructura y relación con la evolución del relieve. Revista Sociedad Geológica España. 32, 17-42.

Song, T., Cawood, P.A., 2001. Effects of subsidiary faults on the geometric construction of listric normal fault systems. AAPG Bulletin. 85(2), 221-232. https://doi.org/10.1306/8626C7A3-173B-11D7-8645000102C1865D.

Soto, R., Casas-Sainz, A. M., Del Río, P., 2007. Geometry of half-grabens containing a mid-level viscous décollement. Basin Research. 19(3), 437-450. https://doi.org/10.1111/j.1365-2117.2007.00328.x.

Vegas, R., Fontboté, J.M., Banda, E., 1979. Widespread neogene rifting superimposed on alpine regions of the Iberian Peninsula. Proceedings Symposium Evolution and Tectonics of the Western Mediterranean and Surrounding Areas, EGS, Viena. Instituto Geográfico Nacional, Madrid, Special Publication. 201, 109-128.

Villamor, P., Berryman, K.R., 1999. La tasa de desplazamiento de una falla como aproximación de primer orden en las estimaciones de peligrosidad sísmica. I Congreso Nacional de Ingeniería Sísmica, Asociación Española de Ingeniería Sísmica. 153-163.

Wells, D.L., Coppersmith, K.J., 1994. New Empirical Relationships among Magnitude, Rupture Length, Rupture Width, Rupture Area, and Surface Displacement. Bull. Seismol. Soc. Am. 84, 974-1002.

Withjack, M.O., Schlische, R.W., 2006. Geometric and experimental models of extensional fault-bend folds. Geological Society, London, Special Publications. 253(1), 285-305.

Withjack, M.O., Islam, Q.T., La Pointe, P.R., 1995. Normal faults and their hanging-wall deformation: An experimental study. AAPG Bulletin. 79, 1-18. https://doi.org/10.1144/GSL.SP.2006.253.01.15.

Young, M.J., Gawthorpe, R.L., Hardy, S., 2001. Growth and linkage of a segmented normal fault zone; the Late Jurassic Murchison-Statfjord North Fault, northern North Sea. Journal of Structural Geology. 23, 1933-1952. https://doi.org/10.1016/S0191-8141(01)00038-4.

The authors declare that they have no known competing financial interests or personal relationships that could have appeared to influence the work reported in this paper.

FIGURE CAPTIONS:

Figure 1:

(a) Location of the Iberian Chain within the Iberian Peninsula. (b) Geological sketch of the Iberian Chain, with location of the main Neogene-Quaternary extensional basins. (c) Simplified geological map of the Jiloca graben, with location of Figures 2, 6 and 9.

Figure 2:

Geological map of the Sierra Palomera area (on DEM image from Instituto Geográfico Nacional) showing the main structures associated to the Sierra Palomera fault. Location of Figures 3, 4, 8, 10a, 11 is indicated, as well as that of OSL samples in La Cecilia and La Sima alluvial fans (see Table 1).

Figure 3:

Cross section of the Jiloca Graben at its central sector, initially reconstructed from surface geology and shallow borehole data (modified from Rubio and Simón, 2007). See location in Figure 2.

Figure 4:

(a) Field view of one of the rupture surfaces within the damage zone of the Sierra Palomera fault; it cuts Lower Jurassic limestones and shows associated fault breccia. (b) Stereoplot (equal area, lower hemisphere) showing orientations of fault planes and slickenlines collected in that zone.

Figure 5:

The Sierra Palomera mountain front. (a) Field panoramic view. (b) Hillshade oblique image rendered from Digital Elevation Model (5 m grid) of Instituto Geográfico Nacional (IGN). (c) Detail of a trapezoidal facet within the fault scarp. (d) Hillshade oblique image (5-m-grid DEM, IGN) showing a close view to the alluvial fans sourced at the mountain front; La Cecilia and La Sima alluvial fans are identified.

Figure 6:

Morphotectonic map of the Sierra Palomera area.

Figure 7:

Throw *vs.* distance (T-D) graph along the Sierra Palomera fault. Lower curve: fault throw *s.s.* recorded by the *FES2* marker. Upper curve: total tectonic throw of *FES2* including the bending component.

Figure 8:

Villafranchian alluvial deposits (V) tilted by an accommodation monocline above La Peñuela fault. Jurassic limestones (J) of the footwall block crops out at the bottom of the gully. See location in Figure 2.

Figure 9:

Results of the magnetometric survey covering the Sierra Palomera piedmont. (a) Location of profiles 01 to 10 (which is the same as for the electromagnetic survey), with the residual values of field intensity (nT) plotted as a colour palette. Black thin lines depict the Sierra Palomera fault trace. Grey thick lines depict the spatial correlation of trending changes on the successive transects, and therefore of the described domains (A, B and C). (b) Residual earth magnetic field profiles plotted with a normalized horizontal length, in which domains A, B and C roughly parallel to the Sierra Palomera fault are defined (data are in nT; see text for details).

Figure 10:

(a) Hillshade relief map of the barranco de la Sima alluvial fan rendered from digital elevation model (DEM, 5 m grid) of the Instituto Geográfico Nacional. See location in Figure 2. (b) Residual magnetic field anomalies at the central sector of the alluvial fan, at the contact between domains A and B. (c) Detailed topographic profile showing a slope anomaly in the longitudinal profile of the alluvial fan surface, from which an apparent antithetic throw of ca. 2.5 m can be inferred.

Figure 11:

(a) Uninterpreted photomosaic of La Sima trench, see location in Figure 2. (b) Detailed log. 1 to 12: Quaternary units described in the text. Greek characters: faults referred in the text. The location and age of samples dated by OSL is indicated. Stereoplots (equal area, lower hemisphere) show orientations of faults and fractures measured within the trench: (c) Central fault zone. (d) Footwall block, including monocline. (e) Synthetic stereoplot of fault planes, including a main set parallel to the prevailing structural trend (NNW-SSE, black great circles) and a subsidiary set oriented NNE-SSW (blue great circles); fault planes rotated at the monocline have been restored to their original orientation. (f) Synthetic stereoplot of fractures without displacement.

Figure 12:

Evolutionary model of sedimentation and deformation recorded at the La Sima trench from retrodeformational analysis. Each sketch represents a stage subsequent to the paleoseismic event (and, in some cases, to deposition of sedimentary units) labelled above. Unexposed sectors below the trench have been locally reconstructed in the sketches in order to complete the evolutionary model. Bold traces indicate which faults are active during each event. Total horizontal extension and throw calculated in Table 2 are shown.

Figure 13:

(a) Refined cross section of the Jiloca graben at its central sector, in which the new inferred, subsidiary faults have been incorporated. (b) Upper fringe of the same cross section (vertical scale x2) showing offset of planation surfaces *FES2* and *FES3.*

Figure 14:

Plot of S_{mf} (mountain-front sinuosity index) *vs.* V_f (valley width/height ratio, measured 250 m upstream from the fault trace), showing the relative position of the Sierra Palomera Fault among extensional fault-generated mountain fronts of eastern Spain. For comparison, the S_{mf} -V_f plots for the neighbouring Concud fault (Lafuente et al, 2011b), faults bounding the Maestrat grabens (eastern Iberian Chain; Perea, 2006), and Valencia region and Betic chains (Silva *et al*., 2003) are also included. Class 1, 2, 3: activity classes (active, moderate and inactive, respectively); the curve represents the tendency for normal faults in SE Spain according to Silva *et al*. (2003).

Figure 15:

Interpretation of paleostress axes from orientation of non-rotated, conjugate fault planes measured within La Sima trench. Stress inversion based on model by Anderson (1951).

Table 1:

Parameters and results of OSL dating of samples collected at the La Sima trench (S1 to S7; Luminiscence Dating Laboratory of University of Georgia, USA), and La Cecilia and La Sima alluvial fans (Laboratorio de Datación y Radioquímica de la Universidad Autónoma de Madrid, Spain).

Table 2:

Synthesis of deformation events inferred at La Sima trench: faults activated during each event; net slip values calculated from the trench log and the retrodeformational analysis (positive: synthetic with the Sierra Palomera fault; negative: antithetic; Figs. 11, 12), and associated values of horizontal extension. Further explanation in text.

Table 1:

Sample	Laboratory reference	Stratigraphic location	Depth (m)	H_2O (%)	Quartz Grain (µm)	^{238}U (ppm)	^{232}Th (ppm)	K (%)	Dose rate (Gy/ka)	Equivalent dose (Gy)	Age (ka)
S1	UGA15OSL-1013	Unit 9 (top)	1.0	5±2.5	80-125	1.42±0.33	5.86±1.14	0.6±0.1	1.50±0.15	146.0±3.9	97.4±10.2
S2	UGA15OSL-1014	Unit 9b	2.1	5±2.5	80-250	0.73±0.12	2.24±0.46	0.2±0.1	0.68±0.10	>256	>378
S3	UGA15OSL-1015	Unit 8	1.6	5±2.5	125-250	0.95±0.15	2.45±0.54	0.3±0.1	0.84±0.11	>300	>355
S4	UGA15OSL-1017	Unit 6 (base)	2.8	5±2.5	150-250	1.35±0.25	5.42±0.88	0.5±0.1	1.27±0.13	>300	>236
S5	UGA15OSL-1018	Unit 11	0.4	5±2.5	125-250	1.29±0.20	4.15±0.71	0.5±0.1	1.26±0.12	62.0±3.4	49.2±5.4
S6	UGA15OSL-1019	Unit 7 (top)	0.7	5±2.5	125-250	0.96±0.20	4.73±0.71	0.5±0.1	1.21±0.12	>300	>248
S7	UGA15OSL-1020	Unit 6 (top)	1.2	5±2.5	80-125	1.41±0.21	4.54±0.75	0.8±0.1	1.56±0.13	>300	>193
La Cecilia	MAD-6326BIN	Alluvial fan	3.0	2.31	2-10	2.97	1.54	0.01±0.1	1.63	47.1±2.5	28.9±2.0
La Sima	MAD-6327BIN	Alluvial fan	0.4	6.25	2-10	3.73	1.90	0.18±0.1	2.31	44.3±1.4	19.2±1.1

Table 2:

Event	Active faults	Net slip[1] (cm)	Average dip (°)	Horizontal extension[1] (cm)	Net slip[1] per event (cm)	Horizontal extension[2] per event (cm)
T	σ	+ 10	53	6	+ 45	15
	τ	+ 5	60	2		
	π1	+ 15	70	5		
	ρ	+ 15	64	7		
U	ε1	+ 15	74	4	+ 105	45
	λ1 + λ2	+ 40	60	20		
	χ	+ 20	59	10		
	μ	+ 15	60	7		
	π2	+ 15	60	7		
V	θ2	- 10	63	5	- 10	5
W	α	+ 10	86	1	+ 60	80
	ε0 + ε1	+ 115	64	50		
	β	- 30	74	8		
	θ1 + θ2 + κ1 to κ4	- 35	63	16		
X	ε2	+ 5	62	2	- 45	65
	θ2+θ3	- 50	74	14		
Y	ε3	0	55	0	- 35	20
	γ1 + γ2 + γ3	- 35	80	6		
Z	ε1	+ 10	64	4	- 110	80
	ε4	- 10	42	7		
	θ2 + θ3 (+ open fissure)	- 110	74	30		
	Total synthetic faults	+ 290		125 (7.8 %)[3]		
	Total antithetic faults	- 280		86 (5.4 %)[3]		
Accumulated deformation:		***Throw[2] (cm)***				***Horizontal extension[2] (cm)***
	Bending monocline	≈ - 220				≈ 100 (6.2 %)[3]
	Total structures	**- 210**				≈ **310** (19.4 %)[3]

[1] Excluding deformation associated to the monocline.

[2] Including deformation associated to both faults and monocline.

[3] Percentage with respect to the restored log length ≈ 1600 cm.

Figure (with caption below and on the same page)

Click here to access/download;Figure (with caption below and on the same page);Fig 1.tif

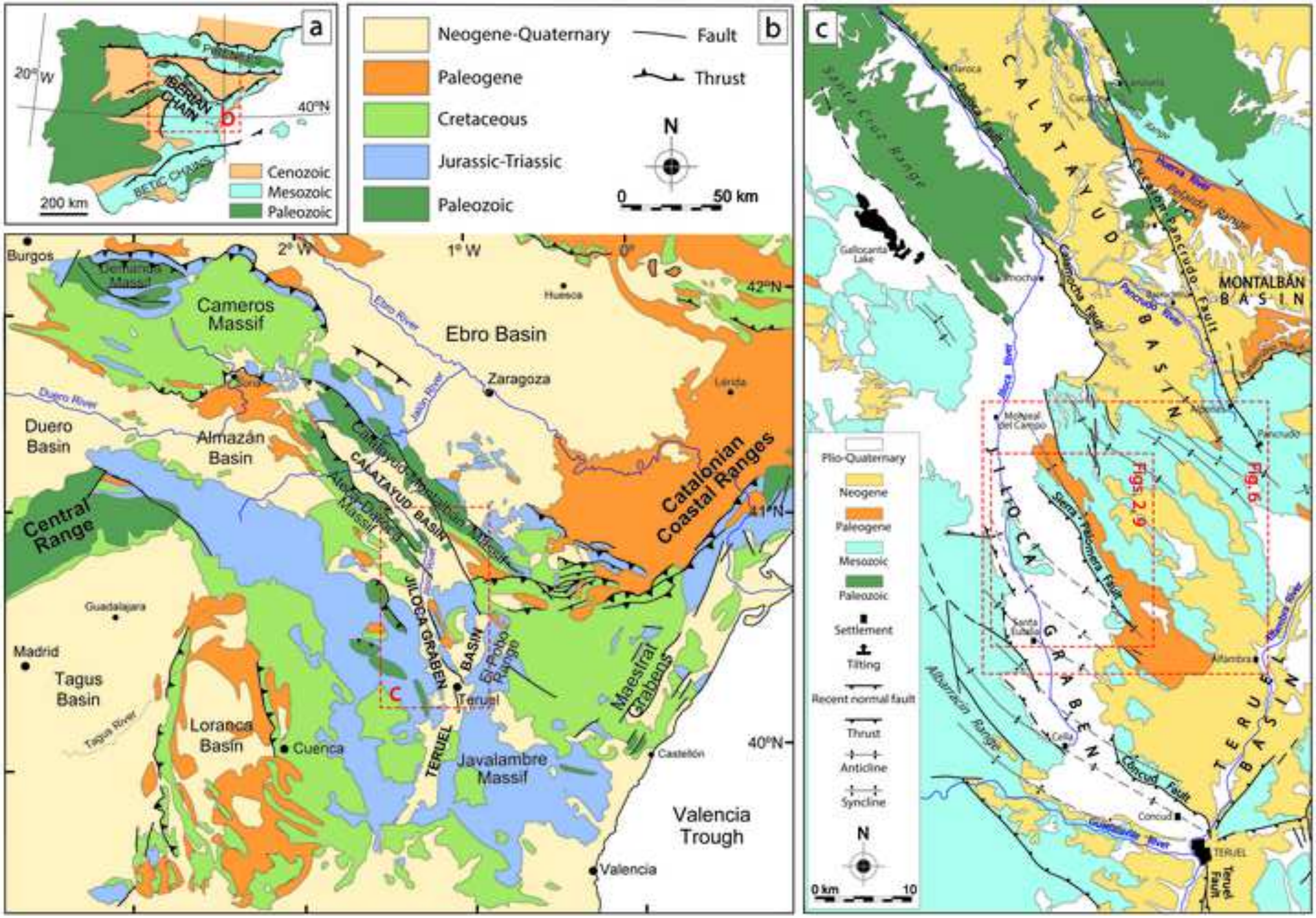

Figure (with caption below and on the same page)

Click here to access/download;Figure (with caption below and on the same page);Fig 1bn.tif

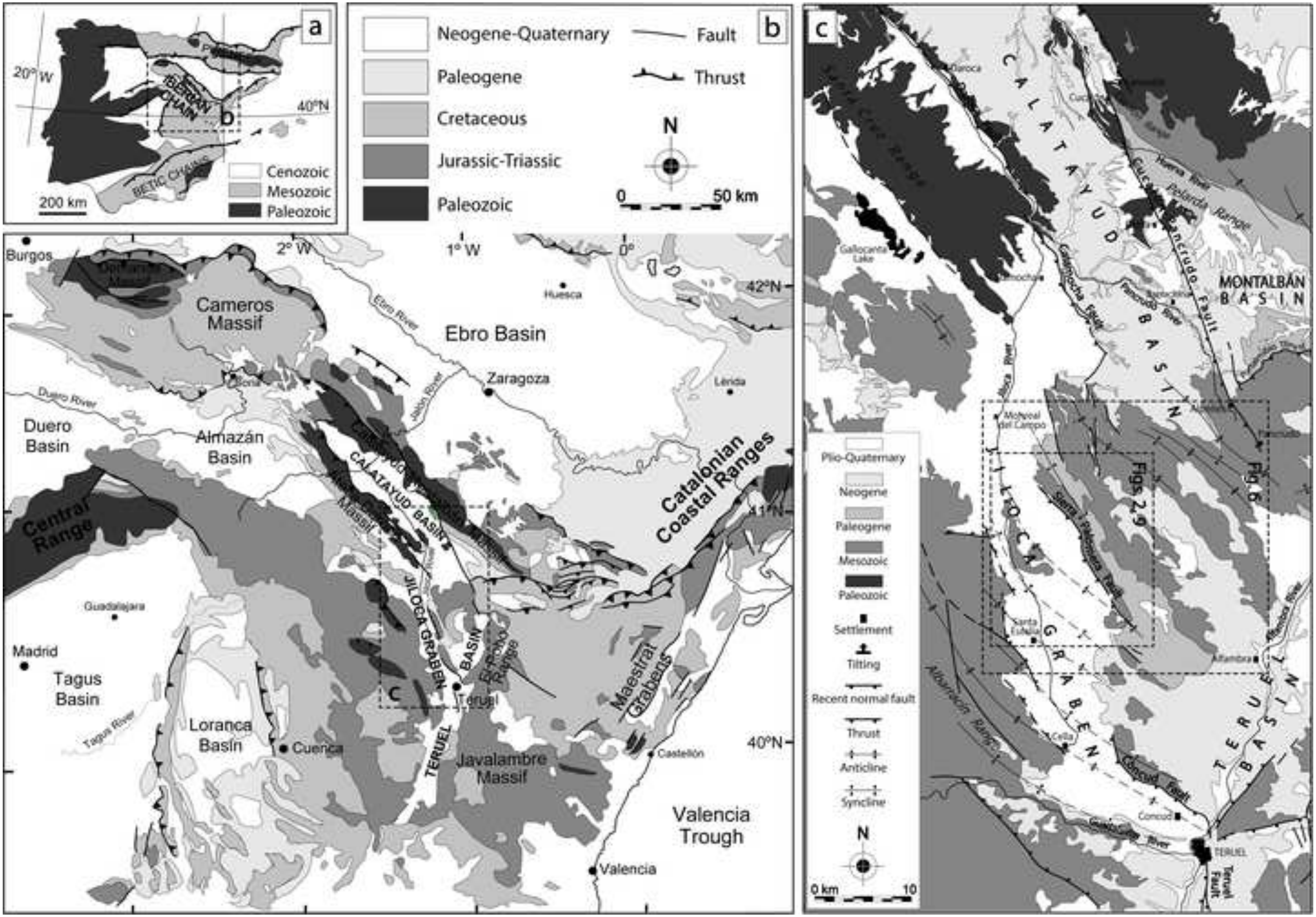

Figure (with caption below and on the same page)

Click here to access/download;Figure (with caption below and on the same page);Fig 2.tif

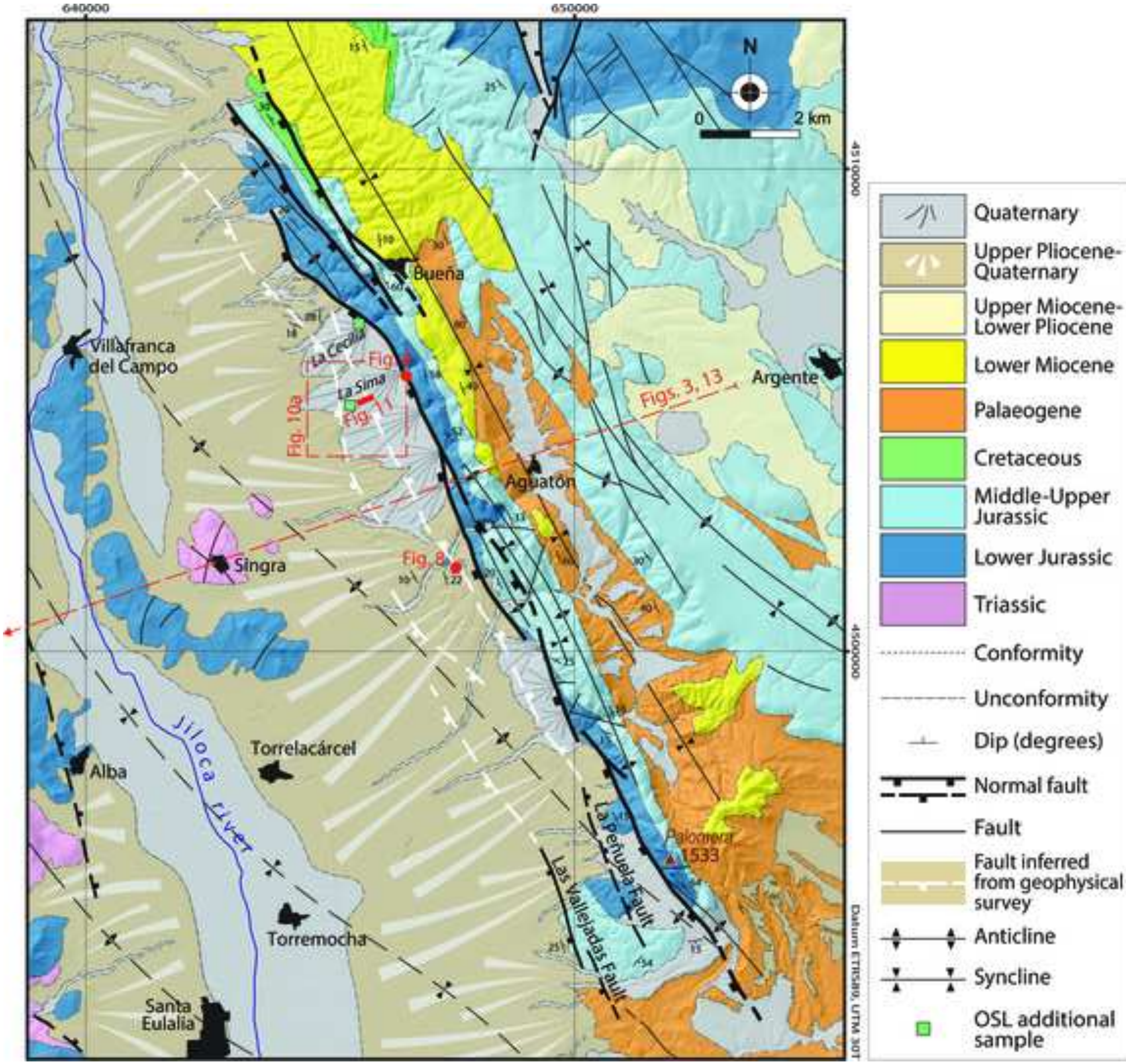

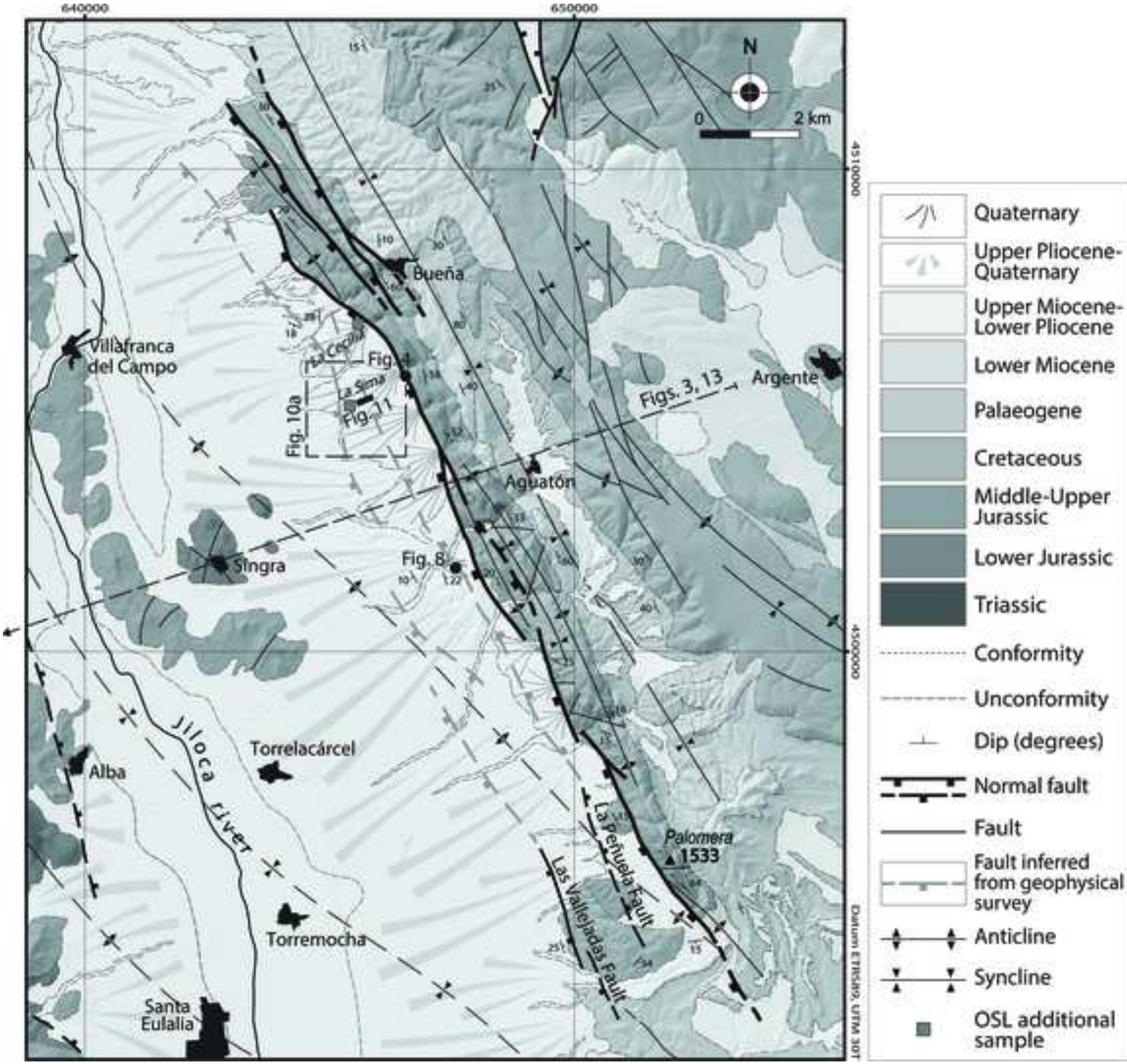
640000
650000
4510000
4500000
N
0
2 km
Bueña
Villafranca del Campo
La Cecilia
Fig. 4
La Sima
Fig. 11
Fig. 10a
Figs. 3, 13
Argente
Aguatón
Singra
Fig. 8
Jiloca river
Torrelacárcel
Alba
La Peñuela Fault
Las Vallejadas Fault
Palomera
1533
Torremocha
Santa Eulalia
Datum ETRS89, UTM 30T
Quaternary
Upper Pliocene-Quaternary
Upper Miocene-Lower Pliocene
Lower Miocene
Palaeogene
Cretaceous
Middle-Upper Jurassic
Lower Jurassic
Triassic
Conformity
Unconformity
Dip (degrees)
Normal fault
Fault
Fault inferred from geophysical survey
Anticline
Syncline
OSL additional sample

Figure (with caption below and on the same page)

Click here to access/download;Figure (with caption below and on the same page);Fig 3.tif

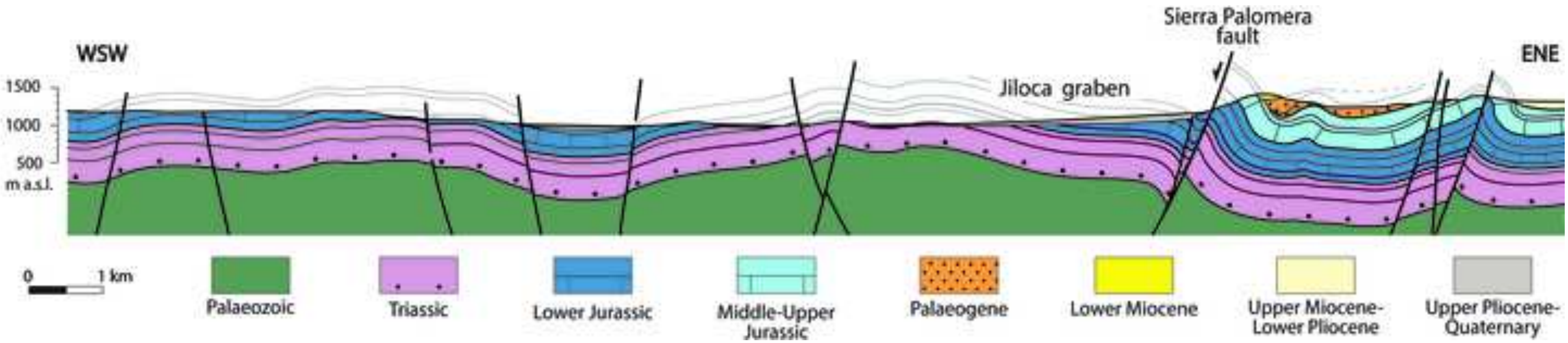

Figure (with caption below and on the same page)

Click here to access/download;Figure (with caption below and on the same page);Fig 3bn.tif

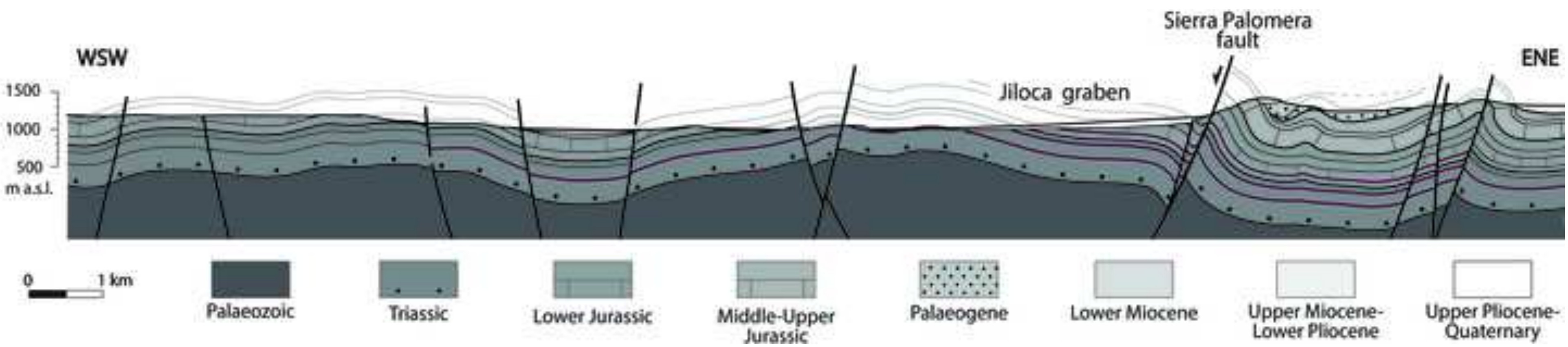

Figure

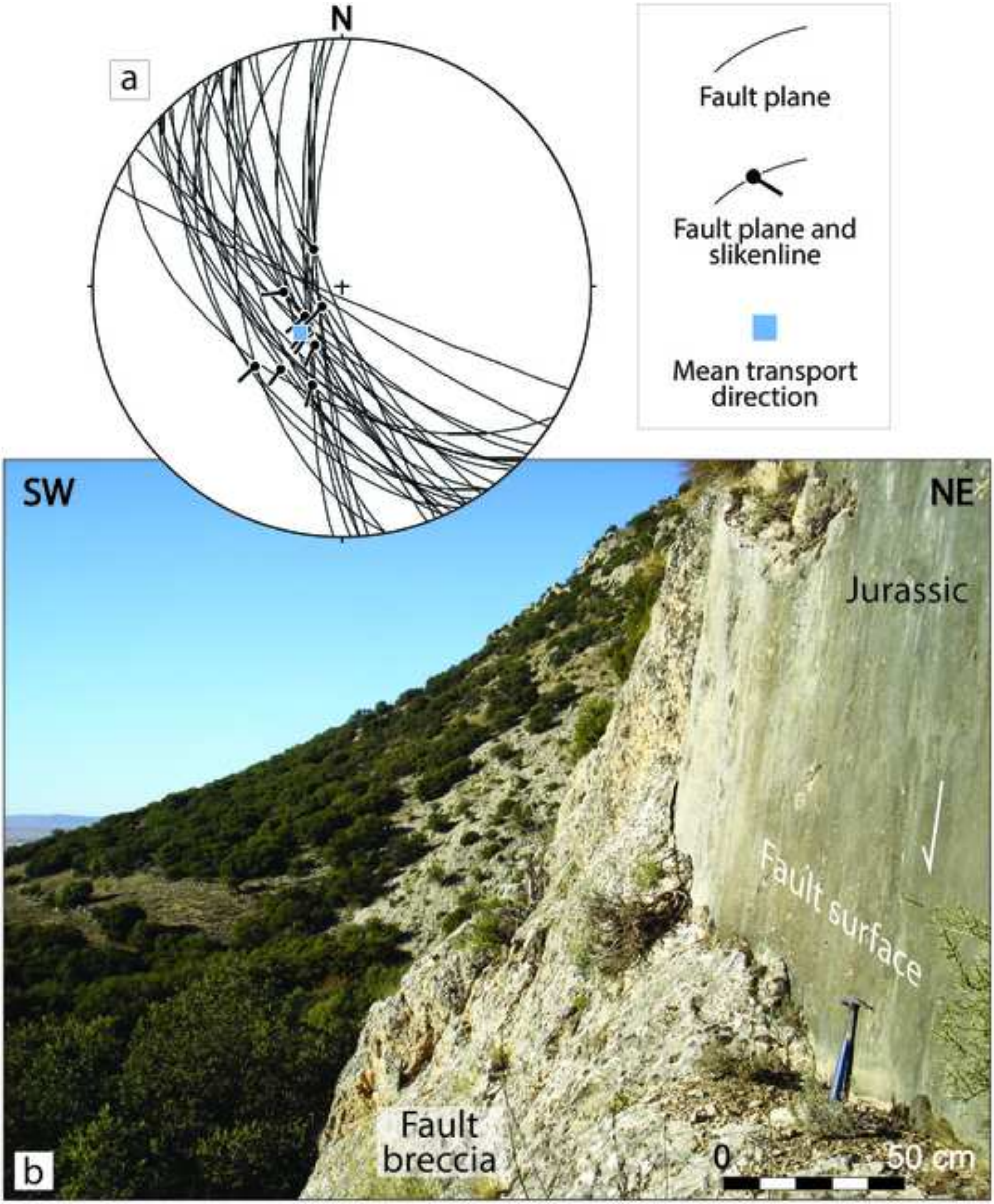
N
a
Fault plane
Fault plane and slikenline
Mean transport direction
SW
NE
Jurassic
Fault surface
Fault breccia
0
50 cm
b

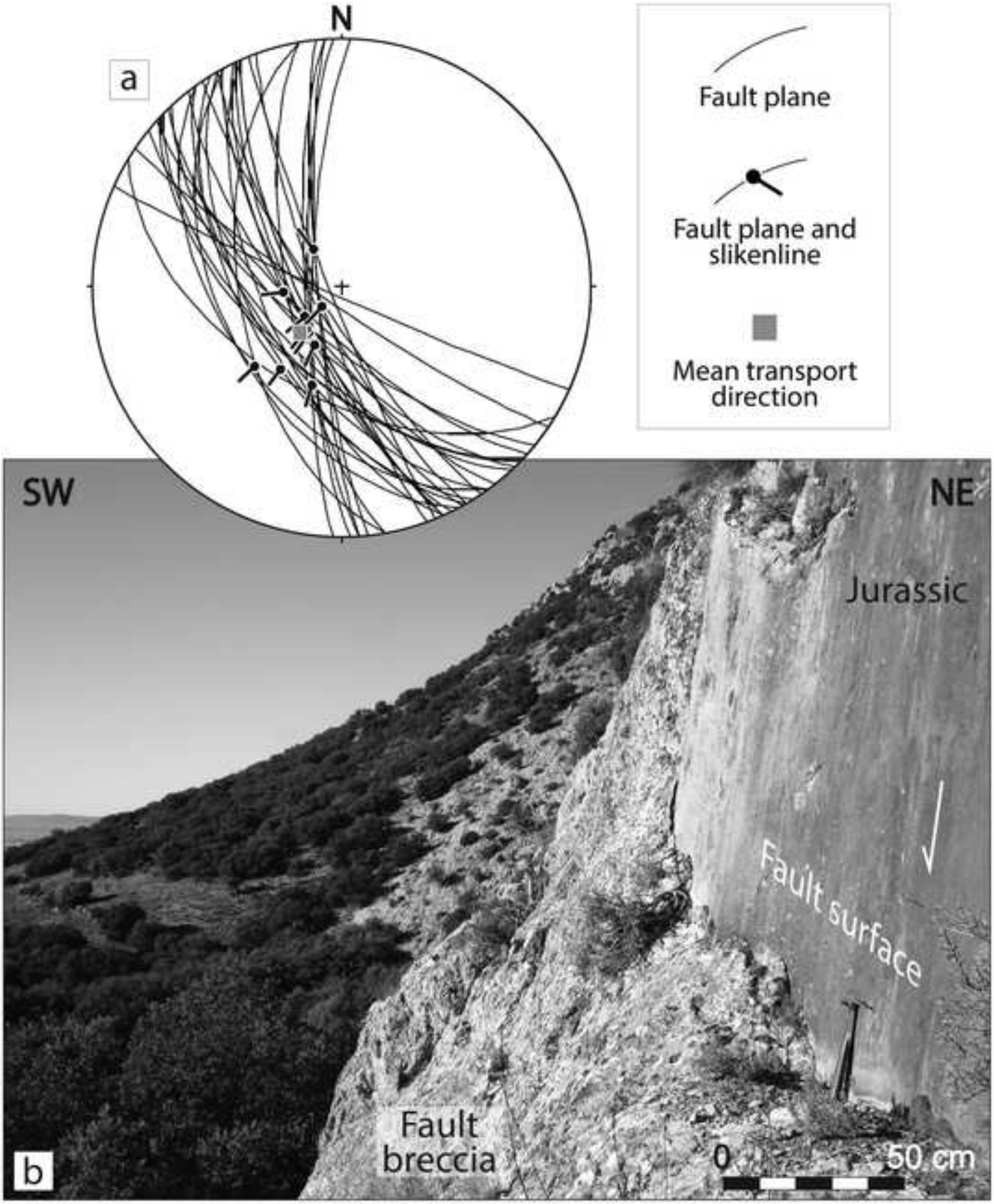
N
a
Fault plane
Fault plane and slikenline
Mean transport direction
SW
NE
Jurassic
Fault surface
Fault breccia
0
50 cm
b

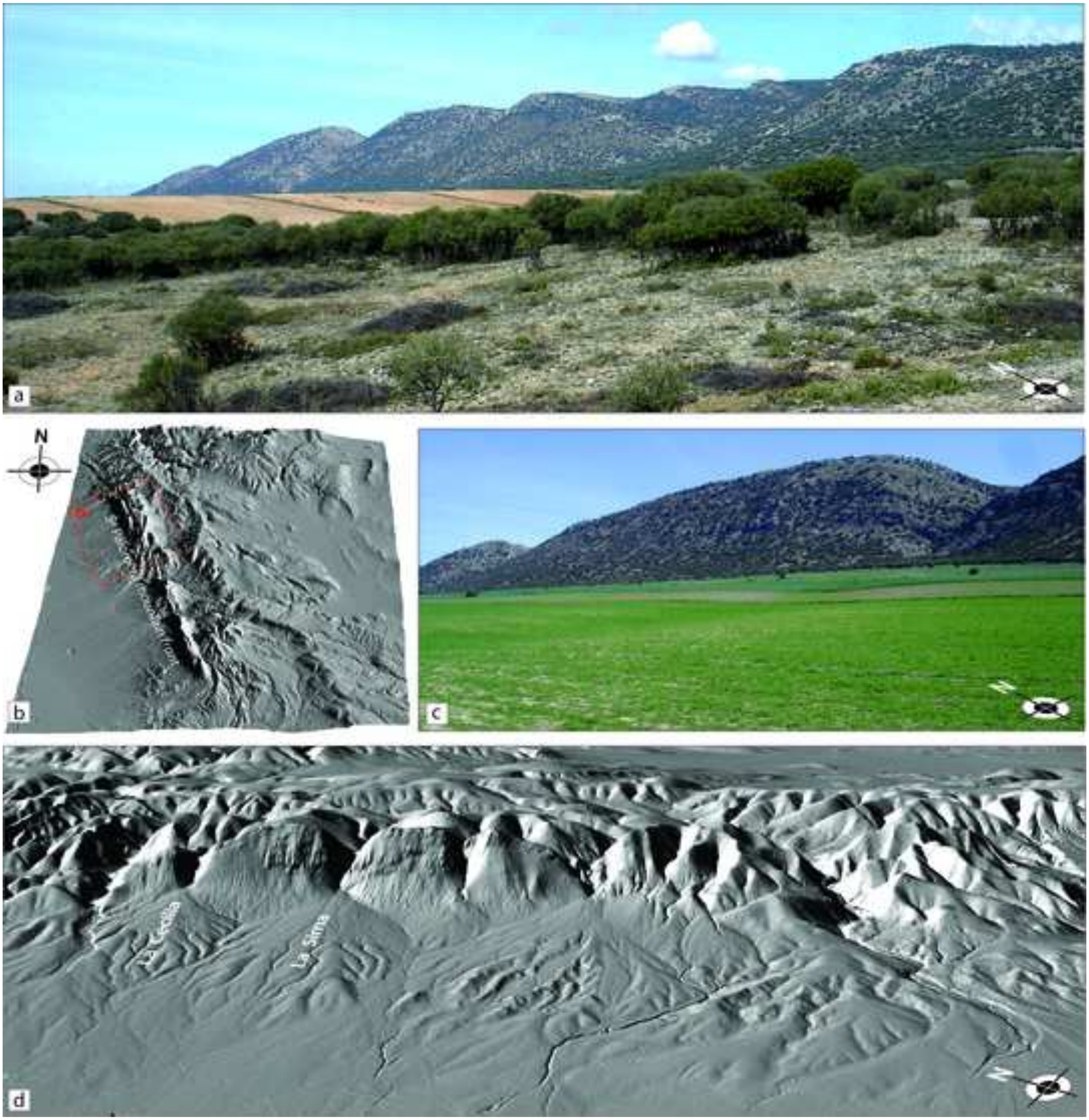
a
N
b
c
La Cecilia
La Sima
d

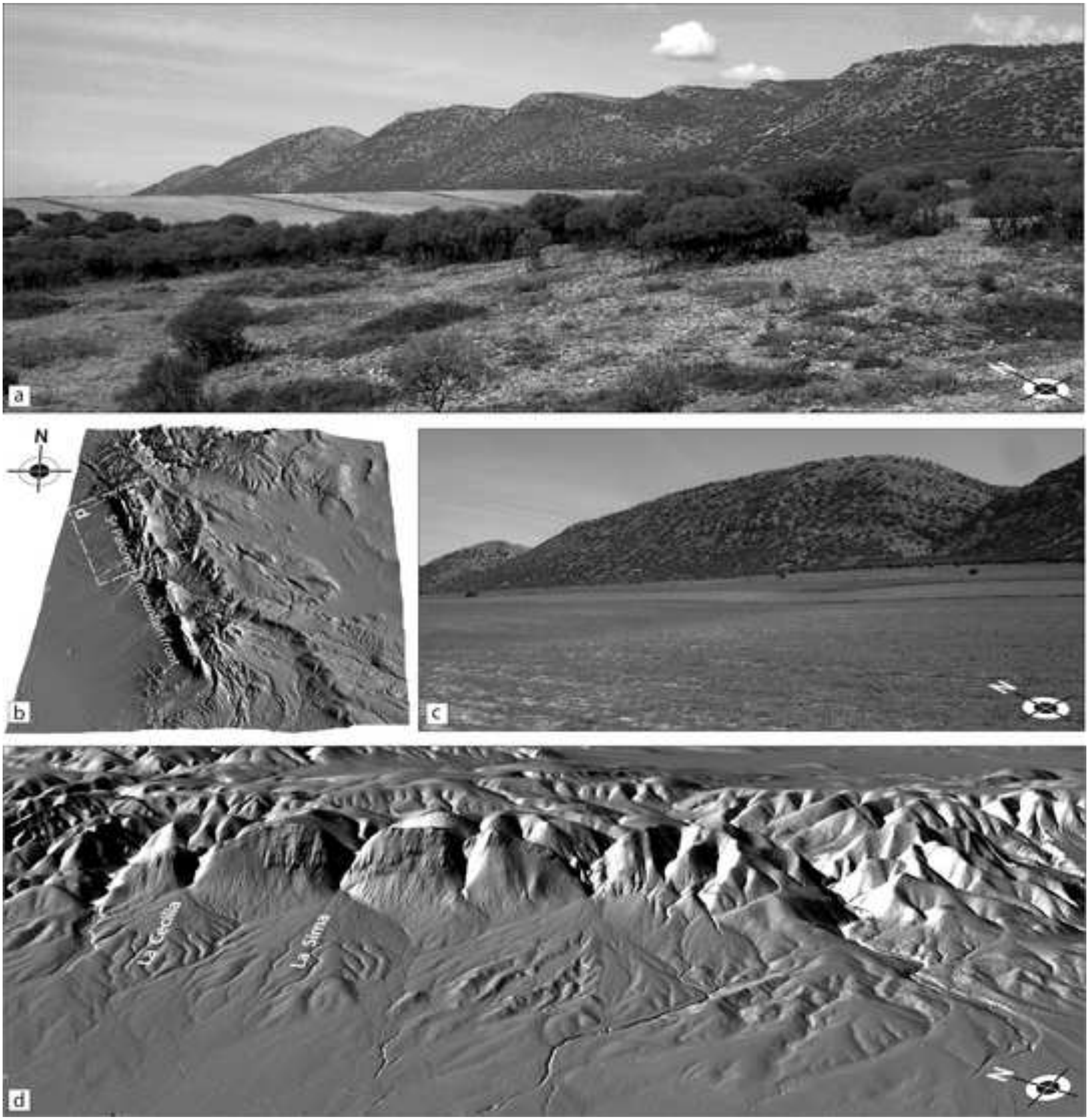
a
N
b
c
d
La Cecilia
La Sirna

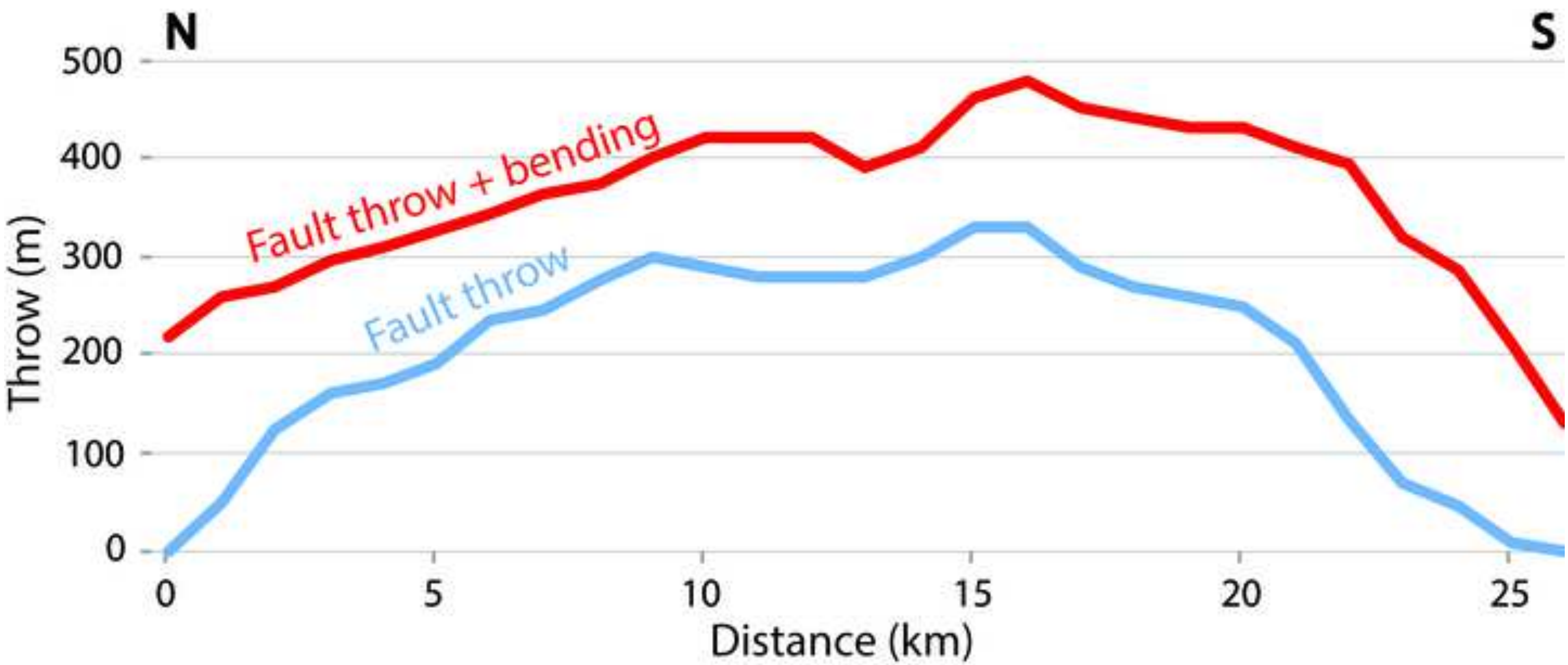
N
S
Fault throw + bending
Fault throw
Throw (m)
500
400
300
200
100
0
0
5
10
15
20
25
Distance (km)

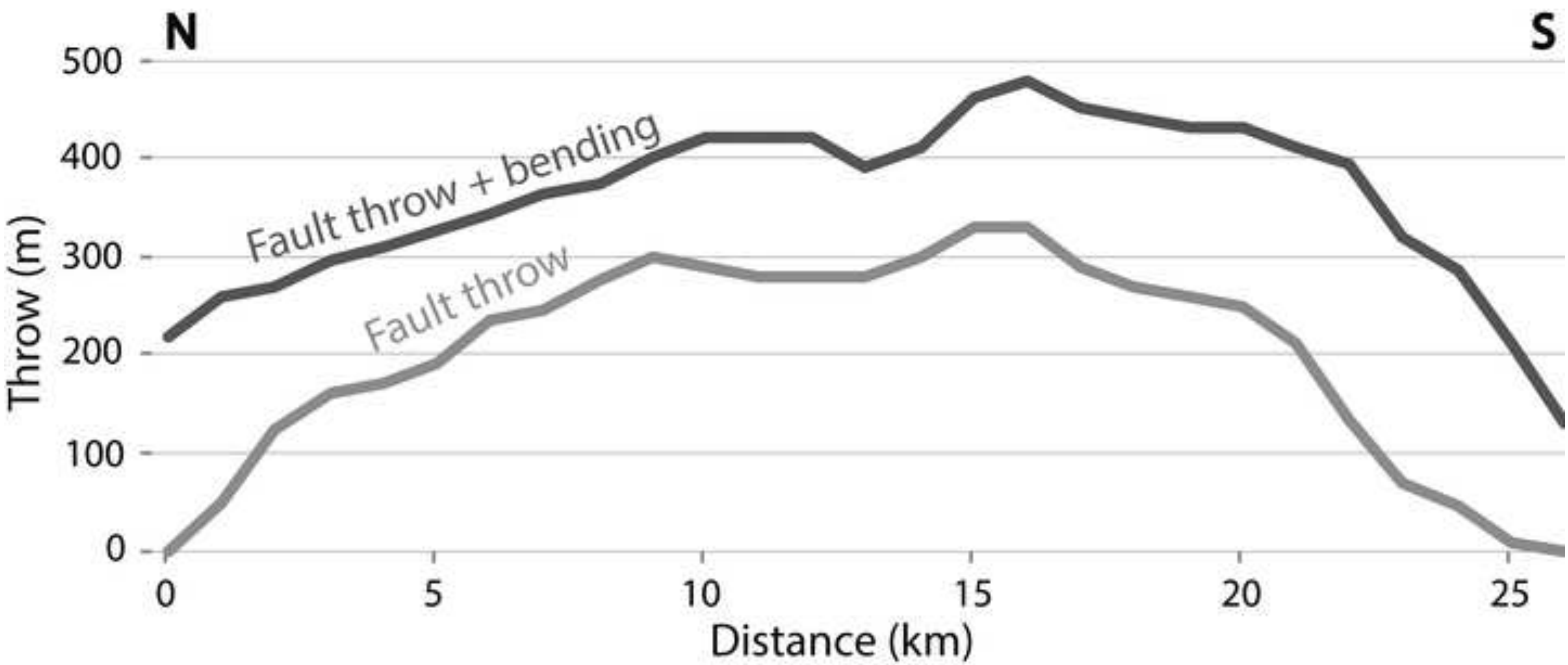
N
S
500
400
300
200
100
0
Throw (m)
Fault throw + bending
Fault throw
0
5
10
15
20
25
Distance (km)

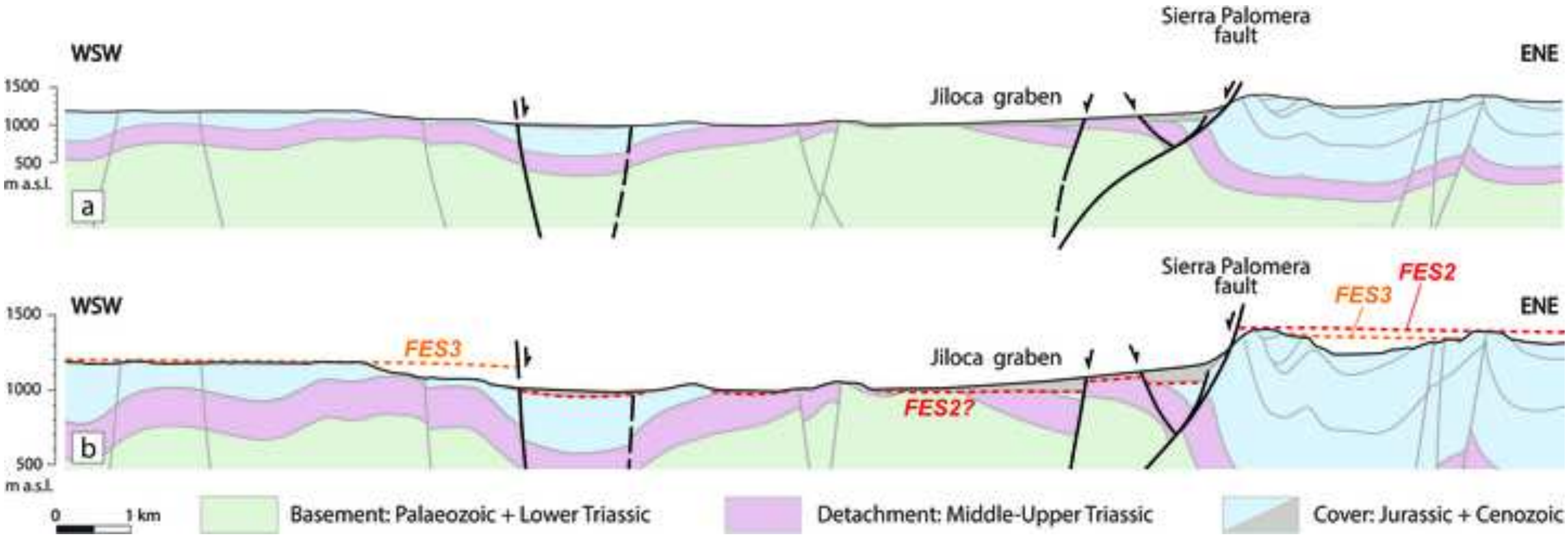
Sierra Palomera fault
WSW
ENE
1500
1000
500
m a.s.l.
Jiloca graben
a
Sierra Palomera fault
FES2
FES3
WSW
ENE
1500
FES3
Jiloca graben
1000
FES2?
b
500
m a.s.l.
0
1 km
Basement: Palaeozoic + Lower Triassic
Detachment: Middle-Upper Triassic
Cover: Jurassic + Cenozoic

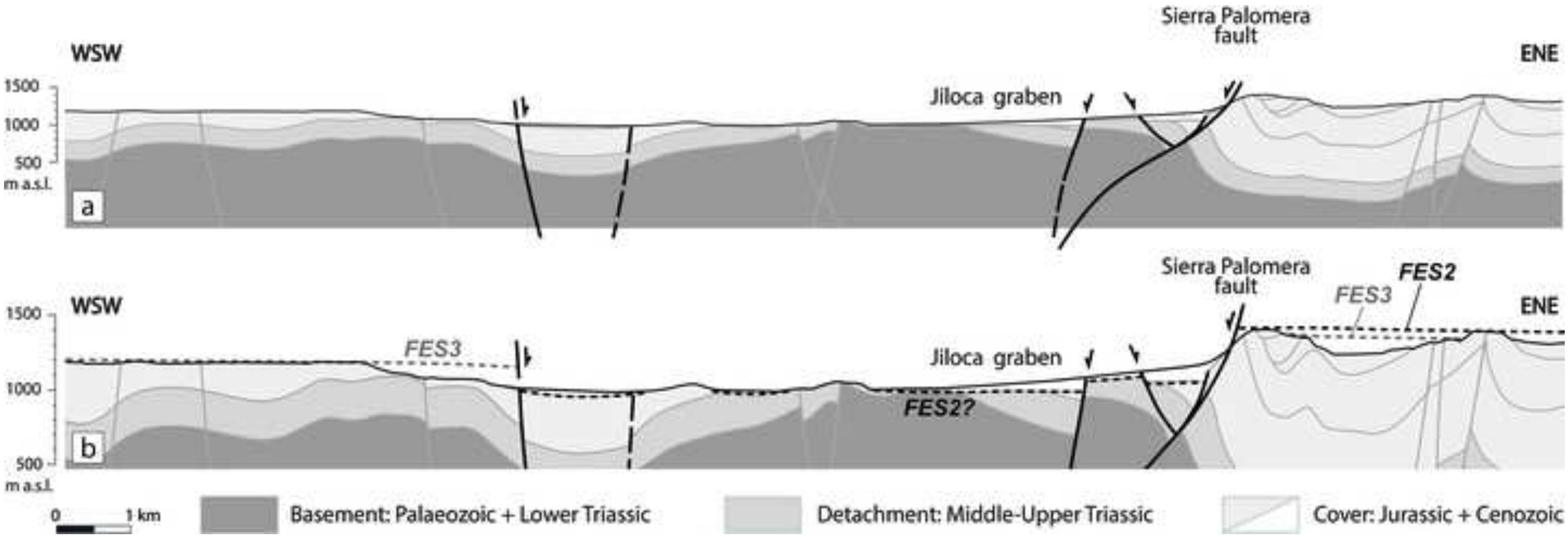
Sierra Palomera
fault
WSW
ENE
1500
1000
500
m a.s.l.
Jiloca graben
a
Sierra Palomera
fault
FES2
FES3
WSW
ENE
1500
FES3
Jiloca graben
1000
FES2?
b
500
m a.s.l.
0
1 km
Basement: Palaeozoic + Lower Triassic
Detachment: Middle-Upper Triassic
Cover: Jurassic + Cenozoic

Figure

Click here to access/download;Figure (with caption below and on the same page);Fig 14.tif

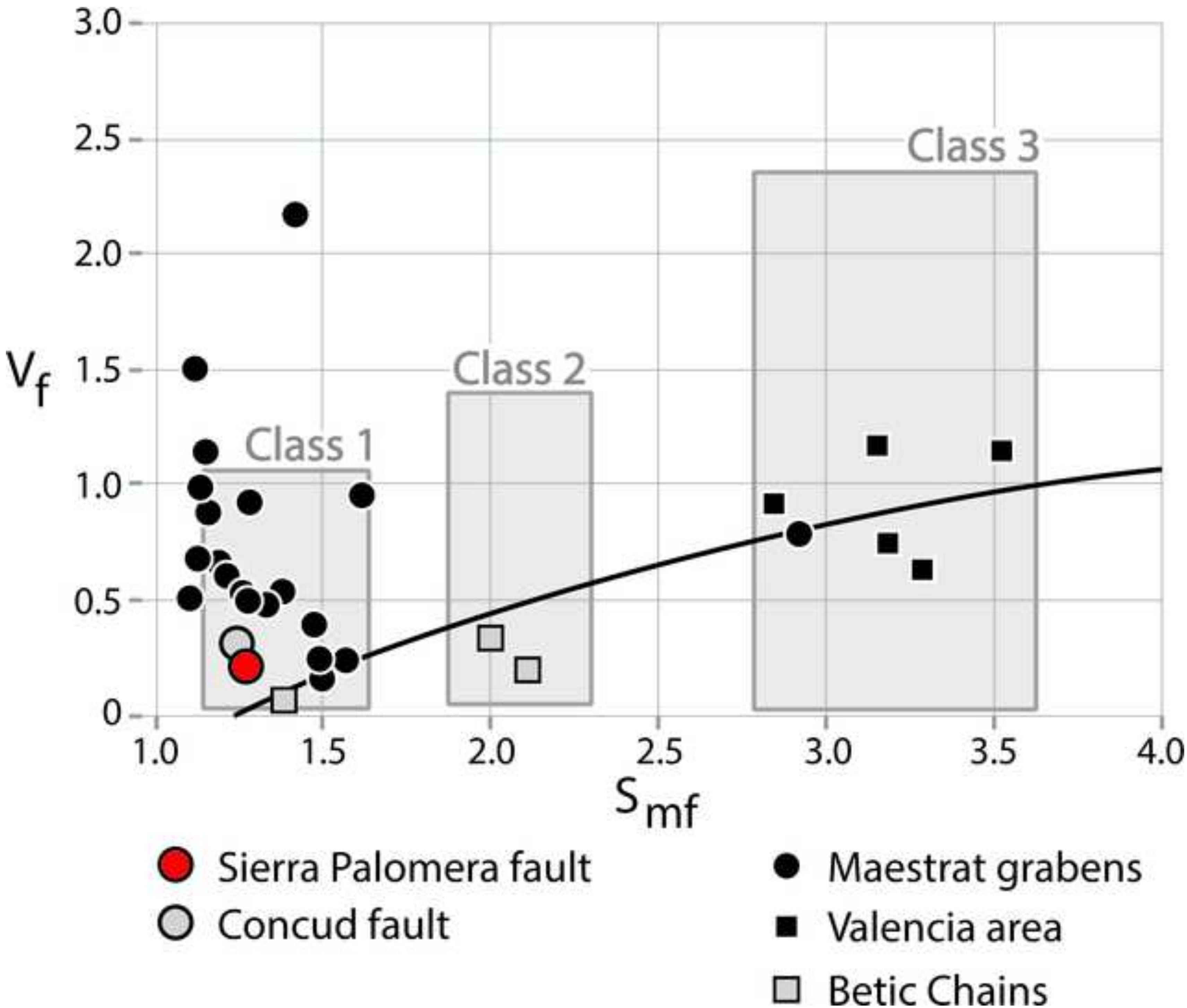

Figure

Click here to access/download;Figure (with caption below and on the same page);Fig 14bn.tif

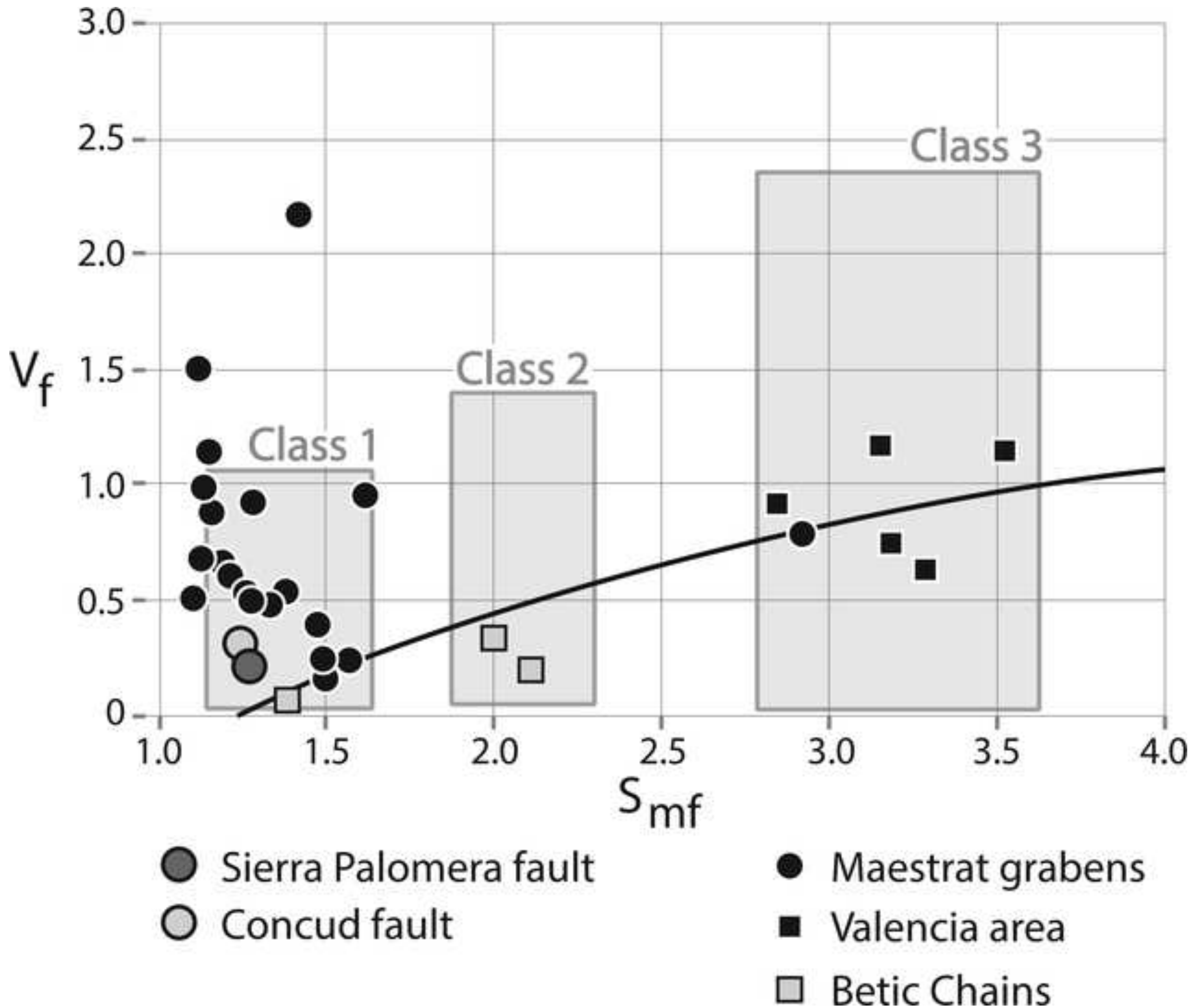

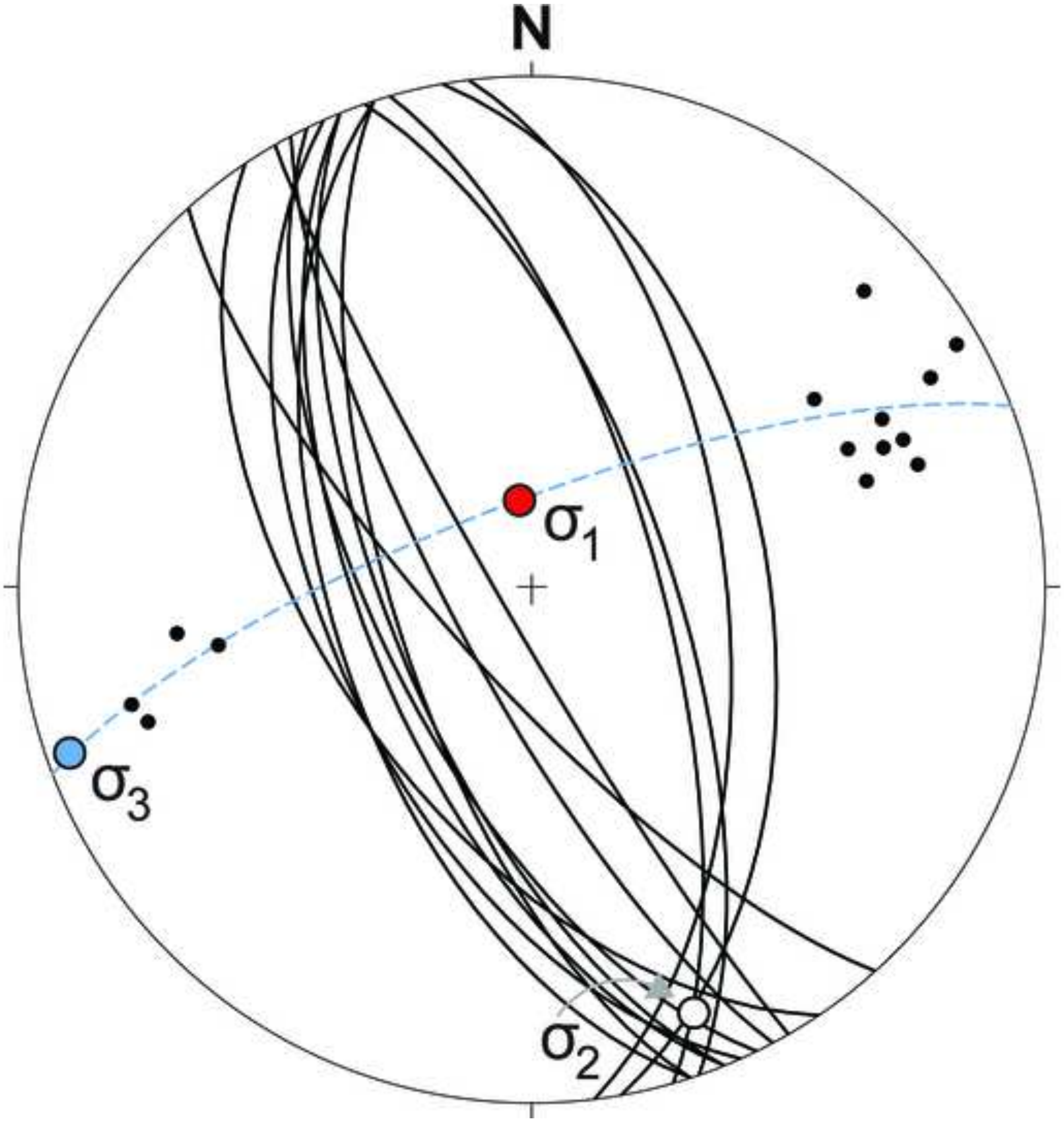
N
σ1
σ3
σ2

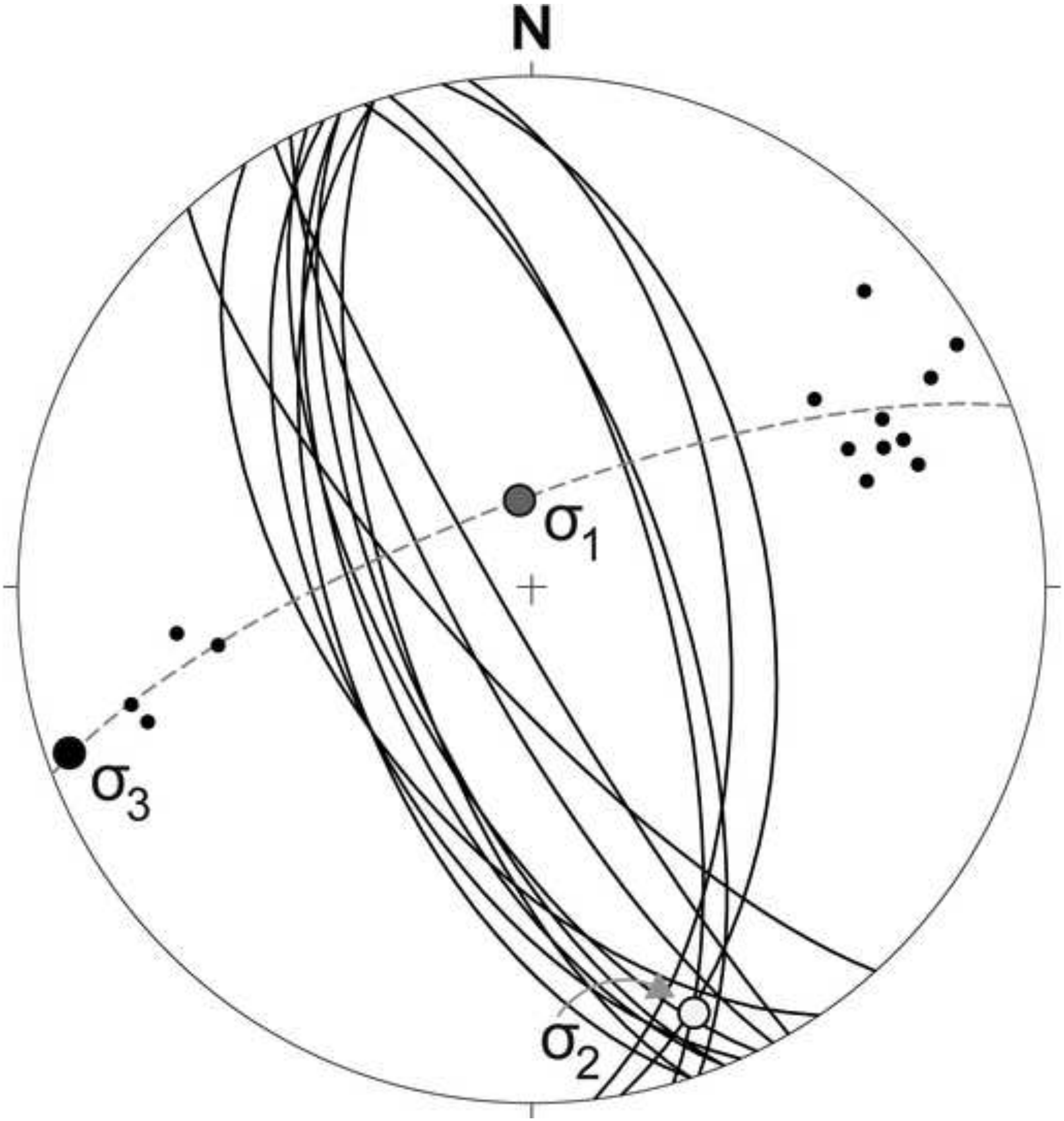
N
σ1
σ2
σ3

Figure (with caption below and on the same page) Click here to access/download;Figure (with caption below and on the same page);Fig 6.tif

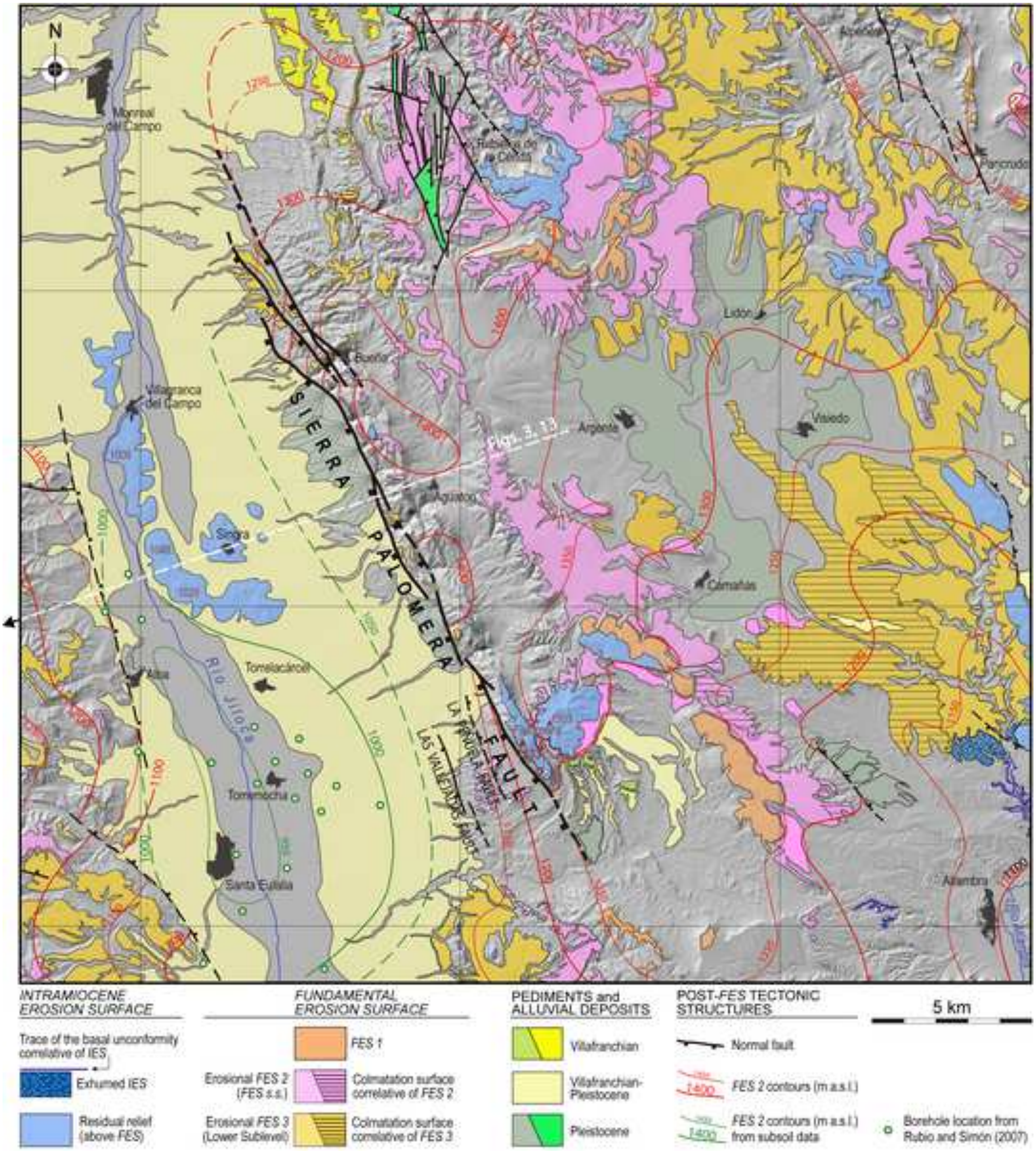

Figure (with caption below and on the same page)

Click here to access/download;Figure (with caption below and on the same page);Fig 6bn.tif

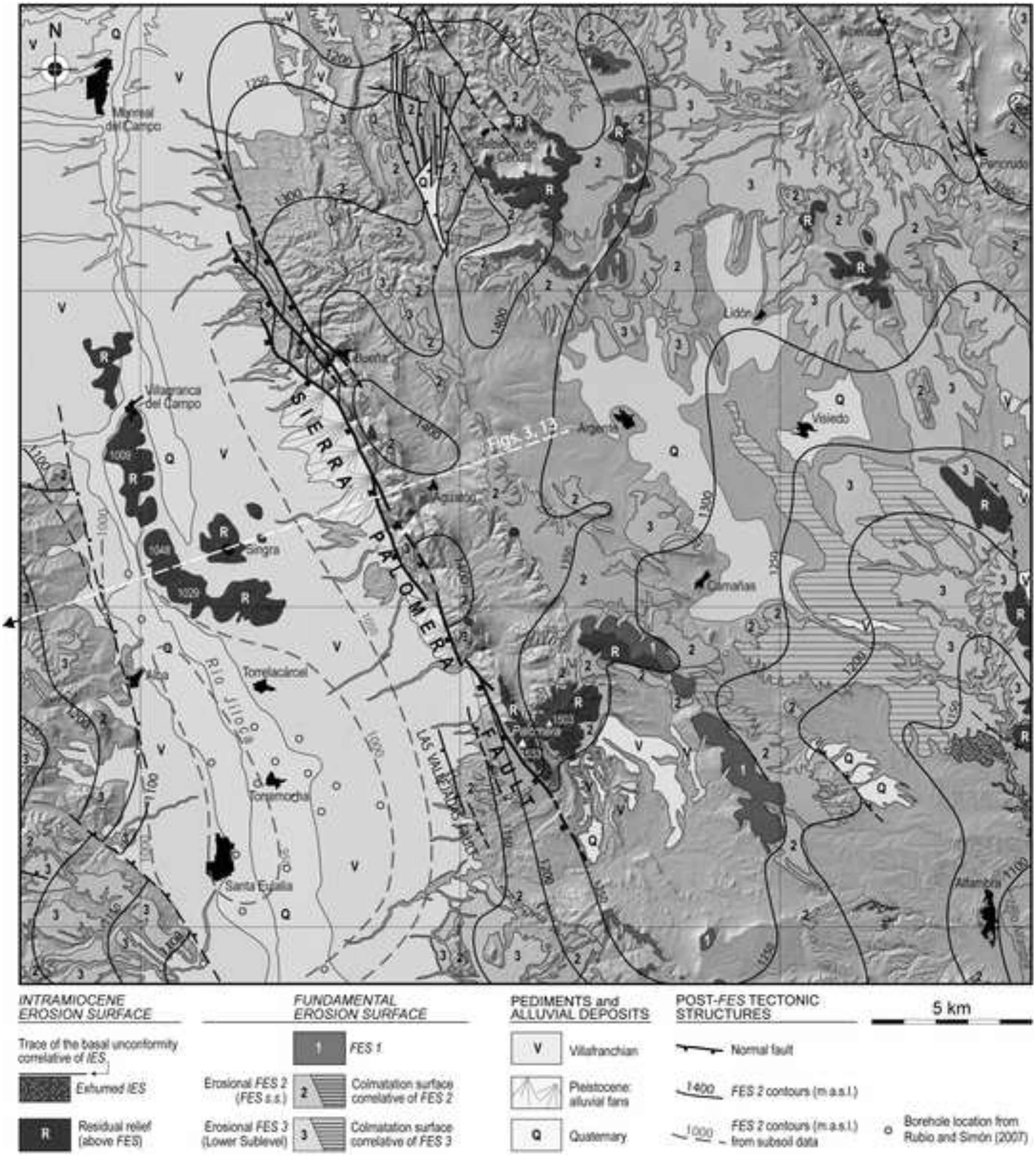

Figure (with caption below and on the same page)

Click here to access/download;Figure (with caption below and on the same page);Fig 8.tif

Figure (with caption below and on the same page)

Click here to access/download;Figure (with caption below and on the same page);Fig 8bn.tif

Figure (with caption below and on the same page)

Click here to access/download;Figure (with caption below and on the same page);Fig 9.tif

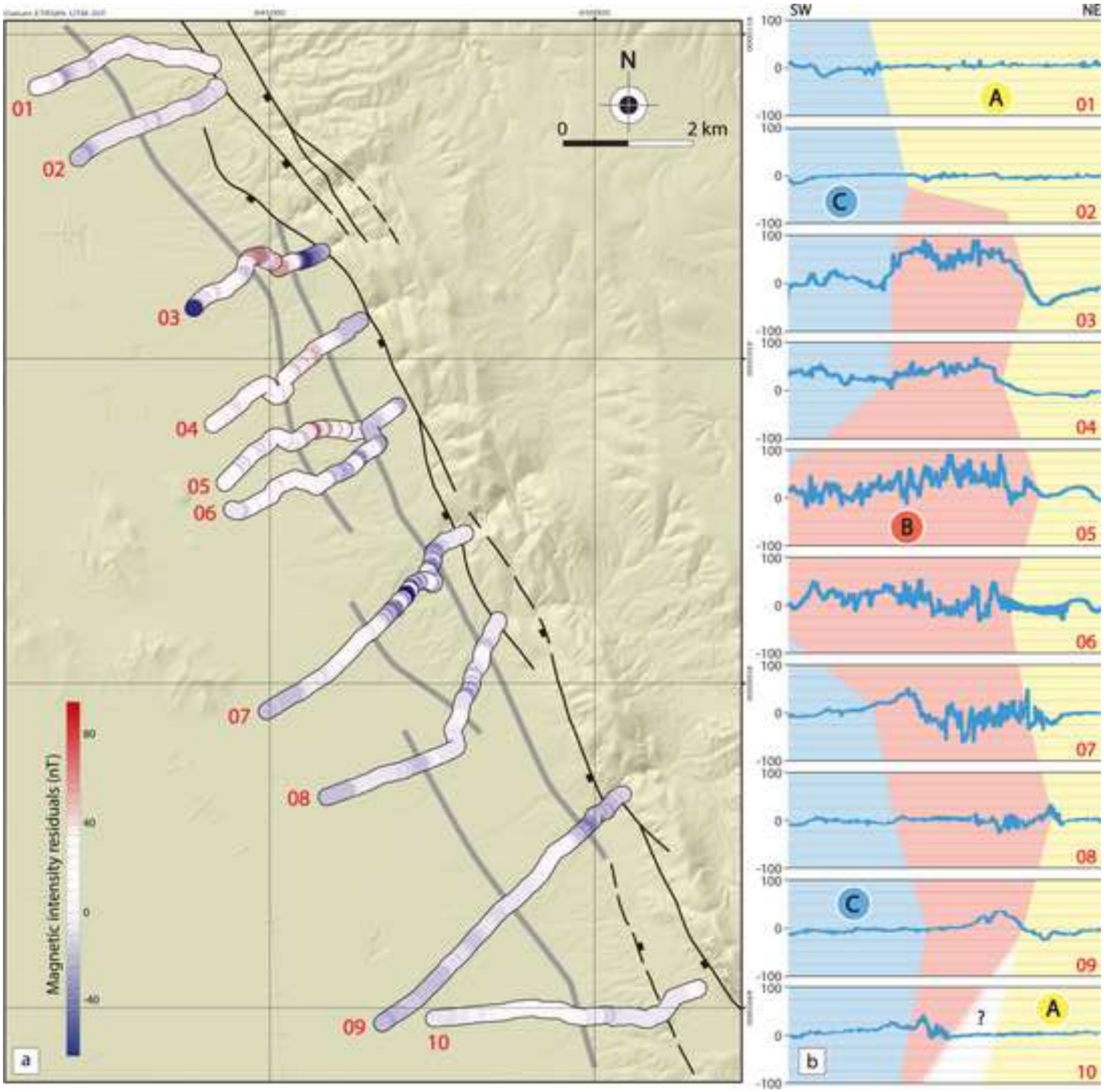

Figure (with caption below and on the same page)

Click here to access/download;Figure (with caption below and on the same page);Fig 9bn.tif

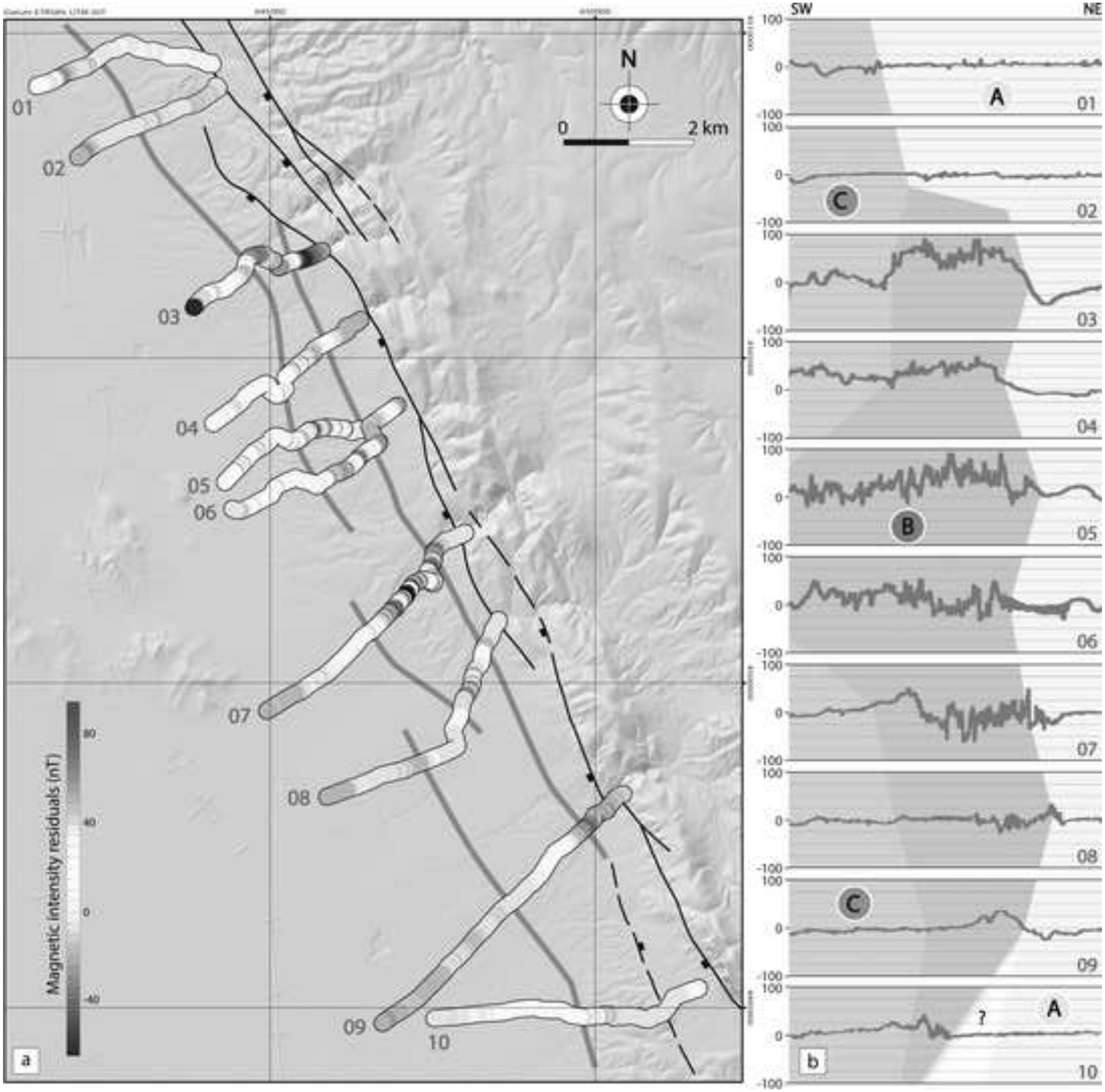

Figure (with caption below and on the same page)

Click here to access/download;Figure (with caption below and on the same page);Fig 10.tif

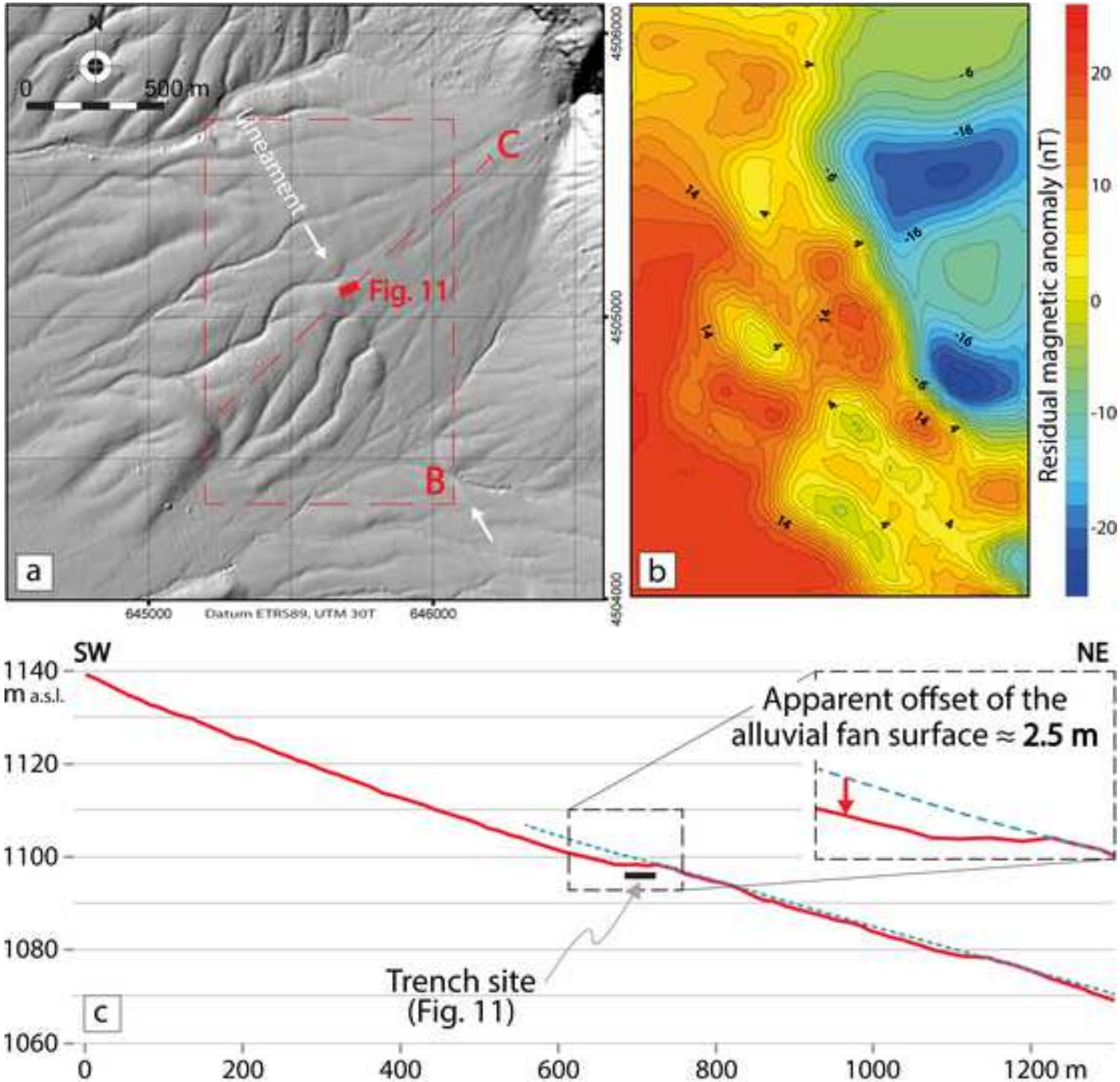

Figure (with caption below and on the same page)

Click here to access/download;Figure (with caption below and on the same page);Fig 10bn.tif

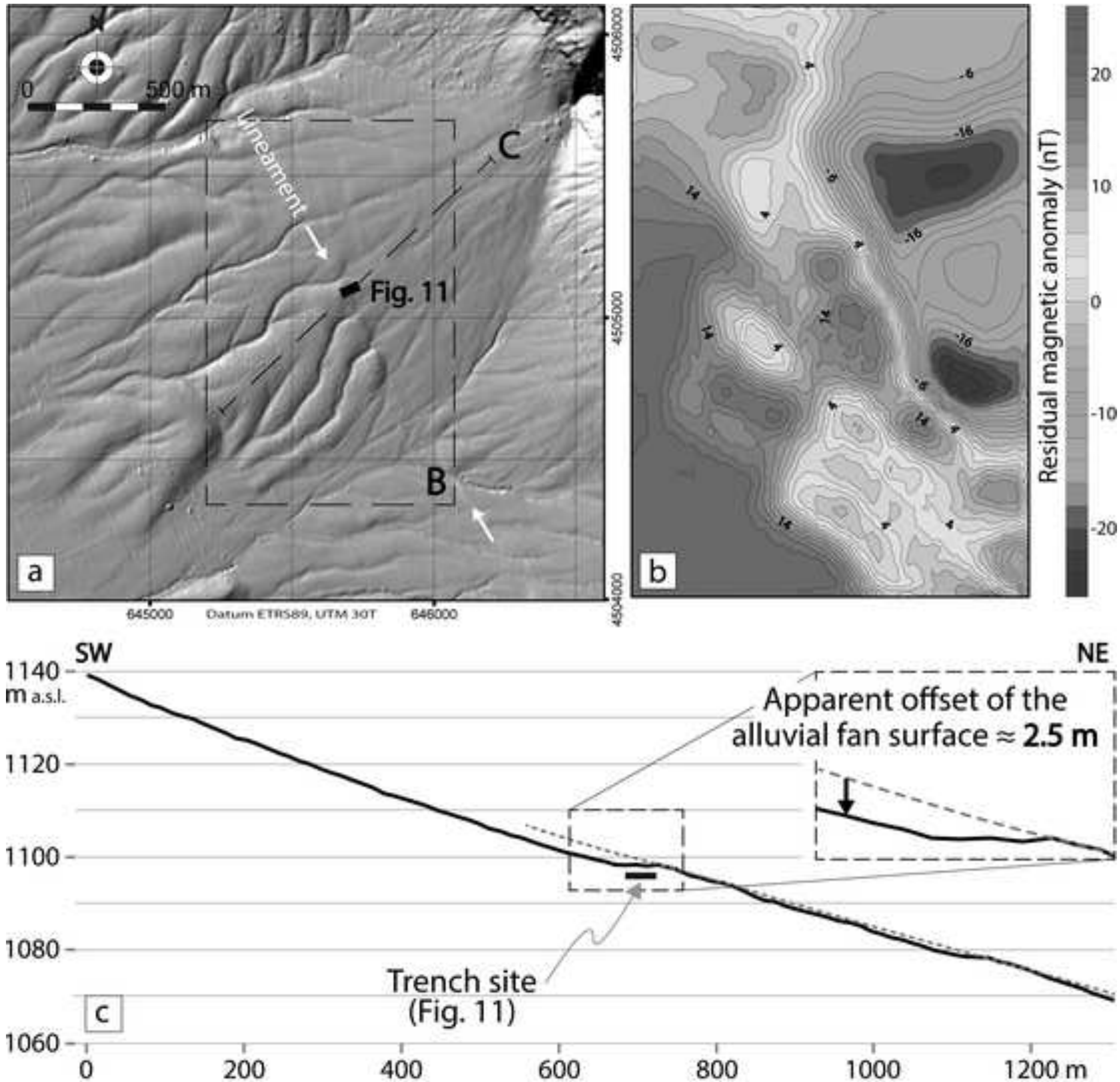

Figure (with caption below and on the same page)

Click here to access/download;Figure (with caption below and on the same page);Fig 11.tif

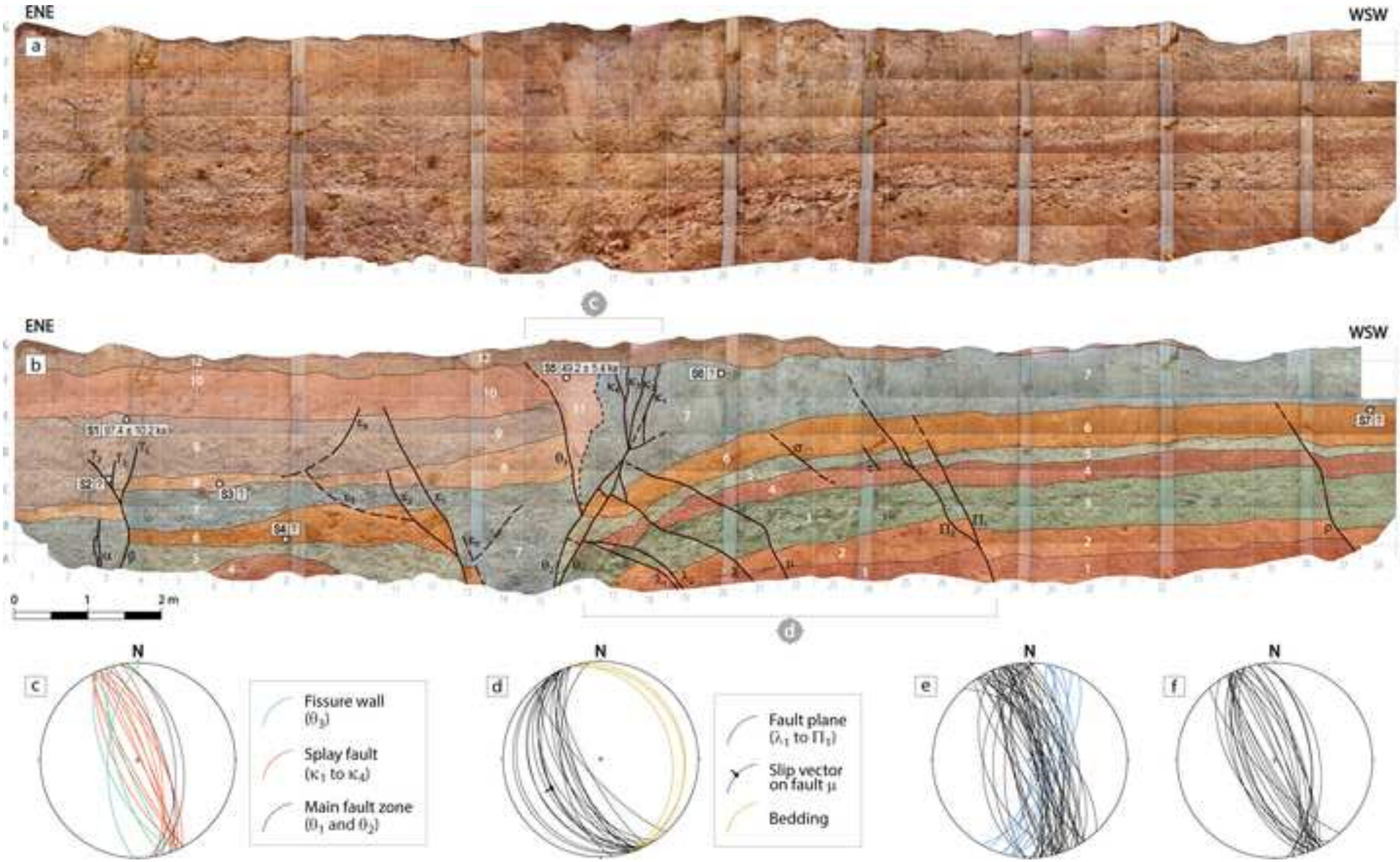

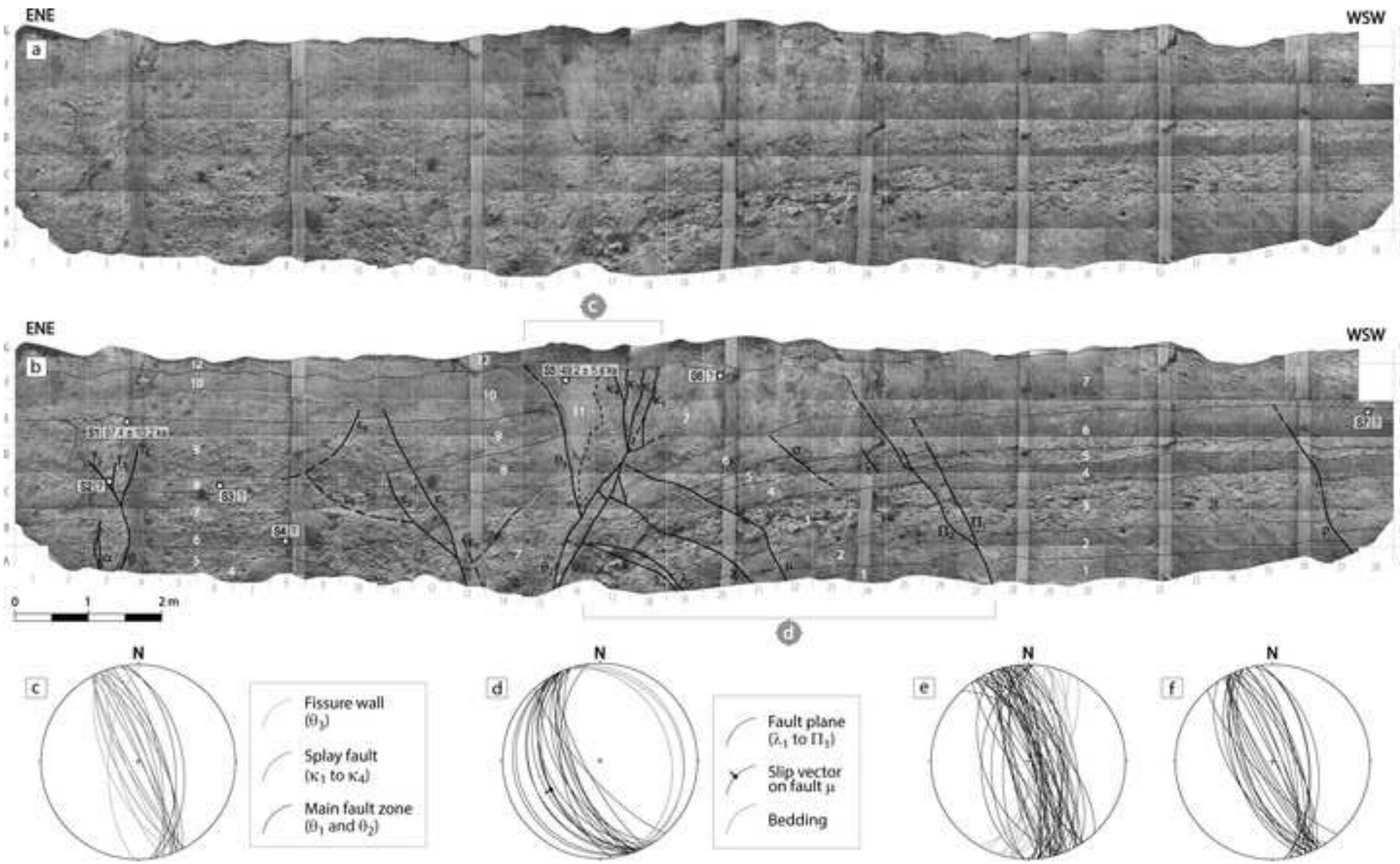
ENE
WSW
a
b
c
d
0
1
2 m
N
c
Fissure wall
(θ3)
Splay fault
(κ1 to κ4)
Main fault zone
(θ1 and θ2)
d
Fault plane
(λ1 to Π1)
Slip vector
on fault μ
Bedding
e
f

Figure (with caption below and on the same page) Click here to access/download;Figure (with caption below and on the same page);Fig 12.tif

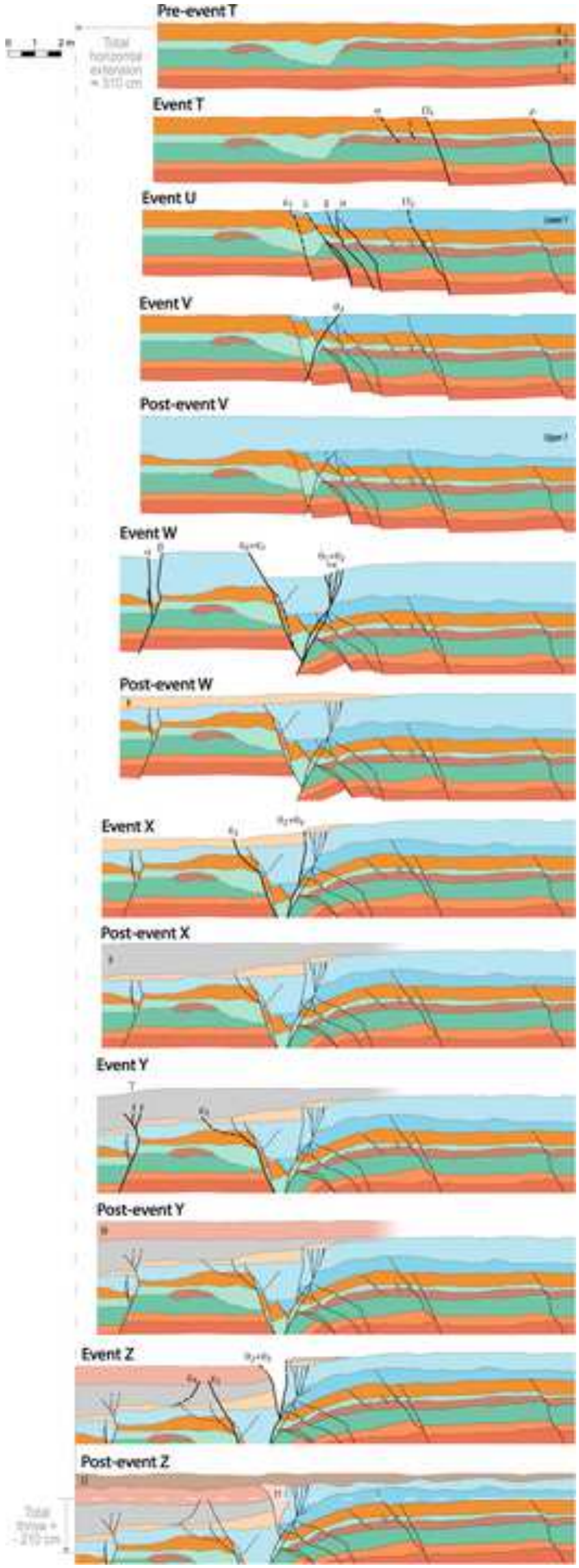

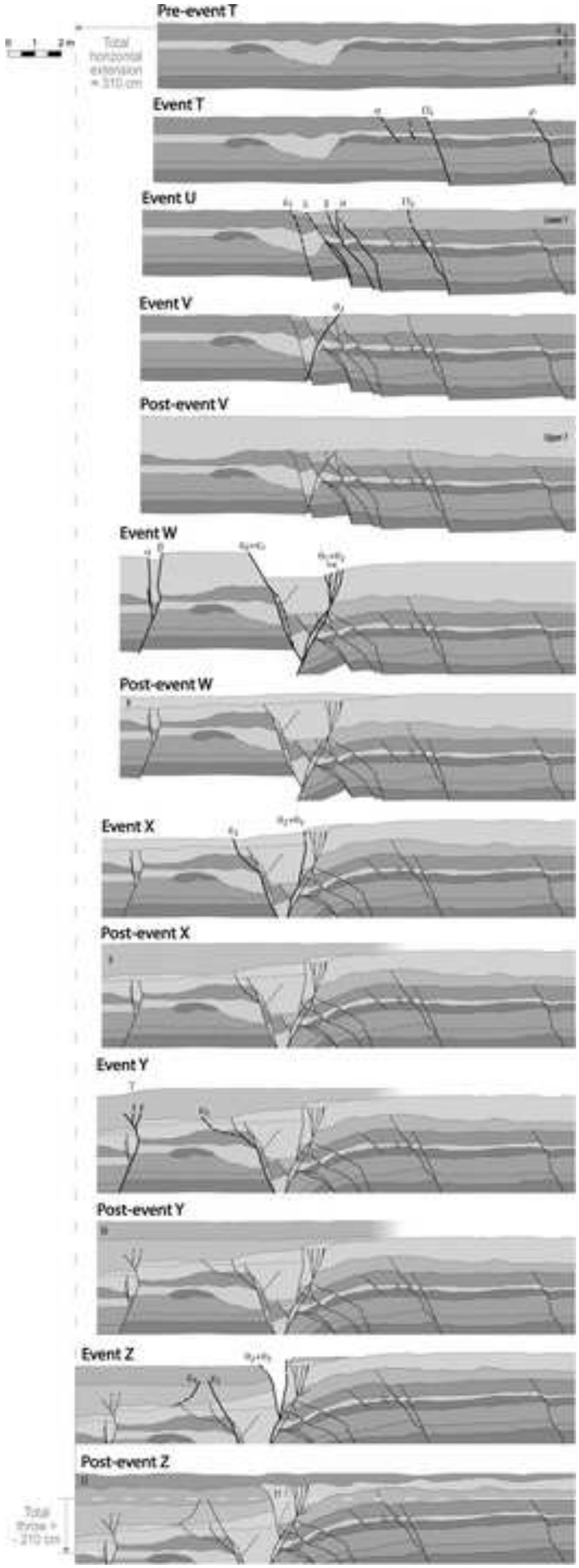
Pre-event T
Event T
Event U
Event V
Post-event V
Event W
Post-event W
Event X
Post-event X
Event Y
Post-event Y
Event Z
Post-event Z

Declaration of interests

☒ The authors declare that they have no known competing financial interests or personal relationships that could have appeared to influence the work reported in this paper.

☐The authors declare the following financial interests/personal relationships which may be considered as potential competing interests:

CRediT author statement

A. Peiro: Methodology, Formal analysis, Investigation, Writing - Original Draft, Visualization; **J.L. Simón:** Conceptualization, Validation, Investigation, Writing - Original Draft, Supervision; **L.E. Arlegui:** Investigation, Visualization; **L. Ezquerro:** Validation, Investigation; **A.I. García-Lacosta:** Formal analysis, Investigation, Visualization; **M.T. Lamelas:** Formal analysis, Investigation, Visualization; **C.L. Liesa:** Validation, Investigation, Writing – Review & Editing; **A. Luzón:** Validation, Investigation, Writing - Original Draft; **L. Martín-Bello:** Investigation; **Ó. Pueyo-Anchuela:** Investigation, Methodology, Formal analysis, Writing - Original Draft; **N. Russo:** Investigation, Visualization.